



TECHNISCHE UNIVERSITÄT MÜNCHEN

TUM Campus Straubing für Biotechnologie und Nachhaltigkeit

## **Advances in the production of poly(oxymethylene) dimethyl ethers and methanolic formaldehyde solution**

Yannic-Henrik Tönges

Vollständiger Abdruck der von der promotionsführenden Einrichtung TUM Campus Straubing für Biotechnologie und Nachhaltigkeit der Technischen Universität München zur Erlangung des akademischen Grades eines

**Doktors der Ingenieurwissenschaften (Dr.-Ing.)**

genehmigten Dissertation.

Vorsitzender: Prof. Dr. rer. nat. Nicolas Plumeré  
Prüfer der Dissertation: 1. Prof. Dr.-Ing. Jakob Burger  
2. Prof. Dr.-Ing. Erik von Harbou

Die Dissertation wurde am 17.08.2022 bei der Technischen Universität München eingereicht und von der promotionsführenden Einrichtung TUM Campus Straubing für Biotechnologie und Nachhaltigkeit am 20.01.2023 angenommen.



# Danksagung

Die vorliegende Arbeit entstand während meiner Tätigkeit als wissenschaftlicher Mitarbeiter der Professur für Chemische und Thermische Verfahrenstechnik am Campus Straubing für Biotechnologie und Nachhaltigkeit der Technischen Universität München.

Zuerst möchte ich mich bei meinem Doktorvater, Prof. Jakob Burger, bedanken: für die Bereitstellung des Themas, für die zahlreichen fachlichen Diskussionen und Denkanstöße und für das Vertrauen in meine Arbeit. Vielen Dank für die Betreuung, die zum Gelingen dieser Arbeit beigetragen hat!

Prof. Erik von Harbou danke ich vielmals für die Begutachtung und Prüfung dieser Arbeit und Prof. Nicolas Plumeré für die Übernahme des Prüfungsvorsitzes. Vielen Dank auch an meinen Mentor, Juniorprofessor Maximilian Kohns.

Besonderer Dank gilt allen Co-Autoren meiner Veröffentlichungen, insbesondere Maximilian Held und Vincent Dieterich, die sich mit mir immer wieder detailliert mit allen erdenklichen technischen Fragestellungen auseinandergesetzt haben.

Herzlichen Dank an alle meine Kollegen der Professur für Chemische und Thermische Verfahrenstechnik, für den regen fachlichen Austausch im Arbeitsalltag, viele schöne Gespräche, und vor allem gute Freundschaften. Die Zusammenarbeit mit euch hat nicht nur zu dieser Arbeit beigetragen, sondern die Promotion zu einer sehr schönen Zeit gemacht. Besonderen Dank hier an Johannes Voggenreiter und Eva Kirchinger für die zahlreichen Diskussionen zur Modellierung und Umsetzung verfahrenstechnischer Prozesse. Herzlichen Dank auch an Birgit Aich-Bauer für die Unterstützung in administrativen Fragen.

Abschließend bedanke ich mich bei meinen Eltern, die mir mein Studium ermöglicht haben, bei meiner Schwester Lisa, und bei Anne, auf deren Unterstützung ich mich immer verlassen kann.

Yannic Tönges

Mainz, März 2023



# Abstract

Poly(oxymethylene) dimethyl ethers (OME) are a much-discussed synthetic and renewable fuel for reducing soot and nitrous oxide formation and, if produced as e-fuel, CO<sub>2</sub> emissions. There are two main routes for OME synthesis: OME synthesis directly from methanol and formaldehyde and OME synthesis via the two intermediates, methylal and trioxane. The latter two are also produced from methanol and formaldehyde, and formaldehyde is produced from methanol. In the first part of this work, the energetic efficiency of the OME production from CO<sub>2</sub> employing electrical energy is calculated. CO<sub>2</sub> capture is included in the analysis by considering direct air capture and post-combustion capture technologies. CO<sub>2</sub> is converted to methanol using hydrogen produced by electrolysis. Both routes for OME synthesis are evaluated, and the energetic efficiency of OME production is evaluated for different levels of heat integration and variable electrolysis efficiencies. The energetic efficiency is compared to different e-fuels to set OME in an overall context. Since both routes require large amounts of formaldehyde solution of low water content, a novel process for producing said solution is proposed in the second part of this work. The designed process produces methanolic formaldehyde solutions with high yield, avoiding aqueous solution as a side product. The separation of water is achieved by a combination of thin-film evaporation and distillation. Optimal operating points concerning energy demand and residual water content are determined with multi-criteria optimization. The novel process saves carbon losses of up to 8% in comparison to its predecessor. Finally, the production cost of OME is investigated. Because all OME production is based on the platform chemical methanol, the production cost of OME depends on the methanol cost. Several routes for providing formaldehyde solutions from methanol are investigated and evaluated in combination with the OME synthesis. The routes are assessed, energy balances are calculated, and a techno-economic analysis is performed. The levelized product cost for OME is calculated as a function of the methanol cost and plant size for every route.



# Kurzfassung

Poly(oxymethylene) dimethyl ether (OME) sind vielversprechende, synthetische und erneuerbare Kraftstoffe die die Bildung von Ruß und Stickoxiden unterdrücken und, wenn sie als e-fuel produziert werden, CO<sub>2</sub> emission verringern. OME können über zwei Routen hergestellt werden: in der direkten Synthese von OME aus Methanol und Formaldehyd und in der Synthese aus den Zwischenprodukten Trioxane und Methylal. Letztere werden ebenso aus Methanol und Formaldehyd hergestellt, Formaldehyd selbst wird auch aus Methanol produziert. Im ersten Teil der vorliegenden Arbeit wird die Energieeffizienz der Herstellung von OME aus CO<sub>2</sub> und Strom berechnet. Technologien zur CO<sub>2</sub>-Abtrennung aus Luft und Verbrennungsabgasen und der jeweilige Energieaufwand werden in der Analyse berücksichtigt. Das gewonnene CO<sub>2</sub> wird mithilfe von Elektrolyse-Wasserstoff zu Methanol reagiert. Beide Routen zur OME Synthese werden evaluiert, und die Energieeffizienz der OME Herstellung wird für verschiedene Stufen von Wärmeintegration und variable Elektrolysewirkungsgrade berechnet. Abschließend wird die Energieeffizienz mit anderen e-fuels verglichen. Da beide Routen der OME Herstellung große Mengen von Formaldehydlösungen mit niedrigem Wassergehalt benötigen, wird im zweiten Teil der vorliegenden Arbeit ein neuer Prozess zur Bereitstellung dieser Lösung vorgestellt. Der entwickelte Prozess kann mit hoher Selektivität methanolische Formaldehydlösungen produzieren, ohne dass dabei wässrige Formaldehydlösungen als Nebenprodukt anfallen. Die Abtrennung von reinem Wasser aus Produkt wird dabei durch eine Kombination von Dünnschichtverdampfung und Destillation erreicht. Die optimalen Betriebspunkte für Prozess und Einzelapparate werden mittels mehrkriterielle Optimierung identifiziert. Der neue Prozess spart gegenüber seinem Vorgänger bis zu 8% an Kohlenstoffverlusten ein. Abschließend werden die Herstellungskosten für OME untersucht. Da die OME Herstellung immer auf Methanol als Plattform-Chemikalie basiert, hängen auch die Herstellungskosten für OME direkt vom Methanolpreis ab. Die OME Synthese wird in Kombination mit mehreren Routen zur Herstellung von Formaldehydlösungen aus Methanol untersucht und ausgewertet. Für alle Routen werden Energiebilanzen berechnet und eine Techno-Ökonomische Analyse durchgeführt um diese zu bewerten. Die Herstellungskosten für OME werden als Funktionen von Methanolpreis und Anlagengröße berechnet.





# Declaration

This dissertation contains material that has been published previously or that is included in submitted publications. In the following, these publications are listed together with a statement on the contributions of the author of the present dissertation.

- M. Held, Y. Tönges, D. Pélerin, M. Härtl, G. Wachtmeister, J. Burger: On the energetic efficiency of producing polyoxymethylene dimethyl ethers from CO<sub>2</sub> using electrical energy, *Energy Environ. Sci.*, 12 (2019). [10.1039/C8EE02849D](https://doi.org/10.1039/C8EE02849D).

*The author developed, implemented and tested the method, set up and performed the simulations, and evaluated the results. The author wrote the manuscript.*

- Y. Tönges, J. Burger: Design of a process for the provision of methanolic formaldehyde solutions of low water content from aqueous formaldehyde solutions, *Chem Eng Res Des*, 189 (2023). <https://doi.org/10.1016/j.cherd.2022.11.022>.

*The author developed, implemented, and tested the method, set up and performed the simulations, and evaluated the results. The author wrote the manuscript.*

- Y. Tönges, V. Dieterich, S. Fendt, H. Spliethoff, J. Burger: Techno-economic analysis of large scale production of poly(oxymethylene) dimethyl ether from methanol in water-tolerant processes, *Fuels*, 4 (2023). <https://doi.org/10.3390/fuels4010001>.

*The author set up and performed the simulations, and evaluated the results. The author performed parts of the economic analysis. The author wrote the manuscript.*



# Contents

<b>1</b>	<b>Introduction</b>	<b>1</b>
<b>2</b>	<b>Overview over the thesis</b>	<b>5</b>
2.1	OME routes and structure of the present work . . . . .	5
2.2	Chemical System . . . . .	7
<b>3</b>	<b>Modeling and Simulation</b>	<b>9</b>
3.1	Process simulation and evaluation . . . . .	9
3.2	Property model . . . . .	9
3.2.1	FA synthesis and concentration, MAL synthesis . . . . .	9
3.2.2	OME synthesis, TRI synthesis . . . . .	10
3.2.3	Enthalpy model . . . . .	10
3.2.4	True and overall composition in FA solutions . . . . .	11
<b>4</b>	<b>Energetic efficiency of OME production</b>	<b>13</b>
4.1	Literature review . . . . .	13
4.2	Boundaries . . . . .	14
4.3	Methodology . . . . .	15
4.3.1	Energetic efficiency . . . . .	15
4.3.1.1	Definition. . . . .	15
4.3.1.2	Maximum attainable energetic efficiency. . . . .	15
4.3.2	Studied routes and stoichiometry . . . . .	16
4.3.3	Material balances of single processes including losses . . . . .	18
4.3.4	Temperatures and enthalpies of process streams . . . . .	18
4.3.5	Energy balances . . . . .	19
4.3.6	Heat integration . . . . .	20
4.4	Process design and calculations . . . . .	21
4.4.1	Carbon capture . . . . .	21
4.4.2	Electrolysis . . . . .	22
4.4.3	ME synthesis . . . . .	22
4.4.4	FA synthesis and concentration . . . . .	22

4.4.5	TRI synthesis . . . . .	24
4.4.6	MAL synthesis . . . . .	24
4.4.7	OME <sub>3-5</sub> synthesis . . . . .	25
4.5	Results . . . . .	26
4.5.1	Material balance . . . . .	26
4.5.1.1	Material balance based on stoichiometry. . . . .	26
4.5.1.2	Material balance based on reference processes. . . . .	27
4.5.2	Energy Balance . . . . .	27
4.5.2.1	Contribution of individual processes to the total energy demand (Scenario S1). . . . .	29
4.5.2.2	Effect of heat integration (Scenarios S2 and S3). . . . .	29
4.5.3	Energetic efficiency . . . . .	30
4.6	Discussion . . . . .	31
4.6.1	Material balance . . . . .	31
4.6.1.1	Hydrogen balance. . . . .	31
4.6.1.2	Carbon balance. . . . .	32
4.6.1.3	Side products and waste. . . . .	32
4.6.2	Energetic efficiency in the context of other e-fuels . . . . .	32
4.6.3	Limitations and assumptions . . . . .	36
4.6.4	Other objectives beside energetic efficiency . . . . .	36
<b>5</b>	<b>Novel process for the provision of methanolic formaldehyde solutions</b>	<b>39</b>
5.1	State of the art . . . . .	39
5.2	Methodology . . . . .	41
5.2.1	Model of physico-chemical properties . . . . .	41
5.2.2	Model of thin-film evaporation . . . . .	42
5.2.3	Model of distillation . . . . .	44
5.2.4	Process and specification . . . . .	44
5.2.5	Simulation and optimization . . . . .	47
5.3	Results . . . . .	49
5.3.1	Validation of the TFE model . . . . .	49
5.3.2	Objective trade-offs . . . . .	50
5.3.2.1	Material and energy balance . . . . .	51
5.4	Discussion . . . . .	53
5.4.1	Model of the thin-film evaporation . . . . .	53
5.4.2	Objective trade-offs . . . . .	53
5.4.3	Variations of the process concept . . . . .	54

---

<b>6</b>	<b>Techno-economic analysis of OME production from methanol</b>	<b>57</b>
6.1	Literature review . . . . .	57
6.2	Methodology . . . . .	59
6.2.1	Description of processes . . . . .	59
6.2.1.1	Overview routes . . . . .	59
6.2.1.2	Formaldehyde production . . . . .	60
6.2.1.3	Formaldehyde concentration . . . . .	61
6.2.1.4	OME production . . . . .	62
6.2.1.5	Detailed descriptions . . . . .	62
6.2.2	Process simulation . . . . .	62
6.2.2.1	Unit modeling and design . . . . .	62
6.2.3	Process economics . . . . .	65
6.3	Results and discussion . . . . .	66
6.3.1	Material balances . . . . .	66
6.3.2	Energy balance . . . . .	67
6.3.3	Economics . . . . .	68
6.3.3.1	Base case . . . . .	68
6.3.3.2	Sensitivitiy studies . . . . .	70
<b>7</b>	<b>Conclusion</b>	<b>75</b>
<b>A</b>	<b>Appendix: Property model</b>	<b>97</b>
A.1	Model of physico-chemical properties . . . . .	97
A.1.1	FA synthesis and concentration, MAL synthesis . . . . .	97
A.1.2	OME synthesis, TRI synthesis . . . . .	98
A.2	Property data parameter values . . . . .	99
<b>B</b>	<b>Appendix: Energetic efficiency of OME production</b>	<b>107</b>
B.1	Additional information on the synthesis processes . . . . .	107
B.1.1	Carbon Capture . . . . .	107
B.1.2	FA synthesis. . . . .	108
B.1.3	TRI synthesis. . . . .	108
B.1.4	ME synthesis . . . . .	109
B.2	Overall material balance . . . . .	110
B.3	Pinch analyses for Route A . . . . .	113
B.3.1	Scenario 1: All processes separately. . . . .	113
B.3.2	Scenario 2: Two blocks. . . . .	115
B.3.3	Scenario 3: One block. . . . .	117

B.4	Pinch analyses for Route B . . . . .	118
B.4.1	Scenario 1: All processes separately. . . . .	118
B.4.2	Scenario 2: Two blocks. . . . .	121
B.4.3	Scenario 3: One block. . . . .	123
B.5	Overall energy balance . . . . .	124
B.6	LHV efficiencies of Route A and B . . . . .	125
B.7	Stream tables (ME to OME <sub>3-5</sub> ) . . . . .	126
B.7.1	Stream tables for single processes in Route A. . . . .	126
B.7.2	Stream tables for single processes in Route B . . . . .	129
B.8	Energy demand tables (ME to OME <sub>3-5</sub> ) . . . . .	134
B.8.1	Energy demand tables for single processes in Route A. . . . .	134
B.8.2	Energy demand tables for single processes in Route B. . . . .	136
<b>C</b>	<b>Appendix: Novel process for the provision of methanolic formalde-</b>	
	<b>hyde solutions</b>	<b>139</b>
C.1	Model TFE: Influence of discretization . . . . .	139
C.2	Reactive vapor-liquid equilibrium topology of formaldehyde solutions . .	142
C.3	Additional process data cases I and II . . . . .	143
C.4	Influence of the residence time in the TFE on OP <sub>I</sub> . . . . .	147
<b>D</b>	<b>Appendix: Techno-economic analysis of OME production</b>	<b>149</b>
D.1	Additional information on the processes . . . . .	149
D.1.1	Process I: Production of FA with complete conversion of ME . . .	149
D.1.1.1	Process II: Production of FA with incomplete conversion of ME . . . . .	151
D.1.1.2	Process II': Production of FA and fast condensation . . .	152
D.1.1.3	Process III: Thin-film evaporation . . . . .	154
D.1.1.4	Process III*, Thin-film evaporation . . . . .	156
D.1.1.5	Process IV, Pervaporation . . . . .	157
D.1.1.6	Process V: Extractive distillation . . . . .	161
D.1.1.7	Process VI: Chemical separation of water and extractive distillation . . . . .	163
D.1.1.8	Process VII: OME production . . . . .	166
D.2	Assumptions Techno-Economic Assessment . . . . .	168

# List of Symbols

## Latin symbols

$a_i$	Activity of component $i$
$A$	Surface area
$c$	Cost
$c_p$	Isobaric heat capacity
$H$	Enthalpy
$h_i$	Specific enthalpy of component $i$
$h_i^f$	Standard enthalpy of formation of component $i$
$K$	Number of components
$K_a$	Activity based chemical equilibrium constant
$k$	Heat transfer coefficient
$\dot{m}$	Mass flow rate
$N$	Number of stages
$n$	Chain length
$p$	Pressure
$p_i^s$	Vapor pressure of component $i$
$\dot{Q}_i$	Heat duty of unit $i$
$\dot{q}_i$	Heat duty of unit $i$ per kg product
$\dot{Q}_{tot}$	Total heat duty
$R$	Universal gas constant
$T$	Temperature
$T^\theta$	Standard temperature
$T_c$	Critical temperature
$W$	Electrical energy
$x_i^{(n/m),k}$	Mole/mass fraction of component $i$ in $k$
$y_i^{(n/m),k}$	Mole/mass fraction of component $i$ in $k$ in the gas phase

## Greek symbols

$\gamma_i$	Activity coefficient of component $i$
$\Delta h_{v,i}$	Enthalpy of vaporization
$\Delta h_{R,i}$	Reaction enthalpy
$\eta$	Energetic efficiency
$\nu_{ij}$	Stoichiometric coefficient of component $i$ in reaction $j$
$\rho^{(n)}$	Molar liquid density
$\tau$	Residence time

## Abbreviations

A	Absorber
AEL	Alkaline Electrolysis
B	Burner (in Flowsheets)
BEV	Battery Electric Vehicle
C	Column
CAPEX	Capital Expenditure
CC	Carbon Capture
CCC	Cold Composite Curve (in Pinch Analyses)
CCU	Carbon Capture and Utilization
CEPCI	Chemical Engineering Plant Cost Index
CON	Condenser (in Flowsheets)
CPS	CO <sub>2</sub> from Point Sources
DAC	Direct Air Capture
DE	Diesel equivalent
DME	Dimethyl Ether
E	Various unit operations with phase change
e-fuel	electricity-based fuel
EL	Electrolysis
EUR	Euro
FA	Formaldehyde
FT	Fischer-Tropsch diesel
GHG	Greenhouse Gas
HCC	Hot Composite Curve (in Pinch Analyses)
HF	Hemiformal



---

HF <sub>n</sub>	Polyoxymethylene hemiformal
HHV	Higher Heating Value
HtF	Hydrogen-to-Fuel
HX	Heat exchanger (in Flowsheets)
ICE	Internal Combustion Engine
LCA	Life Cycle Assessment
LHV	Lower Heating Value
LPC	Levelized product cost
M	Membrane Unit (in Flowsheets)
MAL	Polyoxymethylene ether
MCO	Multi-criteria optimization
MEA	Mono-ethanol amine
ME	Methanol
MG	Methylene glycole
MG <sub>n</sub>	Polyeoxymethylene glycole
OME <sub>n</sub>	Polyoxymethylene dimethyl ether of chain length n
OP	Operating point
OPEX	Operational Expenditure
PCC	Post-Combustion Capture
PEG	Polyethylene glycol dimethyl ether
PEMEL	Polymer Electrolyte Membrane Electrolysis
PFD	Process flow diagram
PtF	Power-to-Fuel
R	Reactor (in Flowsheets)
RR	Reflux Ratio
SOEL	Solid Oxide Electrolysis
TCO	Total Costs of Ownership
TFE	Thin Film Evaporator (in Flowsheets)
TRI	Trioxane
TRL	Technology Readiness Level
TTW	Tank-To-Wheel
USD	US Dollar
VLE	Vapor-liquid equilibrium
WA	Water
WACC	Weighted Average Cost of Capital
WTT	Well-To-Tank
WTW	Well-To-Wheel



# 1 Introduction

Polyoxymethylene dimethyl ethers (OME, also POM-DME or PODE), oligomers of the structure  $\text{CH}_3\text{O}(\text{CH}_2\text{O})_n\text{CH}_3$  with chain length  $n$ , are diesel-like fuels which suppress soot formation during the combustion in internal combustion engines (ICEs) [1–7]. When discussing OME, one has to distinguish between  $\text{OME}_1$  (also called methylal (MAL) or dimethoxymethane) and OME of longer chains ( $\text{OME}_n$ ). The normal boiling point of MAL (315 K [4]) is too low for its direct use in conventional diesel ICEs. By contrast,  $\text{OME}_n$  of longer chains, in particular  $\text{OME}_{3-5}$ , comprise boiling points in the range of conventional diesel fuels. Hence, they can be applied without major changes to current ICEs, filling station infrastructure, and fuel distribution systems [6, 7]. Besides their use as a neat fuel,  $\text{OME}_{3-5}$  can also be used as a blend component. Compared with the reference case of running a car on fossil diesel, the use of  $\text{OME}_{3-5}$  reduces  $\text{NO}_x$  and soot emissions (43% and 25% respectively) disproportionately to the amount of fuel replaced with OME as a blend component [5–7].

OME can be produced based on synthesis gas and methanol either from fossil resources, biomass, or carbon dioxide ( $\text{CO}_2$ ) and hydrogen produced by employing renewable energy for water electrolysis [8]. The latter kind of fuel production concept, using only water, carbon dioxide, and electrical energy as feedstock, is generally known under the term Power-to-Liquid (PtL). The products are referred to as electricity-based fuels (e-fuels), and OME currently rank among the most promising e-fuels for future sustainable and clean mobility [9, 10]. Production processes for OME have been developed only in the last 25 years, first being patented in 1998 from BP [11] and in 2005 from BASF [12]. Recent patents focus in particular on the production of  $\text{OME}_{3-5}$ , mainly from Chinese companies [13–15]. There are several routes for OME production via different intermediate steps [4, 16], and recent scientific publications investigated the kinetics of OME formation [17–19] and have proposed a lot of new process concepts for the production of OME [9, 20–24].

In contrast, the provision of feedstocks for these processes has rarely been discussed in detail, and these feedstocks are often assumed to be available. No matter which route is employed for the OME production, all currently viable technologies are based on methanol as a platform chemical and require a formaldehyde source, preferably of very

low water content, to supply the OME monomer units, the oxymethylene groups ( $\text{CH}_2\text{O}$ ) [25–27]. The required formaldehyde is itself produced from methanol [28]. Methanolic formaldehyde solutions of low water content can be used as such feedstock for the production of OME [21, 23, 29–32] or various intermediates, like, e.g., MAL [33], which is currently produced on an industrial scale [34]. However, there is very little scientific literature about the production of methanolic formaldehyde solutions. Further, providing these solutions poses some challenges because formaldehyde is usually handled and sold in aqueous solutions of 0.37 to 0.50 g/g formaldehyde [28, 35]. Methanolic formaldehyde solutions accrue in small amounts inside some existing formaldehyde plants as a side product, but it is very difficult to produce them exclusively, i.e., selectively with a high yield. This is because water is always formed as a side product in the formaldehyde synthesis from methanol [28]. When the reactor product is condensed/absorbed, one obtains solutions of formaldehyde, water, and, if the conversion was not complete, also methanol. While gaseous side products like  $\text{CO}_2$  and hydrogen are conveniently removed during the condensation, the resulting (formaldehyde+water+methanol) mixtures are more challenging to separate as they are reactive mixtures. For use as feedstock for OME production, large amounts of water have to be removed since water inhibits OME formation. To address this problem, the present work includes the presentation of a novel process that selectively produces methanolic formaldehyde solutions of low water content on a large scale.

Further, a couple of critical issues regarding the production and assessment of OME have to be thoroughly studied and solved, i.e., the availability and price of  $\text{CO}_2$ , the availability and price of renewable electrical energy, and not least the energetic efficiency and economics of the fuel production technology. PtL technologies only enable carbon-based  $\text{CO}_2$ -neutral fuels if the same amount of  $\text{CO}_2$  is used as feedstock for the fuel production as is released during fuel combustion [8, 34]. The carbon intensity of both direct and indirect electrified mobility highly depends on the carbon intensity of the energy required for fuel synthesis or electricity production. Well-to-wheel life cycle assessment (LCA) studies of the production and use as a fuel of OME and MAL have shown their reduction potential for  $\text{CO}_2$  and local emissions [36, 37]. The results show the great potential of MAL to reduce greenhouse gas emissions, but the cumulative energy demand (including production) per driven kilometer when operating MAL in an ICE vehicle is roughly doubled compared to fossil diesel fuels. Further, the cost-competitive production of renewable energy is still a major challenge in particular for the profitability of e-fuels [38, 39].

In contrast to the simulation data on OME production and its carbon balance, there is only sparse literature on the energetic assessment of OME production. While there is

process data including material and energy balances for single process steps [28, 40–44], the potential of OME production has to be assessed considering the entire route from well-to-tank if not from well-to-wheel. If a carbon-based e-fuel is used in ICEs, the tank-to-wheel efficiency mainly depends on the lower heating value (LHV) of the fuel due to the same conversion principle in the vehicle. Basing the well-to-tank efficiency on the LHV makes various fuels comparable in terms of efficiency without neglecting the well-to-wheel perspective, as long as they are used in ICEs. As with any synthetic fuel, it is crucial to know this well-to-tank efficiency for OME to evaluate its technical viability as a fuel and assess whether it can compete with fossil and other synthetic fuels. Part of the present work consequently focuses on an evaluation of the energetic efficiency of OME production from CO<sub>2</sub> and compares it with various other e-fuels. Finally, the economic viability of OME as a fuel has to be evaluated, as only a cost-competitive production can ensure market acceptance and, therefore, a significant impact from the benefits that OME offer. Several studies on the cost of OME production have recently been published. These studies are based on various starting materials, like biomass [21], PtX-hydrogen and CO<sub>2</sub> [10, 45] or methanol [46, 47] and are built on different levels of detail and technical maturity in their analysis. However, all existing studies have at least one of the following caveats: they are either rough estimates using strong simplifications or report costs depending on one single specific raw material source. No study yet reports OME production cost as a function of the methanol cost based on a detailed, and thus meaningful, model describing currently technical feasible processes. Since OME production always requires methanol as a platform chemical, reporting OME production cost depending on a variable methanol cost is highly advantageous. Due to the size of the market for methanol, the OME price will most likely be tied to the methanol price for the foreseeable future. Further, this allows flexible consideration of varying sources for said methanol; it could stem from CO<sub>2</sub> utilization, biomass, or fossil resources, and the results for OME production cost hold. Therefore the present work concludes with a techno-economic analysis (TEA) and derives the OME production cost as a function of a variable methanol cost and various plant sizes.



## 2 Overview over the thesis

### 2.1 OME routes and structure of the present work

Figure 1 shows the two routes for OME production examined in the present work, the direct Route A and the indirect Route B.

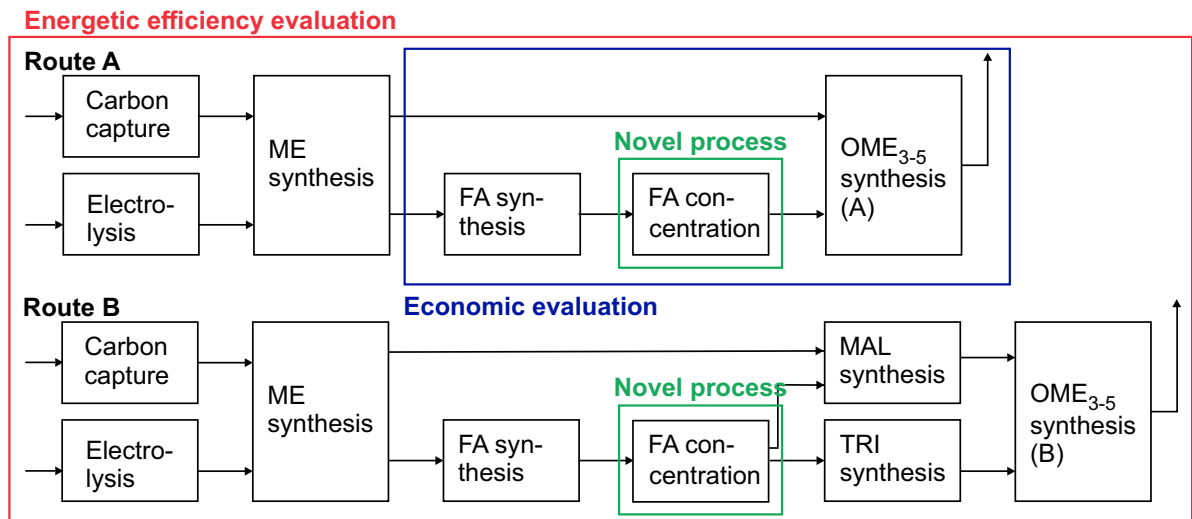


**Figure 1:** Routes for the production of OME<sub>3-5</sub> from CO<sub>2</sub> using electrical energy. The system boundaries for the topics of the present work are shown as colored rectangles: red for the energetic efficiency evaluation (Chapter 4), green for the novel FA concentration process (Chapter 5), and blue for the economic evaluation (Chapter 6).

All currently feasible OME production routes are based on methanol (ME) as a platform chemical. Here the methanol is produced from CO<sub>2</sub> (collected via carbon capture) and hydrogen (H<sub>2</sub>, produced by electrolysis) [40]. Part of the methanol is converted to formaldehyde (FA) in the FA synthesis [28], which needs to be concentrated in the next step prior to OME production. In Route A OME is then produced directly from ME and FA [43]. Route B requires the synthesis of the additional intermediates methylal (MAL) and trioxane (TRI), which are subsequently reacted to OME [44].

The topics investigated in the subsequent chapters and their respective system boundaries are highlighted as colored rectangles in Figure 1. The first part of the present

work (Chapter 3, not shown in Figure 1) presents the modeling and simulation method used for the analysis of the two routes. The second part of the present work (Chapter 4, red rectangle) investigates the energetic efficiency of OME production. For this evaluation, it is necessary to consider the energy demand of all processes of the complete process chain. While the methanol for OME production can stem from various sources, e.g., biomass or fossil resources, we limit it to methanol produced from  $\text{CO}_2$  and  $\text{H}_2$  for the investigation of the energetic efficiency. This allows the evaluation of OME as a carbon-neutral e-fuel. Routes A and B are compared to each other and to various e-fuels in terms of carbon yield and energetic efficiency. The third part of the present work (Chapter 5, green rectangle) investigates the FA concentration in detail. While this step is required in both routes and many other processes, it is seldom addressed in scientific literature and is often assumed to be available. It is also very challenging, as it involves the separation of complex reactive mixtures that often show solid precipitation. A novel process for this step, the provision of methanolic FA solution via the concentration of FA solution, is presented and optimized in Chapter 5. The last part of the present work (Chapter 6, blue rectangle) evaluates the economic performance of OME production. This evaluation is based on methanol as raw material, as reporting OME production cost depending on a variable methanol cost is highly advantageous (due to the flexibility this offers). We further limit the TEA to Route A (cf. Chapter 6 for details). Various technologies are considered for the FA concentration, including the novel process, and the resulting (sub-)routes are compared in terms of economic performance.

Besides Route A and B, multiple other processes have been proposed for the production of OME. Oestreich et al. [48] proposed a process similar to Route A, but in which OME is extracted from the process and separated from side products via absorption in large amounts of fossil fuel. This process only allows the use of OME for blending, not as pure fuel, as is intended here. Ouda et al. proposed a process for OME production based on the anhydrous dehydrogenation of methanol [49]. While this would improve production efficiency, the underlying technology is still in fundamental development, and the study is based on idealized separators. It is also possible to produce OME from dimethyl ether (DME), and a formaldehyde source [50]; the route looks similar to Route B, with DME instead of MAL. However, the process still requires improvement of catalysts to suppress side-product formation [50] and is not yet feasible. Further, some publications suggest the production of OME from biomass as feedstock [20, 51, 52]. The processes downstream of methanol production are the same as in Figure 1, but methanol (or DME) is produced from synthesis gas derived from biomass gasification. Other concepts for the production of OME directly from synthesis gas or methane are still in fundamental research and far from technical feasibility.

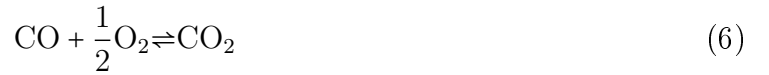
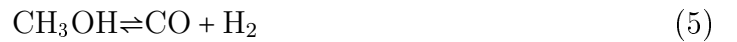
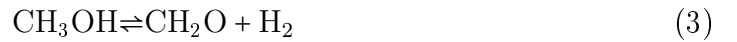
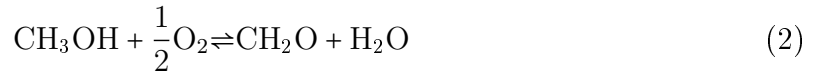


## 2.2 Chemical System

Both routes start with CO<sub>2</sub> capture and water electrolysis for H<sub>2</sub> production. In the subsequent methanol synthesis, CO<sub>2</sub> and H<sub>2</sub> are pressurized and reacted to methanol (ME, CH<sub>3</sub>OH), forming water (WA, H<sub>2</sub>O) as a side product: [40]



In both routes, parts of the methanol are converted to formaldehyde (FA, CH<sub>2</sub>O). Methanol is reacted with oxygen (in air) over silver or metal-oxide catalysts to FA, WA, H<sub>2</sub>, CO, and CO<sub>2</sub> [28, 53].



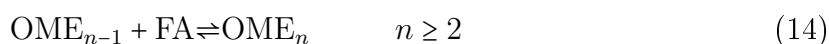
In all state-of-the-art processes, the FA is produced in a gas phase reactor and afterward chemically absorbed in water or methanol. Thereby, formaldehyde reacts both with water to poly(oxymethylene) glycols (MG<sub>n</sub>, HO-(CH<sub>2</sub>O)<sub>n</sub>-H) and with methanol to poly(oxymethylene) hemiformals (HF<sub>n</sub>, HO-(CH<sub>2</sub>O)<sub>n</sub>-CH<sub>3</sub>) [54].



These reactions occur at a considerable rate even without the presence of catalysts [55], resulting in a complex reactive phase behavior of FA solutions. Since the equilibrium of Reactions (7) to (12) lies far on the side of the products, there are only very small

amounts of monomeric FA present in aqueous and methanolic solutions. It is not possible to use simple distillation to remove large quantities of water [33]. Therefore, it is challenging to produce methanolic FA solutions of low water content, which can be used in the subsequent OME production, necessitating the formaldehyde concentration step. Three different technologies are considered for the FA concentration here. First, highly concentrated FA solutions are typically produced in fall-film evaporators or thin-film evaporators [56–58], cf. Chapter 5 for a novel process based on this option. Second, membrane separation processes, like pervaporation, can also be used to remove water from FA solutions [59, 60]. The third possibility is to employ extractive distillation of aqueous FA solutions to obtain concentrated gaseous FA, which is dissolved in methanol subsequently [61]. A variety of these technologies is also compared and included in the TEA of OME production in Chapter 6.

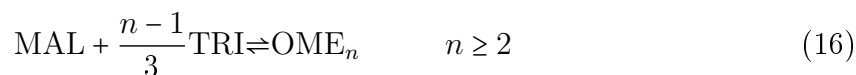
For the last step, the OME synthesis, the two routes differ. In the direct Route A, OME are formed from ME and FA and the respective HF, cf. Reactions (13)-(14) [43].



The OME process in Route A is tolerant to small amounts of water (up to 0.1 g/g in the feed) [43] and Route A generally requires fewer processing steps than Route B. On the downside, water has to be removed in the same process in which OME is produced, which is challenging [27, 43]. The indirect Route B additionally produces trioxane (TRI) [41]



and methylal [62], cf. Reaction (13). TRI and MAL are subsequently reacted to OME in a water-free process [1, 26, 27, 44].



# 3 Modeling and Simulation

## 3.1 Process simulation and evaluation

All processes downstream of the methanol synthesis are evaluated using steady-state process simulation. The simulations are performed in the software Aspen Plus V8.8 based on the following property model. Details on the modeling of the individual units are given in the respective chapters concerning the processes. All processes are evaluated regarding technical feasibility, and material and energy balances are derived from the simulation. For the techno-economic analysis, the equipment is also explicitly sized, and the purchasing cost for each item is retrieved.

## 3.2 Property model

### 3.2.1 FA synthesis and concentration, MAL synthesis

For the FA synthesis, MAL synthesis, and FA concentration processes, we adopt an activity-based fluid phase equilibrium model for the components FA, WA, ME, HF<sub>1</sub>-HF<sub>*n*</sub>, MG<sub>1</sub>-MG<sub>*n*</sub>, and MAL from Kuhnert et al. [63]. The vapor-liquid equilibrium (VLE) of these components and the Reactions (7) to (12) up to a chain length of *n*=10 are included in the model. The VLE is modeled via extended Raoult's law assuming an ideal gas phase

$$py_i = p_i^s x_i \gamma_i, \quad i \in \{\text{FA, WA, ME, MG}_1, \text{HF}_1, \text{MAL}\} \quad (17)$$

where *p* is the pressure, *y<sub>i</sub>* and *x<sub>i</sub>* the mole fractions of component *i* in the gas and liquid phase, respectively, and *p<sub>i</sub><sup>s</sup>* the vapor pressure of the component *i*. Correlations for the vapor pressures *p<sub>i</sub><sup>s</sup>* and a model for the activity coefficients *γ<sub>i</sub>* are taken from Kuhnert et al. [63]. Correlations for the vapor pressures *p<sub>i</sub><sup>s</sup>* and a model for the activity coefficients *γ<sub>i</sub>* are taken from Kuhnert et al. [63]. Therein, the non-ideality of the liquid phase is modeled via a tailor-made UNIFAC group-contribution method. The chemical

equilibrium of Reactions (7) to (12) is modeled with activity-based equilibrium constants following Kuhnert et al. [63]. For thin-film evaporators, the reactions in the liquid phase are instead modeled as described by the kinetics from Ott et al. [64], cf. Sections 5.2.1-5.2.2 for details.

For the noncondensable gases N<sub>2</sub>, O<sub>2</sub>, CO, CO<sub>2</sub>, H<sub>2</sub>, property data for vapor pressures, enthalpies of formation in the gas phase, enthalpies of vaporization, ideal gas heat capacities are adopted from the DIPPR database [65]. Gas solubilities are neglected for these components.

### 3.2.2 OME synthesis, TRI synthesis

For the OME synthesis in Route A, we adopt the activity-based fluid phase equilibrium and reactor model from Schmitz et al. [66], which is slightly different from the one used for the FA synthesis. This model is also used for the estimation of the energy balances of the TRI and OME synthesis in Route B in Chapter 4. Details are given in Appendix A.

### 3.2.3 Enthalpy model

In the process analysis and simulation, enthalpy streams are used. Neglecting excess enthalpies, they are calculated via

$$\dot{H}_{\text{stream}} = \sum_{i=1}^K \dot{m}_i h_i(T_{\text{stream}}). \quad (18)$$

Where  $K$  is the number of components in the stream,  $\dot{m}_i$  is the mass flow rate of the  $i$ -th component, and  $h_i(T_{\text{stream}})$  the specific enthalpy of the pure component  $i$  at the physical state of the stream. The specific enthalpies at temperature  $T_{\text{stream}}$  are normalized to the enthalpy of formation  $h_i^f(T^\theta)$  in the gaseous state at standard temperature  $T^\theta$  for gaseous streams:

$$h_i(T_{\text{stream}}) = h_i^f(T^\theta) + \int_{T^\theta}^{T_{\text{stream}}} c_{p,i}^g dT, \quad (19)$$

and for liquid streams:

$$h_i(T_{\text{stream}}) = h_i^f(T^\theta) + \int_{T^\theta}^{T_{\text{stream}}} c_{p,i}^g dT - \Delta h_{v,i}(T_{\text{stream}}). \quad (20)$$

The pressure dependence of the enthalpies is neglected.  $c_{p,i}^l$  and  $c_{p,i}^v$  are the isobaric, specific heat capacities in the liquid and vapor phase, respectively.  $\Delta h_{v,i}$  denotes the enthalpy of vaporization. The used correlations for the mentioned quantities are given in Appendix A.

### 3.2.4 True and overall composition in FA solutions

In FA systems, it is often expedient to differentiate between the true composition, which considers all MG and HF as individual species, and the overall composition, which is obtained when all MG/HF are conceptually decomposed into FA, ME, and WA. In the calculations of the present work, the true composition is considered throughout, while for presenting the results, we always refer to overall mass fractions. Exceptions from that rule are explicitly stated.



# 4 Energetic efficiency of OME production

## 4.1 Literature review

For any synthetic fuel, the energetic efficiency of its production is crucial to its applicability and market potential. Therefore, the following chapter focuses on the efficiency of OME production compared to other synthetic fuels. Some related work has been done on the energetic assessment of (i) biomass-based OME and (ii) the production of OME from ME and water-free FA:

(i) Besides OME as e-fuel, two studies promote biomass as a feedstock for OME [20, 51]. A significant reduction of total life cycle CO<sub>2</sub> emissions can be achieved when switching fuel from fossil diesel fuel to biomass-based OME<sub>1-8</sub> produced in an indirect route. While diesel emissions amount to 127 g CO<sub>2</sub>-eq. per MJ, OME<sub>1-8</sub> scales only to 18 g CO<sub>2</sub>-eq. per MJ (for forest residue) or 26 g CO<sub>2</sub>-eq. per MJ (for whole tree) [37]. However, the biomass-based production of OME<sub>1-8</sub> has a high life cycle energy demand of 1.40 GJ per MJ OME<sub>1-8</sub> (for forest residue) and 1.46 g GJ per MJ OME<sub>1-8</sub> (for whole tree) [37]. Thereof, 1.24 GJ per MJ OME<sub>1-8</sub> are needed for the chemical conversion of biomass to OME<sub>1-8</sub>.

(ii) Ouda et al. [67] investigate the theoretical maximum production efficiency of OME based on the reaction mechanism. Therein, the theoretical maximum hydrogen-to-OME<sub>4</sub> efficiency (based on higher heating value (HHV)) is given as 67 % or 87 %, depending on FA reaction chemistry. Another study by Ouda et al. [49] presents an idealized process concept and gives an estimated efficiency of 61.03 % for the production of OME from ME. Herein, the separation of OME<sub>3-5</sub> from the reaction product is modeled using an idealized separator; the energy consumption is simply assumed to be 30 % of the LHV of the final product. Further work [68] presents a novel OME process, respective simulation data, and the overall efficiency of the production. The results should, however, be handled with caution since the process concept employs a debatable distillation sequence [43].

In the following chapter, the present work reports resilient numbers about the energetic

efficiency of OME<sub>3-5</sub> production from CO<sub>2</sub>, H<sub>2</sub>O and electrical energy. Presented are the well-to-tank efficiency of OME<sub>3-5</sub> production via the direct Route A and the indirect Route B, and our findings are discussed in the context of other e-fuels. State-of-the-art CO<sub>2</sub> capture, hydrogen (H<sub>2</sub>) production via water electrolysis, and the state-of-the-art synthesis of ME, FA, and OME<sub>3-5</sub> are taken into account. The FA concentration is realized in one step in combination with the FA production. Heat losses are minimized by maximum heat integration via pinch analysis. Thus, a rather optimistic evaluation of the state-of-the-art technology is obtained.

The following chapter is organized as follows. In the next section, boundary conditions, definitions, and the methodology for determining the energetic efficiency are presented. Afterward, the results are presented, discussed, and compared with literature results for other e-fuels.

## 4.2 Boundaries

The large-scale production of OME<sub>3-5</sub> is considered. However, results are discussed normalized for 1 kg of OME<sub>3-5</sub>. Literature suggests different optimal product compositions depending on whether the indirect [44] or the direct [43] route is used. The production via the direct process leads to a product composition of  $x_{\text{OME}_3} = 0.498$  g/g,  $x_{\text{OME}_4} = 0.307$  g/g and  $x_{\text{OME}_5} = 0.194$  g/g [43]. The indirect process described in literature [44] was altered to produce a product of the same average OME chain length (3.59). This leads to a slightly different product composition ( $x_{\text{OME}_3} = 0.471$  g/g,  $x_{\text{OME}_4} = 0.373$  g/g,  $x_{\text{OME}_5} = 0.155$  g/g). However, these two products contain the same amount of carbon, require the same material amounts as feed and have the same LHV (18.9 MJ per kg [44]). Therefore, comparability of the OME syntheses and their upstream processes is achieved. Altering one process to produce exactly the same composition as the other is not advised, as the difference stems from different chemical systems in the respective routes having different reaction selectivities. The alternation would shift the process far from its optimal operating point.

Raw materials are pure water (assumed to be available), air and CO<sub>2</sub>. Regarding the CO<sub>2</sub>, three origins are studied: pure CO<sub>2</sub>, CO<sub>2</sub> in flue gases and CO<sub>2</sub> in air. No other products than OME<sub>3-5</sub> are produced in parallel. Thus, no other processes than the ones needed for OME production are considered for the integration of material or energy. The energetic analysis investigates only operational energy, not the energy for building the plants.



## 4.3 Methodology

### 4.3.1 Energetic efficiency

#### 4.3.1.1 Definition.

Since a fuel application is discussed, the energetic efficiency of a process is based on the lower heating values of its educts and products:

$$\eta_{\text{Process}} = \frac{\sum_{i \in \text{Products}} m_i \cdot LHV_i}{\sum_j Q_j + \sum_k W_k + \sum_{l \in \text{Educts}} m_l \cdot LHV_l} \quad (21)$$

where  $m_i$  and  $m_l$  denote the masses of product  $i$  and educt  $l$ .  $LHV_i$  and  $LHV_l$  are their specific lower heating values at 298 K.  $Q_j$  are the externally supplied heats in the process.  $W_k$  are the externally supplied electrical energies. The energetic efficiency is evaluated for single processes and several integrated processes. The water that is fed to the process chain is in liquid state. The vaporization of the input water is included in the electrical energy demand of the electrolysis.

#### 4.3.1.2 Maximum attainable energetic efficiency.

In a Power-to-Liquid or Power-to-Fuel (PtF) process,  $\text{CO}_2$  reacts with  $\text{H}_2$  that is produced by electrolysis. Assuming that a) the only external energy supply is the supply of electrical energy for the electrolysis of water (ideal process), and b) no electricity is generated in the fuel production process, the maximum attainable efficiency is given as follows:

$$\eta_{\text{Power-to-Fuel}}^{\text{max}} = \frac{m_{\text{Fuel}} \cdot LHV_{\text{Fuel}}}{W_{\text{Electrolysis}}} \quad (22)$$

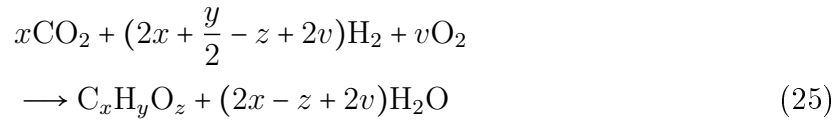
With

$$\eta_{\text{Electrolysis}} = \frac{m_{\text{H}_2} \cdot LHV_{\text{H}_2}}{W_{\text{Electrolysis}}} \quad (23)$$

follows:

$$\eta_{\text{Power-to-Fuel}}^{\text{max}} = \eta_{\text{Electrolysis}} \frac{m_{\text{Fuel}} \cdot LHV_{\text{Fuel}}}{m_{\text{H}_2} \cdot LHV_{\text{H}_2}} \quad (24)$$

The minimum amount of  $H_2$  to produce 1 mol of the fuel  $C_xH_yO_z$  while reducing  $v$  mol of oxygen is defined by the overall reaction stoichiometry:



Employing the molecular weight of the fuel,  $(12x + y + 16z)$  g per mol, and the one of  $H_2$ , 2 g per mol, it follows:

$$\eta_{\text{Power-to-Fuel}}^{\text{max}} = \eta_{\text{Electrolysis}} \cdot \frac{12x + y + 16z}{4x + y - 2z + 4v} \cdot \frac{LHV_{\text{Fuel}}}{LHV_{H_2}} \quad (26)$$

$\eta_{\text{Power-to-Fuel}}^{\text{max}}$  can only be achieved if all energy required in the fuel production (reaction heat, separation energy) is supplied by process-internal heat integration and no losses of intermediates occur.

The stoichiometric coefficients and the LHVs for the different e-fuels considered in the present work are given in Table 1.

**Table 1:** Lower heating values and stoichiometric coefficients used in Equation 25 for different e-fuels ( $C_xH_yO_z$ ). (II) and (III) denote MAL/ OME production using Reaction (II) (current FA technology) or Reaction (III) (selective dehydrogenation) for FA synthesis, respectively (cf. Table 2). For multiple references which differ in LHVs, mean values are taken. Fischer-Tropsch-diesel (FT) is assumed to consist only of multiple  $CH_2$  groups.

Fuel & Ref.	x	y	z	v	LHV /
					MJ per kg
$H_2$ [69, 70]	0	2	0	0	120.0
$CH_4$ [70]	1	4	0	0	50.0
DME [9, 71]	2	6	1	0	27.6
ME [69, 70, 72]	1	4	1	0	20.0
MAL(II) [65]	3	8	2	0.5	22.8
MAL(III) [65]	3	8	2	0	22.8
FT [69, 72]	n	2n	0	0	43.2
OME <sub>3-5</sub> (II) [44]	5.59	13.18	4.59	1.80	18.9
OME <sub>3-5</sub> (III) [44]	5.59	13.18	4.59	0	18.9

### 4.3.2 Studied routes and stoichiometry

Figure 2 shows the two Routes discussed in the present work, the direct Route A and the indirect Route B.

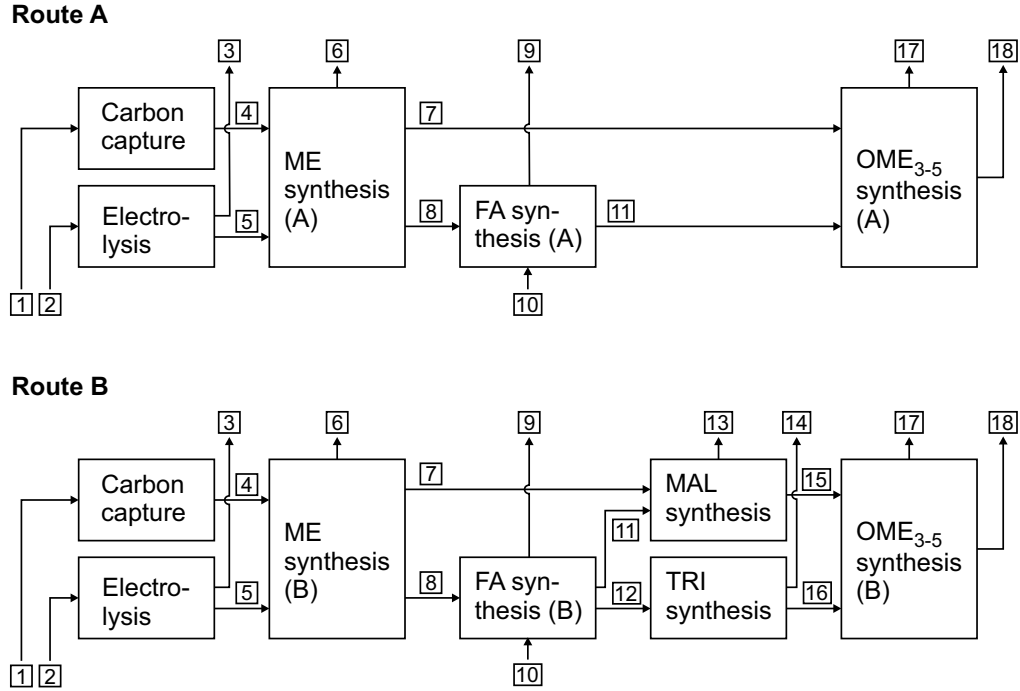


**Figure 2:** Studied routes for the production of OME<sub>3-5</sub> from CO<sub>2</sub> using electrical energy. Streams' main constituents: 1: Diluted CO<sub>2</sub>; 2, 6, 9, 13, 14, 17: WA; 3: O<sub>2</sub>; 4: CO<sub>2</sub>; 5: H<sub>2</sub>; 7, 8: ME; 10: Air; 11, 12: FA (aqueous); 15: MAL; 16: TRI; 18: OME<sub>3-5</sub>

The routes consist of several process steps. Note that the FA synthesis here combines FA production and concentration in one simplified step. In the following, both routes are analyzed in detail based on industrial processes for every step. Further stoichiometric material balances of both routes are calculated solely based on stoichiometry. In Table 2, Reactions (I)-(VII) show the stoichiometries that are used in the individual steps after CC and electrolysis.

For the FA synthesis, we consider two different technologies: Reaction (II) is closer to the state-of-the-art FA synthesis technology in which the produced H<sub>2</sub> is burned with oxygen to water [28]. Reaction (III) is the direct dehydrogenation of ME where the H<sub>2</sub> formed as a byproduct during dehydrogenation could be recycled. Thereby, it would decrease the electricity demand of the electrolysis [73–77]. For both Reactions (II) and (III), the overall stoichiometry of the entire route from CO<sub>2</sub> to OME<sub>n</sub> is given in Reactions (VIII) and (IX) of Table 2.

The overall stoichiometry is identical for both routes and provides idealized material balances with minimum educt demands.

**Table 2:** Reaction stoichiometry for the single processes of the OME<sub>3-5</sub> synthesis from CO<sub>2</sub> and H<sub>2</sub>

Process step / Reaction	Nr.
ME synthesis	
$\text{CO}_2 + 3\text{H}_2 \longrightarrow \text{CH}_3\text{OH} + \text{H}_2\text{O}$	(I)
FA synthesis (via partial oxidation)	
$\text{CH}_3\text{OH} + \frac{1}{2} \text{O}_2 \longrightarrow \text{CH}_2\text{O} + \text{H}_2\text{O}$	(II)
FA synthesis (via direct dehydrogenation)	
$\text{CH}_3\text{OH} \longrightarrow \text{CH}_2\text{O} + \text{H}_2$	(III)
MAL synthesis	
$2\text{CH}_3\text{OH} + \text{CH}_2\text{O} \longrightarrow \text{CH}_3\text{OCH}_2\text{OCH}_3 + \text{H}_2\text{O}$	(IV)
TRI synthesis	
$3\text{CH}_2\text{O} \longrightarrow (\text{CH}_2\text{O})_3$	(V)
OME <sub>n</sub> synthesis (via Route A)	
$2\text{CH}_3\text{OH} + n\text{CH}_2\text{O} \longrightarrow \text{CH}_3\text{O}(\text{CH}_2\text{O})_n\text{CH}_3 + \text{H}_2\text{O}$	(VI)
OME <sub>n</sub> synthesis (via Route B)	
$\text{CH}_3\text{OCH}_2\text{OCH}_3 + \frac{n-1}{3}(\text{CH}_2\text{O})_3 \longrightarrow \text{CH}_3\text{O}(\text{CH}_2\text{O})_n\text{CH}_3$	(VII)
CO <sub>2</sub> to OME <sub>n</sub> with FA synthesis via reaction (II)	
$(n+2) \text{CO}_2 + (3n+6) \text{H}_2 + \frac{n}{2} \text{O}_2 \longrightarrow \text{OME}_n + (2n+3) \text{H}_2\text{O}$	(VIII)
CO <sub>2</sub> to OME <sub>n</sub> with FA synthesis via reaction (III)	
$(n+2) \text{CO}_2 + (2n+6) \text{H}_2 \longrightarrow \text{OME}_n + (n+3) \text{H}_2\text{O}$	(IX)

### 4.3.3 Material balances of single processes including losses

In the following, every process is investigated in more detail including material losses. For this task, reference processes are selected from literature. The reference processes comprise standard process units (reactors, heat exchangers, distillation columns, compressors, etc.). Flowsheets, apparatus design and material streams between them are adopted from the original literature. In case the stream tables are not given in the original studies, they are derived from the available information in literature. All steps are scaled to provide exactly the amount of material required in the subsequent step. The selection of the reference processes and their modifications are described in more detail in Section 4.4.

### 4.3.4 Temperatures and enthalpies of process streams

If available, the temperatures of all process streams are taken from the original literature of the respective reference process. If not available, temperatures are chosen such that

feed and product streams of distillation columns are boiling liquids and streams entering and leaving reactors are at reaction temperature. The employed enthalpy model is described in Section 3.2.3, all property data is given in Appendix A.

### 4.3.5 Energy balances

If the heat and power duties of the equipment of a process are given in the respective literature and the process was not altered for the present work, the values of the heat duties are only scaled to the production of 1 kg of OME<sub>3-5</sub>. In cases where no heat and power duties are given or the process was altered, the heat and power duties were estimated based on the following assumptions.

- Pumps and compressors:

Preliminary calculations showed that work required for pumping liquids was negligible compared to other energetic contributions. Only the compression of gases in the ME and FA synthesis requires significant electrical power input. The work required for compression of gases is calculated for an isothermal compression of an ideal gas at 298 K.

- Distillation columns:

The condenser duty  $\dot{Q}_C$  of a column is estimated from the enthalpy of vaporization  $\Delta h_{v,i}(T)$  of the components of the top product, their mass flows  $\dot{m}_i$ , and the reflux ratio  $RR$ :

$$\dot{Q}_C = (RR + 1) \cdot \sum_{i=1}^K (\Delta h_{v,i}(T) \cdot \dot{m}_i) \quad (27)$$

The reboiler duty  $\dot{Q}_B$  is calculated via the energy balance of the whole column

$$\dot{Q}_B = \dot{H}_{\text{Bottom}} + \dot{H}_{\text{Top}} - \dot{H}_{\text{Feed}} - \dot{Q}_C \quad (28)$$

with  $\dot{H}_{\text{Bottom}}$ ,  $\dot{H}_{\text{Top}}$ ,  $\dot{H}_{\text{Feed}}$  being the enthalpy streams of bottom product, top product, and feed, respectively.

If there was no information on  $RR$  in the literature of the reference process, the reflux ratio was assumed to be 0.5.






















- Reactors and thin film evaporators (TFEs):

Heat input or output is calculated via the energy balance:

$$\dot{Q} = \dot{H}_{\text{out}} - \dot{H}_{\text{in}} \quad (29)$$

### 4.3.6 Heat integration

Heat integration is evaluated by pinch analysis [78, 79]. We chose a pinch temperature of  $\Delta T_{\text{pinch}} = 10$  K for all units [80]. Due to the high number of involved processes, there are many possible scenarios to perform inter-processual heat integration among them. Three scenarios S1-S3 are selected and illustrated in Figure 3.

	S1	S2	S3
Carbon capture			
Electrolysis			
ME synthesis			
FA synthesis			
TRI synthesis*			
MAL synthesis*			
OME <sub>3-5</sub> synthesis			

**Figure 3:** Considered scenarios for heat integration of Route A and B. \*: TRI and MAL synthesis only for Route B. The bars connect processes that are integrated.

In scenario S1, there is no heat integration between different processes but heat integration within single processes. Every process could be built at a different site. The output streams of all processes are cooled down to 298 K, and all input streams are heated up from 298 K to operating temperature.

In scenario S2, all processes up to the synthesis of ME are grouped and integrated – as well as all subsequent steps in a second group. ME is the only intermediate along the chain that is easy to transport: it is liquid and chemically stable. In scenario S2, the production of ME is moved locally to the place where cheap electricity for electrolysis and abundant CO<sub>2</sub> is available. The final synthesis of OME fuel from ME could be done somewhere else.

In scenario S3, heat integration among all processes is allowed. This requires all processes of the PtF route to be built in one single site and enables the maximum of inter-processual heat integration.

The temperatures of input and output streams of all integrated processes are matched. Heat losses between two subsequent processes are assumed to be negligible. In all scenarios, it is assumed that excess heat of  $T > 298$  K that cannot be utilized by heat integration is used to supply district heat or is removed by air cooling.

## 4.4 Process design and calculations

The flowsheets of all processes downstream of the ME synthesis are given in Figure 4 to 6. The process flow diagram of the ME synthesis itself is highly complex – an abstraction of it is given in Appendix B. To increase comprehensibility, pumps and compressors are not illustrated in the flowsheets if their corresponding energy demand is neglected. A detailed overview of all processes is given in Appendix B, comprising the following:

- Tables of material streams
- Tables of process heat duties (with corresponding temperature levels) and power duties

In total, we consider 18 different cases for the production of OME<sub>3-5</sub>, comprising of two different production Routes (A and B), three heat integration scenarios (S1-S3), and three different CC technologies.

### 4.4.1 Carbon capture

Three forms of carbon supply are considered: pure CO<sub>2</sub> from point sources (CPS) and two carbon capture processes, post-combustion capture (PCC) and direct air capture (DAC):

- In CPS, CO<sub>2</sub> is available at zero energy cost (source not defined).
- PCC describes the capture of CO<sub>2</sub> from flue gas. We consider amine scrubbing via mono-ethanol amine (MEA) as a PCC reference process. A regeneration temperature of 393 K and an absorption temperature of 313 K are assumed in accordance with the literature [81]. We further assume air cooling after regeneration. Hence, 3.33 MJ heat needs to be supplied at 393 K to capture one kg CO<sub>2</sub> with a purity of 99% [81].
- DAC describes the capture of CO<sub>2</sub> from air. As DAC reference, we chose the only commercially available technology in Europe from Climeworks AG. The total heat requirement for this process is 6.30 MJ supplied at 368 K to recover one kg CO<sub>2</sub> (purity 97%). The total electricity demand is 0.9 MJ per kg CO<sub>2</sub> [82–84].

Both chosen technologies show high Technology Readiness Levels (TRLs) of 9 for PCC and 7 for DAC [85]. For further energetic calculations, we assume that both processes provide pure CO<sub>2</sub>. A detailed overview on CC technologies can be found in Appendix B [85–89].

### 4.4.2 Electrolysis

We selected polymer electrolyte membrane electrolysis (PEMEL) as a reference process for our work because it can be operated with high flexibility and thus can deal with fluctuations of renewable energy supply [90]. Latest research states that 5.0 kWh of electrical energy is required for the production of 1 Nm<sup>3</sup> hydrogen via PEMEL [91]. This corresponds to an electrical energy demand of 200.2 MJ per kg H<sub>2</sub> and an energetic efficiency of  $\eta_{\text{PEMEL}}=60\%$ . Excess heat of 60.5 MJ per kg H<sub>2</sub> is removed during the process at low temperature (323-353 K) [92]. This excess heat is not utilized by heat integration in the present work.

Electrolysis efficiency highly depends on the used technology, the operation schedule, and the plant size. Therefore, we discuss our findings based on PEMEL also in the light of two other common technologies, the alkaline electrolysis (AEL) and the solid oxide electrolysis (SOEL). AEL efficiencies are in the range of PEMEL. SOEL offers higher efficiency potential but requires operation temperatures of over 1000 K. After shutting the SOEL cells down, they have to be heated up to operating temperature prior to restarting. This impedes an intermittent operation [73, 93].

### 4.4.3 ME synthesis

As a reference process for the ME synthesis from H<sub>2</sub> and CO<sub>2</sub>, we chose the heterogeneous catalysis process, which is commercially available [40, 94, 95]. We adopted a process from literature [40] in which the reactor is operated at 76 bar and 483 K. After the reactor, ME is purified by distillation. The list of heat duties, as well as the power duty for the feed compressor, are given in detail by the original paper [40], which already includes pinch analysis to optimize the process. The carbon yield is 94.1 %. The losses accrue in a combustible off-gas stream which has not been considered in the original work [40]. We have added a burner that burns the off-gas at 900 K. The released heat is used in heat integration.

### 4.4.4 FA synthesis and concentration

We selected the BASF silver process [28] as a reference process for our work, cf. Figure 4. Herein, gaseous ME is converted to FA in the presence of a silver catalyst. In the reactor, dehydrogenation of ME (Reaction (II), Table 2), as well as partial oxidation (Reaction (III), Table 2), happen in parallel, although the produced hydrogen is mostly oxidized with oxygen to water.



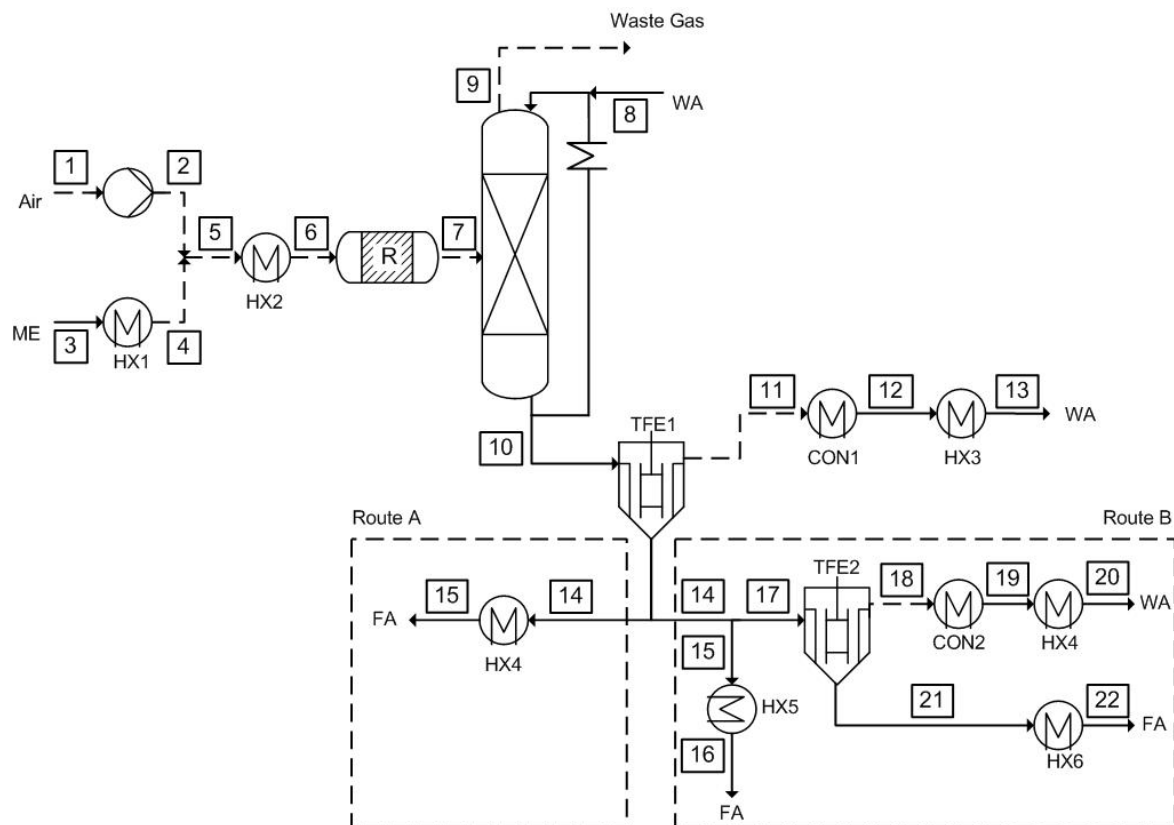


**Figure 4:** Process flow diagram (PFD) of the FA synthesis, Route A and B based on the BASF silver process [28].

The resulting mixture is fed to a packed absorption column. Since there is no material balance given in Reuss et al. [28], one is estimated based on the information given in the publication. Air is fed in stoichiometric rate based on Reaction (III), Table 2. The composition of the off-gas stream (9) is given in the original work [28]. We assume that it contains neither ME nor FA. The carbon yield is 89.5 %. For the calculation of temperature levels, a column pressure of 1.4 bar is assumed [96]. The concentration of FA yielded in the absorption column is 0.550 g/g [28].

Since the subsequent processes need higher FA concentrations than the reference process provides, an additional concentration step is required. We assumed that it is possible to remove pure water from FA solutions in a single step using pervaporation units or thin-film evaporators (TFEs). TFEs [57, 97] are commonly used to concentrate FA solutions and can provide solutions of various strengths. We added TFEs to increase the FA concentration (to 0.849 g/g for OME synthesis (Route A), 0.773 g/g for TRI synthesis (Route B), and 0.627 g/g for MAL synthesis (Route B)). Note that this is a simplifying assumption that is justified for evaluating the energetic efficiency of the

overall chain of OME production. This process step is investigated in more detail in Chapter 5.

#### 4.4.5 TRI synthesis

For the synthesis of TRI, there is only sparse open literature available. A pressure swing process for the TRI synthesis is selected as a reference for our work without modifications [41], cf. Figure 5.

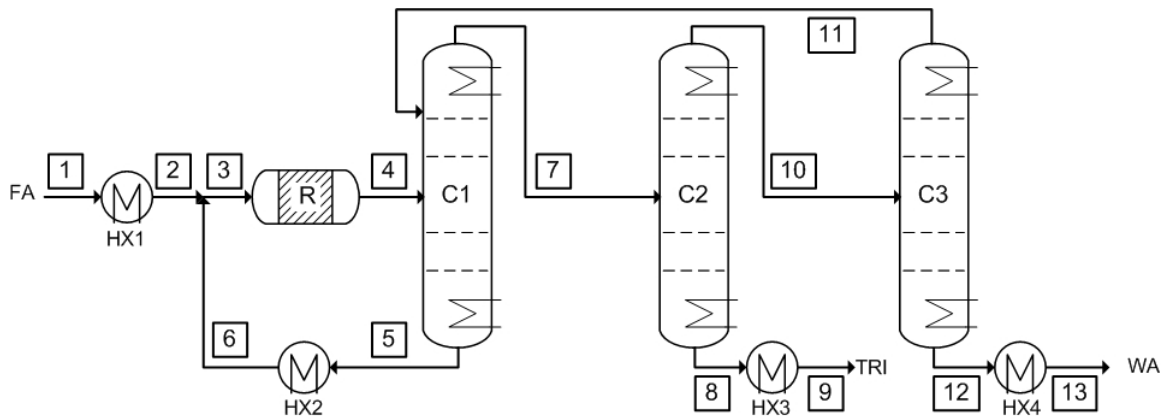


**Figure 5:** PFD of the TRI synthesis plant, based on Grützner et al. [41].

Pressures are adopted from the original work. The stream table is derived from the therein depicted ternary diagrams and PFD of the process; see Appendix B for details. The temperatures of the streams and the heat duties of the units are estimated as described in Section 4.3.4. The PFD of the TRI synthesis is depicted in Figure 5. The carbon yield of the process is 99.7 %.

#### 4.4.6 MAL synthesis

Figure 6 shows the PFD of the adopted reference process for the synthesis of MAL from ME and aqueous FA [62]. In contrast to the original work, the ME-rich stream (8) is recycled back to the reactor to avoid ME losses. Thereby, the composition of stream (6) is kept as given. Furthermore, we slightly altered the composition of the feed in order to correct minor inconsistencies in the material balance of the original process. The carbon yield of the process is 99.9 %.

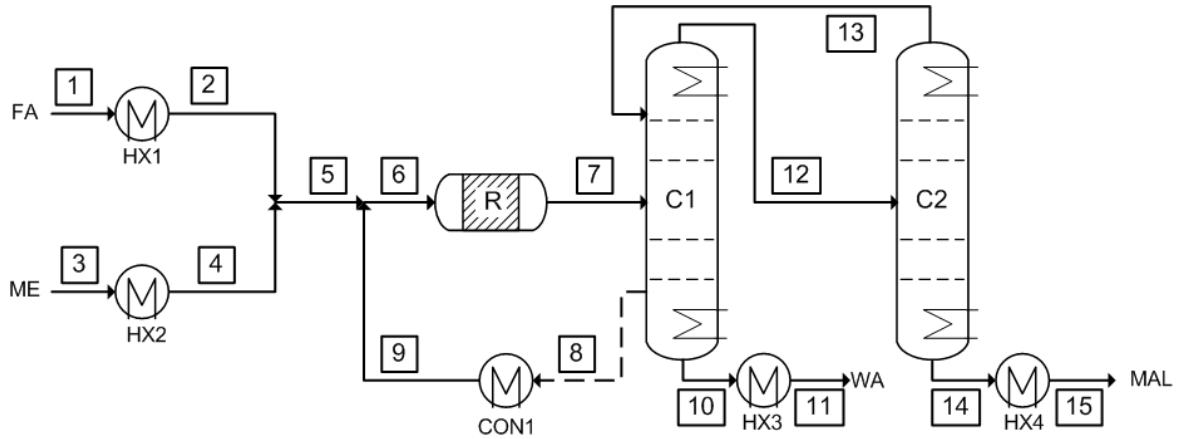


**Figure 6:** PFD of the MAL synthesis plant, based on Weidert et al. [62] and Drunsel et al. [42], modified by recycling of stream 8.

#### 4.4.7 OME<sub>3-5</sub> synthesis

Figure 7 shows the reference process adopted for the OME<sub>3-5</sub> synthesis via Route A [43] and B [44].

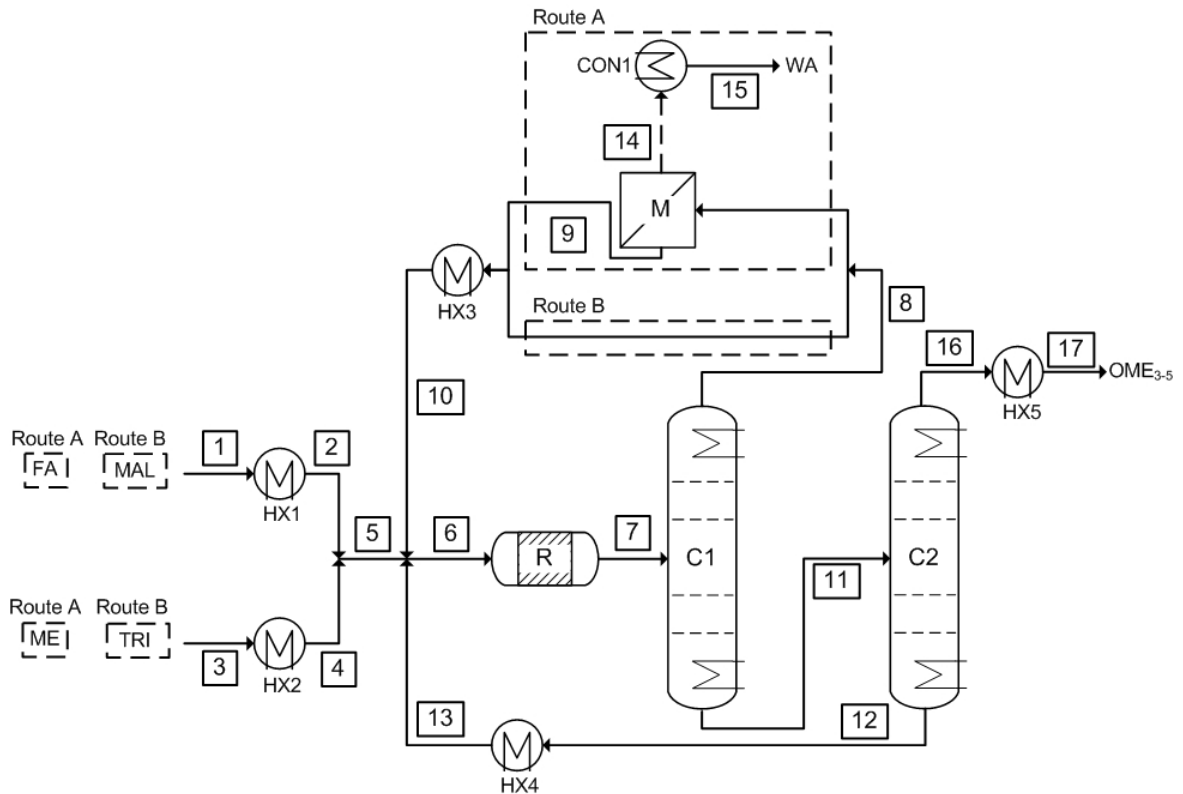


**Figure 7:** PFD of the OME<sub>3-5</sub> synthesis plant, Route A based on Schmitz et al. [43], Route B based on Burger et al. [44].

For Route A, the process has been validated in continuous lab-scale experiments [59, 98].

Since the membrane unit is not further specified in the original work for Route A [43], a concept for a pervaporation unit was designed based on similar processes [99, 100]. The pervaporation unit is composed of a membrane unit (M1) which separates water from the feed, a vacuum pump for the removal of inert gas (attached to M1, not displayed), a condenser (CON1), and a pump after CON1 (not displayed). To enable permeation of water, the absolute pressure on the permeate side is 0.032 bar, realized through the condensation of the permeate. The retentate cools down to provide the energy for evaporation. The retentate is then reheated up to reactor temperature by the heat exchanger (HX3). The carbon yield of the process is 100.0 %.

For Route B, the water-free OME<sub>3-5</sub> process [44] was adapted without major changes. The process flow diagram is identical to the one in Route A except that the pervaporation unit is not required due to a water-free process. In order to produce a product of the same average chain length as in Route A, the feed composition of the process is changed. TRI was added to increase the OME chain length of the product compared to the reference process. This affects not only product and feed compositions but also the recycling streams' mass flow rates. As a result, the heat duties of the columns change in comparison to the original process. The carbon yield of the process is 100.0 %.

## 4.5 Results

### 4.5.1 Material balance

#### 4.5.1.1 Material balance based on stoichiometry.

Table 3 shows the masses of educts and intermediates required to produce 1 kg of OME<sub>3-5</sub> in a stoichiometric process without losses if FA is produced by partial oxidation (Reaction (II), Table 2). The values are identical for Route A and B. For the stoichiometric production of 1 kg OME<sub>3-5</sub>, 1.600 kg CO<sub>2</sub> and 0.218 kg H<sub>2</sub> are required. 1.192 kg of water are formed as byproduct.

If FA is produced by selective dehydrogenation (Reaction (III), Table 2) and the hydrogen that is produced thereby is recycled to the ME synthesis, then the H<sub>2</sub> and the O<sub>2</sub> that are produced in the electrolysis and the side product WA are decreased by 0.047 kg H<sub>2</sub> (-21.4 %) per kg OME<sub>3-5</sub>, 0.374 kg O<sub>2</sub> (-21.4 %), and 0.420 kg WA (-35.2 %) respectively per kg OME<sub>3-5</sub>. Complete stream tables of the idealized processes based on stoichiometry are reported in Appendix B.

**Table 3:** Masses of inputs and intermediates required to produce 1 kg of OME<sub>3-5</sub>. Numbers of streams referring to Figure 2. \*: Route B exclusively

Stream	Component	Destination	Mass stream / kg per kg OME <sub>3-5</sub>
1	Diluted CO <sub>2</sub>	to CC	-
2	WA	to EL	1.965
3	O <sub>2</sub>	side product	1.746
4	CO <sub>2</sub>	to ME	1.600
5	H <sub>2</sub>	to ME	0.218
7	ME	to OME	0.417
8	ME	to FA	0.747
10	Air	to FA	-
11	FA	to OME	0.701
11*	FA	to MAL	0.195
12*	FA	to TRI	0.505
15*	MAL	to OME	0.495
16*	TRI	to OME	0.505
18	OME <sub>3-5</sub>	final product	1.000
Σ of 6, 9, 13*, 14*, 17	WA	side product	1.192

#### 4.5.1.2 Material balance based on reference processes.

When conversion losses are considered, the educt streams grow: 1.829 kg CO<sub>2</sub> (+14.2 %) and 0.250 kg H<sub>2</sub> (+14.5 %) are necessary for the production of 1 kg OME<sub>3-5</sub> via Route A. For Route B, the results are almost identical (1.833 kg CO<sub>2</sub> and 0.251 kg H<sub>2</sub>). 66 % of the hydrogen produced in the electrolysis is lost in the process chain. This hydrogen loss is mainly due to the formation of water in several process steps (ME, FA, MAL, OME<sub>3-5</sub> synthesis). The loss of carbon is only 13 %.

As there is currently no FA production process solely based on Reaction (III), a material balance based on a reference process is not available. However, the potential benefits through direct dehydrogenation are discussed later in Section 4.6.1. Complete stream tables including losses are given in Appendix B.

#### 4.5.2 Energy Balance

Lists of heat and power duties of the units in all processes are given in Appendix B, normalized to the production of 1 kg OME<sub>3-5</sub>. The composite curves of all pinch analyses,

as well as the values of the remaining external heat demands after heat integration, are shown in Appendix B. The remaining heat demands that have to be supplied for each process are shown graphically in Figure 8. This includes thermal as well as electrical energy, while the latter is highlighted by cross-hatched marking. Scenarios S1-S3 are illustrated for both Routes A and B. Furthermore, the results are differentiated with respect to the used CC technology (CPS, PCC, DAC).

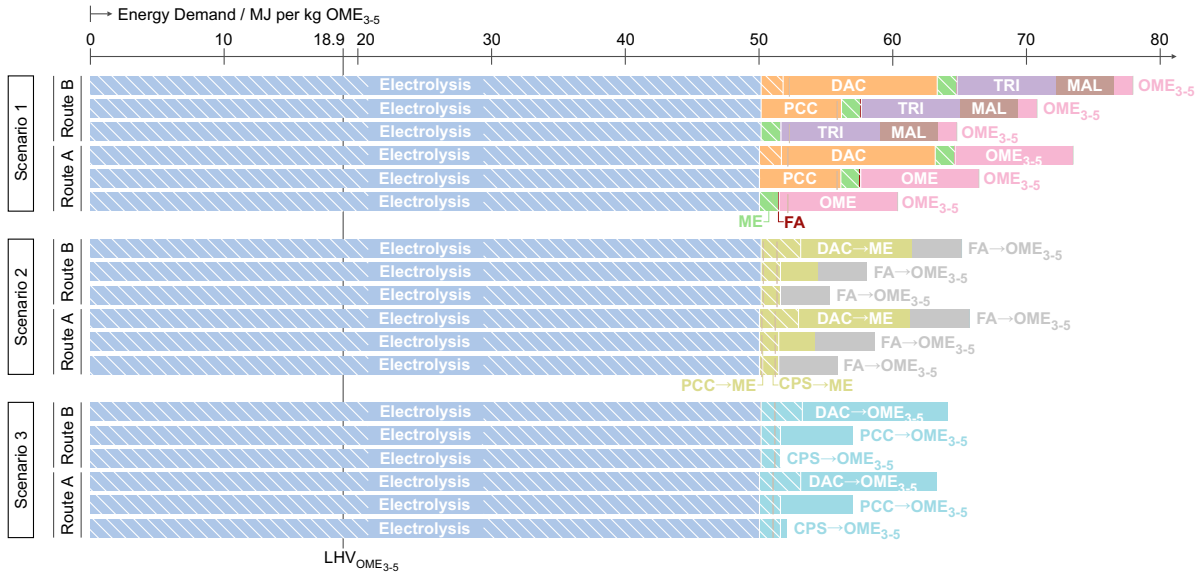


**Figure 8:** Proportionate energy demand share of single process steps of  $\text{OME}_{3.5}$  production, in MJ per kg  $\text{OME}_{3.5}$ . Electrical energy is shown in cross-hatched bars, thermal energy is shown in filled bars.

For all 18 cases, the overall energy demand varies between 51.6 MJ (Route B, CPS, S3) and 78.0 MJ (Route B, DAC, S1) per kg  $\text{OME}_{3.5}$ . The share of electrical energy of the total energy demand varies from 68.3 % (Route B, DAC, S1) to 100.0 % (Route B, CPS, S3). For scenarios S2 and S3, the heat demand can be reduced significantly compared to S1. While in Route B, the sum of all heat demands is higher than in Route A; it has more potential for inter-processual heat integration.

In all cases, the electrolysis has by far the largest share of the energy demand. Roughly 50 MJ of electrical energy is required to operate the electrolysis. Additional demands in electrical energy arise from the ME and FA synthesis (with 1.4 and 0.04 MJ) and DAC (with 1.6 MJ) for all routes and scenarios. Hence, the electrolysis has a share of 94.2 to 97.2 % of the total electrical energy demand. To quantify the contribution of the individual processes to the total energy demand, the findings of scenario S1 are described in more detail in the following. Subsequently, the effect of heat integration is illustrated considering scenarios S2 and S3.

#### 4.5.2.1 Contribution of individual processes to the total energy demand (Scenario S1).

As we assumed zero energy costs for the integration of CO<sub>2</sub> from CPS, this case allows for a discussion of the results from a PtF perspective where the capture of CO<sub>2</sub> is neglected. However, we also show the results for the integration of CC technologies into the PtF process chain.

When providing CO<sub>2</sub> via CPS at zero energy cost, the production of 1 kg OME<sub>3-5</sub> requires 8.9 MJ of heat for Route A and 13.2 MJ for Route B. In Route A, the external heat demand stems only from the OME<sub>3-5</sub> synthesis. The other processes do not require additional heat. In Route B, the OME<sub>3-5</sub> synthesis requires only 1.4 MJ of heat, as it starts from the intermediates MAL and TRI. However, their synthesis over-compensates that with a total heat demand of 11.8 MJ. In both routes, the ME and FA synthesis cause only 2.2 % and 0.1 % of the total energy demand, all of it in the form of electrical energy for the compression of gases.

When using PCC or DAC to provide CO<sub>2</sub>, the energy demand is increased. As both Routes A and B need virtually the same amount of CO<sub>2</sub>, the capture of CO<sub>2</sub> requires the same amount of energy for both routes. For scenario S1, CC via PCC leads to a roughly 6 MJ (+10 %) larger thermal energy demand for both routes while the electrical energy demand stays constant. CC via DAC leads to an increased demand of electrical energy of roughly 1.6 MJ (+3 %) and thermal energy demand of 11.5 MJ (+18 %).

#### 4.5.2.2 Effect of heat integration (Scenarios S2 and S3).

The high level of inter-processual heat integration leads to significantly reduced heat demands for both routes compared to scenario S1. The difference between Route A and B is quite small in these scenarios. In scenario S2 and S3, the excess heat from the ME and FA synthesis is used in the downstream processes (MAL, TRI, and OME<sub>3-5</sub>). Compared to scenario S1, the heat demand is reduced significantly: In scenario S2, the remaining heat demand is 4.4 MJ for Route A and 3.7 MJ for Route B. In scenario S3, the remaining heat demand is 0.6 MJ for Route A and 0.0 MJ for Route B. Although the excess heat of the ME and FA synthesis can be integrated into other processes, the conversion of chemically bound energy (hydrogen) in these processes to thermal energy is thermodynamically disadvantageous. The hydrogen was produced by electrical energy beforehand, in a rather energy-inefficient electrolysis process.

When PCC is used, its heat demand is partly covered in scenario S2 by excess heat of the ME synthesis, and 2.8 MJ heat has to be supplied externally. In scenario S3, the

excess heat of the ME synthesis is also needed in the OME<sub>3-5</sub> synthesis. Hence, the heat demand for PCC is only partially covered. A remainder of 5.4 MJ for Route A and 5.5 MJ for Route B has to be supplied externally for PCC.

The supply of CO<sub>2</sub> via DAC sets an additional heat demand of 11.5 MJ per kg OME<sub>3-5</sub> which is in no case covered by heat integration. It is only partly compensated in scenario S2 (reduced to 8.2 MJ for both routes) and very slightly reduced in scenario S3 (to 9.6 MJ for Route A and to 10.8 MJ for Route B).

The temperature level of the heat required for the PCC and DAC process is comparably low. Integrating the high temperature excess heat of the FA or ME synthesis to cover this demand would be possible but thermodynamically disadvantageous.

### 4.5.3 Energetic efficiency

The energetic efficiency as defined in Equation 21 is calculated for all 18 cases from the data of Figure 8. The results are shown in Figure 9. The filled symbols show the

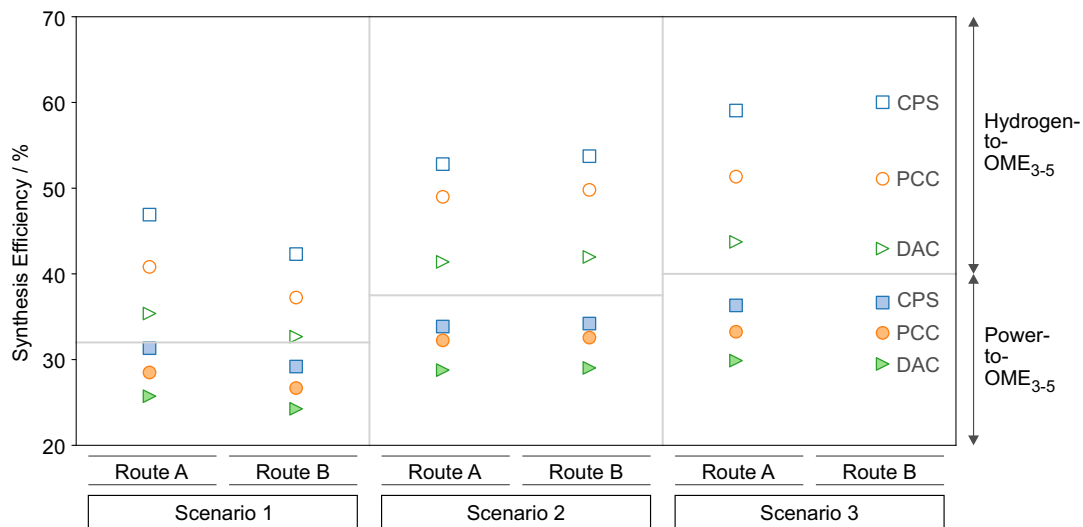


**Figure 9:** LHV-based energetic efficiency of OME<sub>3-5</sub> production from electrical energy and CO<sub>2</sub> (Power-to-OME<sub>3-5</sub>) and from H<sub>2</sub> and CO<sub>2</sub> (Hydrogen-to-OME<sub>3-5</sub>). The Power-to-OME<sub>3-5</sub> efficiencies are based on an electrolysis efficiency of 60 %.

efficiency starting from electrical energy to the LHV of OME<sub>3-5</sub> (Power-to-OME<sub>3-5</sub>). The open symbols do leave out the electrolysis ( $\eta_{\text{Electrolysis}} = 60\%$ ) and show the efficiencies starting from the LHV of hydrogen to the LHV of OME<sub>3-5</sub> (Hydrogen-to-OME<sub>3-5</sub>). The use of heat integration leads to a significant efficiency increase. For scenario S3, this results in efficiencies of up to 36 % for Power-to-OME<sub>3-5</sub> and up to 59 % for Hydrogen-to-OME<sub>3-5</sub>. For Route B, the results are similar.



As the supply of CO<sub>2</sub> via CPS is assumed to have no energy demand at all, this source leads to the highest efficiencies of all carbon capture variants. The supply of CO<sub>2</sub> via PCC has a small negative effect on the efficiency in scenarios S1 and S3, resulting in efficiency drops of about three percentage points. In scenario S2, the additional heat demand is partly covered by excess heat from the ME synthesis; therefore, there is only a small effect on the efficiency when compared to CPS (about 1.5 percentage points). The supply of CO<sub>2</sub> through DAC leads to drastically lower efficiencies (between 24.3 % to 29.9 % Power-to-OME<sub>3-5</sub>) for both routes and all heat integration scenarios.

## 4.6 Discussion

### 4.6.1 Material balance

#### 4.6.1.1 Hydrogen balance.

In the stoichiometric material balance with FA synthesis via partial oxidation (via dehydrogenation), both routes need 2.54 (2.00) times as much H<sub>2</sub> than is actually present in the OME product. 60.7 % (40.9 %) of the total H<sub>2</sub> input are lost during the process chain. The huge losses in H<sub>2</sub> result mainly from the formation of water in the ME, FA, and OME synthesis. If direct dehydrogenation of ME to FA (Reaction (III)) could be applied, 0.047 kg of H<sub>2</sub> per kg OME<sub>3-5</sub> could be saved through recycling. This corresponds to 35.5 % of the overall H<sub>2</sub> losses. The remaining 64.5 % can hardly be avoided. They are needed as a reduction agent for the CO<sub>2</sub> to produce ME and oxidize to water that accrues either directly in the ME synthesis or later as a side-product of the etherification of ME to OME, cf. Reaction (IX).

If we could implement the direct dehydrogenation of FA and recycle the H<sub>2</sub>, the power demand in the electrolysis would drop by 9.4 MJ per kg of OME<sub>3-5</sub>. At first sight, this sounds promising. However, one must be aware that the new FA synthesis would be an endothermic process that does not provide excess heat. The current excess heat of 5.6 MJ per kg of OME<sub>3-5</sub> is used for heat integration in scenarios S2 and S3 and would have to be provided by other means. Additionally, it would lead to a heat demand for the endothermic reactor of the FA synthesis. This would deplete a large part of the gained energy savings but might still be favorable because providing heat is thermodynamically more attractive than providing electrical energy.

On top of these stoichiometric considerations, 15 % additional H<sub>2</sub> is currently lost and burnt in off-gases in the ME and FA synthesis. This bears some potential for optimization.

#### 4.6.1.2 Carbon balance.

In the stoichiometric material balance, there are no losses of carbon. However, the reference processes via both routes require approximately 15 % more carbon ( $\text{CO}_2$ ) than for stoichiometry. The carbon is primarily lost in the FA synthesis. For e-fuels, the  $\text{CO}_2$  neutrality is crucial. Two aspects need to be considered: a) The electrical energy should be produced  $\text{CO}_2$ -neutral. However, it is beyond the scope of the present work to discuss the electrical energy supply of the future. b) The carbon intensity of the  $\text{CO}_2$  supply should be close to zero. This is given when CC technologies are operated with renewable energy. Further, the captured  $\text{CO}_2$  should stem from the atmosphere (DAC) or from a source where it would have been emitted to the atmosphere when not captured, e.g., PCC from flue gases.

DAC has the advantage of being location-wise independent of other industries. However, it has a high energy demand. If  $\text{CO}_2$ -containing flue gases are available near the PtF plant, PCC outperforms DAC in terms of energetic efficiency. Assuming that CPS provides  $\text{CO}_2$  at zero energy cost, this would be even better.

#### 4.6.1.3 Side products and waste.

The main side products in the production of  $\text{OME}_{3-5}$  are  $\text{CO}_2$  and water. No other significant wastes are produced. Both routes rely on the same processes for ME and FA production. Further, the formation of  $\text{OME}_{3-5}$  leads to the same amount of produced water for both routes. Therefore the amount of side products is the same for both routes, 0.235 kg  $\text{CO}_2$  and 1.536 kg water per kg  $\text{OME}_{3-5}$ . Whether the water needs further purification to remove traces of impurities depends on the concrete implementation and operating conditions of the unit utilized for water removal in each process. These topics are beyond the scope of the present work.

### 4.6.2 Energetic efficiency in the context of other e-fuels

The energetic efficiency of the production of  $\text{OME}_{3-5}$  is compared to the production of other e-fuels in Figure 10, i.e. methane ( $\text{CH}_4$ ), dimethyl ether (DME), methanol (ME), methylal (MAL) and Fischer-Tropsch diesel (FT). The left panel illustrates the maximum energetic efficiency according to Equation 26, based on the stoichiometric coefficients of Table 1. They range between  $(0.72 \text{ to } 0.92) \cdot \eta_{\text{EL}}$ , where the coefficients (0.72 to 0.92) describe the  $\text{H}_2$ -to-Fuel (HtF) efficiencies.

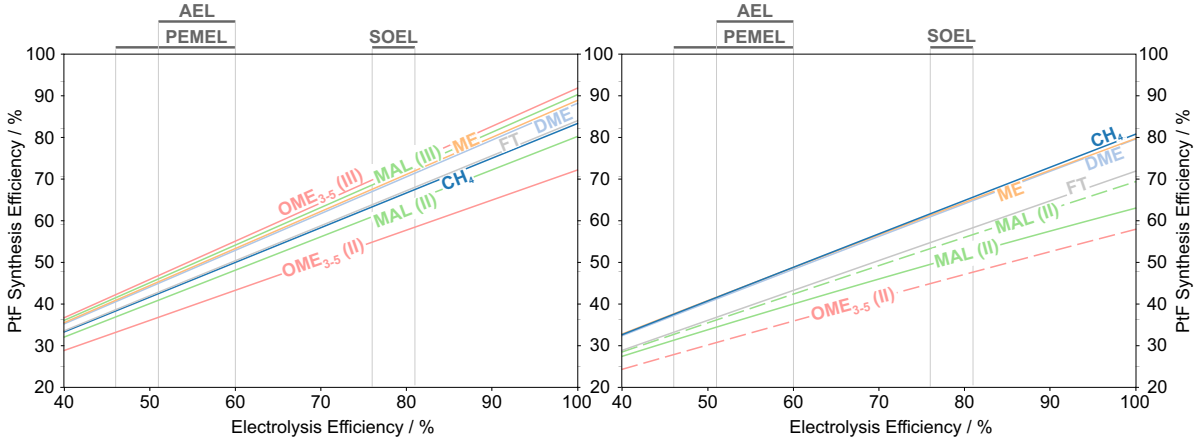


**Figure 10:** Left panel: Maximum attainable energetic efficiency for the production of different e-fuels as a function of the energetic efficiency of the electrolysis. Indicated ranges for the efficiencies of AEL (51-60 %), PEMEL (46-60 %), SOEL (76-81 %) are from existing plants [91]. These values are in good alignment with the efficiencies given in Detz et al. [101] (AEL: 63 %, PEMEL: 56 %, SOEL: 68 %) and Shaner et al. [102] (PEMEL: 61 %). Curves are displayed for CH<sub>4</sub>, DME, ME, MAL, FT fuel  $-(\text{CH}_2)_n$  and OME<sub>3-5</sub>. For MAL and OME<sub>3-5</sub>, (II) indicates the production via the current FA technology (Reaction (II)) and (III) via selective dehydrogenation as FA technology (Reaction (III)). Underlying LHVs are listed in Table 1. Right panel: Literature based PtF synthesis efficiencies of the same e-fuels. For OME<sub>3-5</sub> and intermediates of the OME<sub>3-5</sub> production (ME, MAL), dashed lines indicate own calculations. In these cases, we assumed that CO<sub>2</sub> is available for free and that maximum heat integration is achieved (cf. scenario S3). Solid lines are computed via data given in literature (CH<sub>4</sub>[103], DME[104], ME[40], MAL[36], FT[105]).

If required FA is provided via partial oxidation of ME, we get the following values for HtF efficiencies: 0.83 for CH<sub>4</sub>, 0.88 for DME, 0.89 for ME, 0.80 for MAL, 0.84 for FT and 0.72 for OME<sub>3-5</sub>. Here ME shows the highest efficiency. However, if FA for the production of MAL or OME<sub>3-5</sub> could be provided via direct dehydrogenation of ME, their production efficiency could even surpass the one of ME, with HtF efficiencies of 0.90 for MAL and 0.92 for OME<sub>3-5</sub>. These efficiency improvements through direct dehydrogenation were already pointed out by Ouda et al. [67]

Besides the rather theoretical maximum attainable energetic efficiency, we compare OME<sub>3-5</sub> as well with the other e-fuels considering real processes, including conversion losses. However, the efficiencies of other PtF processes from literature are often not comparable for a number of reasons. First, a variety of different efficiency definitions results from different system boundaries. In particular, there is no consensus on (i) whether to use the LHV or the HHV efficiency [70], (ii) to which extent heat integration is applied [106], (iii) whether material or heat from other processes is included [107–109],

and (iv) whether the CO<sub>2</sub> supply is considered [110, 111]. Second, the PtF efficiency strongly depends on the efficiency of the electrolysis. We consider only literature studies having the following boundaries: no utilization of waste heat to generate electricity, no integration of material and heat from processes outside the PtF process chain, the efficiency of the electrolysis is known, efficiency definition allows the derivation of comparable LHV-based efficiency, and energy demand of CC is excluded.

To compare the production process over a range of potential energetic efficiencies of the electrolysis, we define the PtF efficiency conditional on the electrolysis efficiency as follows:

$$\eta_{\text{Power-to-Fuel}} = f(\eta_{\text{Electrolysis}}) \quad (30)$$

By applying Equation 21 to the entire PtF process chain and isolating the electrical work of the electrolysis from the other energy demand, we get:

$$\eta_{\text{Power-to-Fuel}} = \frac{m_{\text{Fuel}} \cdot LHV_{\text{Fuel}}}{W_{\text{Electrolysis}} + \sum_j Q_j + \sum_{k \neq \text{Electrolysis}} W_k} \quad (31)$$

Inserting Equation 23 yields the desired function:

$$\eta_{\text{Power-to-Fuel}} = \frac{m_{\text{Fuel}} \cdot LHV_{\text{Fuel}}}{\frac{m_{\text{H}_2} LHV_{\text{H}_2}}{\eta_{\text{Electrolysis}}} + \sum_j Q_j + \sum_{k \neq \text{Electrolysis}} W_k} \quad (32)$$

While  $\eta_{\text{Electrolysis}}$  may vary, all other terms on the right-hand side of Equation 32 are considered as constant and taken from the literature. The results for all considered PtF processes are shown in the right panel of Figure 10 as solid lines. For OME<sub>3-5</sub>, the case of CPS, Route A, scenario S3 is selected. As ME and MAL are intermediates in the OME<sub>3-5</sub> production, their production efficiency can be calculated from the data and assumptions used to calculate the Power-to-OME<sub>3-5</sub> efficiency. To achieve this, the respective processes are scaled to produce only the desired product, and pinch analysis is used to determine the heat demand for maximum heat integration (analogously to scenario S3). These values calculated in the present work (ME, MAL, OME<sub>3-5</sub>) are illustrated as dashed lines. For the reference electrolysis efficiency of 60 %, we get the following PtF efficiencies: 48.8 % for CH<sub>4</sub>, 48.4 % for DME, 48.8 % for ME, 40.0 % [36]/ 42.4 % (own value) for MAL, 43.3 % for FT, and 36.3 % for OME<sub>3-5</sub>.

CH<sub>4</sub>, DME, and ME show already efficiencies close to the maximum attainable ones. They are small molecules that are produced with high selectivity in the respective processes. On the other end, there are MAL, FT, and OME<sub>3-5</sub> which are larger molecules requiring either multiple transformation steps (OME<sub>3-5</sub> and MAL) or have reduced prod-

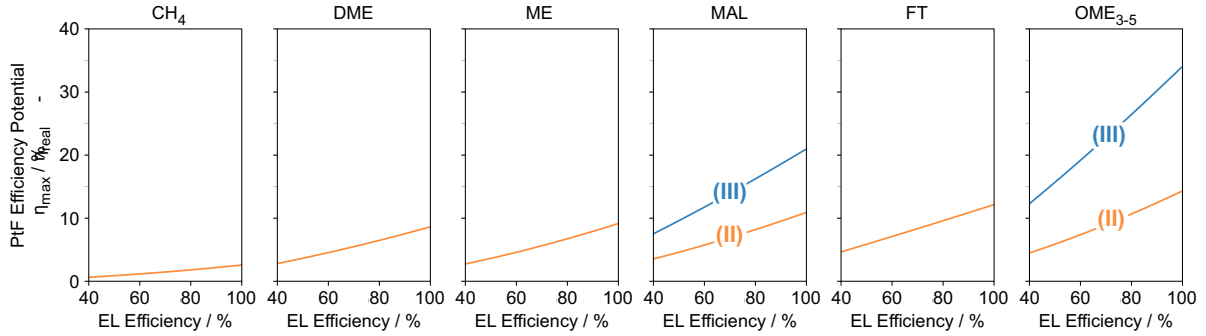


**Figure 11:** Difference between the stoichiometric efficiencies (left panel of Figure 10) and the efficiencies of real processes (right panel of Figure 10) for the considered e-fuels. For MAL and OME<sub>3-5</sub>, the investigated production process is compared to the stoichiometric process via partial oxidation (II) and direct dehydrogenation of ME to FA (III). For OME<sub>3-5</sub>, the efficiency calculated in the present work is used for this comparison (Route A, scenario S3, CO<sub>2</sub> via CPS), for all other e-fuels curves are relying on processes from literature.

uct selectivity due to byproducts (FT). The difference between the MAL efficiency from literature [36] and our calculation is due to different assumptions on the ME production technology. To cross-check the validity of our findings, we compared the HtF efficiencies of all e-fuels (for electrolysis efficiency of 100 % in the right panel of Figure 10) with further values from literature (where only the HtF efficiencies were stated – no detailed process data to include them into Figure 10). For CH<sub>4</sub>, our HtF efficiency of 80.8 % is in good alignment with the value from literature (80.0 % [106]). The same holds for DME (79.6 % vs. 82.4 % [72]), ME (79.7 % vs. 79.7 % [72]) and FT (71.9 % vs. 69.3 % [72]). Our results for the energetic efficiency of MAL and OME<sub>3-5</sub> production have also been confirmed by subsequently published studies [112–114].

A measure for the research and development potential of each e-fuel is given by its deviation from the stoichiometric (ideal) process, which sets the thermodynamic limit for each e-fuel. Therefore, we illustrate the difference between the stoichiometric efficiencies (left panel of Figure 10) and the efficiencies of real processes (right panel of Figure 10) in Figure 11. While CH<sub>4</sub> production is already very close to its maximal production efficiency, the other e-fuels fall short up to 8.6 (DME) and 14.2 percentage points (OME<sub>3-5</sub>), for an electrolysis efficiency of 100 %. If direct dehydrogenation could be applied, MAL and OME<sub>3-5</sub> show even more potential, with a deviation of 27.2 (MAL) and 33.9 percentage points (OME<sub>3-5</sub>) from their maxima (for an electrolysis efficiency of 100 %).

Both Figure 10 and Figure 11 show the high influence of the electrolysis efficiency on the overall efficiency.

### 4.6.3 Limitations and assumptions

The present work uses idealizing assumptions that lead to rather optimistic efficiencies: Only the main units of the processes have been considered – auxiliary processes such as wastewater and waste gas treatment have not been included. Although many PCC units already contain units for removal of  $\text{NO}_x$ ,  $\text{SO}_x$ , and particles [115], additional gas cleaning of the  $\text{CO}_2$  might be necessary. These steps would add an additional energy demand that has not been investigated. The assumed pinch temperature of 10 K is possibly not suitable for all heat exchangers. Heat losses of the plants have been neglected. Additionally, the assumption of a reflux ratio of 0.5 is not necessarily correct for all columns. A detailed analysis of the reflux ratio is beyond the scope of this chapter’s analysis, but the reflux ratio significantly influences the energy balance of a column.

On the other hand, most individual processes from the literature were not optimized for OME production. The process chain is considered stand-alone. Improvements of the energetic efficiency could be obtained by various measures: The OME production processes could be integrated into other sites like refineries, power plants, or steel mills. Heat integration for single processes could be improved if process conditions such as pressures in distillation columns were altered. Further, the individual processes might be integrated with each other on a material basis – e.g., the oxygen produced in the electrolysis could be used in the FA synthesis instead of air. All the above is related to substantial research and development efforts and should be addressed in future work. For heat integration, the number of heat exchangers has not been limited. In practice, the corresponding investment will only be taken for the most significant streams. Optimizing only the energetic efficiency leads to a large heat exchanger network without considering the respective investment.

### 4.6.4 Other objectives beside energetic efficiency

Chemical process design is a multi-objective problem [116], as is the selection of an e-fuel. Focussing solely on maximizing the energetic efficiency is not advisable. Both the capital expenditure (CAPEX) to build an  $\text{OME}_{3.5}$  production plant and the operational expenditure (OPEX) during its operation have so far not been considered. However, CAPEX and OPEX should be optimized together with the energetic efficiency and other aspects. Comparing Route A and B, Route A is expected to have a significantly lower CAPEX because two processes are skipped.

Assessments of the production costs of multiple e-fuels have been done recently by Brynolf et al. [90], Detz et al. [101], and other studies (ME[117–119], FT[120], OME[47]),

and the production cost of OME in particular is investigated in Chapter 6.

For a life cycle assessment of OME production, energy demands for logistics, fuel storage, and construction of all synthesis plants should be included [106].

When comparing different e-fuels, other factors should be considered as well, e.g., application-related criteria like the toxicity, the combustion emissions, and the cost of storage and handling of the fuel. Whether the non-toxicity, the sootless combustion [1, 2, 4–7, 20], cheap storage and smooth integration into existing fuel logistics and infrastructure [6, 7] of OME<sub>3-5</sub> justify a lower energetic efficiency compared to other fuels, has to be assessed in concrete application scenarios.

When comparing e-fuel operated ICE vehicles with battery electric vehicles (BEVs), a sound technology assessment should consider cradle-to-cradle greenhouse gas (GHG) emissions, costs for charging/ fueling infrastructure, and customer-related criteria like total costs of ownership (TCO) and technology acceptance (e.g., range or second-hand market prices).





# 5 Novel process for the provision of methanolic formaldehyde solutions

## 5.1 State of the art

The following chapter presents a novel process for the provision of methanolic formaldehyde solutions of low water content. These solutions are required to produce OME [29, 121] and many other products, e.g., various specialty resins and coatings and whenever water hinders the formation of formaldehyde reaction products [122]. In contrast to the commonly traded aqueous FA solution, it is crucial that the water content in this methanolic FA solution is as low as possible, as water shifts the chemical equilibrium in the OME reactor to the educts and inhibits OME formation [29, 121]. However, they are difficult to produce in large amounts; there is always water formed as a by-product in FA production, and FA reacts with both methanol and water. These Reactions (7) to (12) occur fast and without the presence of catalysts [55]. Both  $MG_n$  and  $HF_n$  are present in various chain lengths, resulting in a complex, i.e., reactive, phase behavior of FA solutions in thermal separations. Very high FA concentrations usually lead to solid precipitation of long-chained MG/HF, complicating processing and storage even further [123, 124]. It is possible to obtain ME-free aqueous FA solutions by removing excess ME from FA, WA, ME solutions via distillation. However, removal of water with conventional distillation is limited due to the azeotropes that WA forms with FA [125]. While there is no scientific literature that describes processes to produce methanolic formaldehyde solution, there are several patents on respective process concepts. To obtain methanolic FA solutions from WA, FA, ME solutions without producing other FA products, there are generally two strategies: (a) isolation of pure FA followed by dissolution or absorption in ME, or (b) selective water removal.

For possibility (a), some patents [61, 126] suggest using extractive distillation or extraction to produce pure gaseous formaldehyde, which could be absorbed in methanol. Another option is the production of paraformaldehyde and its subsequent dissolution in methanol. In the industrial production of paraformaldehyde, an aqueous solution from an FA plant (0.5 g/g FA) is usually concentrated in a combination of distillation,

fall-film evaporation, and thin-film evaporation up to 0.9 g/g FA [56, 57]. Afterward, the solution is usually dried in a prilling tower to produce solid paraformaldehyde [127]. For the production of methanolic FA solution, the production of paraformaldehyde has the disadvantage of solid handling. Therefore, the question arises of whether the drying step leading to the solid can be omitted. Besides physical separation, FA can also be isolated by a reversible chemical conversion to trioxane or methylal [41, 62]. These are separated from water and used as an FA substitute or as an FA carrier, cf. OME production Route B.

For possibility (b), the selective removal of water, membrane processes like pervaporation have been suggested by several patents for various FA-containing mixtures [60, 128]. The viability of this concept has been experimentally demonstrated for removing small amounts of water in an OME production process [59]. Similarly, adsorption has been suggested and tested [129]. Multiple patents suggest using evaporation or condensation with a short residence time to produce methanolic FA solution. This can be done in columns [130], thin-film evaporators (TFEs) [58, 97], or through fast cooling [131]. However, all of these processes produce aqueous FA as side products. While the use of thin-film evaporators is well established for the production of short-term stable, highly concentrated aqueous FA solutions in the industry [57, 58, 97], it has rarely been investigated in scientific literature. Mantei et al. [10] suggest a process using two TFEs in series to provide FA solutions for OME production. However, they considered the TFEs as idealized splitters, and there is no formaldehyde recovery, leading to FA losses of 8% in the effluent water. Recent studies on TFEs have investigated their wetting behavior and heat transfer [132], the influence of wiper type, speed, and liquid viscosity [133], or modeled the complex fluid dynamics in the unit [134]. However, the FA concentration in TFEs has barely been investigated scientifically. As notable exception, Schilling et al. [135] modeled the concentration of FA solutions in TFEs using a stage model with phase equilibrium and reaction kinetics in the liquid phase.

Employing such a model to design and optimize the whole process can significantly improve the achieved performance of processes for the provision of methanolic FA solution via thin-film evaporation. Such an optimization has to consider multiple conflicting objectives, and an efficient way to deal with these is multi-criteria optimization (MCO) or Pareto optimization. MCO is used to find the set of all best compromises between objectives without weighing them, and it has been applied widely in chemical and process engineering [116, 136, 137]. In the present work, the  $\epsilon$ -constraint method as presented by Haimes et al. [138] is employed. It minimizes the most important objective while all others are limited by constraints. A systematic variation of the constraints gives the complete set of all Pareto optimal solutions [139].

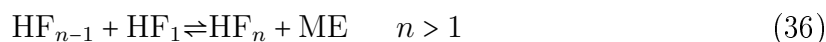
The following chapter presents the conceptual design of a process to produce methanolic FA solution with high yield, i.e., no other FA products or carbon losses and low water content in the product. High yields are essential if the methanolic FA solutions are intended for large-scale OME production. Solid formation, additives, and selective agents/materials (e.g., for adsorption/membrane) are avoided. The process combines thin-film evaporation and distillation and can be added to formaldehyde plants with complete or incomplete conversion of methanol. Literature models for fluid properties and apparatuses are implemented into a process simulator. Apparatus design and operating parameters are optimized using multiple (competing) objectives: energy demand in all units, residual product water content, and unit sizes.

## 5.2 Methodology

The presented process for the provision of methanolic FA solutions relies on a combination of distillation and thin-film evaporation to remove pure water (0.997 g/g) from FA solutions, cf. Section 5.2.4 for a detailed process description. The thin-film evaporation exhibits much lower residence times than distillation in columns and therefore allows separation steps not possible in the latter. This necessitates a different model for distillation columns and thin-film evaporation, as described in the following.

### 5.2.1 Model of physico-chemical properties

The property model described in Section 3.2 is applied. However, since the residence times in thin-film evaporators are very short, the reactions of FA with ME and WA usually do not reach chemical equilibrium in these units. Therefore the model is extended to consider the respective reaction kinetics in the liquid phase in these units. For the implementation of the kinetic, the formation and degradation of MG and HF are formulated as described by Ott et al. [64].



### 5.2.2 Model of thin-film evaporation

In thin-film evaporators, the feed solution runs down a heated shell in a thin film that may be stabilized by wiper blades on a rotor. The bottom product of the TFE is the liquid residual. The top product gas is fed to a condenser, which is considered a total condenser in the present work. The light-boiling monomeric formaldehyde, methanol, and short-chain oligomers are preferably evaporated, while long-chain oligomers stay back in the liquid phase. Because the residence time is short, the long-chain oligomers do not have the time to decompose into shorter species. Ultimately, this leads to an enhanced accumulation of formaldehyde in the liquid residual when compared to slower evaporation methods.

A model for the simulation of a continuous thin-film evaporation of aqueous FA solutions was developed by Schilling et al. [135]. We developed a model for the thin-film evaporation of FA solutions containing both water and methanol; Figure 12 shows the respective scheme. The evaporation is modeled as an open evaporation with a finite number  $N_{\text{TFE}}$  of stages, which are no equilibrium stages but are modeled as described below. Each stage has a liquid holdup, which is quantified via the liquid residence time  $\tau_{\text{TFE}}$ . The liquid stream leaving a stage is fed to the next, and the gaseous streams are collected and completely condensed, cf. middle part of Figure 12. This allows the simulation of a closed evaporation (one stage) or an open evaporation (multiple stages) by choosing different values for  $N_{\text{TFE}}$ .

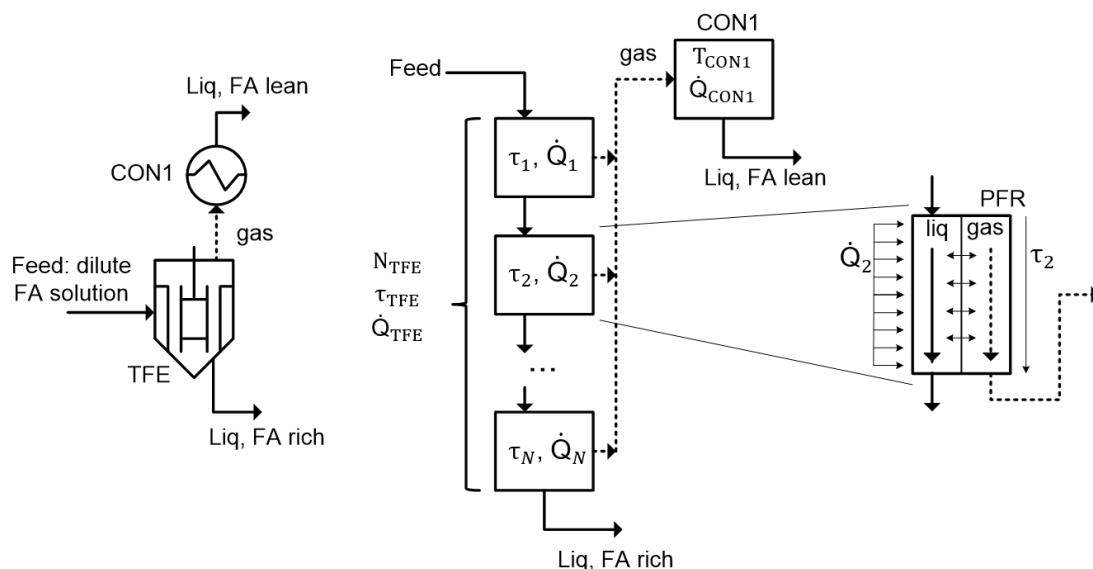


**Figure 12:** Process flow diagram (left) and model scheme (center, right) of the thin-film evaporator (TFE) [135].  $\dot{Q}_i$  is the heat duty on stage  $i$ ,  $\tau_i$  is the liquid residence time on stage  $i$ . Liquid streams are indicated with full lines, gaseous streams with dashed lines.

Every individual stage represents a closed film evaporation in a two-phase plug flow reactor (PFR), cf. right part of Figure 12. In the implementation (in Aspen Plus), the PFR is discretized into many differential control volumes; in every of the differential volumes, the liquid phase is ideally mixed, considers the reaction kinetics, and is in vapor-liquid equilibrium with the gas phase. The kinetic by Ott et al. [64] is adopted to model the MG and HF formation/degradation in the PFR according to Reactions (33) to (36). It describes the reactions rates as follows,

$$r_1 = k_1 a_{\text{FA}} a_{\text{WA}} - k_1^* a_{\text{MG}_1} \quad (37)$$

$$r_{2,n} = k_2 a_{\text{MG}_{n-1}} a_{\text{MG}_1} - k_2^* a_{\text{MG}_n} a_{\text{WA}} \quad n > 1 \quad (38)$$

$$r_3 = k_3 a_{\text{FA}} a_{\text{ME}} - k_3^* a_{\text{HF}_1} \quad (39)$$

$$r_{4,n} = k_4 a_{\text{HF}_{n-1}} a_{\text{HF}_1} - k_4^* a_{\text{HF}_n} a_{\text{ME}} \quad n > 1 \quad (40)$$

$$\frac{dx_i}{dt} = \sum_1^R r_j \nu_{i,j} \quad (41)$$

where  $x_i$  is the mole fraction (true composition) of component  $i$ , and  $a_i = x_i \gamma_i$  is the activity of component  $i$ .  $k_j$  is the rate constant of the forward reaction  $j$  and  $k_j^*$  of the reverse reaction. The summation is over all reactions  $R$ . The stoichiometric coefficient  $\nu_{i,j}$  is +1 for products, and -1 for educts. Reactions (34) and (36) are both considered up to a chain length of  $n = 10$ .

The rate constants are pH-dependent; the pH value of the feed can be adjusted in order to reduce the speed of the reactions and enhance the separation. A pH value of 4.51 was chosen for all simulations in the present work. At this value, the reaction rates of the degradation of both MG and HF of various chain lengths are close to their minima [64]. The total heat duty  $\dot{Q}_{\text{TFE}}$  and the total residence time  $\tau_{\text{TFE}}$  are distributed equally over all stages:

$$\dot{Q}_i = \frac{\dot{Q}_{\text{TFE}}}{N_{\text{TFE}}} \quad i = 1, \dots, N_{\text{TFE}} \quad (42)$$

$$\tau_i = \frac{\tau_{\text{TFE}}}{N_{\text{TFE}}} \quad i = 1, \dots, N_{\text{TFE}} \quad (43)$$

Assuming a constant pressure on all stages and a fully specified feed stream, the TFE model has four degrees of freedom to specify in the simulation: the pressure  $p_{\text{TFE}}$ , the total heat duty  $\dot{Q}_{\text{TFE}}$ , the total residence time  $\tau_{\text{TFE}}$  and the number of stages  $N_{\text{TFE}}$ .

We believe Schilling et al. [135] used a CSTR approach for the kinetic instead of our PFR approach (they did not clearly specify). Thus the models are probably not one-to-one

comparable. They have also performed measurements of the chain length distribution of the  $MG_n$  in TFE products. We validate the simulation model of the present work using this reported experimental data [135], cf. Section 5.3.1. For the simulation, the feed rate and condition and the pressure in the TFE are set as described in the experiment; the total heat duty is chosen in such a way that the evaporated top product has the same mass flow as in the experiment. The number of stages is set to 8. The residence time is not disclosed in Schilling et al. [135] and is therefore estimated from the given apparatus size and the volume flow rate of the feed. We assumed a constant film thickness of 0.1 mm in the unit. Using a simplified geometry, the liquid holdup is calculated as the volume of a hollow cylinder of the corresponding thickness and an inner diameter (50 mm) and length (300 mm) equal to the TFE used by Schilling et al. [135]. The resulting heat flow rate of around 13 kW/m<sup>2</sup> is typical in TFEs [140].

The operating point of the TFE in the process studied later in the present work differs strongly from the operating point studied by Schilling et al. [135], not least because ME is present. Thus a sensitivity study regarding the number of stages was done using feed streams relevant in the present work's process. Based on this sensitivity, the stage number was set to two stages to simulate the process in the present work. Adding more stages did not change the results, cf. Appendix C for details.

### 5.2.3 Model of distillation

The distillation columns are modeled using the equilibrium stage model, assuming physical and chemical equilibrium on all stages. In contrast to the TFE, higher temperatures leading to larger reaction rates and higher liquid holdups leading to long residence times justify the assumption of chemical equilibrium [64, 125]. Condenser (assumed total) and reboiler are modeled with one additional stage, respectively, the pressure drop along the column is neglected.

### 5.2.4 Process and specification

The goal of the process is to provide a methanolic FA solution that can be used directly in a water-tolerant OME production process [43]. This methanolic formaldehyde solution will be further referred to as OME feedstock. It has a FA/ME mass ratio of 1.647 and a water content as low as possible, maximally 0.1 g/g [30, 43]. Higher water content would be detrimental since water shifts the chemical equilibrium in the OME reactor to the educts and inhibits OME formation [121]. Raw materials are pure ME and the typical main products of FA production plants, i.e., solutions with up to 0.5 g/g FA

in water and methanol. Two formaldehyde products are studied as feed: (Case I) a solution composed of 0.503 g/g FA, 0.294 g/g WA and 0.203 g/g ME from a FA plant with incomplete conversion [130] and (Case II) a solution of 0.5 g/g FA and WA and no methanol (e.g., from a FA silver process or FORMOX process with full methanol conversion [28]). All FA in the feed shall be yielded in the OME feedstock; there shall be no other FA containing side products.

The process suggested in the present work is shown in Figure 13. The feed (1) is fed to distillation column C1, where parts of the methanol are removed (In Case II, column C1 is not required, and the feed is fed directly to the thin-film evaporator TFE1).

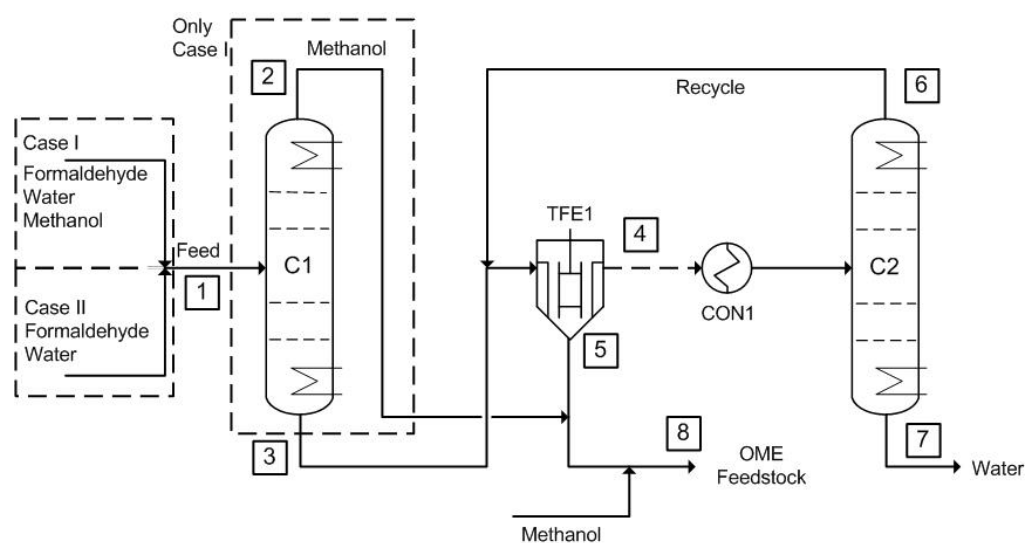


**Figure 13:** Flow diagram of the studied process, column C1 is only required if methanol is present in the Feed (1).

Column C1 is operated at low pressure to yield FA in the bottom and remove purified methanol as the top product (2). Its bottom product (3) is fed to the thin-film evaporator TFE1, in which it is partially evaporated, yielding a gaseous, FA-lean top product (4). The liquid residual (5) of the TFE is a concentrated FA solution with small amounts of ME and WA. It is mixed with ME to yield the product (8). The top product (4) of TFE1 is condensed in the condenser CON1, and fed to the distillation column C2. C2 is operated at elevated pressure to shift the FA-WA azeotrope to higher FA concentrations, yield the FA in the top, and remove purified WA as the bottom product (7). The top product (6) is recycled, mixed with stream (3), and fed to TFE1. The amount of water in stream (6) is limited through the pressure-dependent azeotrope FA-WA and a respective distillation boundary in the ternary system, cf. Appendix C.

The specifications of the individual units are listed in Table 4 and motivated as follows:

- Column C1: The pressure in C1 should be as low as possible while still allowing condensing with non-chilled water. Low pressure (and respective low temperatures) drives the FA into the bottom product.  $p_{C1}$  is set to 0.5 bar (in the present work, values for pressure always refer to the absolute pressure bar (a)) here, resulting in a condensation temperature of 47 °C for the top product methanol. The purity of the top product is set to 0.99 g/g ME. A higher purity is not required, as the stream is used for blending the final product. The influence of the purity specification is studied in a sensitivity study to show its minor importance, cf. the results in Section 5.3.2. The number of stages  $N_{C1}$ , the feed stage  $N_{C1}^{\text{Feed}}$ , and the reflux ratio of the column  $RR_{C1}$  remain as degrees of freedom and are subject to optimization.
- TFE1: The pressure should be as low as possible to drive the FA into the bottom product, but it is again limited by the cooling temperature in the condenser CON1. To enable the use of non-chilled water, the pressure is set to 0.2 bar, resulting in the temperature of 45 °C in CON1. The residence time  $\tau_{\text{TFE}}$  in the unit is set to 11.3 s (analogous to the experiment used to validate the model, cf. Section 5.2.2). Shorter residence times might be favorable in terms of the FA recovered in the bottom product but would result in a more expensive TFE and difficulties in producing a sufficiently high heat flux. Longer residence times lead to a higher heat demand in the process but would still be feasible, cf. Appendix C for a sensitivity study. The remaining degree of freedom, the heat  $\dot{Q}_{\text{TFE}}$  supplied to the TFE, is subject to optimization.
- Column C2: As mentioned before, elevated pressure is needed: 4 bar is chosen as it still allows to use 4 bar steam from the network for heating. The purity of the bottom product was set to 0.997 g/g WA (Higher purities are also feasible, the required purity depends on the waste-water treatment plant associated with the site of the process). The number of stages  $N_{C2}$ , the feed stage  $N_{C2}^{\text{Feed}}$ , and the reflux ratio of the column  $RR_{C2}$  remain as degrees of freedom and are subject to optimization.



**Table 4:** Specifications and optimization parameters of the studied process for Case I and Case II

Unit/Entity	Specification	
	Case I	Case II
Feed	$x_{\text{FA}}^{(1)} = 0.503$ g/g $x_{\text{WA}}^{(1)} = 0.294$ g/g $x_{\text{ME}}^{(1)} = 0.203$ g/g $T^{(1)} = 75.1$ °C $p^{(1)} = 1.0$ bar	$x_{\text{FA}}^{(1)} = 0.5$ g/g $x_{\text{WA}}^{(1)} = 0.5$ g/g $x_{\text{ME}}^{(1)} = 0.0$ g/g $T^{(1)} = 75.1$ °C $p^{(1)} = 1.0$ bar
C1	$p_{\text{C1}} = 0.5$ bar $x_{\text{ME}}^{(2)} = 0.99$ g/g $RR_{\text{C1}} = \text{opt. param.}$ $N_{\text{C1}} = \text{opt. param.}$ $N_{\text{C1}}^{\text{Feed}} = \text{opt. param.}$	
TFE1	$p_{\text{TFE}} = 0.2$ bar $\dot{Q}_{\text{TFE}} = \text{opt. param.}$	$p_{\text{TFE}} = 0.2$ bar $\dot{Q}_{\text{TFE}} = \text{opt. param.}$
C2	$p_{\text{C2}} = 4.0$ bar $x_{\text{WA}}^{(7)} = 0.997$ g/g $RR_{\text{C2}} = \text{opt. param.}$ $N_{\text{C2}} = \text{opt. param.}$ $N_{\text{C2}}^{\text{Feed}} = \text{opt. param.}$	$p_{\text{C2}} = 4.0$ bar $x_{\text{WA}}^{(1)} = 0.997$ g/g $RR_{\text{C2}} = \text{opt. param.}$ $N_{\text{C2}} = \text{opt. param.}$ $N_{\text{C2}}^{\text{Feed}} = \text{opt. param.}$

### 5.2.5 Simulation and optimization

The simulation was implemented in ASPEN PLUS Version 8.8. Since the kinetic does not fit Aspen's standard format, it was implemented as a custom Fortran user model. The complete process is optimized using two objectives:

- Minimize the overall mass fraction  $x_{\text{WA}}^{(8)}$  of water in the product.
- Minimize the specific total heat demand  $\dot{q}_{\text{tot}}$ , i.e., the sum of the heat provided to the units C1, C2, TFE1 divided by the mass flow rate of the product. To avoid infinite numbers of stages in the columns, which would be obtained naturally at minimum energy demand, a constraint is introduced that chooses stage numbers so that the energy demand in the columns is 6% above the theoretical minimum (see below).

The optimization parameters that are varied are given in Table 4. As both objectives are partly conflicting, a multi-criteria optimization (MCO) is done. The optimization problem can be classified as a mixed-integer nonlinear programming problem (MINLP). Because the simultaneous finding of all optimal parameters turned out to be numerically

unstable in the process simulator (here: ASPEN PLUS Version 8.8), the application of many established optimization methods, e.g., black-box optimization or genetic algorithms, turned out to be not feasible. Therefore the following heuristic was used to determine the Pareto front of the MCO:

1. The numbers of stages of both columns are initially set to 50 and the feed stages to 25.
2. While keeping the number of stages and feed stages in C1 and C2 constant, the Pareto front is determined by optimizing the continuous parameters ( $RR_{C1}$ ,  $RR_{C2}$ ,  $\dot{Q}_{TFE}$ ). To sample the Pareto front, the  $\epsilon$ -constraint method as described by Haimes et al. [138] was used. A constraint was set on  $x_{WA}^{(8)}$  and varied between 0.18 and 0.09 g/g, while for every  $x_{WA}^{(8)}$  the total heat duty  $\dot{q}_{tot}$  was minimized using the sequential quadratic programming (SQP)[141, 142] algorithm included in ASPEN PLUS.
3. A Pareto-optimal point in the Pareto knee is selected as operating point. This is done as follows. The Pareto optimal points are indexed with  $k$ ,  $k=1$  ( $k = k_{max}$ ) being the one with highest (lowest)  $x_{WA}^{(8)}$ . The slope  $m(k)$  of the Pareto front at some point  $k$  is approximated by the difference quotient:

$$m(k) = \frac{x_{WA}^{(8)}(k) - x_{WA}^{(8)}(k+1)}{\dot{q}_{tot}(k) - \dot{q}_{tot}(k+1)} \quad k = 1, \dots, k_{max}-1. \quad (44)$$

Further, the overall slope of the front is defined as

$$m_{overall} = \frac{x_{WA}^{(8)}(k=1) - x_{WA}^{(8)}(k=max)}{\dot{q}_{tot}(k=1) - \dot{q}_{tot}(k=max)}, \quad (45)$$

The point with the smallest  $k$  but meeting

$$m(k) \geq 0.35 m_{overall} \quad (46)$$

is selected as operating point (OP) for the following steps. This procedure and the value 0.35 of the tuning parameter in Equation Eq. (46) might not be universal, but produced good solutions in our problem, cf. the section Results.

4. The number of stages and the feed stage for C1 and C2 are updated. Both columns are simulated isolated using changed specifications. The reflux ratios are not specified; instead, an additional purity is specified for each column to the values of the selected operating point in Step 3,  $x_{ME}^{(3)}$  for C1 and  $x_{WA}^{(6)}$  for C2.  $N, Q$ -curves, i.e., trade-offs between the number of stages and reboiler duties, are generated for

both columns. The number of stages and the feed stages are selected so that the reboiler duty is 1.06 times the minimum reboiler duty.

5. If the numbers of stages have changed, go to Step 2; otherwise, stop.

While this heuristic was found to produce good solutions fast, it cannot guarantee to find the global optimum of the MINLP, of course.

## 5.3 Results

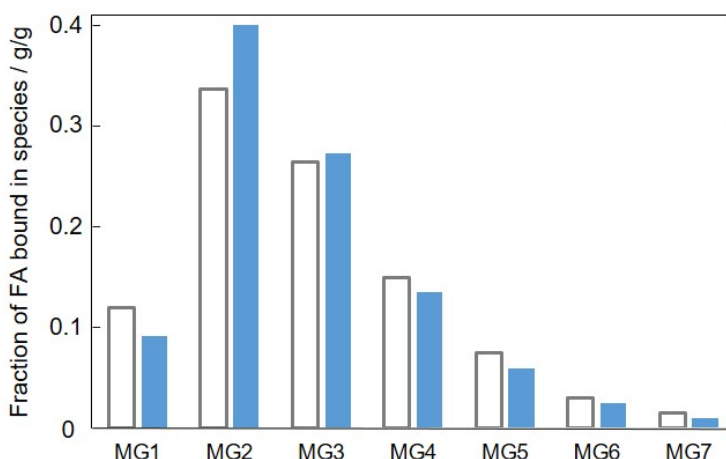
### 5.3.1 Validation of the TFE model

Table 5 shows the overall FA mass fractions in the top and bottom product of the TFE at the operating point studied experimentally by Schilling et al. [135]. The model's simulation results are in good agreement with the experimental results from the original work. Furthermore, the distribution of the FA bound in the individual MG species in the bottom product is also in good agreement with the experimental results, cf. Figure 14.

**Table 5:** Simulation results and adopted measurements [135] of the TFE product compositions.

	Feed	Top	Bottom
$\dot{m}$ /g/h (experimental [135])	1547.4	1005.2	542.2
$\dot{m}$ /g/h (simulation)	1547.4	1005.2	542.2
$x_{\text{FA}}$ /g/g (experimental [135])	0.298	0.113	0.641
$x_{\text{FA}}$ /g/g (simulation)	0.298	0.113	0.644

In contrast to a highly concentrated FA solution in chemical equilibrium where more FA is bound in long-chained MG, most of the FA is bound in  $\text{MG}_{1-4}$ . This is why FA solutions produced in TFEs are (at least short-term) stable and do not show immediate solid precipitation.



**Figure 14:** Distribution of the FA bound in the individual MG species in the TFE bottom product in the experiment done by Schilling et al. [135]. Empty bars: experiment [135], filled bars: simulation results.

### 5.3.2 Objective trade-offs

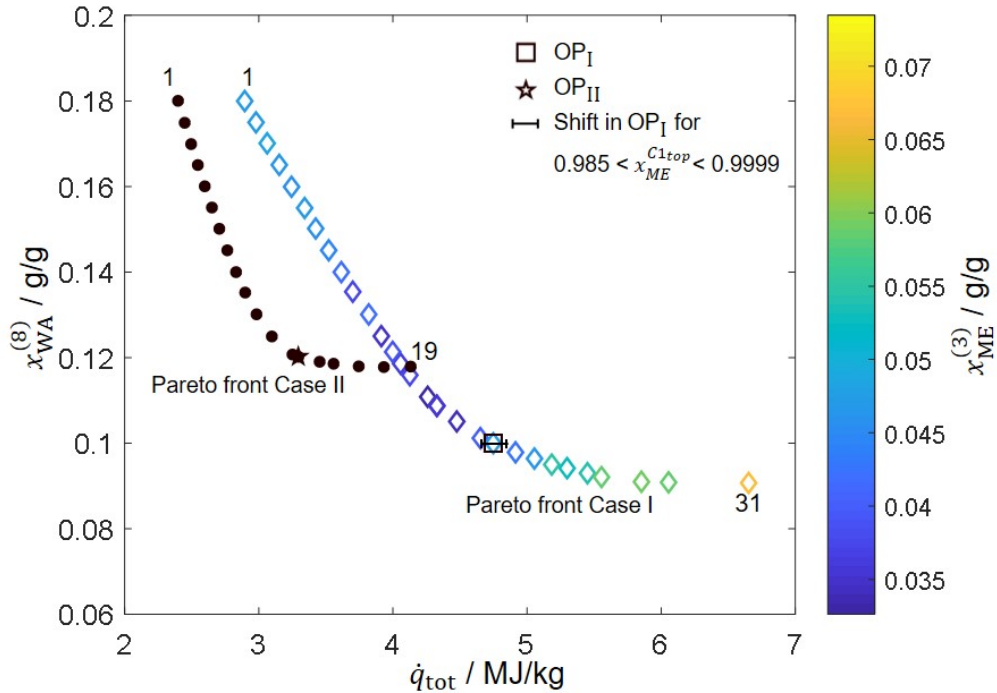
In this section, the main results for Case I and II are presented and discussed. Detailed information, including stream tables,  $N, Q$ -curves, and numerical values of the optimization parameters of all Pareto-optimal points, are given in Appendix C. The property model is also used to investigate the reactive VLE topology in distillation columns for the system FA+WA+ME, the results are also given in Appendix C.

Figure 15 shows the Pareto front in the objective space for both Cases I and II. The Pareto-optimal points of the final iteration are numbered from 1 to 31 and 1 to 19. The two objectives  $x_{\text{WA}}^{(8)}$  and  $\dot{q}_{\text{tot}}$  are conflicting for both cases.  $x_{\text{WA}}^{(8)}$  can be reduced by increasing  $\dot{q}_{\text{tot}}$  up to a certain point. From there on, a further increase will lead to drastically higher heat demand while not affecting  $x_{\text{WA}}^{(8)}$ . The minimum product water content for Case I is 0.092 g/g, for Case II 0.118 g/g. That means that methanol in the feed helps to yield a lower  $x_{\text{WA}}^{(8)}$ . Case II clearly has a lower  $\dot{q}_{\text{tot}}$  than Case I for all  $x_{\text{WA}}^{(8)}$  larger than 0.118 g/g.

In Case I, the mass fraction  $x_{\text{ME}}^{(3)}$  of ME in the bottom product of C1 is at its maximum for the minimum product water content and the maximum  $\dot{q}_{\text{tot}}$ , cf. color code in Figure 15. This indicates that the presence of ME increases the heat duty in the TFE and C2 but also lowers the product water content. With increasing  $x_{\text{WA}}^{(8)}$ ,  $x_{\text{ME}}^{(3)}$  is reduced until it reaches a minimum on the Pareto front at  $x_{\text{WA}}^{(8)}=0.13$ . For high  $x_{\text{WA}}^{(8)}$ ,  $x_{\text{ME}}^{(3)}$  slightly increases again. Here the increased heat duty in C1 required for a low  $x_{\text{ME}}^{(3)}$  outweighs its benefit on the heat duty in C2 and the TFE.

Though not varied during the optimization, the influence of the purity specification for

the top product of C1 on the final operating point was investigated for Case I. The bar in Figure 15 shows that OP I shifts insignificantly when varying  $x_{\text{ME}}^{(2)}$  between 0.985 and 0.9999 g/g. Therefore, the exact specification of  $x_{\text{ME}}^{(2)}$  is judged not decisive. As intended, the operating points chosen in Step 3 of the optimization heuristic lie in the knee of the corresponding Pareto fronts.



**Figure 15:** Results of the Pareto optimization in Case I (diamonds) and II (circles). For Case I, the mass fraction  $x_{\text{ME}}^{(3)}$  of ME in the bottom of C1 is highlighted as color code. The operating points selected in Step 3 of the optimization heuristic are highlighted as star/rectangle. The bar shows the influence of the specification  $x_{\text{ME}}^{(2)}$  on OP I.

### 5.3.2.1 Material and energy balance

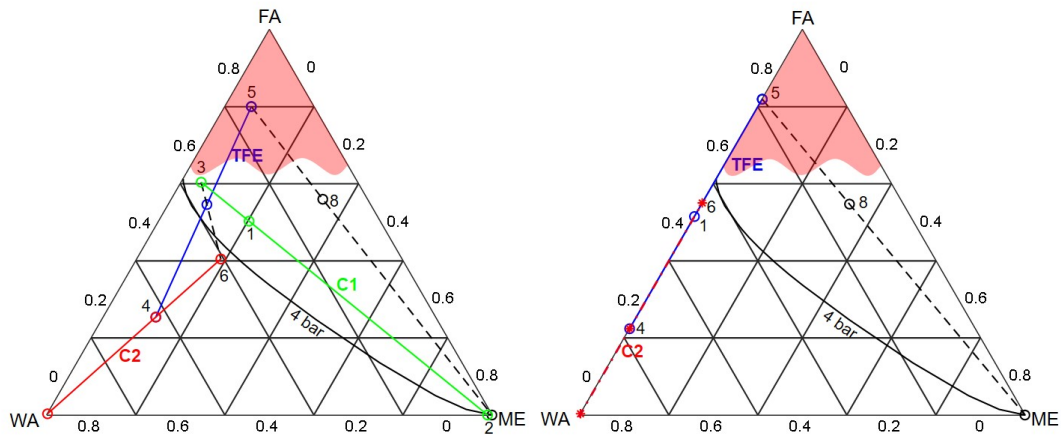
Table 6 gives the heat duties and other results of the process units. Figure 16 shows the ternary diagrams with the overall compositions of all process streams for the selected operating points indicated in Figure 15.

Figure 16 left (Case I) shows that the separation of the solution in the TFE (Streams (3),(4),(5)) allows for crossing the distillation boundary and provides a bottom product (5) that would show solid precipitation upon ripening in storage. The TFE is the key separation step that enables overcoming the azeotrope formed by FA and WA. The

bottom product (5) is immediately mixed with ME to stabilize it and produce the final product (8).

**Table 6:** Results for the process units for Case I and Case II. All heat duties are normalized on the product mass flow rate  $\dot{m}^{(8)}$ .

Distillation columns	C1	C2	C2	Evaporator & Condenser	TFE1	CON1	TFE1	CON1
	Case I	Case I	Case II		Case I	Case I	Case II	Case II
$\dot{q}_{\text{top}}$ / MJ/kg	- 1.52	- 1.62	- 1.36	$\dot{q}_{\text{CON}}$ / MJ/kg		- 1.30		- 1.63
$T_{\text{top}}/^\circ\text{C}$	47.84	134.73	136.17	$T_{\text{CON}}/^\circ\text{C}$		57.21		45.00
$\dot{q}_{\text{bot}}$ / MJ/kg	1.59	1.91	1.67	$\dot{q}_{\text{TFE}}$ / MJ/kg	1.23		1.62	
$T_{\text{bot}}/^\circ\text{C}$	83.20	143.47	143.47	$T_{\text{TFE}}/^\circ\text{C}$	116.85		122.08	
$p$ / bar	0.50	4.00	4.00	$p$ / bar	0.20	0.20	0.20	0.20
$N$	28.00	22.00	25.00					
$N^{\text{Feed}}$	16.00	14.00	14.00					
$RR$	6.09	1.81	1.83					



**Figure 16:** Ternary diagrams of the process for Case I (left) and II (right). Distillation boundary (full black line) depicted at the pressure in C2 (4 bar). For all streams the compositions are given as overall mass fractions. Colored full lines show the splits in the corresponding units, dashed lines result from mixing of streams. The red shaded area qualitatively indicates the region of solid precipitation, solutions of these compositions can not be produced in distillation columns.

Column C1 is operated in the distillation region below the distillation boundary (4 bar) to remove water (7) from the TFE's top product (4). The recycling of the top product of C1 (6) yields all FA into the desired product. Balanced lever arms in the splits of the units in Figure 16 indicate that the recycle is similar in rate as the feed or the product. In Case II (Figure 16 right), the situation is similar. Since there is no ME present, both

the split in the TFE and the one in C2 lie on the binary edge WA-FA of the ternary diagram. However, both units fulfill the same function as in Case I, and the units also show balanced lever arms. The mass flow rate of the recycle stream (6) is only 0.36 (0.23) times the mass flow rate of the product in Case I (II). The losses of FA are 0.13 % for both Case I and II. The total specific heat duty for the chosen operating points is 4.73 MJ/kg product for Case I and 3.29 MJ/kg product for Case II.

## 5.4 Discussion

### 5.4.1 Model of the thin-film evaporation

The model of the TFE calculates the overall and true composition of TFE products and the required heat duty in the unit well for aqueous solutions [135]. However, the model has only been confirmed in experiments for aqueous FA solutions so far, not methanolic aqueous FA solutions. Further, the underlying property model assumes that  $MG_{n \geq 2}$  and  $HF_{n \geq 2}$  have such low vapor pressures that they do not exist in the vapor phase. This assumption is sufficient to describe the reactive phase behavior of FA solutions in VLE [143]; however, it might not sufficiently describe all the kinetically controlled separations in a TFE. In the future, the experimental base should be broadened to obtain confidence in the model. The operating points identified in the present work provide a good starting point for experimental planning.

### 5.4.2 Objective trade-offs

The simulations indicate the feasibility of the presented process for both cases I and II. The process is able to yield almost all fed FA as methanolic FA with only insignificant losses in stream (7). The FA losses are very small in both cases since only purified water is removed as side product.

Starting with aqueous formaldehyde solution (Case II) leads to a smaller heat demand per produced kg OME feedstock. However, methanol present in the fed formaldehyde solution (either naturally or admixed, Case I) has also advantages. First, lower product water contents can be achieved. Second, the upstream FA plant has less strict specifications. The incomplete conversion of ME to FA in the upstream FA plant in Case I could decrease carbon losses via a better selectivity in the FA reactor. Further, there are other arguments for plants with incomplete conversion, such as safety and process control aspects [35]. Third, the TFE requires less heat per kg product in Case

I (1.23 MJ/kg) than in Case II (1.62 MJ/kg). This reduces the required surface area of the TFE and, therefore, its investment cost. This is particularly significant because the TFE is expected to have a major share of the investment cost. On the other hand, the additional costs for C1 also have to be considered.

The heat demand of the process can be lowered in both cases through heat integration. In Case I, the temperature difference between C2's condenser and C1's reboiler is large enough to allow a heat integration where the heat in C1's reboiler is entirely provided by C2. In both cases, one could lower the temperature in the TFE by reducing the pressure, while increasing the pressure in C2. This would allow using the heat from C2's condenser in the TFE. However, chilled or cooled water would have to be supplied to the condenser of the TFE.

The difference between Cases I and II in the minimum achievable product water content  $x_{\text{WA}}^{(8)}$  can be explained by the effect of ME on the separation in the TFE. ME and its reaction products  $\text{HF}_n$  displace water in the TFE's bottom product. This is because FA binds more preferably to ME than to WA [144], and the resulting  $\text{HF}_n$  have a very low vapor pressure. However, the presence of ME in the process also leads to a higher heat demand in C2 and a higher recycle flow rate.

When comparing Case I and II in terms of heat demand and investment cost, one should also consider that both cases are based on different upstream FA production processes.

### 5.4.3 Variations of the process concept

Several variants of the process concept were also investigated. They are shortly discussed in the following. If there is a significant demand for aqueous FA solution besides methanolic FA solution, the recycles are not necessary. FA solution could be separated in one step in a TFE into a concentrated part (which is used to produce methanolic FA) and dilute part (which is used in an FA plant's absorber as absorbent or sold as aqueous FA after concentration).

In both cases I and II, CON1 could be used as a partial condenser. If the condensation is done fast, this would result in an FA-rich gaseous residual and an FA-lean condensate. The condenser CON1 would thereby serve as a pre-fractionator of column C2: the gaseous residual could be fed to the top part of C2, and the liquid condensate could be fed to the bottom of C2. While this would reduce the heat demand in C2, it would require fast cooling and energy-intensive compression of the gaseous residual. A complete omission of CON1 would result in a similar trade-off between reduced heat demand and additional work for compression.

In both cases, Column C2 could be heated by feeding 4 bar steam to the column bottom.



The steam is used as stripping gas and allows to eliminate a reboiler equipment.

In Case I, it is possible to feed the recycle stream (6) to column C1 instead of the TFE. This would increase the heat demand in C1 but decrease the heat demands of the TFE and C2 due to a slightly lower recycle. Whether this alternation helps or harms the overall performance depends on the composition of the feed. For the presented feed composition, it did not yield an improvement.

If C1 is omitted in Case I (to save investment), the total specific heat demand would rise to 34.8 MJ per kg OME feedstock (more than seven times the demand than with C1), due to the accumulation of too much ME in the recycle. This is clearly not an option. However, for other feed compositions, the process could be viable without C1.

In the studied process, the pre-concentration of FA is realized in column C2, and the concentration is done in one step in the TFE. In the industrial production of paraformaldehyde, the concentration of FA is usually realized by a pre-concentration in a fall film evaporator (FFE) and subsequent concentration in a TFE. A two or more step concentration instead of just one TFE may be advantageous for the studied process as well. Adding a fall film evaporator before the TFE might increase the concentration of FA and would likely reduce the investment cost, as the required heat exchange surface is much cheaper to realize in FFEs than in TFEs. Since an economic analysis is not part of the present work, this option was not explored in detail.

Further, although the assumed film thickness of 0.1 mm is common in TFEs, a TFE with a film thickness of 0.5-1.0 mm could be the cheaper option. This would save on heat exchanger surface and investment costs for the TFE, which are usually relatively high. On the other hand, this would result in a less effective separation, shifting the operating point of the process and resulting in higher operating costs.

In a variation of Case I, the feed could be fed directly to the TFE. In this setup, the column C1 has to be placed either in stream (4) or stream (6). While this change increases the heat demand in the TFE, it reduces the heat demands in C1 and C2. Simulations showed the respective process slightly inferior to the one presented in Case I for the given feed. However, the alternation might have advantages for other feed compositions, i.e., other FA plants with incomplete conversion.

Note that all described process concepts can be combined with pervaporation units or similar equipment to further increase product purity and remove even more water from the product.



# 6 Techno-economic analysis of OME production from methanol

## 6.1 Literature review

For any potential renewable fuel not yet on the market, studies on production cost are highly relevant and revealing. Therefore several studies on the cost of OME production have been published. Schmitz et al. [47] calculated costs for both routes of OME production as a function of the methanol cost through a very rough estimation of production costs based on analogies to refineries. However, they essentially neglected the challenging water removal in the formaldehyde concentration and the cost of formaldehyde production. Therefore, the results should be considered rather as a lower bound to the production cost. Similarly, Burger and Hasse [46] reported the production cost of OME<sub>3-5</sub> as a function of the methanol cost. However, they did not describe how the result was obtained. Ouda et al. [68] report an OME production cost of 951 USD per ton of OME<sub>3-5</sub> at a small production capacity (35 kt per annum). However, the production process is based on the direct dehydrogenation of methanol to formaldehyde which is still fundamental research, and the cost estimate seems premature. Mantei et al. [10] present a very detailed study that gives the cost of production for OME from Power-to-X (PtX) hydrogen and CO<sub>2</sub> for four routes. They report the production cost of OME<sub>3-5</sub> as a function of the costs of hydrogen and CO<sub>2</sub>. For the cost of hydrogen and CO<sub>2</sub> of 4241 EUR/t and 309 EUR/t, respectively, they reported the OME cost of 2382-2458 EUR/t. They concluded that  $\geq 80\%$  of the cost was related to raw material cost and that the production cost of OME only slightly varied among the four studied routes. Oyedun et al. [21] present production costs of 1.66-1.93\$/l for OME for fuel blending produced from biomass. They use fixed raw material costs and a simplified OME production process for their assessment. They conclude that OME yield, capital cost, and biomass cost significantly influence OME cost and that the minimum OME cost can be obtained at a plant capacity of 4000 Mt/d [21]. Schemme et al. [45] present a study that gives the OME production cost when hydrogen is used as raw material for three different hydrogen costs, they use idealized assumptions on water removal in the

formaldehyde concentration. For their base case of 4.6 EUR/kg<sub>H<sub>2</sub></sub>, they report manufacturing costs of 1.85 EUR/l<sub>DE</sub> for DME and 3.96 EUR/l<sub>DE</sub> for OME, with the other investigated fuels ranging between the two [45].

However, all the studies mentioned above have at least one of the following caveats: either they are very coarse estimates under strongly simplifying assumptions, e.g., formaldehyde production is essentially free of cost [47], or they report the cost depending on one single raw material, e.g., Pt<sub>x</sub> hydrogen [10]. There is no study yet, that reports OME production cost as a function of the methanol cost and plant size based on a detailed, and thus meaningful, process model. Reporting OME production cost depending on the methanol cost is advantageous over reporting it for several individual raw materials upstream of methanol for the following reasons: First, there is an enormous market for methanol, and the OME price will therefore be tied to the methanol price for the foreseeable future. Second, the exclusion of the methanol production allows the flexible consideration of varying sources for said methanol; it could stem from CO<sub>2</sub> utilization, biomass, or fossil resources, and the results for OME production cost hold. Third, this system boundary allows the assessment of a methanol production that is located somewhere where sustainable energy is cheap, while the OME production can be located anywhere, e.g., near the market for OME. In contrast to hydrogen or formaldehyde, methanol is liquid, stable, and easy to transport.

In the following, the present work presents a techno-economic analysis and derives the OME cost as a function of a variable methanol cost. The costs of production for various plant sizes are determined. Multiple routes for the production and concentration of FA are analyzed and compared, including rather novel ones, cf. Chapter 5. It is shown to what extent these process improvements have an influence on the production cost. Further, the influence of different remaining water contents in the feed of the OME process is considered explicitly in the analysis. The investigated processes are evaluated with process simulation, and heat integration is considered via a steam cycle. Techno-economic analysis, based on Towler [145] and Peters [146] is used to evaluate and report the capital and operational cost of all process steps.

## 6.2 Methodology

### 6.2.1 Description of processes

#### 6.2.1.1 Overview routes

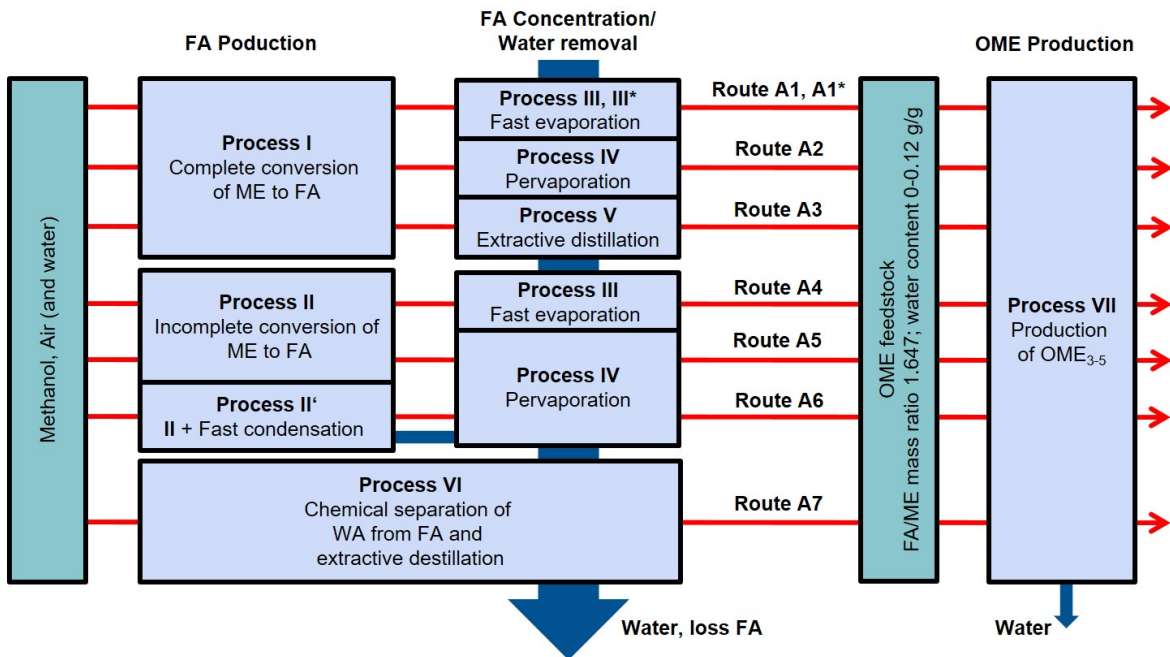
We rely on process routes that are considered feasible in academic literature and described well enough to be evaluated. We study the class of water-tolerant OME processes, i.e., processes that synthesize OME<sub>3-5</sub> directly from methanol and concentrated formaldehyde solutions (Route A). Processes that include dry formaldehyde (monomeric formaldehyde / paraformaldehyde / trioxane), in contrast, are still in fundamental development (i.e., first trials of novel reactor concepts [68], improvement of catalysts to suppress side-product formation [50]) or involve the production of expensive intermediates (trioxane). Therefore, we have omitted Route B from our consideration for the TEA. Mantei et al. [10] have shown that if Route B processes are included in the analysis (e.g., by using idealizing assumptions), then the results on OME production cost are not significantly different. This is because the cost mainly depends on the raw material cost, which is conceptually the same in Routes A and B.

Figure 17 shows the water-tolerant OME production Route A starting from methanol. Three process steps are needed: FA production, FA concentration/water removal, and OME production. For the latter one, the process presented by Schmitz et al. [43] is used without modification (Process VII). Simulation data [43] and a demonstration plant exist [147]. The feed for that process is a liquid mixture of formaldehyde and methanol (with a FA/ME mass ratio of 1.647) and small amounts of water, referred to as OME feedstock. Its water content should be as low as possible since water shifts the chemical equilibrium in the reactor to the educts and inhibits OME formation [29]. This is why the upstream FA concentration/water removal step is essential.

To the best of our knowledge, there is currently no industrial process to produce OME feedstock from methanol without producing large amounts of couple products such as aqueous FA solution. We collected ideas from the patent literature for this task and conceptually designed 7 routes from methanol to OME feedstock without major side products, which are assessed and compared; cf. Figure 17.

Routes A1-A6 combine a process for formaldehyde production with a process for water removal. Route A7 integrates both tasks into one process. Raw materials of all routes are pure methanol, water and air (21 vol% O<sub>2</sub>, 79 vol% N<sub>2</sub>). They enter the production at 25°C. All side products and auxiliary materials (e.g., extracting agents) are preferably recovered as pure components and recycled. For comparison, all routes are scaled to

produce the same mass flow rate of OME<sub>3-5</sub>.



**Figure 17:** Overview of all processes considered in the economic analysis. Processes are numbered as follows. I: FA production that provides a 0.5 g/g FA-WA solution, herein the BASF process [28]. II: FA production with incomplete conversion [130]. III/III\*: Separation of FA solutions in a fast evaporator or column [10, 58]. IV: Pervaporation to remove water from FA solutions [59, 60]. V: Extractive distillation of FA solutions [61]. II': FA production with incomplete conversion and fast condensation of water from reactor product [131]. VI: Production of Methylal and separation of water, oxidation of MAL to FA and following extractive distillation [126]. VII: OME production adopted from Schmitz et al. [43].

### 6.2.1.2 Formaldehyde production

Processes to produce FA solutions are well established in the industry. Two process types for FA production from methanol are distinguished: Process I yields complete ME conversion in one pass through the reactor (e.g., Formox processes, off-gas recycle processes). The reactor delivers a mixture of FA and WA with very little ME (0-2wt%). Many such processes are used in industry; herein, we chose the BASF process for producing a 0.5 g/g aqueous FA solution as described in Ullmann's Encyclopedia of Industrial Chemistry [28]. Process II operates with incomplete ME conversion in one pass; here, the reactor delivers mixtures of FA, ME, and WA with a distinctly higher FA/WA ratio than in process I [28]. In process II, there is usually subsequent removal and recycling

of ME from the reactor product to achieve complete conversion of ME. However, this is not needed for our purpose. Process II is appealing for the production of methanolic formaldehyde solution because the reactor product already contains less water per unit of FA than in processes with complete conversion. We use data from Vancells [130] for process II. In a variation of process II, process II', part of the reactor product is rapidly condensed to further reduce the water content [131].

### 6.2.1.3 Formaldehyde concentration

In routes A1-A6, water must be removed from the FA solutions provided by an FA process of type I or II. Three different technologies are considered for this purpose. First, highly concentrated FA solutions are typically produced in fall-film evaporators or thin-film evaporators [56–58]. This option is considered as Process III/III\* in Figure 17. Process III is presented in Chapter 5, it combines thin-film evaporation with a distillation column to recover FA and minimize FA losses. Process III\* is a simpler scheme adopted from Mantei et al. [10] to enable comparisons with their results. It uses two thin-film evaporators in series without formaldehyde recovery. It has, therefore, FA losses of up to 8% in effluent water [10]. Besides evaporation, we also consider two alternative technologies: Process IV is a membrane separation of water from FA solutions; the chosen reference process employs pervaporation [59, 60]. Process V is based on the extractive distillation of aqueous FA solutions to obtain concentrated gaseous FA, which is dissolved in methanol subsequently [61]. We added a FA concentration column for formaldehyde recovery from the effluent water in process V. In Route A7, Process VI combines FA production and concentration. FA is reacted to MAL before water is removed. MAL is then oxidized to FA, and pure gaseous FA is obtained in subsequent extractive distillation [126]. The FA is then dissolved in ME to obtain OME feedstock. The main difference between the routes lies in the FA concentration / water removal technology. However, the upstream FA production in Routes A1-A6 also influences the overall performance: It significantly influences carbon losses via the FA reactor's selectivity. Further, Route A1-A7 lead to OME feedstock of different water content. This influences the efficiency of the OME process, which was explicitly considered in the assessment.

#### 6.2.1.4 OME production

For Process VII we adopt the process of Schmitz et al. [43], which converts OME feedstock to OME<sub>3-5</sub> and water over an acidic solid catalyst, ion exchange resin Amberlyst 46. The reactor effluent is separated in a direct distillation sequence in three fractions: (1) light OME, ME, FA, WA; (2) product OME<sub>3-5</sub>; (3) heavy OME. Water is separated from (1) using a pervaporation unit before it is recycled with fraction (3) to the reactor.

#### 6.2.1.5 Detailed descriptions

All processes and the basic apparatus designs are adopted from the corresponding sources indicated in the caption of Figure 17. Process flow diagrams of all processes and detailed descriptions are given in Appendix D. Consistent material balances are derived from the simulations performed in the present work; the required information is adopted from the original literature as described in Appendix D.

### 6.2.2 Process simulation

The processes I-VII are simulated rigorously as steady-state processes in the software Aspen Plus V8.8, cf. Section 3.2 for the property model. Aspen Process Economic Analyzer is used for equipment sizing.

#### 6.2.2.1 Unit modeling and design

Heat duties of all units are derived from the process simulations performed in the present work. The equipment cost calculation requires the respective cost determining factors for each unit given in Table 7.

**Table 7:** Cost determining factors for each unit for the techno-economic analysis

Unit	Cost determining factors
Distillation columns, absorbers	Column height and diameter, Column internals: Trays/Packing
Reactors	Heat duty, Catalyst mass
Heat exchangers, evaporators, condensers, Thin-film-evaporators, Off-gas-burners	Heat exchange area
Membrane units	Membrane surface area



The units are modeled as follows:

- Distillation and absorption columns: All columns are simulated using the equilibrium stage model, assuming physical equilibrium and chemical equilibrium considering Reactions (7)-(12) on all stages. For distillation columns, the condenser (=total condenser) and reboiler are modeled with one additional stage, respectively. The pressure drop along the column is neglected. If not given in the reference, the stage numbers are chosen so that 1.2 times the minimum required reboiler heat duty is used. The feed stage is found using the built-in feed stage optimization of Aspen Plus. The remaining two degrees of freedom per column were fixed by the specification of top and bottom product concentrations as given in the original source; the corresponding concentrations are highlighted in the respective stream tables as bold (cf. Appendix D). The extractive distillation columns in processes V and VI were not modeled with an equilibrium stage model because of missing property data (for extraction agents). Instead, the minimum reflux ratio is calculated based on Underwood's equation [142] and is used to estimate the approximate heat duties, cf. Appendix D. For these extractive distillation columns, height and diameter are adopted from the original work. For all other columns, height and diameter are estimated with the Aspen Process Economic Analyzer, both packed and trayed columns are sized with the default option as DTW Tower.
- Reactors: Reactor product compositions, conversion and selectivity are adopted from the original source. The heat duty  $\dot{Q}$  is calculated via the energy balance:

$$\dot{Q} = \dot{H}_{\text{out}} - \dot{H}_{\text{in}} \quad (47)$$

Reactor cost is based on  $\dot{Q}$  and the temperature level; no further design was done.

- Heat exchangers, condensers, evaporators: Heat is generally provided via a steam network operating at the pressure stages given in Table 8. The water condensate leaves the heat exchanger at the same temperature as the steam entered. Cooling is done preferably by producing steam at the maximum pressure level. Low temperature (LT) cooling is done using the media listed in Table 8. Cooling demand at temperatures above 40°C is realized via cooling water, which enters the heat exchanger at 25°C and leaves it at a maximum of 60°C. Cooling below 40°C requires different cooling mediums at an increased cost. Ammonia and salt solutions were only used for condensation at a constant temperature. Using the mean logarithmic temperature difference and the respective heat transfer coefficient for the heat

exchanger type (cf. Appendix D) the area of the heat exchanger is determined.

$$A = \frac{\dot{Q}}{k * \Delta T_{\text{mean}}} \quad (48)$$

The steam level and cooling media are chosen so that a minimum temperature difference of 10 K [142] throughout the heat exchanger is not undercut. Heat integration along the process chain from ME to OME is realized via the steam network. Heat below 160 °C is not considered for steam generation, therefore, not considered for heat integration unless stated otherwise in the process description. Note that it is likely possible to use part of this excess heat to supply district heat, but this depends on the boundary conditions of the plant and is not further considered here.

**Table 8:** First part: Pressure stages and temperatures of the employed steam network; second part: Temperatures of the cooling media and the process stream.

Steam network pressure levels			
	$T_{\text{Steam}}$	$T_{\text{out}}^{\text{Stream}} / \text{°C}$ (consumption)	$T_{\text{out}}^{\text{Stream}} / \text{°C}$ (production)
Steam 40 bar	290	280	300
Steam 20 bar	220	210	230
Steam 4 bar	150	140	160
LT Cooling media			
Cooling medium	$T_{\text{min.}}^{\text{Product}} / \text{°C}$	$T_{\text{in}}^{\text{medium}} / \text{°C}$	$T_{\text{out(max)}}^{\text{medium}} / \text{°C}$
Cooling water	40	25	60
Chilled water	20	10	60
Ammonia	10	0	0
Salt solutions	-5	-15	-15
Salt solutions	-10	-20	-20

- Thin film evaporators (TFEs) and other kinetic separators: Fast evaporation of aqueous and methanolic FA solutions results in a reactive phase equilibrium that does not reach the chemical equilibrium. These units are modeled as open evaporation with multiple stages considering the vapor-liquid equilibrium and the reaction kinetics of Reactions (33)-(36) [64] on every stage. Details on the model are given in Chapter 5.
- Pervaporation: The primary energy demand for pervaporation results from the permeate's phase change and is calculated from its heat of vaporization. The

membrane surface area is calculated based on the correlation given by Schmitz et al. [59] from the given output stream's specification.

Pumps are not explicitly sized; they are considered using the factor model in the economic analysis. Burners are modeled like reactors with ascribed heat exchangers but are based on a different cost correlation.

### 6.2.3 Process economics

Capital expenditure (CAPEX) and operational expenditure (OPEX) are estimated using an equipment factored estimating method for each route. The cost determining factors of the main process equipment is determined based on the simulation results, and subsequently, the purchasing cost for each item is retrieved. For standard equipment, e.g., heat exchangers or columns, cost equations have been adopted from Towler and Sinnott, [145] and Peters and Timmerhaus [146]. All purchasing costs have been updated for the year 2018 using the Chemical Engineering Plant Cost Index (CEPCI). Costs in US Dollar have been converted using the average exchange rate of 0.85 EUR/USD in 2018 and a location factor of 1.11 for Germany [145].

The purchasing costs are multiplied by cost factors accounting for additional charges, e.g., installation, power supply, engineering. For this study, cost factors have been taken from Peters and Timmerhaus [146]. A detailed overview of the applied cost factors is given in Appendix D. The working capital is estimated as 15% of the total capital investment. A plant lifetime of 20 years is assumed with a Weighted Average Cost of Capital (WACC) of 5%, resulting in a capital charge factor of 0.08, which is used to calculate the annuity.

Indirect OPEX costs are determined using factors from Peters and Timmerhaus [146]. Distribution and R&D costs are neglected to only account for costs directly linked to the production. The direct OPEX is calculated based on the material and energy balances of the process. It is assumed that generated steam can be sold for the same price as the buying costs. Steam and cooling costs vary depending on the steam pressure level and the employed cooling medium, cf. Table 9.

The labor costs are estimated based on Towler and Sinnott [145]. Three shift positions are assumed for a continuous fluid processing plant at a large site. To account for vacations and other employee absences, 4.5 shifts are assumed. This results in 13.5 operation positions with a working time of 37 h per week. A detailed overview of all considered OPEX factors and raw material costs, utility costs, and labor costs is given in Appendix D. The levelized product cost (LPC), including annuity on CAPEX and all OPEX, is calculated per t of produced OME.

**Table 9:** Steam and cooling cost depending on steam pressure level and employed cooling medium.

Pressure level	Cost/credit/ EUR/t
Steam 40 bar	23.5
Steam 20 bar	23.1
Steam 4 bar	22.8
Cooling medium	Cost / EUR/kWh
Cooling water	0.005
Chilled water	0.0075
Ammonia	0.015
Salt solutions	0.02
Salt solutions	0.025

A plant size of 100 kt OME production per year and a methanol cost of 401 EUR/t (average price Methanex 2018) are assumed as the base case. Variations of plant size and methanol cost are also considered.

The achieved cost estimates for the CAPEX are categorized as class 4 estimates by the American Association of Cost Engineering (AACE) International and usually provide a relative uncertainty of  $\pm 30\%$  [148]. The uncertainty in the levelized product cost for OME is smaller, as the current methanol cost is an input parameter. It follows as

$$\text{Rel.Uncertainty(LPC)} = \pm 30\% \left( 1 - \frac{\text{Raw material cost}}{\text{Total cost of production}} \right). \quad (49)$$

## 6.3 Results and discussion

### 6.3.1 Material balances

Detailed stream tables for all processes are given in Appendix D. The carbon yield of all investigated routes is given in Table 10 along with the other performance indicators. All routes perform similarly regarding carbon yield. There are rather small carbon losses in all routes because the dilute FA solutions are usually concentrated and recycled for maximum utilization. Therefore, the carbon yield is mainly determined by the yield of the FA plant and the FA reactor's selectivity. Consequently, routes with the same FA process (A1-A3, A4-A5) have similar carbon yields among them. Routes A1-A3, as well as routes A6 and A7, lead to approximately 0.93 mol/mol carbon yield. Routes A4 and A5 have a lower yield of 0.82 mol/mol due to a lower selectivity in the respective FA

reactor. Route A1\* is an exception and has significant losses in the FA concentration process. Despite the same FA production process as Routes A1-A3, it leads to a carbon yield of 0.88 mol/mol, 0.05 mol/mol lower. The carbon losses in the OME process are negligible for all routes.

**Table 10:** Key results for all routes for a plant size of 100 kt OME production per year and a methanol prize of 401 EUR/t.

Route	A1	A1*	A2	A3	A4	A5	A6	A7
Carbon yield / mol/mol	0.935	0.881	0.927	0.925	0.817	0.812	0.928	0.926
Heat demand / GJ /t OME	6.18	5.05	3.36	13.36	2.51	-1.11	6.57	8.70
CAPEX / Mio EUR	32.39	28.32	24.66	27.80	31.83	23.34	28.66	27.18
OPEX / Mio EUR / a	57.66	59.32	53.46	68.63	62.40	54.57	48.23	64.63
LCOP / EUR / t OME	597.26	611.30	550.31	704.13	644.41	560.43	500.69	662.98

### 6.3.2 Energy balance

Detailed tables of the energy balances for single units with respective temperature levels are given in Appendix D. Table 10 and Figure 18 show the overall heat demand per t OME from the steam network and the heat demand and excess per t OME at the respective temperature levels for the base case. Excess is displayed as a negative bar, demand as a positive bar. It shows the net heat demand at the steam levels 40, 20, and 4 bar (steam production and consumption) for all routes. Heat is integrated within every pressure level via the steam network, but not to lower pressure levels, as this would destroy exergy. LT cooling has to be provided at low temperatures below 25 °C. Due to the exothermic oxidation of methanol to formaldehyde, all routes provide large amounts of excess heat. For routes A1, A2, A4, A5, and A6, this excess heat would suffice to provide all required heat input in the FA production and concentration step. Furthermore, routes A2, A4, and A5 provide usable excess heat that can be integrated into the OME process via the steam network. Routes A3 and A7 have a higher heat demand; they require more heating and provide no excess heat for the OME process. Route A1\* has a very similar heat demand to Route A1, but the heat demand is at a lower temperature level.

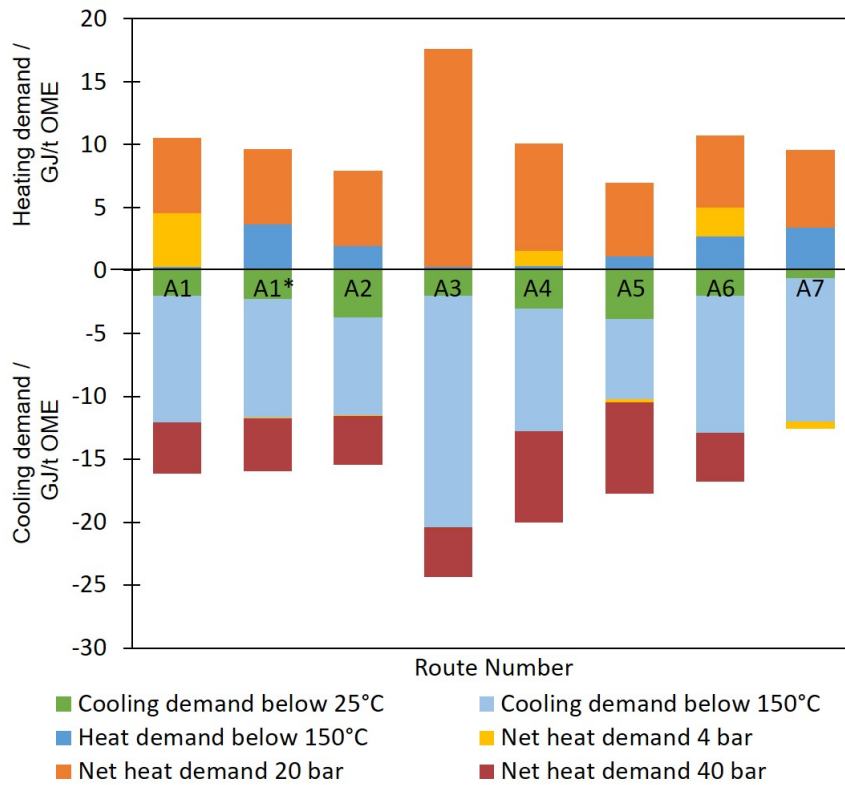


**Figure 18:** Net heat demand per t OME at every steam level (40, 20, 4 bar) for all routes. Excess heat is negative, heat demand positive.

### 6.3.3 Economics

#### 6.3.3.1 Base case

##### Equipment cost:

Figure 19 gives the estimated equipment costs of all routes for a plant of 100 kt OME production per year. The costs are broken down by equipment type. The most significant cost contributors are heat exchangers, distillation columns, and evaporators. The equipment costs in the OME process mainly stem from the two distillation columns. The estimated equipment costs for FA production and concentration vary widely between the investigated routes A1-A7, from 3.9 (Route A2) to 5.8 Mio (Route A1) EUR. Considering that CAPEX costs occur at the beginning of the project and constitute the capital at risk over time, the financial risk differs significantly between the process options.

Routes A1, A1\*, and A4 have high equipment costs, primarily due to the expensive thin-film evaporators. Routes A3, A6, and A7 have moderate costs. Their largest cost contributors are distillation columns and a large number of unit operations.

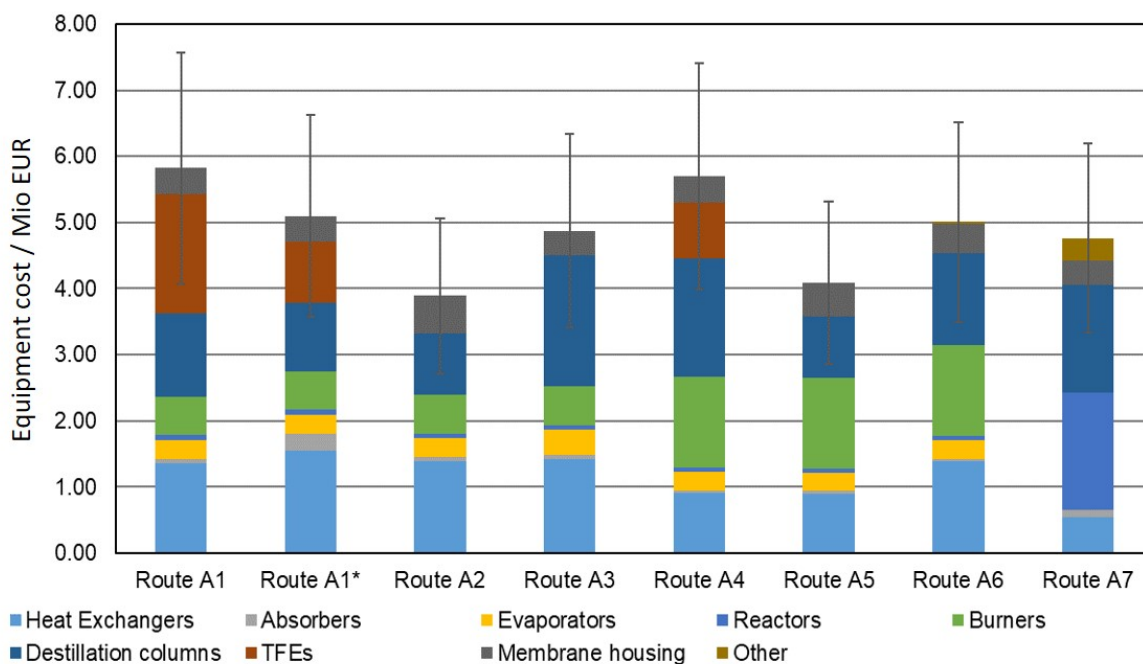


**Figure 19:** Equipment cost of all Routes for a plant size of 100 kt OME /a. The whiskers show the uncertainty in the total equipment cost for each route ( $\pm 30\%$  [148]).

Membrane units like they appear in Routes A2 and A5 have only a small contribution to the overall cost, making these routes cheap options. However, the high uncertainty regarding the membrane costs should be considered, and the membrane material has been treated as a consumable only considered in the OPEX. Despite its large number of units, Route A7 has a relatively low total equipment cost. The discussed differences in the equipment costs between the routes are correspondingly pronounced in the total CAPEX, cf. Table 10.

### Operational cost:

Figure 20 and Table 10 show the OPEX for a plant size of 100 kt OME per year and a methanol price of 401 EUR/t. It ranges from 48.2 (Route A6) to 68.6 (Route A3) Mio EUR per year for the routes.

The variance in the OPEX is less noticeable than in the CAPEX; this is mainly because the raw material costs cause nearly two-thirds of the entire OPEX. Raw material costs are followed by indirect OPEX cost, which summarizes several smaller indirect cost contributors and the operating labor cost. The differences between the routes arise from the differing carbon yields, utility consumptions, and potentials for steam generation. Routes A3, A4, and A7 show the highest OPEX. In Routes A3 and A7, this is due to high heat demand and a lack of significant steam revenue; in Route A4 due to carbon losses in the FA process. Routes A2, A5, and A6 show a low OPEX due to the low

costs for the employed pervaporation units. Note that membrane material replacement only accounts for 0.6% of the OPEX cost. Route A1\* has a slightly higher OPEX than Route A1 due to its higher carbon losses. For all routes, the annuity of the CAPEX only contributes around 4% to the manufacturing cost; the OPEX has a much larger share. This is partly caused by the rather low WACC and long plant lifetimes that were assumed. While this seems striking, comparable studies result in similar proportions of OPEX and CAPEX [10, 45].

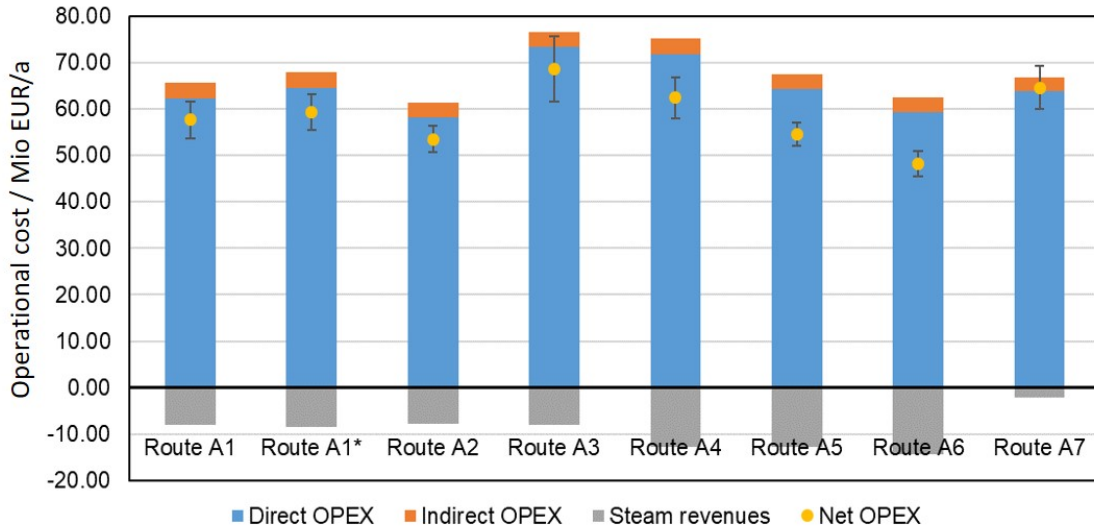


**Figure 20:** Operational cost / a of all routes for a plant size of 100 kt OME / a. The whiskers show the uncertainty in the operational costs.

### 6.3.3.2 Sensitivity studies

#### Manufacturing cost for OME:

The levelized product cost for OME was analyzed for variations of methanol cost and plant size in sensitivity studies. The LPC as a function of the methanol cost is shown in Figure 21 for a plant size of 100 kt OME<sub>3-5</sub>/a, the average LPC is:

$$\text{LPC}_{\text{OME}} = 79.07 \text{ EUR/t} + 1.31 * c_{\text{Methanol}} \text{ (EUR/t)} \quad (50)$$

Further, the minimum feasible manufacturing cost for OME ( $c_{\text{OME}}^{\text{min.}}$ ) is calculated based solely on the methanol cost and the stoichiometrically required methanol for the production of 1 t of OME (cf. Reactions (3), (13) to (14)).

$$c_{\text{OME}}^{\text{min.}} = 1.112 * c_{\text{Methanol}} \text{ (EUR/t)} \quad (51)$$



In order to better differentiate between routes, the minimum feasible manufacturing cost is subtracted from the LPC for routes A1 to A7. This yields the process-dependent cost ( $c_{\text{OME}}^{\text{PD}}$ ), cf. Figure 22.

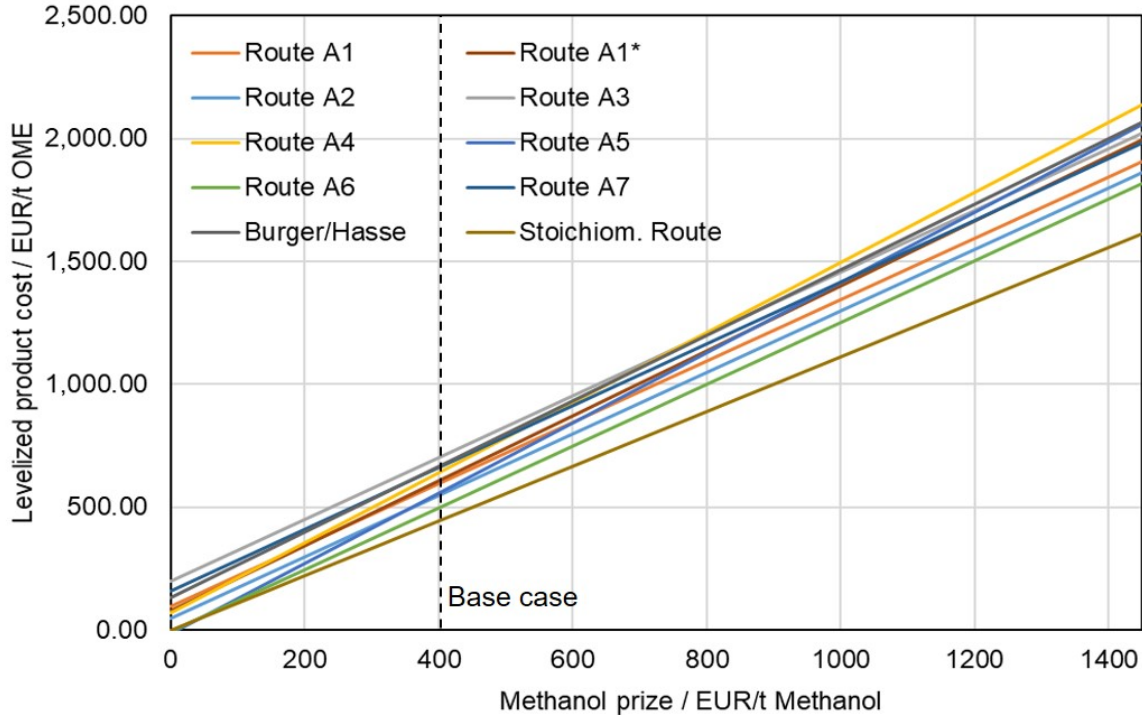


**Figure 21:** Levelized product cost per t OME for all routes as a function of the methanol cost for a plant size of 100 kt/a.

The y-intercept at 0 EUR/t methanol is determined by the fixed cost of the route, and the slope by its carbon yield. OME production via routes A2 and A6 is the cheapest for methanol costs higher than 350 EUR/t; both routes have a high carbon yield and low CAPEX and OPEX, and both routes employ pervaporation. Route A5 also employs pervaporation and has low costs for low ME costs, but the high carbon losses in the FA process II lead to high manufacturing costs for higher ME costs. Routes with considerable carbon losses, i.e., Routes A4 and A5 via their lower FA reactor selectivity and Route A1\* via the FA losses in the concentration process, show a larger slope. Therefore, they become less competitive with higher methanol costs. For lower ME costs, they perform reasonably well. Route A3 leads to the highest manufacturing cost for ME costs lower than 700 EUR/t. For higher costs, it is more economical than Routes A4 and A5 due to their significant carbon losses. Routes A1 and A7 both lead to mid-range costs for all methanol costs.

One should consider the significant uncertainty in the equipment cost estimation and that all graphs are close together. The uncertainty is less pronounced in the LPC due

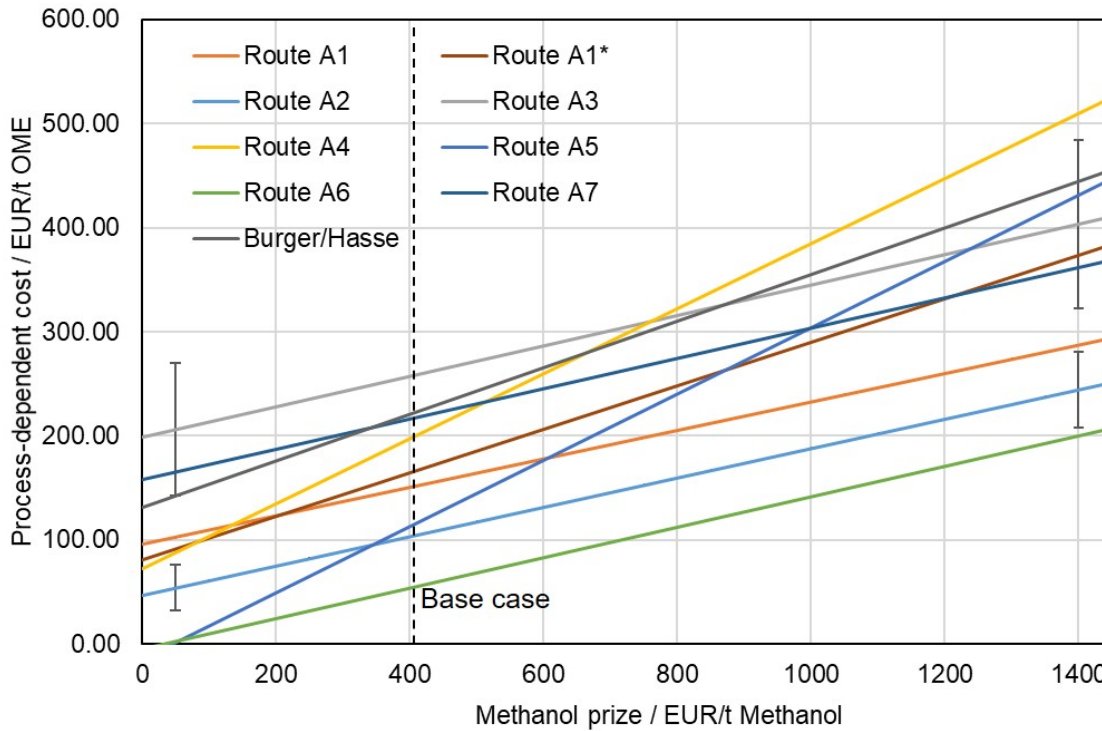


**Figure 22:** Process-dependent cost per t OME for all routes as a function of the methanol cost for a plant size of 100 kt/a.

to the large share of the ME cost but is still significant ( $\pm 30\%$  to  $\pm 1.5\%$ , depending on route and methanol cost). In Figure 22, where a large share of the methanol cost is already deducted, the uncertainty grows again. To visualize the size of the uncertainty, it is shown for Route A2 (smallest uncertainty) and Route A5 (largest uncertainty) for the methanol cost of 50 and 1400 EUR/t. For the base case (methanol costs of 401 EUR/t), the uncertainty is between  $\pm 5\%$  to  $\pm 10\%$ , depending on the route.

For this cost, the OME manufacturing cost range between 586 and 821 EUR/t. These results are in good agreement with other publications that analyze comparable routes. Burger and Hasse [46] give OME cost of 668 EUR/t for methanol costs of 401 EUR/t. Their results are also shown in Figure 21 and 22 for other methanol costs. Schmitz et al. give OME costs of 522 EUR/t for methanol costs of 255 EUR/t. For these methanol costs, our study results in slightly lower OME costs of 310 to 513 EUR/t. This is mainly due to lower carbon losses in the FA production and steam revenues. Compared with Route A1\*, which was suggested by Mantei et al., the improved thin-film evaporation in Route A1 saves 2.3% on the manufacturing cost for a methanol price of 401 EUR/t. For higher ME costs of up to 1500 EUR/t, these savings rise to 4.7%. While these savings are within the uncertainty, they result solely from the material balance, which is much less uncertain.

The influence of the plant size on the levelized product cost is also investigated in a sensitivity study for all routes. Figure 23 gives the results for the fixed methanol cost of 401 EUR/t.

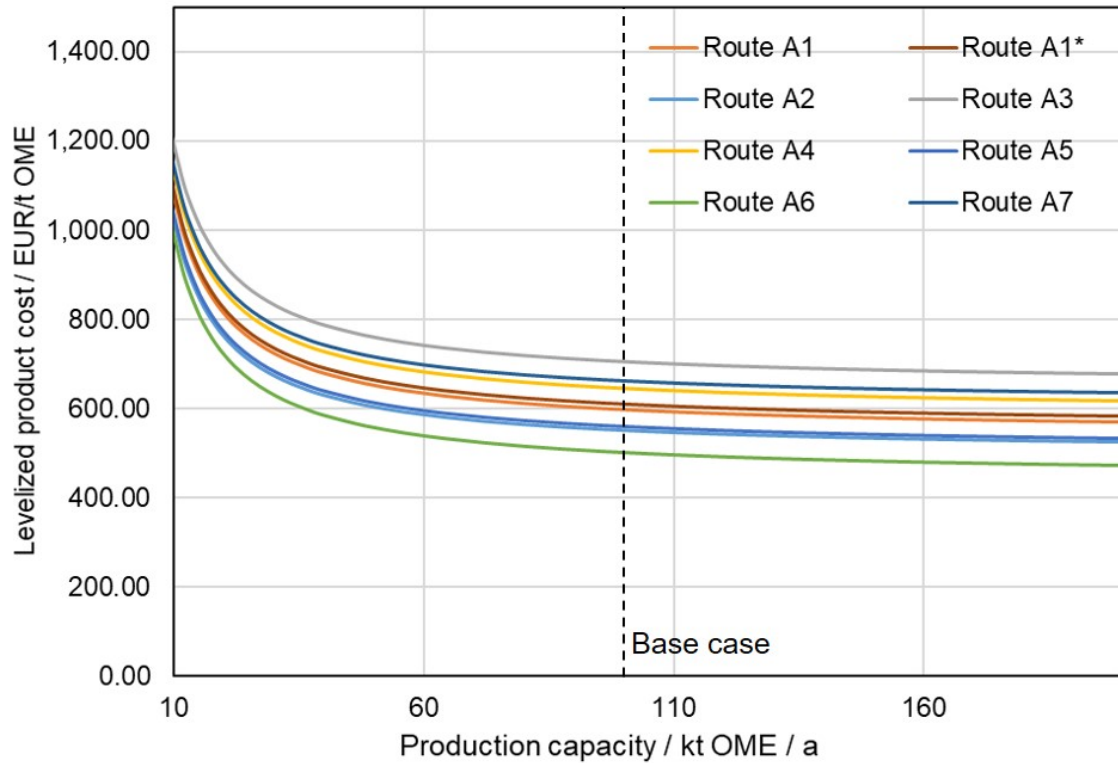


**Figure 23:** Levelized product cost per t OME for all routes as a function of the plant size for a ME cost of 401 EUR/t.

The levelized product cost increases drastically with smaller plant sizes for all routes. Below production capacities of 50,000 tons OME per year, the cost increase strongly. For larger production capacities, the raw material cost dominates all other cost contributors. The discussed differences between the routes hold for all plant sizes. However, note that the scale-up is simplified; it considers the increased cost via the unit size used as input for the cost correlation by Towler & Sinnott [145].

While this study achieves very good agreement with comparable works, there are some limitations to consider. First, the uncertainty stemming from the employed techno-economic has to be considered when evaluating the cost. Second, some aspects of the investigated technologies were deemed beyond the scope. The removal of wastewater was not considered here. While the removed wastewater is quite pure, it may cause further costs for some routes, which might not be negligible. Further, we assumed that all carbon should be converted to OME. Joint products could lead to lower production costs for OME. Of course, the involved processes could be improved further. For instance, the

FA reactor could be trimmed toward hydrogen recovery. There is also the possibility to use methanol or wastewater as an absorbent in the FA absorber, which could lower the water content of FA solutions [149]. Although these options were not considered in the present work, major cost reductions seem unlikely as the levelized product cost is determined mainly by the methanol cost.

## 7 Conclusion

Synthetic fuels have the potential to drastically reduce CO<sub>2</sub> emissions and help with the urgently needed climate change mitigation. Poly(oxymethylene) dimethyl ether (OME) in particular are much-discussed, as their boiling points are in the range of conventional diesel fuels, which allows for them to be applied swiftly without major changes to current internal combustion engines or filling station infrastructure. However, a couple of critical questions still had to be answered regarding their production, energetic efficiency, and cost.

To have a meaningful influence on CO<sub>2</sub> emission, OME production must have a high energetic efficiency in all processes required for their production from CO<sub>2</sub>. Therefore, the efficiency of OME<sub>3-5</sub> production from electrical energy and CO<sub>2</sub> was investigated for the whole process chain. Two routes A and B based on industrial processes were analyzed, and the influence of various levels of heat integration was discussed, considering the location of the different processes. For the provision of CO<sub>2</sub>, three different carbon capture (CC) technologies were included: pure CO<sub>2</sub> already being available, CO<sub>2</sub> from flue gas via post-combustion capture and CO<sub>2</sub> captured from air. Both Routes A and B are identical in their carbon balance. Regardless of the carbon source, 1.6 kg of CO<sub>2</sub> is bound in 1 kg product while approximately 1.83 kg CO<sub>2</sub> are required as raw material. The OME<sub>3-5</sub> production directly from ME and FA (Route A) without CC results in an energy demand between 52.1 and 60.0 MJ per kg OME<sub>3-5</sub>, depending on the level of heat integration. This equals an LHV efficiency of 31.3 to 36.3 %. The OME<sub>3-5</sub> production via the additional intermediates TRI and MAL (Route B) results in an energy demand between 51.6 and 64.8 MJ per kg OME<sub>3-5</sub>, depending on the level of heat integration. This equals an LHV efficiency of 29.2 to 36.7 %.

For no inter-processual heat integration, Route A clearly has the advantage of the lower energy demand of the individual processes. Route B, on the other hand, has more potential for inter-processual heat integration, which leads to the same LHV efficiency for the fully integrated process chain. However, to achieve this level of heat integration, substantial investment in a heat exchanger network would be necessary. In general, the OME<sub>3-5</sub> production via Route B would require a higher capital expenditure due to the larger number of processes and units.

Major energy demand drivers are hydrogen electrolysis and the OME<sub>3-5</sub> synthesis. An optimized electrolysis process would offer the biggest potential for an efficiency increase. Furthermore, there are big hydrogen losses in the ME and FA processes. Due to the conversion of hydrogen to water, there is a large amount of heat released in these two processes. This heat is used to cover the heating demand of all other processes in the process chain. A reduction of these losses in the ME and FA process would, therefore, only increase the efficiency of the process chain if the OME<sub>3-5</sub> synthesis would be improved as well.

The upper bound of the OME<sub>3-5</sub> production efficiency is given by the stoichiometric material balance and amounts to  $0.72 \cdot \eta_{\text{Electrolysis}}$  (and  $0.92 \cdot \eta_{\text{Electrolysis}}$  if FA could be supplied via direct dehydrogenation of ME).

When comparing current PtF technologies for  $\eta_{\text{Electrolysis}} = 60\%$ , the efficiency of the OME<sub>3-5</sub> production (36.3 %) ranks lower than most other e-fuels. Methane, dimethyl-ether, and ME show much better efficiencies (48.4 - 48.8 %), methylal and Fischer-Tropsch diesel production are more efficient too (40.0 % - 43.3 %). If hydrogen itself is considered as an e-fuel, it is obviously the most efficient as it only requires an electrolysis process (60 % in this comparison scenario) and is the basic feedstock of all other e-fuels. It is shown that the discussed results hold qualitatively for all electrolysis efficiencies.

Further, the provision of feedstocks for OME production, which, in contrast to OME production itself, is seldom discussed, has to be analyzed and optimized. These feedstocks are usually assumed to be available, but they are very challenging to produce. Therefore, a novel process for the provision of these solutions based on thin-film evaporation was designed and presented. A model for the simulation of thin-film evaporation of formaldehyde solutions containing both water and methanol was developed and validated for aqueous formaldehyde solutions. The model allows the analysis of a wide range of operating points for the concentration of methanolic, aqueous formaldehyde solutions in TFEs. While the underlying reaction kinetic [64] is reliable, the model currently remains predictive, and the extension to methanol should be validated by future experiments with TFEs. A process for the provision of methanolic FA solution of high yield and low water content was designed, simulated, and optimized. Two types of feed were considered; a mixture of FA, WA, and ME (Case I) and aqueous FA solution (Case II). The process consists of one distillation column to remove methanol as top product, a TFE that overcomes the azeotrope FA-WA and yields a highly concentrated FA solution as bottom product, and one distillation column operating at high pressure to remove pure water from the TFEs top product. In both cases, the simulations show the feasibility of the process. There are no significant losses of carbon. Small recycle streams (up to 0.36 times the product mass flow rate) allow for small process equipment and low

heat demand. The process has a small number of units, all of which are well-established in practice. Further, the results show that the presence of methanol in the TFE enables lower water contents in the product but also leads to a higher total heat demand. The minimum achievable water contents in the product are 0.092 g/g (Case I) and 0.118 g/g (Case II). For all water contents in the product larger than 0.118 g/g, Case II leads to a lower total heat demand. The minimum total heat demand for providing a methanolic FA solution to be used directly in existing processes for OME production is 3.29 MJ/kg. The model should be refined based on experiments in the future to better understand the complex correlation between heat duty, residence time, and pressure in TFEs and their influence on the product composition. Especially the interplay with the upstream FA plant reactors is highly interesting, as the product of such a plant can contain various amounts of formaldehyde, methanol, and water depending on the reactor conversion and selectivity.

Lastly, the cost-competitive production of OME is still a significant challenge in its acceptance. Previous studies on the economics of OME production only focus on one specific raw material for their production, often with a fixed price, or rely on strongly simplifying assumptions in their analysis. The present work presents the first techno-economic analysis that is based on a highly reliable process model and gives the cost of production for OME as a function of a variable methanol price and various plant sizes. The latter means that the results hold for future changes in the methanol price and are universally applicable independent of the raw material used for methanol production. Several (sub-)routes for OME production from methanol via the water-tolerant OME process (Route A) were investigated. Different technologies for removing water from formaldehyde solutions were evaluated, simulated, and compared. Techno-economic analysis was used to calculate the manufacturing cost of OME as a function of the methanol cost and plant size. Key performance indicators were identified, and all routes were compared. For a current methanol market cost of 401 EUR/t, the levelized product cost of OME range between 586 and 821 EUR/t. The routes using pervaporation result in the lowest levelized product cost for all methanol costs higher than 300 EUR/t. They have high carbon yields and low energy and investment costs. Routes that rely on extractive distillation result in high OME costs. For methanol costs up to 350 EUR/t, they result in the highest levelized product costs. For higher methanol costs, the routes with the highest carbon losses, based on one of the FA plants with incomplete conversion, become even more expensive. Processes based on pervaporation perform well, but there are still questions regarding the long-term stability of the membrane, and there is high uncertainty in the membrane cost. Thin-film evaporation performs reasonably well when combined with distillation for maximum FA recovery. Compared to previous

processes, the novel thin-film evaporation process saves costs of up to 4.7%. Extractive distillation is not recommended unless highly pure FA is required.

The most influential parameter on both energetic efficiency and costs of any route is the carbon yield. Thus, for future OME production, the selectivity in the ME and FA production process should be maximized, and the FA losses in the subsequent concentration and OME production should be minimized. Provided that there will be sufficient research and development in the future, OME<sub>3-5</sub> has the potential to become an economic alternative to conventional e-fuels. This holds in particular when considering other important fuel properties besides the efficiency, like the required logistics, the toxicity, or safety-related and ecological aspects.



# Literature

- [1] J. Burger, M. Siegert, E. Ströfer, H. Hasse: Poly(oxymethylene) dimethyl ethers as components of tailored diesel fuel: Properties, synthesis and purification concepts, *Fuel* 89 (2010) 3315–3319.
- [2] B. Lump, D. Rothe, C. Pastötter, R. Lämmermann, E. Jacob: Oxymethylene ethers as diesel fuel additives of the future, *MTZ worldwide eMagazine* 72 (2011) 34–38.
- [3] Q. Zhang, W. Wang, Z. Zhang, Y. Han, Y. Tan: Low-Temperature Oxidation of Dimethyl Ether to Polyoxymethylene Dimethyl Ethers over CNT-Supported Rhenium Catalyst, *Catalysts* 6 (2016) 43.
- [4] C. J. Baranowski, A. M. Bahmanpour, O. Kröcher: Catalytic synthesis of polyoxymethylene dimethyl ethers (OME): A review, *Applied Catalysis B: Environmental* 217 (2017) 407–420.
- [5] M. Härtl, P. Seidenspinner, E. Jacob, G. Wachtmeister: Oxygenate screening on a heavy-duty diesel engine and emission characteristics of highly oxygenated oxymethylene ether fuel OME1, *Fuel* 153 (2015) 328–335.
- [6] D. Pélerin, K. Gaukel, M. Härtl, G. Wachtmeister: Simplifying of the Fuel Injection System and lowest Emissions with the alternative Diesel Fuel Oxymethylene Ether, in: 16th Conference: The Working Process of the Internal Combustion Engine, Institute of Internal Combustion Engines and Thermodynamics, Graz University of Technology, Graz, 2017.
- [7] D. Pélerin, K. Gaukel, M. Härtl, G. Wachtmeister: Recent results of the sootless Diesel fuel oxymethylene ether, in: 4. International Motor Congress, Springer Vieweg, Wiesbaden, 2017, pp. 439–456. doi:10.1007/978-3-658-17109-4\\_28.
- [8] G. Centi, S. Perathoner: Opportunities and prospects in the chemical recycling of carbon dioxide to fuels, *Catalysis Today* 148 (2009) 191–205.

- [9] S. Schemme, R. C. Samsun, R. Peters, D. Stolten: Power-to-fuel as a key to sustainable transport systems - An analysis of diesel fuels produced from CO<sub>2</sub> and renewable electricity, *Fuel* 205 (2017) 198–221.
- [10] F. Mantei, R. E. Ali, C. Baensch, S. Voelker, P. Haltenort, J. Burger, R.-U. Dietrich, N. Von Der Assen, A. Schaadt, J. Sauer, O. Salem: Techno-economic assessment and Carbon footprint of processes for the large-scale production of Oxymethylene Dimethyl Ethers from Carbon Dioxide and Hydrogen, *Sustainable Energy & Fuels* 6 (2021) 528–549.
- [11] G. P. Hagen, M. J. Spangler: Preparation of polyoxymethylene dimethyl ethers by catalytic conversion of formaldehyde formed by oxidation of dimethyl ether. Patent US 6392102B1, 2000.
- [12] S. Blagov, H. Hasse, E. Ströfer: Polyoxymethylene dimethyl ether synthesis reaction process for product separation. Patent DE102005027701A, 2005.
- [13] Beijing Coreteam Engineering Technology Co. Ltd.: Patent CN102701923A (2012).
- [14] Kairui Environmental Technology Co. Ltd.: Patent CN205556510U, 2016.
- [15] Beijing Dongfang Hongsheng New Energy Application Technology Research Institute Co. Ltd.: Patent CN108164400A, 2018.
- [16] B. Niethammer, S. Wodarz, M. Betz, P. Haltenort, D. Oestreich, K. Hackbarth, U. Arnold, T. Otto, J. Sauer: Alternative Liquid Fuels from Renewable Resources, *Chemie-Ingenieur-Technik* 90 (2018) 99–112.
- [17] P. Haltenort, K. Hackbarth, D. Oestreich, L. Lautenschütz, U. Arnold, J. Sauer: Heterogeneously catalyzed synthesis of oxymethylene dimethyl ethers (OME) from dimethyl ether and trioxane, *Catalysis Communications* 109 (2018) 80–84.
- [18] L. Lautenschütz, D. Oestreich, P. Haltenort, U. Arnold, E. Dinjus, J. Sauer: Efficient synthesis of oxymethylene dimethyl ethers (OME) from dimethoxymethane and trioxane over zeolites, *Fuel Processing Technology* 165 (2017) 27–33.
- [19] D. Wang, F. Zhao, G. Zhu, C. Xia: Production of eco-friendly poly(oxymethylene) dimethyl ethers catalyzed by acidic ionic liquid: A kinetic investigation, *Chemical Engineering Journal* 334 (2018) 2616–2624.

- [20] X. Zhang, A. O. Oyedun, A. Kumar, D. Oestreich, U. Arnold, J. Sauer: An optimized process design for oxymethylene ether production from woody-biomass-derived syngas, *Biomass and Bioenergy* 90 (2016) 7–14.
- [21] A. O. Oyedun, A. Kumar, D. Oestreich, U. Arnold, J. Sauer: The development of the production cost of oxymethylene ethers as diesel additives from biomass, *Biofuels, Bioproducts and Biorefining* 12 (2018) 694–710.
- [22] J. Burre, D. Bongartz, S. Deutz, C. Mebrahtu, O. Osterthun, R. Sun, S. Völker, A. Bardow, J. Klankermayer, R. Palkovits, A. Mitsos: Comparing pathways for electricity-based production of dimethoxymethane as a sustainable fuel, *Energy & Environmental Science* 14 (2021) 3686–3699.
- [23] M. Martin, J. Redondo, I. E. Grossmann: Optimal Integrated Facility for Oxymethylene Ethers Production from Methanol, *ACS Sustainable Chemistry and Engineering* 8 (2020) 6496–6504.
- [24] O. Emenike, S. Michailos, K. J. Hughes, D. Ingham, M. Pourkashanian: Techno-economic and environmental assessment of BECCS in fuel generation for FT-fuel, bioSNG and OME x, *Sustainable Energy & Fuels* 5 (2021) 3382–3402.
- [25] H. Li, H. Song, L. Chen, C. Xia: Designed SO<sub>4</sub><sup>2-</sup>/Fe<sub>2</sub>O<sub>3</sub>-SiO<sub>2</sub> solid acids for polyoxymethylene dimethyl ethers synthesis: The acid sites control and reaction pathways, *Applied Catalysis B: Environmental* 165 (2015) 466–476.
- [26] Z. Xue, H. Shang, C. Xiong, C. Lu, G. An, Z. Zhang, C. Cui, M. Xu: Synthesis of polyoxymethylene dimethyl ethers catalyzed by sulfonic acid-functionalized mesoporous SBA-15, *RSC Advances* 7 (2017) 20300–20308.
- [27] J. Wu, H. Zhu, Z. Wu, Z. Qin, L. Yan, B. Du, W. Fan, J. Wang: High Si/Al ratio HZSM-5 zeolite: an efficient catalyst for the synthesis of polyoxymethylene dimethyl ethers from dimethoxymethane and trioxymethylene, *Green Chemistry* 17 (2015) 2353–2357.
- [28] G. Reuss, W. Disteldorf, A. O. Gamer, A. Hilt: Formaldehyde, in: *Ullmann's Encyclopedia of Industrial Chemistry*, Wiley-VCH Verlag GmbH & Co. KGaA, Weinheim, Germany, 2000.
- [29] N. Schmitz, J. Burger, H. Hasse: Reaction Kinetics of the Formation of Poly(oxymethylene) Dimethyl Ethers from Formaldehyde and Methanol in Aqueous Solutions, *Industrial & Engineering Chemistry Research* 54 (2015) 12553–12560.

- [30] Z. Han, C. Fu: Investigating the Effects of Water in Feedstock on the Energetic Efficiency of Producing Polyoxymethylene Dimethyl Ethers, *Applied Sciences* 10 (2020) 7474.
- [31] J. Zhang, D. Fang, D. Liu: Evaluation of Zr-Alumina in Production of Polyoxymethylene Dimethyl Ethers from Methanol and Formaldehyde: Performance Tests and Kinetic Investigations, *Industrial and Engineering Chemistry Research* 53 (2014) 13589–13597.
- [32] E. Ströfer, H. Hasse, S. Blagov: Verfahren zur herstellung von polyoxymethylendimethylethern aus methanol und formaldehyd. Patent WO2006134088, 2006.
- [33] M. Ott: Reaktionskinetik und Destillation formaldehydhaltiger Mischungen (Berichte aus der Verfahrenstechnik), Ph.D. thesis, 2004.
- [34] J. Artz, T. E. Müller, K. Thenert, J. Kleinekorte, R. Meys, A. Sternberg, A. Bardow, W. Leitner: Sustainable Conversion of Carbon Dioxide: An Integrated Review of Catalysis and Life Cycle Assessment, *Chemical Reviews* 118 (2017) 434–504.
- [35] G. J. Millar, M. Collins: Industrial Production of Formaldehyde Using Polycrystalline Silver Catalyst, *Industrial & Engineering Chemistry Research* 56 (2017) 9247–9265.
- [36] S. Deutz, D. Bongartz, B. Heuser, A. Kätelhön, L. Schulze Langenhorst, A. Omari, M. Walters, J. Klankermayer, W. Leitner, A. Mitsos, S. Pischinger, A. Bardow: Cleaner production of cleaner fuels: wind-to-wheel - environmental assessment of CO<sub>2</sub>-based oxymethylene ether as a drop-in fuel, *Energy & Environmental Science* 11 (2018) 331–343.
- [37] N. Mahbub, A. O. Oyedun, A. Kumar, D. Oestreich, U. Arnold, J. Sauer: A life cycle assessment of oxymethylene ether synthesis from biomass-derived syngas as a diesel additive, *Journal of Cleaner Production* 165 (2017) 1249–1262.
- [38] J. C. Abanades, E. S. Rubin, M. Mazzotti, H. J. Herzog: On the climate change mitigation potential of CO<sub>2</sub> conversion to fuels, *Energy & Environmental Science* 10 (2017) 2491–2499.
- [39] G. Centi, E. A. Quadrelli, S. Perathoner: Catalysis for CO<sub>2</sub> conversion: a key technology for rapid introduction of renewable energy in the value chain of chemical industries, *Energy & Environmental Science* 6 (2013) 1711–1731.

- 
- [40] M. Pérez-Fortes, J. C. Schöneberger, A. Boulamanti, E. Tzimas: Methanol synthesis using captured CO<sub>2</sub> as raw material: Techno-economic and environmental assessment, *Applied Energy* 161 (2016) 718–732.
- [41] T. Grützner, H. Hasse, N. Lang, M. Siegert, E. Ströfer: Development of a new industrial process for trioxane production, *Chemical Engineering Science* 62 (2007) 5613–5620.
- [42] J.-O. Drunsel, M. Renner, H. Hasse: Experimental study and model of reaction kinetics of heterogeneously catalyzed methylal synthesis, *Chemical Engineering Research and Design* 90 (2012) 696–703.
- [43] N. Schmitz, E. Ströfer, J. Burger, H. Hasse: Conceptual Design of a Novel Process for the Production of Poly(oxymethylene) Dimethyl Ethers from Formaldehyde and Methanol, *Industrial and Engineering Chemistry Research* 56 (2017) 11519–11530.
- [44] J. Burger, E. Ströfer, H. Hasse: Production process for diesel fuel components poly(oxymethylene) dimethyl ethers from methane-based products by hierarchical optimization with varying model depth, *Chemical Engineering Research and Design* 91 (2013) 2648–2662.
- [45] S. Schemme, J. L. Breuer, M. Köller, S. Meschede, F. Walman, R. C. Samsun, R. Peters, D. Stolten: H<sub>2</sub>-based synthetic fuels: A techno-economic comparison of alcohol, ether and hydrocarbon production, *International Journal of Hydrogen Energy* 45 (2020) 5395–5414.
- [46] J. Burger, H. Hasse: Processes for the production of OME fuels, in: *Internationaler Motorenkongress*. Springer Vieweg, Wiesbaden., Springer Vieweg, Wiesbaden, 2020. doi:10.1007/978-3-658-30500-0\_12.
- [47] N. Schmitz, J. Burger, E. Ströfer, H. Hasse: From methanol to the oxygenated diesel fuel poly(oxymethylene) dimethyl ether: An assessment of the production costs, *Fuel* 185 (2016) 67–72.
- [48] D. Oestreich, L. Lautenschütz, U. Arnold, J. Sauer: Production of oxymethylene dimethyl ether (OME)-hydrocarbon fuel blends in a one-step synthesis/extraction procedure, *Fuel* 214 (2018) 39–44.
- [49] M. Ouda, F. K. Mantei, M. Elmehlawy, R. J. White, H. Klein, S.-E. K. Fa-teen: Describing oxymethylene ether synthesis based on the application of non-

- stoichiometric Gibbs minimisation, *Reaction Chemistry & Engineering* 3 (2018) 277–292.
- [50] M. Drexler, P. Haltenort, U. Arnold, J. Sauer: Continuous Synthesis of Oxymethylene Ether Fuels from Dimethyl Ether in a Heterogeneously Catalyzed Liquid Phase Process, *Chemie Ingenieur Technik* 94 (2022) 256–266.
- [51] X. Zhang, A. Kumar, U. Arnold, J. Sauer: Biomass-derived Oxymethylene Ethers as Diesel Additives: A Thermodynamic Analysis, *Energy Procedia* 61 (2014) 1921–1924.
- [52] U. Arnold, J. Sauer, L. Lautenschütz, D. Oestreich: Production of Oxygenate Fuels from Biomass-derived Synthesis Gas: DGMK International Conference Synthesis Gas Chemistry, volume 2015,2 of *DGMK Tagungsbericht*, DGMK, Hamburg, 2015.
- [53] J. Thrane, U. V. Mentzel, M. Thorhauge, M. Høj, A. D. Jensen: A review and experimental revisit of alternative catalysts for selective oxidation of methanol to formaldehyde, *Catalysts* 11 (2021) 1329.
- [54] J. F. Walker: Formaldehyde, Reinhold Publishing Corporation, 1964.
- [55] I. Hahnenstein, M. Albert, H. Hasse, C. G. Kreiter, G. Maurer: NMR Spectroscopic and Densimetric Study of Reaction Kinetics of Formaldehyde Polymer Formation in Water, Deuterium Oxide, and Methanol, *Industrial and Engineering Chemistry Research* 34 (1995) 440–450.
- [56] H.-J. Mann, W. Pohl, K. Simon, W. Weigert: Production of free flowing paraformaldehyde. Patent US3595926A, 1969.
- [57] E. Ströfer, T. Gruetzner, H. Hasse, N. Lang, M. Ott: Verfahren zur erzeugung hochkonzentrierter formaldehydlösungen. Patent WO2004078678A3, 2003.
- [58] E. Ströfer, M. Sohn, H. Hasse, K. Schilling: Highly concentrated formaldehyde solution, production and reaction thereof. Patent US7193115B2, 2002.
- [59] N. Schmitz, C. F. Breitzkreuz, E. Ströfer, J. Burger, H. Hasse: Separation of water from mixtures containing formaldehyde, water, methanol, methylal, and poly(oxymethylene) dimethyl ethers by pervaporation, *Journal of Membrane Science* 564 (2018) 806–812.
- [60] A. Dams, A. Fried, F. Hammann: Verfahren zur Gewinnung konzentrierter wäßriger Formaldehydlösungen durch Pervaporation. Patent DE4337231A1, 1993.

- 
- [61] H. Morishita, J. Masamoto, T. Hata: Process for producing high purity formaldehyde. Patent US4962235A, 1989.
- [62] J.-O. Weidert, J. Burger, M. Renner, S. Blagov, H. Hasse: Development of an Integrated Reaction-Distillation Process for the Production of Methylal, *Industrial and Engineering Chemistry Research* 56 (2017) 575–582.
- [63] C. Kuhnert, M. Albert, S. Breyer, I. Hahnenstein, H. Hasse, G. Maurer: Phase Equilibrium in Formaldehyde Containing Multicomponent Mixtures: Experimental Results for Fluid Phase Equilibria of (Formaldehyde + (Water or Methanol) + Methylal)) and (Formaldehyde + Water + Methanol + Methylal) and Comparison with Predictions, *Industrial & Engineering Chemistry Research* 45 (2006) 5155–5164.
- [64] M. Ott, H. H. Fischer, M. Maiwald, K. Albert, H. Hasse: Kinetics of oligomerization reactions in formaldehyde solutions: NMR experiments up to 373K and thermodynamically consistent model, *Chemical Engineering and Processing: Process Intensification* 44 (2005) 653–660.
- [65] Department of Chemical Engineering, Brigham University, Provo, Utah: Thermophysical Properties Laboratory Project 801, *Thermophysical Properties Laboratory Project 801* (2009).
- [66] N. Schmitz: Production of poly(oxymethylene) dimethyl ethers from formaldehyde and methanol, Phd thesis, Technical University of Kaiserslautern, 2018.
- [67] M. Ouda, G. Yarce, R. J. White, M. Hadrich, D. Himmel, A. Schaadt, H. Klein, E. Jacob, I. Krossing: Poly(oxymethylene) dimethyl ether synthesis-A combined chemical equilibrium investigation towards an increasingly efficient and potentially sustainable synthetic route, *Reaction Chemistry and Engineering* 2 (2017) 50–59.
- [68] M. Ouda, F. Mantei, K. Hesterwerth, E. Bargiacchi, H. Klein, R. J. White: A hybrid description and evaluation of oxymethylene dimethyl ethers synthesis based on the endothermic dehydrogenation of methanol, *Reaction Chemistry & Engineering* 3 (2018) 676–695.
- [69] G. N. Tiwari, B. Agrawal: *Building Integrated Photovoltaic Thermal Systems: For Sustainable Developments*, Royal Society of Chemistry, 2022. doi:10.1016/c2019-0-02586-1.
- [70] B. Anicic, P. Trop, D. Goricanec: Comparison between two methods of methanol production from carbon dioxide, *Energy* 77 (2014) 279–289.

- [71] Z. Azizi, M. Rezaeimanesh, T. Tohidian, M. R. Rahimpour: Dimethyl ether: A review of technologies and production challenges, *Chemical Engineering and Processing: Process Intensification* 82 (2014) 150–172.
- [72] A. Tremel, P. Wasserscheid, M. Baldauf, T. Hammer: Techno-economic analysis for the synthesis of liquid and gaseous fuels based on hydrogen production via electrolysis, *International Journal of Hydrogen Energy* 40 (2015) 11457–11464.
- [73] M. Bertau, H. Offermanns, L. Plass, F. Schmidt, H.-J. Wernicke: *Methanol: The Basic Chemical and Energy Feedstock of the Future*, Springer Berlin Heidelberg, Berlin, Heidelberg, 2014.
- [74] W. Maus, E. Jacob, M. Härtl, P. Seidenspinner, G. Wachtmeister: Synthetic Fuels - OME1: A Potentially Sustainable Diesel Fuel, in: H. P. Lenz (Ed.), *35th International Motor Symposium in Vienna*, volume 777, VDI, Düsseldorf, 2014.
- [75] R. van Basshuysen, F. Schäfer: *Handbuch Verbrennungsmotor*, Springer Fachmedien Wiesbaden, Wiesbaden, 2015.
- [76] A. M. Bahmanpour, A. Hoadley, A. Tanksale: Critical review and exergy analysis of formaldehyde production processes, *Reviews in Chemical Engineering* 30 (2014).
- [77] S. Su, P. Zaza, A. Renken: Catalytic dehydrogenation of methanol to water-free formaldehyde, *Chemical Engineering & Technology* 17 (1994) 34–40.
- [78] E. Blass: *Entwicklung verfahrenstechnischer Prozesse: Methoden, Zielsuche, Lösungssuche, Lösungsauswahl*, *Chemische Technik / Verfahrenstechnik*, 2. ed., Springer, Berlin and Heidelberg, 1997.
- [79] J. D. Lewins: *Teaching Thermodynamics*, Springer, Boston, 1986.
- [80] G. D. Smith, R. L. Jaffe, D. Y. Yoon: Conformational Characteristics of 1,3-Dimethoxypropane and Poly(oxytrimethylene) Based upon ab Initio Electronic Structure Calculations, *The Journal of Physical Chemistry* 100 (1996) 13439–13446.
- [81] R. Socolow, M. Desmond, R. Aines, J. Blackstock, O. Bolland, T. Kaarsberg, L. Nathan, M. Mazzotti, A. Pfeffer, K. Sawyer, J. Sirola, B. Smit, J. Wilcox: *Direct Air Capture of CO<sub>2</sub> with Chemicals: A Technology Assessment for the APS Panel on Public Affairs*, 2011.



- 
- [82] X. Zhang, C. Bauer, C. L. Mutel, K. Volkart: Life Cycle Assessment of Power-to-Gas: Approaches, system variations and their environmental implications, *Applied Energy* 190 (2017) 326–338.
- [83] J. A. Wurzbacher, C. Gebald, N. Piatkowski, A. Steinfeld: Concurrent Separation of CO<sub>2</sub> and H<sub>2</sub>O from Air by a Temperature-Vacuum Swing Adsorption/Desorption Cycle, *Environmental Science & Technology* 46 (2012) 9191–9198.
- [84] J. A. Wurzbacher, C. Gebald, A. Steinfeld: Separation of CO<sub>2</sub> from air by temperature-vacuum swing adsorption using diamine-functionalized silica gel, *Energy & Environmental Science* 4 (2011) 3584.
- [85] M. Bui, C. S. Adjiman, A. Bardow, E. J. Anthony, A. Boston, S. Brown, P. S. Fennell, S. Fuss, A. Galindo, L. A. Hackett, J. P. Hallett, H. J. Herzog, G. Jackson, J. Kemper, S. Krevor, G. C. Maitland, M. Matuszewski, I. S. Metcalfe, C. Petit, G. Puxty, J. Reimer, D. M. Reiner, E. S. Rubin, S. A. Scott, N. Shah, B. Smit, J. P. M. Trusler, P. Webley, J. Wilcox, N. Mac Dowell: Carbon capture and storage (CCS): the way forward, *Energy & Environmental Science* 11 (2018) 1062–1176.
- [86] M. E. Boot-Handford, J. C. Abanades, E. J. Anthony, M. J. Blunt, S. Brandani, N. Mac Dowell, J. R. Fernández, M.-C. Ferrari, R. Gross, J. P. Hallett, R. S. Haszeldine, P. Heptonstall, A. Lyngfelt, Z. Makuch, E. Mangano, R. T. J. Porter, M. Pourkashanian, G. T. Rochelle, N. Shah, J. G. Yao, P. S. Fennell: Carbon capture and storage update, *Energy & Environmental Science* 7 (2014) 130–189.
- [87] A. Goeppert, M. Czaun, G. K. Surya Prakash, G. A. Olah: Air as the renewable carbon source of the future: An overview of CO<sub>2</sub> capture from the atmosphere, *Energy and Environmental Science* 5 (2012) 7833–7853.
- [88] P. Markewitz, W. Kuckshinrichs, W. Leitner, J. Linssen, P. Zapp, R. Bongartz, A. Schreiber, T. E. Müller: Worldwide innovations in the development of carbon capture technologies and the utilization of CO<sub>2</sub>, *Energy & Environmental Science* 5 (2012) 7281–7305.
- [89] X. Zhang, X. Zhang, H. Dong, Z. Zhao, S. Zhang, Y. Huang: Carbon capture with ionic liquids: overview and progress, *Energy & Environmental Science* 5 (2012) 6668–6681.
- [90] S. Brynolf, M. Taljegard, M. Grahn, J. Hansson: Electrofuels for the transport sector: A review of production costs, *Renewable and Sustainable Energy Reviews* 81 (2018) 1887–1905.

- [91] A. Buttler, H. Spliethoff: Current status of water electrolysis for energy storage, grid balancing and sector coupling via power-to-gas and power-to-liquids: A review, *Renewable and Sustainable Energy Reviews* 82 (2018) 2440–2454.
- [92] M. Carmo, D. L. Fritz, J. Mergel, D. Stolten: A comprehensive review on PEM water electrolysis, *International Journal of Hydrogen Energy* 38 (2013) 4901–4934.
- [93] M. Sterner, I. Stadler: *Energiespeicher: Bedarf, Technologien, Integration*, Springer Vieweg Berlin, Heidelberg, 2014.
- [94] A. Otto, T. Grube, S. Schiebahn, D. Stolten: Closing the loop: captured CO<sub>2</sub> as a feedstock in the chemical industry, *Energy & Environmental Science* 8 (2015) 3283–3297.
- [95] É. S. Van-Dal, C. Bouallou: Design and simulation of a methanol production plant from CO<sub>2</sub> hydrogenation, *Journal of Cleaner Production* 57 (2013) 38–45.
- [96] A. K. Kralj: Silver and oxide hybrids of catalysts during formaldehyde production, *Energy* 35 (2010) 2528–2534.
- [97] E. Ströfer, N. Lang, U. Lichtfers, U. Steinbrenner, H. Hasse: Separation of liquid mixtures in a film evaporator. Patent US7414159B2, 2003.
- [98] N. Schmitz, C. F. Breitkreuz, E. Ströfer, J. Burger, H. Hasse: Vapor-liquid equilibrium and distillation of mixtures containing formaldehyde and poly(oxymethylene) dimethyl ethers, *Chemical Engineering and Processing - Process Intensification* 131 (2018) 116–124.
- [99] U. Sander, P. Soukup: Design and operation of a pervaporation plant for ethanol dehydration, *Journal of Membrane Science* 36 (1988) 463–475.
- [100] B. K. Srinivas, M. M. El-Halwagi: Optimal design of pervaporation systems for waste reduction, *Computers & Chemical Engineering* 17 (1993) 957–970.
- [101] R. J. Detz, J. N. H. Reek, B. C. C. van der Zwaan: The future of solar fuels: when could they become competitive?, *Energy & Environmental Science* 11 (2018) 1653–1669.
- [102] M. R. Shaner, H. A. Atwater, N. S. Lewis, E. W. McFarland: A comparative technoeconomic analysis of renewable hydrogen production using solar energy, *Energy & Environmental Science* 9 (2016) 2354–2371.

- 
- [103] A. Sternberg, A. Bardow: Power-to-What? - Environmental assessment of energy storage systems, *Energy & Environmental Science* 8 (2015) 389–400.
- [104] M. Fasihi, C. Breyer: Synthetic Methanol and Dimethyl Ether Production based on Hybrid PV-Wind Power Plants, in: 11th IRES Conference, Düsseldorf, 2017.
- [105] F. G. Albrecht, D. H. König, N. Baucks, R.-U. Dietrich: A standardized methodology for the techno-economic evaluation of alternative fuels - A case study, *Fuel* 194 (2017) 511–526.
- [106] H. Blanco, A. Faaij: A review at the role of storage in energy systems with a focus on Power to Gas and long-term storage, *Renewable and Sustainable Energy Reviews* 81 (2018) 1049–1086.
- [107] D. Mignard: Methanol synthesis from flue-gas CO<sub>2</sub> and renewable electricity: A feasibility study, *International Journal of Hydrogen Energy* 28 (2003) 455–464.
- [108] E. Tsupari, J. Kärki, E. Vakkilainen: Economic feasibility of power-to-gas integrated with biomass fired CHP plant, *Journal of Energy Storage* 5 (2016) 62–69.
- [109] M. Götz, J. Lefebvre, F. Mörs, A. McDaniel Koch, F. Graf, S. Bajohr, R. Reimert, T. Kolb: Renewable Power-to-Gas: A technological and economic review, *Renewable Energy* 85 (2016) 1371–1390.
- [110] R. J. Pearson, M. D. Eisaman, J. W. G. Turner, P. P. Edwards, Z. Jiang, V. L. Kuznetsov, K. A. Littau, L. di Marco, S. R. G. Taylor: Energy Storage via Carbon-Neutral Fuels Made From CO<sub>2</sub>, Water, and Renewable Energy, *Proceedings of the IEEE* 100 (2012) 440–460.
- [111] T. Schulzke: Synergies from Direct Coupling of Biomass-to-Liquid and Power-to-Liquid Plants, *Chemical Engineering & Technology* 40 (2017) 254–259.
- [112] D. Bongartz, J. Burre, A. Mitsos: Production of Oxymethylene Dimethyl Ethers from Hydrogen and Carbon Dioxide - Part I: Modeling and Analysis for OME1, *Industrial and Engineering Chemistry Research* 58 (2019) 4881–4889.
- [113] J. Burre, D. Bongartz, A. Mitsos: Production of Oxymethylene Dimethyl Ethers from Hydrogen and Carbon Dioxide - Part II: Modeling and Analysis for OME3-5, *Industrial and Engineering Chemistry Research* 58 (2019) 5567–5578.
- [114] J. Burre, D. Bongartz, A. Mitsos: Erratum: Production of Oxymethylene Dimethyl Ethers from Hydrogen and Carbon Dioxide-Part I: Modeling and Analysis for OME1 & Part II: Modeling and Analysis for OME3-5 (*Ind. Eng. Chem.*

- Res. (2019) 58: 14 (5567-5578) DOI: 10.1021/acs.iecr.8b05577), *Industrial and Engineering Chemistry Research* 59 (2020) 21615–21616.
- [115] Y. Wang, L. Zhao, A. Otto, M. Robinius, D. Stolten: A Review of Post-combustion CO<sub>2</sub> Capture Technologies from Coal-fired Power Plants, *Energy Procedia* 114 (2017) 650–665.
- [116] M. Bortz, J. Burger, N. Asprion, S. Blagov, R. Böttcher, U. Nowak, A. Scheithauer, R. Welke, K. H. Küfer, H. Hasse: Multi-criteria optimization in chemical process design and decision support by navigation on Pareto sets, *Computers and Chemical Engineering* 60 (2014) 354–363.
- [117] J. A. Herron, J. Kim, A. A. Upadhye, G. W. Huber, C. T. Maravelias: A general framework for the assessment of solar fuel technologies, *Energy & Environmental Science* 8 (2015) 126–157.
- [118] J. Kim, C. A. Henao, T. A. Johnson, D. E. Dedrick, J. E. Miller, E. B. Stechel, C. T. Maravelias: Methanol production from CO<sub>2</sub> using solar-thermal energy: process development and techno-economic analysis, *Energy & Environmental Science* 4 (2011) 3122.
- [119] J. Kim, T. A. Johnson, J. E. Miller, E. B. Stechel, C. T. Maravelias: Fuel production from CO<sub>2</sub> using solar-thermal energy: system level analysis, *Energy & Environmental Science* 5 (2012) 8417.
- [120] I. Dimitriou, P. García-Gutiérrez, R. H. Elder, R. M. Cuéllar-Franca, A. Azapagic, R. W. K. Allen: Carbon dioxide utilisation for production of transport fuels: process and economic analysis, *Energy & Environmental Science* 8 (2015) 1775–1789.
- [121] N. Schmitz, F. Homberg, J. Berje, J. Burger, H. Hasse: Chemical Equilibrium of the Synthesis of Poly(oxymethylene) Dimethyl Ethers from Formaldehyde and Methanol in Aqueous Solutions, *Industrial & Engineering Chemistry Research* 54 (2015) 6409–6417.
- [122] C. W. Demuth: Process for producing methanol-formaldehyde solution of low-water content. Patent US3629997A, 1970.
- [123] T. Grützner, H. Hasse: Solubility of formaldehyde and trioxane in aqueous solutions, *Journal of Chemical and Engineering Data* 49 (2004) 642–646.

- 
- [124] W. Ma, Y. Hu, H. Wang, D. Zhao: The effects of typical salts, acids and ionic liquids on the solubility of formaldehyde in aqueous solutions, *Fluid Phase Equilibria* 460 (2018) 51–56.
- [125] M. Ott, H. Schoenmakers, H. Hasse: Distillation of formaldehyde containing mixtures: Laboratory experiments, equilibrium stage modeling and simulation, *Chemical Engineering and Processing: Process Intensification* 44 (2005) 687–694.
- [126] J. Masamoto, J. Ohtake, M. Kawamura: Process for producing formaldehyde and derivatives thereof. Patent US4967014, 1989.
- [127] H. H. Thigpen, R. J. Clos: Method of manufacture for paraformaldehyde prills. Patent US40550213, 1985.
- [128] H. Vandenmersch, T. Sirch, C. Hittinger, E. Danz: Verfahren zur Herstellung von alkoholischen Formaldehydlösungen mittels Membrantrennverfahren. Patent DE10004562A1, 2000.
- [129] A. Ferre, J. Burger: Coadsorption Equilibria on Molecular Sieves 3A and Densities of Liquid Mixtures Containing Formaldehyde, Methanol, and Water at 295.15 and 313.15 K, *Industrial and Engineering Chemistry Research* 60 (2021) 15256–15263.
- [130] L. Eek Vancells: Method for producing stabilized solutions of formaldehyde with methanol. Patent EP0434783B1, 1990.
- [131] D. L. Klopper, L. G. Stevenson: Method for making alcoholformaldehyde product. Patent US3214891A, 1965.
- [132] S. Jahnke, K. Jasch, S. Scholl: Wiped film evaporators: Segmental assessment of wetting behavior and heat transfer performance, *Chemical Engineering Research and Design* 163 (2020) 67–75.
- [133] K. Jasch, T. Grützner, G. Rosenthal, S. Scholl: Experimental investigation of the residence time behavior of a wiped film evaporator, *Chemical Engineering Research and Design* 165 (2021) 162–171.
- [134] D. Appelhaus, K. Jasch, S. Jahnke, H. Hassani Khab Bin, W. Tegethoff, J. Köhler, S. Scholl: A new approach to simulate the fluid dynamics in a wiped film evaporator using Modelica, *Chemical Engineering Research and Design* 161 (2020) 115–124.

- [135] K. Schilling, M. Sohn, E. Ströfer, H. Hasse: Reaktive Verdampfung formaldehydhaltiger Mischungen und Process Monitoring mit Online-NMR-Spektroskopie, *Chemie Ingenieur Technik* 75 (2003) 240–244.
- [136] N. Asprion, S. Blagov, O. Ryll, R. Welke, A. Winterfeld, A. Dittel, M. Bortz, K. H. Küfer, J. Burger, A. Scheithauer, H. Hasse: Pareto-Navigation in Chemical Engineering, *Computer Aided Chemical Engineering* 29 (2011) 422–426.
- [137] R. Marler, J. Arora: Survey of multi-objective optimization methods for engineering, *Structural and Multidisciplinary Optimization* 26 (2004) 369–395.
- [138] Y. Haimes, L. Lasdon, D. Dang: On a bicriterion formation of the problems of integrated system identification and system optimization, *IEEE Transactions on Systems, Man and Cybernetics SMC-1* (1971) 296–297.
- [139] C.-L. Hwang, A. S. M. Masud: Multiple Objective Decision Making - Methods and Applications, volume 164 of *Lecture Notes in Economics and Mathematical Systems*, Springer Berlin Heidelberg, Berlin, Heidelberg, 1979. doi:10.1007/978-3-642-45511-7.
- [140] P. Stephan, S. Kabelac, M. Kind, D. Mewes, K. Schaber, T. Wetzel: VDI-Wärmeatlas: Fachlicher Träger VDI-Gesellschaft Verfahrenstechnik und Chemieingenieurwesen, Springer-Verlag Berlin Heidelberg, 2019.
- [141] J. Frédéric Bonnans, J. Charles Gilbert, C. Lemaréchal, C. A. Sagastizábal: Numerical optimization: Theoretical and practical aspects, Springer Berlin Heidelberg, 2006.
- [142] R. Smith: Chemical Process Design and Integration, John Wiley & Sons, Ltd, 2005.
- [143] G. Maurer: Vapor-liquid equilibrium of formaldehyde-and water-containing multicomponent mixtures, *AIChE Journal* 32 (1986) 932–948.
- [144] R. Kircher, N. Schmitz, J. Berje, K. Münnemann, W. R. Thiel, J. Burger, H. Hasse: Generalized Chemical Equilibrium Constant of Formaldehyde Oligomerization, *Industrial & Engineering Chemistry Research* 59 (2020) 11431–11440.
- [145] G. Towler, R. K. Sinnott: Chemical engineering design: principles, practice and economics of plant and process design, Elsevier, 2012.
- [146] M. S. Peters, K. D. Timmerhaus, R. E. West: Plant Design and Economics for Chemical Engineers 5th Edition, volume 369, McGraw-Hill, 2003.

- 
- [147] A. Ferre, J. Voggenreiter, Y. Tönges, J. Burger: Demonstrationsanlage für die Synthese von OME-Kraftstoffen, *MTZ - Motortechnische Zeitschrift* 82 (2021) 28–33.
- [148] P. Christensen, L. R. Dysert: Cost Estimate Classification system-as applied in engineering, procurement, and construction for the process industries - TCM Framework: 7.3 - Cost Estimating and Budgeting, AACE International Recommended Practice No. 18R-97 (2005) 1–9.
- [149] S. Schemme, S. Meschede, M. Köller, R. C. Samsun, R. Peters, D. Stolten: Property Data Estimation for Hemiformals, Methylene Glycols and Polyoxymethylene Dimethyl Ethers and Process Optimization in Formaldehyde Synthesis, *Energies* 13 (2020) 3401.
- [150] M. Albert: Thermodynamische Eigenschaften formaldehydhaltiger Mischungen, Phd thesis, 1999.
- [151] A. Lydersen: Estimation of critical properties of organic compounds by the method of group contributions, University of Wisconsin, Madison, 1955.
- [152] J. Burger: A novel process for the production of diesel fuel additives by hierarchical design, Phd thesis, Technical University of Kaiserslautern, 2012.
- [153] M. Albert, H. Hasse, C. Kuhnert, G. Maurer: New Experimental Results for the Vapor-Liquid Equilibrium of the Binary System (Trioxane + Water) and the Ternary System (Formaldehyde + Trioxane + Water), *Journal of Chemical & Engineering Data* 50 (2005) 1218–1223.
- [154] R. Boyd: Some Physical Properties of Polyoxymethylene Dimethyl Ethers, *Journal of Polymer Science* (1961) 133–141.
- [155] J. Marrero-Morejón, E. Pardillo-Fontdevila: Estimation of pure compound properties using group-interaction contributions, *AIChE Journal* 45 (1999) 615–621.
- [156] E. J. Novek, E. Shaulsky, Z. S. Fishman, L. D. Pfefferle, M. Elimelech: Low-Temperature Carbon Capture Using Aqueous Ammonia and Organic Solvents, *Environmental Science & Technology Letters* 3 (2016) 291–296.
- [157] B. E. Launder, J. M. T. Thompson: Capturing CO<sub>2</sub> from the atmosphere: rationale and process design considerations, Cambridge Univ. Press, 2010.

- [158] T. Kuramochi, A. Ramírez, W. Turkenburg, A. Faaij: Comparative assessment of CO<sub>2</sub> capture technologies for carbon-intensive industrial processes, *Progress in Energy and Combustion Science* 38 (2012) 87–112.
- [159] Climeworks AG: Website of Climeworks AG, 2017. URL: <http://www.climeworks.com/>.
- [160] S. Schiebahn, T. Grube, M. Robinius, V. Tietze, B. Kumar, D. Stolten: Power to gas: Technological overview, systems analysis and economic assessment for a case study in Germany, *International Journal of Hydrogen Energy* 40 (2015) 4285–4294.
- [161] V. Schröder: Explosionsgrenzen von Wasserstoff und Wasserstoff/Methan-Gemischen, Technical Report, Bundesanstalt für Materialforschung und -prüfung (BAM), 2002.
- [162] X. Liu, Y. Huang, Y. Wang, Q. Zhang: Critical explosible oxygen concentration of methanol-saturated vapor/O<sub>2</sub>/N<sub>2</sub> mixtures at elevated temperatures and pressures, *Industrial and Engineering Chemistry Research* 53 (2014) 5617–5621.
- [163] M. Qian, M. A. Liauw, G. Emig: Formaldehyde synthesis from methanol over silver catalysts, *Applied Catalysis A: General* 238 (2003) 211–222.
- [164] L. M. Vane, F. R. Alvarez: Effect of membrane and process characteristics on cost and energy usage for separating alcohol-water mixtures using a hybrid vapor stripping-vapor permeation process, *Journal of Chemical Technology and Biotechnology* 90 (2015) 1380–1390.
- [165] C. Lipski, P. Coté: The use of pervaporation for the removal of organic contaminants from water, *Environmental Progress* 9 (1990) 254–261.
- [166] Sigma-Aldrich: Polyethylene glycol 400 data sheet, 2020. URL: <https://pubchem.ncbi.nlm.nih.gov/substance/24852060>.
- [167] Chemical Engineering Plant Cost Index, 2021. URL: <https://www.chemengonline.com/pci-home>.
- [168] Statista: Avg. Exchange Rate Euro/Dollar, 2021. URL: <https://de.statista.com/statistik/daten/studie/200194/umfrage/wechselkurs-des-euro-gegenueber-dem-us-dollar-seit-2001/>.



- [169] Methanex: Methanex Monthly Average Regional Posted Contract Price History, 2020. URL: <https://www.methanex.com/sites/default/files/MxAvgPriceNov302021.xls>.
- [170] Monitoringbericht 2018, 2018. URL: [BundesnetzagenturMonitoringbericht2018](#).
- [171] R. Turton: Analysis, synthesis, and design of chemical processes, Prentice Hall PTR international series in the physical and chemical engineering sciences, 3rd ed., Prentice Hall, Upper Saddle River, N.J, 2009.



# A Appendix: Property model

## A.1 Model of physico-chemical properties

### A.1.1 FA synthesis and concentration, MAL synthesis

Correlations for the vapor pressures (MAL[63], FA[63], MG<sub>n</sub>[63], HF<sub>n</sub>[63], WA[63]) were adopted from literature. The same holds for enthalpies of vaporization (FA[65], MAL [65], ME[150], WA[150], FA [150]) and the ideal gas heat capacities (FA[65], MAL[65], ME [150], WA[150], , FA[150]). Enthalpies of formation are adopted from the literature as well (FA[65], MAL[65], ME[63], WA[63]). The UNIFAC parameters of the activity model for the system WA, FA, ME, MG, HF, MAL are adopted from Kuhnert et al. [63]. The activity-based equilibrium constants  $K_a$  of the formation of MG<sub>n</sub> and HF<sub>n</sub> are also adopted from Kuhnert et al. [63]. For thin-film evaporators, the reaction kinetics in the liquid phase are modeled as described by Ott et al. [64] For the noncondensable gases N<sub>2</sub>, O<sub>2</sub>, CO, CO<sub>2</sub>, H<sub>2</sub>, property data for vapor pressures, enthalpies of formation in the gas phase, enthalpies of vaporization, ideal gas heat capacities are adopted from the DIPPR database [65]. Gas solubilities are neglected for these components.

We found no consistent enthalpy model readily available for the MG<sub>n</sub> and HF<sub>n</sub>. Therefore one is derived based on their vapor pressure and the activity-based equilibrium constants  $K_a$  of the formation of MG<sub>n</sub> and HF<sub>n</sub> [63]. A similar procedure to the following for the derivation of this enthalpy model has already been described by Bongartz et al. [112]

All specific enthalpies are normalized to the enthalpy of formation  $h_i^f(T^\theta)$  in the gaseous state at standard temperature  $T^\theta$  and are calculated based on the following equations :

$$h_i(T_1) = h_i^f(T^\theta) + \int_{T^\theta}^{T_1} c_{p,i}^g dT \quad (52)$$

for gaseous streams, and

$$h_i(T_1) = h_i^f(T^\theta) + \int_{T^\theta}^{T_1} c_{p,i}^g dT - \Delta h_{v,i}(T_1) \quad (53)$$

for liquid streams. Pressure dependence of the enthalpies is neglected.  $c_{p,i}^l$  and  $c_{p,i}^g$  are the isobaric, specific heat capacities in the liquid and gaseous phase, respectively.  $\Delta h_{v,i}$  denotes the enthalpy of vaporization.

The enthalpy of vaporization of  $\text{MG}_1$  and  $\text{HF}_1$  is estimated from their vapor pressure via the Clausius Clapeyron equation assuming an ideal gas phase and negligible liquid volume

$$\frac{1}{p} dp = \frac{\Delta h_{v,i}}{RT^2} dT. \quad (54)$$

The reaction enthalpies  $\Delta_R h(T)$  of Reactions (7) to (12) in the main document for the formation of  $\text{MG}/\text{HF}$  in the liquid phase are calculated from the respective equilibrium constant  $K_a$  via the Van-'t-Hoff-equation:

$$\left( \frac{\partial \ln K_a}{\partial T} \right) = \frac{\Delta_R h(T)}{RT^2}. \quad (55)$$

The specific enthalpies of all  $\text{MG}/\text{HF}$  species in the liquid phase

$$h_{\text{MG}_n}^{liq}(T) = \Delta_R^{liq} h_{\text{MG}_n}(T) + h_{\text{MG}_{n-1}}^{liq}(T) + h_{\text{FA}}^{liq}(T) \quad (56)$$

( $\text{HF}$  analogously) and the enthalpies of  $\text{MG}_1$  and  $\text{HF}_1$  in the gaseous phase are calculated for multiple temperatures in the range of 298.15 K to 415.15 K. This also yields the standard enthalpies of formation (at 298.15 K) for  $\text{MG}_1$  and  $\text{HF}_1$  in the gaseous phase and  $\text{MG}/\text{HF}_{n>1}$  in the liquid phase. Heat capacities are fitted for  $\text{MG}_1$  and  $\text{HF}_1$  in the gaseous phase and  $\text{MG}/\text{HF}_{n>1}$  in the liquid phase so that the enthalpies in the temperature range can be calculated using Eq. (53) instead of Eq. (56). The heat capacities are fitted to a polynomial that meets the required input format of Aspen:

$$c_p/\text{J/molK} = A + BT + CT^2 + DT^3 + ET^4. \quad (57)$$

The enthalpies of  $\text{MG}/\text{HF}_{n>1}$  in the gas phase are not required since they are assumed to be always liquid due to their very low vapor pressure. The critical temperatures  $T_c(\text{MG}_1)$  and  $T_c(\text{HF}_1)$  are estimated with the method of Lyderson. Parameters for all used correlations are given in Section A.2

### A.1.2 OME synthesis, TRI synthesis

The property model used for the OME synthesis in Route A is adopted from Schmitz [66], which has slight differences to the model used for FA and MAL synthesis, cf. Tables 11 and 12. This model is also used for the estimation of the energy balances of the TRI

and OME synthesis in Route B in Chapter 4.

## A.2 Property data parameter values

Table 11 and 12 give the parameters for the chemical equilibrium constants in the system FA, WA and ME without and with OME present. Table 13 gives the critical temperatures and enthalpy of formation for all components. Table 14 gives the vapor pressure of all vaporizable components, Table 15 the enthalpy of vaporization. Tables 16 and 17 give the heat capacities in the gas and liquid phase respectively. Table 18 gives the molar liquid density of all components. For the activity model all UNIFAC parameters are adopted from Schmitz [66].

The chemical equilibrium constants are correlated by Eq. (58).

$$\ln(K) = A + \frac{B}{T} + C * \ln(T) + D * T \quad (58)$$

**Table 11:** Parameters for the correlation of the chemical equilibrium constants (cf. Eq. (58)) in the system FA, WA and ME (without OME present).

Reaction	$A$	$B$	$C$	$D$	Source
Eq. (7)	-30.946	4819.00	3.741	-0.004534	[66]
Eq. (8)	-30.941	5653.00	3.741	-0.004534	[66]
Eq. (9)	-30.933	5361.00	3.741	-0.004534	[66]
Eq. (10)	1130.100	-25100.00	- 198.400	0.316	Refit to Kuhnert et al.[63]
Eq. (11)	1129.500	-25510.00	- 198.400	0.316	Refit to Kuhnert et al.[63]
Eq. (12)	1129.600	-25630.00	- 198.400	0.316	Refit to Kuhnert et al.[63]

**Table 12:** Parameters for the correlation of the chemical equilibrium constants (cf. Eq. (58)) in the system FA, WA, ME and OME<sub>n</sub>. Note that the activity-based equilibrium constants  $K_a$  of the formation of MG<sub>n</sub> and HF<sub>n</sub> from Schmitz [66] differ slightly from those by Kuhnert et al. [63], this seemingly slight difference is crucial if OME is present in FA solutions.

Reaction	$A$	$B$	$C$	$D$	Source
Eq. (7)	-30.946	4819.00	3.741	-0.004534	[66]
Eq. (8)	-30.941	5653.00	3.741	-0.004534	[66]
Eq. (9)	-30.933	5361.00	3.741	-0.004534	[66]
Eq. (10)	1129.700	-25100.00	- 198.400	0.316	[66]
Eq. (11)	1129.000	-25510.00	- 198.400	0.316	[66]
Eq. (12)	1129.000	-25630.00	- 198.400	0.316	[66]
Eq. (13)	0.628	745.73			[66]
Eq. (14)	-9.055	4843.60			[66]

**Table 13:** Critical temperatures and enthalpies of formation of all components. \*: Critical temperature estimated with method of Lydersen [151].

Component	$T_c$ / K	Source $T_c$	$h_i^{f,gas}(T^\theta)$ / kJ/mol	$h_i^{f,liq}(T^\theta)$ / kJ/mol	Source $h_i^f(T^\theta)$
Formaldehyd	420.00	[65]	- 108.60	- 129.01	[65]
Methanol	512.50	[65]	- 200.94	- 239.10	[65]
Water	647.10	[65]	- 241.94	- 285.80	[65]
Methylal	480.60	[65]	- 350.26	-379.80	[65]
TRI	604.00	[65]	- 465.74	-508.60	[65]
OME <sub>2</sub>	552.19	[152]		- 553.49	[44]
OME <sub>3</sub>	603.44	[152]		- 727.21	[44]
OME <sub>4</sub>	646.90	[152]		- 900.93	[44]
OME <sub>5</sub>	683.66	[152]		- 1,074.65	[44]
OME <sub>6</sub>	714.76	[152]		- 1,248.37	[44]
OME <sub>7</sub>	742.96	[152]		- 1,422.10	[44]
OME <sub>8</sub>	769.25	[152]		- 1,595.80	[44]
OME <sub>9</sub>	794.61	[152]		- 1,769.50	[44]
OME <sub>10</sub>	819.90	[152]		- 1,943.30	[44]
MG <sub>1</sub>	599.25	*	- 391.10	- 448.80	This work
MG <sub>2</sub>	616.55	*		- 618.90	This work
MG <sub>3</sub>	635.45	*		- 786.60	This work
MG <sub>4</sub>	653.95	*		- 954.20	This work
MG <sub>5</sub>	672.15	*		- 1,121.90	This work
MG <sub>6</sub>	690.65	*		- 1,289.60	This work
MG <sub>7</sub>	709.75	*		- 1,457.20	This work
MG <sub>8</sub>	729.95	*		- 1,624.90	This work
MG <sub>9</sub>	751.65	*		- 1,792.50	This work
MG <sub>10</sub>	775.45	*		- 1,960.20	This work
HF <sub>1</sub>	535.85	*	- 370.00	- 416.90	This work
HF <sub>2</sub>	570.35	*		- 595.60	This work
HF <sub>3</sub>	598.75	*		- 769.70	This work
HF <sub>4</sub>	622.15	*		- 943.90	This work
HF <sub>5</sub>	643.05	*		- 1,118.10	This work
HF <sub>6</sub>	662.75	*		- 1,292.30	This work
HF <sub>7</sub>	682.25	*		- 1,466.50	This work
HF <sub>8</sub>	702.05	*		- 1,640.60	This work
HF <sub>9</sub>	722.75	*		- 1,814.80	This work
HF <sub>10</sub>	744.95	*		- 1,989.00	This work
CO <sub>2</sub>	304.21	[65]	- 393.51		[65]
N <sub>2</sub>	126.20	[65]	-		[65]
O <sub>2</sub>	154.58	[65]	-		[65]
H <sub>2</sub>	33.19	[65]	-		[65]
CO	132.92	[65]	- 110.53		[65]

Vapor pressures are correlated by Eq. (59).

$$\ln p^s/\text{bar} = A + \frac{B}{T/\text{K} + C} + D * \ln(T/\text{K}) + E * (T/\text{K})^F \quad (59)$$

**Table 14:** Parameters for the correlation of the vapor pressure, cf. Eq. (59).

Component	<i>A</i>	<i>B</i>	<i>C</i>	<i>D</i>	<i>E</i>	<i>F</i>	Source
Formaldehyd	9.85733	- 2,204.13	- 30.1500				[63]
Methanol	11.96733	- 3,626.55	- 34.2900				[63]
Water	11.68343	- 3,816.44	- 46.1300				[63]
Methylal	9.64213	- 2,640.84	- 41.2200				[63]
TRI	9.774429814	-3099.47	-68.92				[153]
OME <sub>2</sub>	68.10393	- 7,223.44		- 8.2522			[154]
OME <sub>3</sub>	63.68203	- 8,042.31		- 7.4100			[154]
OME <sub>4</sub>	81.21393	- 10,017.28		- 9.7511			[154]
OME <sub>5</sub>	86.93933	- 11,323.17		- 10.3994			[154]
OME <sub>6</sub>	93.49400	- 12,720.00		- 11.1491			[152]
OME <sub>7</sub>	99.81200	- 14,090.90		- 11.8697			[152]
OME <sub>8</sub>	106.13000	- 15,461.80		- 12.5903			[152]
OME <sub>9</sub>	112.44800	- 16,832.70		- 13.3109			[152]
OME <sub>10</sub>	118.76600	- 18,203.60		- 14.0315			[152]
MG <sub>1</sub>	12.81810	- 4,762.07	- 51.2100				[63]
HF <sub>1</sub>	14.96843	- 5,646.71					[63]
CO <sub>2</sub>	35.50407	- 2,839.00		- 3.8639	2.81120E-16	6	[65]
N <sub>2</sub>	46.76907	- 1,084.10		- 8.3144	4.41270E-02	1	[65]
O <sub>2</sub>	39.73207	- 1,200.20		- 6.4361	2.84050E-02	1	[65]
H <sub>2</sub>	1.17707	- 94.90		1.1125	3.29150E-04	2	[65]
CO	34.18507	- 1,076.60		- 4.8814	7.56730E-05	2	[65]



Enthalpies of vaporization are correlated by Eq. (60)

$$\Delta h_\nu/\text{J/mol} = A(1 - T_r)^{B+CT_r+DT_r^2}, \quad (60)$$

where  $T_r$  is the reduced temperature  $T_r = T/T_c$ .

**Table 15:** Parameters for the correlation of the enthalpy of vaporization, cf. Eq. (60).

\*: estimated with method of Marrero/Pardillo [155] in the original work,

\*\* : estimated based on the vapor pressure via Clausius Clapeyron equation in this work.

Component	$A$	$B$	$C$	$D$	Tc / K	Source
Formaldehyd	29575.0	0.09830	0.28373		420.00	[65]
Methanol	50451.0	0.33594			512.50	[65]
Water	51546.0	0.28402	- 0.15843	0.23750	647.10	[65]
Methylal	44122.0	0.41418			480.60	[65]
TRI	55800.0	0.38760			604.00	[65]
OME <sub>2</sub>	52246.0	0.36240			552.19	[152]*
OME <sub>3</sub>	58545.0	0.29380			603.44	[152]*
OME <sub>4</sub>	72458.0	0.36130			646.90	[152]*
OME <sub>5</sub>	81911.0	0.35950			683.66	[152]*
OME <sub>6</sub>	92022.0	0.35810			714.76	[152]*
OME <sub>7</sub>	101940.0	0.35750			742.96	[152]*
OME <sub>8</sub>	111860.0	0.35800			769.25	[152]*
OME <sub>9</sub>	121760.0	0.36000			794.61	[152]*
OME <sub>10</sub>	131660.0	0.36360			819.90	[152]*
MG <sub>1</sub>	1.028045E+05	1.490936E+00	-1.308039E+00		599.25	This work**
HF <sub>1</sub>	4.694675E+04	1.751584E-15	-1.702812E-15		535.85	This work**
CO <sub>2</sub>	21730.0	0.38200	-0.43390	0.42213	304.21	[65]
N <sub>2</sub>	7490.5	0.40406	-0.31700	0.27343	126.20	[65]
O <sub>2</sub>	9008.0	0.45420	-0.40960	0.31830	154.58	[65]
H <sub>2</sub>	1012.7	0.69800	-1.81700	1.44700	33.19	[65]
CO	8585.0	0.49210	-0.32600	0.22310	132.92	[65]

The ideal gas heat capacities of all components except MG/HF are correlated by Eq. (61).

$$c_p/\text{J/molK} = A + B \left[ \frac{C/T}{\sinh(C/T)} \right]^2 + D \left[ \frac{E/T}{\cosh(E/T)} \right]^2 \quad (61)$$

**Table 16:** Parameters for the DIPPR correlation of the ideal gas heat capacity, cf. Eq. (61).

Component	<i>A</i>	<i>B</i>	<i>C</i>	<i>D</i>	<i>E</i>	Source
Formaldehyd	33.27	49.54	1,866.60	28.08	934.90	[65]
Methanol	39.25	87.90	1,916.50	53.65	896.70	[65]
Water	33.36	26.79	2,610.50	8.90	1,169.00	[65]
Methylal	74.98	161.66	862.87	789.64	4,671.80	[65]
TRI	56.41	219.62	1554.7	152.18	746.30	[65]
OME <sub>2</sub>	94.91	216.35	- 787.75			[152]
OME <sub>3</sub>	112.74	277.19	- 769.63			[152]
OME <sub>4</sub>	130.39	338.31	- 758.08			[152]
OME <sub>5</sub>	147.95	399.59	- 750.07			[152]
OME <sub>6</sub>	165.45	460.97	- 744.20			[152]
OME <sub>7</sub>	182.91	522.41	- 739.71			[152]
OME <sub>8</sub>	200.34	583.89	- 736.16			[152]
OME <sub>9</sub>	217.75	645.40	- 733.29			[152]
OME <sub>10</sub>	235.15	706.94	- 730.91			[152]
CO <sub>2</sub>	29.37	34.54	1,428.00	26.40	588.00	[65]
N <sub>2</sub>	29.11	8.61	1,429.00	0.10	589.00	[65]
O <sub>2</sub>	29.10	10.04	1,430.00	9.36	590.00	[65]
H <sub>2</sub>	27.62	9.56	1,431.00	3.76	591.00	[65]
CO	29.11	8.77	1,432.00	8.46	592.00	[65]

The ideal gas and liquid heat capacities of MG and HF are correlated by Eq. (62).

$$c_p/\text{J/molK} = A + BT + CT^2 + DT^3 + ET^4 \quad (62)$$

**Table 17:** Parameters for the polynomial correlation of the heat capacity, cf. Eq. (62). Parameters for MG<sub>1</sub>/HF<sub>1</sub> for the heat capacity in the gas phase, for MG<sub>n>1</sub>/HF<sub>n>1</sub> in the liquid phase.

Component	<i>A</i>	<i>B</i>	<i>C</i>	<i>D</i>	<i>E</i>	Source
Heat capacities for MG <sub>1</sub> /HF <sub>1</sub> in gas phase:						
MG <sub>1</sub>	104981.725	-1234.9336	5.43577321	-0.0106073	7.75E-06	This work
HF <sub>1</sub>	105341.756	-1249.7393	5.51496097	-0.0107482	7.85E-06	This work
Heat capacities for MG <sub>n&gt;1</sub> /HF <sub>n&gt;1</sub> in liquid phase:						
MG <sub>2</sub>	213208.791	-2498.6198	10.9720692	-0.0213772	1.5602E-05	This work
MG <sub>3</sub>	319821.427	-3748.3417	16.4598327	-0.0320692	2.3406E-05	This work
MG <sub>4</sub>	426358.029	-4997.1565	21.9435505	-0.0427532	3.1203E-05	This work
MG <sub>5</sub>	532962.682	-6246.8032	27.4310633	-0.0534449	3.9007E-05	This work
MG <sub>6</sub>	639665.527	-7497.5087	32.9228192	-0.064144	4.6815E-05	This work
MG <sub>7</sub>	746318.83	-8747.6581	38.412248	-0.0748389	5.462E-05	This work
MG <sub>8</sub>	852582.263	-9993.3925	43.882994	-0.0854987	6.2401E-05	This work
MG <sub>9</sub>	958747.561	-11238.034	49.3491889	-0.0961502	7.0176E-05	This work
MG <sub>10</sub>	1065730.4	-12491.955	54.8547543	-0.1068756	7.8003E-05	This work
HF <sub>2</sub>	210179.227	-2493.032	10.9979451	-0.021431	1.5644E-05	This work
HF <sub>3</sub>	314970.101	-3735.7838	16.4785839	-0.0321093	2.3438E-05	This work
HF <sub>4</sub>	419831.164	-4979.3708	21.9629339	-0.0427949	3.1236E-05	This work
HF <sub>5</sub>	524815.948	-6224.3275	27.4529348	-0.0534908	3.9042E-05	This work
HF <sub>6</sub>	630124.406	-7472.9883	32.9587962	-0.0642168	4.687E-05	This work
HF <sub>7</sub>	734561.219	-8711.7216	38.4223872	-0.074863	5.4641E-05	This work
HF <sub>8</sub>	838978.813	-9950.2379	43.8850714	-0.0855076	6.2411E-05	This work
HF <sub>9</sub>	944315.853	-11199.229	49.3923452	-0.0962363	7.024E-05	This work
HF <sub>10</sub>	1049359.49	-12444.896	54.8855485	-0.1069386	7.8051E-05	This work

The liquid densities are correlated by Eq. (63).

$$\rho^{(n)}/\text{kmol/m}^3 = \frac{A}{B(1+(1-T/C)^D)} \quad (63)$$

**Table 18:** Parameters for the correlation of the liquid density, cf. Eq. (63).

Component	$A$	$B$	$C$	$D$	Source
Formaldehyd	1.94150	0.2230900	408.000	0.285710	[65]
Methanol	2.32670	0.2707300	512.500	0.247130	[65]
Water	7.19130	0.3261800	647.096	0.285714	[65]
Methylal	1.43550	0.3057600	480.600	0.317550	[65]
TRI	1.15900	0.2594300	604.000	0.285700	[65]
OME <sub>2</sub>	0.90052	0.2777876	552.187	0.285700	[152]
OME <sub>3</sub>	0.70390	0.2725395	603.439	0.285700	[152]
OME <sub>4</sub>	0.55055	0.2625736	646.899	0.285700	[152]
OME <sub>5</sub>	0.47349	0.2625736	683.661	0.285700	[152]
OME <sub>6</sub>	0.41628	0.2625736	714.758	0.285700	[152]
OME <sub>7</sub>	0.37086	0.2625736	742.964	0.285700	[152]
OME <sub>8</sub>	0.33448	0.2625736	769.247	0.285700	[152]
OME <sub>9</sub>	0.30414	0.2625736	794.609	0.285700	[152]
OME <sub>10</sub>	0.27819	0.2625736	819.903	0.285700	[152]
MG <sub>1</sub>	11.24951	0.6269446	1000.000	0.579635	[66]
MG <sub>2</sub>	6.92277	0.6269446	1000.000	0.579635	[66]
MG <sub>3</sub>	4.99977	0.6269446	1000.000	0.579635	[66]
MG <sub>4</sub>	3.91286	0.6269443	1000.000	0.579634	[66]
MG <sub>5</sub>	3.21414	0.6269446	1000.000	0.579635	[66]
MG <sub>6</sub>	2.72715	0.6269446	1000.000	0.579635	[66]
MG <sub>7</sub>	2.36831	0.6269446	1000.000	0.579635	[66]
MG <sub>8</sub>	2.09293	0.6269446	1000.000	0.579635	[66]
MG <sub>9</sub>	1.87491	0.6269446	1000.000	0.579635	[66]
MG <sub>10</sub>	1.69803	0.6269446	1000.000	0.579635	[66]
HF <sub>1</sub>	1.29097	0.2024660	522.746	0.285713	[66]
HF <sub>2</sub>	1.00909	0.2024677	568.472	0.285716	[66]
HF <sub>3</sub>	0.80480	0.2024658	613.300	0.285713	[66]
HF <sub>4</sub>	0.65250	0.2024641	657.763	0.285711	[66]
HF <sub>5</sub>	0.53627	0.2024667	702.330	0.285714	[66]
HF <sub>6</sub>	0.44575	0.2024660	747.428	0.285713	[66]
HF <sub>7</sub>	0.37407	0.2024667	793.462	0.285714	[66]
HF <sub>8</sub>	0.31647	0.2024649	840.832	0.285714	[66]
HF <sub>9</sub>	0.26960	0.2024692	889.933	0.285717	[66]
HF <sub>10</sub>	0.23097	0.2024498	941.193	0.285698	[66]
CO <sub>2</sub>	2.76800	0.2621200	304.210	0.290800	[65]
N <sub>2</sub>	3.20910	0.2861000	126.200	0.296600	[65]
O <sub>2</sub>	3.91430	0.2877200	154.580	0.292400	[65]
H <sub>2</sub>	5.41400	0.3489300	33.190	0.270600	[65]
CO	2.89700	0.2753200	132.920	0.281300	[65]

# B Appendix: Energetic efficiency of OME production

## B.1 Additional information on the synthesis processes

### B.1.1 Carbon Capture

In the present work, we analyzed post-combustion capture (PCC) and direct air capture (DAC) technologies [85–89]. In the following, both technologies are discussed.

Most PCC technologies rely on chemical absorption. The most popular technology is amine scrubbing via monoethanolamine (MEA), which is already available on an industrial scale [81, 88, 156–158].

DAC technologies rely on a variety of different operating principles to separate carbon emissions from the air. The most important ones are physical absorbents (e.g., the commercial products Selexol, Rectisol, Sepasolv MPE), chemical absorbents (e. g. hydroxides, carbonates), adsorbents (e.g., amines on SiO<sub>2</sub> carriers, microporous materials), and cryogenic air separation. DAC systems can be installed apart from power plants. This allows for great freedom in the search for adequate operation sites [81, 87, 157].

Both electricity and heat demand for several CC technologies are given in Table 19. As

**Table 19:** Energy demand for state-of-the-art CC plants

CC Type	Technology	E / MJ per kg CO <sub>2</sub>
PCC	MEA [81]	1.3
PCC	MEA [110]	3.2...4.1
PCC	MEA [95]	3.4
PCC	Amine [157]	2...3
DAC	Class-3-Amin [159]	6.3 <sub>(th.)</sub> + 0.9 <sub>(el.)</sub>
DAC	NaOH/ Ca(OH) <sub>2</sub> [81]	9.9
DAC	NaOH/ Ca(OH) <sub>2</sub> [87]	10...17
DAC	NaOH, KOH [160]	10.8...18.0
DAC	Ca(OH) <sub>2</sub> / CaCO <sub>3</sub> [87]	241

PCC reference, we chose the MEA process with the lowest energy demand [81]. As DAC reference, we chose the only commercially available technology in Europe [159].

### B.1.2 FA synthesis.

In order to derive a material balance from the information in the original work, the following assumptions are used:

The product is assumed to contain 55 wt.-% FA (the original work [28] suggests 40-55 wt.-%). Furthermore, it is stated that the yield of the process is 90 mol-%. The composition of the waste gas is given in vol-%. We assumed that:

- The liquid feed is pure methanol.
- The gaseous feed contains exactly the stoichiometric amount of oxygen.
- The waste gas contains neither ME nor FA.
- There are only small traces of water in the waste gas.

Since the pressures of the units were not given, we assumed a pressure of 1.4 bar for the reactor and column. This assumption is based on data from comparable silver processes [96].

### B.1.3 TRI synthesis.

The material balance for the TRI synthesis was calculated based on graphics given by Grützner et al. [41] and the lever rule. To calculate the mass flows  $\dot{m}_i$  of all streams we used the following levers from Figure 6 of the original work [41], indexes referring to Figure 5 of the original work [41].

Column K1:

The lever rule of the leaving streams is

$$\frac{\dot{m}_5}{\dot{m}_5 + \dot{m}_4} = \frac{\overline{M, 4}}{4, 5}. \quad (64)$$

Where M describes a fictitious mixing point. M has exactly the same mass and concentration as a mixture of  $\dot{m}_3$  and  $\dot{m}_{10}$  or  $\dot{m}_4$  and  $\dot{m}_5$ .

The lever rule of the entering streams is

$$\frac{\dot{m}_{10}}{\dot{m}_{10} + \dot{m}_3} = \frac{\overline{M, 3}}{3, 10}. \quad (65)$$

With the correlation between the line segments containing the mixing point M

$$\overline{M,4} = \overline{M,3} + \overline{3,4} \quad (66)$$

and the material balance of the column

$$\dot{m}_{10} + \dot{m}_3 = \dot{m}_4 + \dot{m}_5 \quad (67)$$

follows

$$\dot{m}_3 = \dot{m}_5 \cdot \frac{\overline{4,5}}{\overline{3,4}} + \dot{m}_{10} \cdot \left( \frac{\overline{3,10}}{\overline{3,4}} + 1 \right). \quad (68)$$

Based on Equation (68)  $\dot{m}_3$  is known. Equation (67) is then used to calculate  $\dot{m}_4$ .  $\dot{m}_8$  follows from the lever rule of column K2

$$\dot{m}_8 = \dot{m}_5 \cdot \frac{\overline{5,7}}{\overline{8,7}}. \quad (69)$$

$\dot{m}_{10}$  follows from the lever rule of column K3

$$\dot{m}_{10} = \dot{m}_8 \cdot \frac{\overline{9,8}}{\overline{9,10}}. \quad (70)$$

Based on these equations, the mass flows of all streams are available. The concentrations of streams 4, 7, 9, and 10 were taken from the ternary diagrams. All other concentrations are calculated based on mass flow and conservation of mass.

### B.1.4 ME synthesis

Since the process flow diagram of the ME production process in the original work [40] is complex and detailed, we show a simplified version to describe only the in- and outgoing streams, see Figure 24.

However, in our calculations, we used the detailed data given by Pérez-Fortes et al. [40]. In the original work, pinch analysis is performed for the ME production as a standalone process. We also consider heat integration between the processes of Routes A and B. To do so, we extracted the heat duties and respective temperature levels of the process from the pinch analysis in the original work.

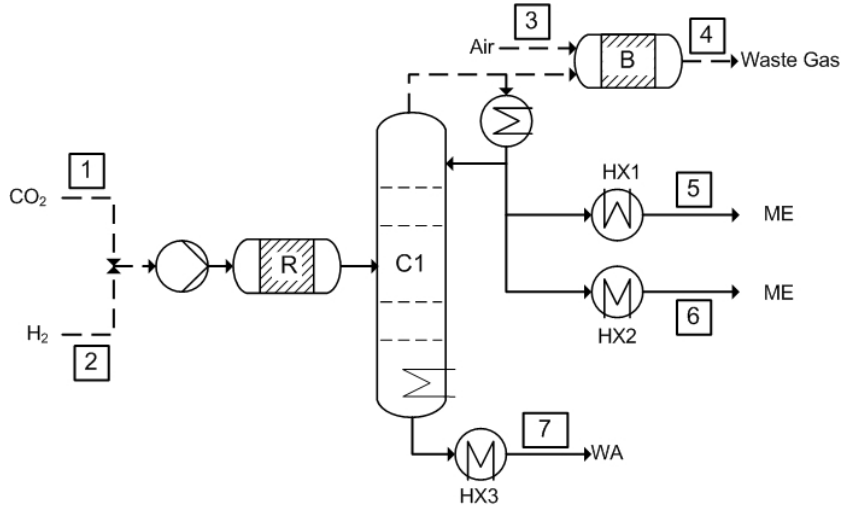


**Figure 24:** Simplified process flow diagram of the ME synthesis plant (Route A and B) based on Pérez-Fortes et al. [40], Van-Dal and Bouallou [95]: R = Reactor, HX = Heat exchanger, B = Burner.

## B.2 Overall material balance

Tables 20 to 24 show the full material balance for the complete process chain. Stream numbers refer to Figure 2 in the main manuscript. Stream (1) is always comprised of (diluted) CO<sub>2</sub>. Since three different forms of CC are considered, there are various possible compositions for stream (1). These compositions are not investigated further in the present work. All processes are scaled to the production of 1 kg OME<sub>3-5</sub> per second (equals to 3600 kg OME<sub>3-5</sub> per hour).

**Table 20:** Idealized material balance for Route A, stream numbers referring to Figure 2 in main manuscript.

	1	2	3	4	5	6	7	8	9	10	11	17	18
	Mass flowrates $\dot{m}_i$ / kg per hour												
OME <sub>3-5</sub>	-	0	0	0	0	0	0	0	0	0	0	0	3600
WA	-	7070	0	0	0	2357	0	0	1513	0	0	422	0
FA	-	0	0	0	0	0	0	0	0	0	2522	0	0
ME	-	0	0	0	0	0	1500	2690	0	0	0	0	0
O <sub>2</sub>	-	0	6285	0	0	0	0	0	0	1345	0	0	0
H <sub>2</sub>	-	0	0	0	786	0	0	0	0	0	0	0	0
CO <sub>2</sub>	5761	0	0	5761	0	0	0	0	0	0	0	0	0



**Table 21:** Material balance for Route A based on reference processes, stream numbers referring to Figure 2 in main manuscript.

	1	2	3	4	5	6	7	8	9	10	11	17	18
	Mass flowrates $\dot{m}_i$ / kg per hour												
OME <sub>3-5</sub>	-	0	0	0	0	0	0	0	0	0	0	0	3600
WA	-	8096	0	0	0	3000	0	0	1660	868	447	868	0
FA	-	0	0	0	0	0	0	0	0	0	2520	0	0
ME	-	0	0	0	0	0	1501	3005	0	0	0	0	0
O <sub>2</sub>	-	0	7197	879	0	449	0	0	0	1251	0	0	0
H <sub>2</sub>	-	0	0	0	900	0	0	0	70	0	0	0	0
CO <sub>2</sub>	6583	0	0	6583	0	408	0	0	411	0	0	0	0
CO	-	0	0	0	0	0	0	0	16	0	0	0	0
N <sub>2</sub>	-	0	0	2784	0	2784	0	0	4116	4116	0	0	0

**Table 22:** Idealized material balance for Route C, stream numbers referring to Figure 2 in main manuscript.

	1	2	3	4	5	6	7	8	9	10	11	17	18
	Mass flowrates $\dot{m}_i$ / kg per hour												
OME <sub>3-5</sub>	-	0	0	0	0	0	0	0	0	0	0	0	3600
WA	-	7070	0	0	0	2357	0	0	0	0	0	422	0
FA	-	0	0	0	0	0	0	0	0	0	2522	0	0
ME	-	0	0	0	0	0	1500	2690	0	0	0	0	0
O <sub>2</sub>	-	0	6285	0	0	0	0	0	0	0	0	0	0
H <sub>2</sub>	-	0	0	0	786	0	0	0	168	0	0	0	0
CO <sub>2</sub>	5761	0	0	5761	0	0	0	0	0	0	0	0	0

**Table 23:** Idealized material balance for Route B, stream numbers referring to Figure 2 in main manuscript.

	1	2	3	4	5	6	7	8	9	10	11	12	13	14	15	16	17	18	
	Mass flowrates $\dot{m}_i$ / kg per hour																		
OME <sub>3-5</sub>	-	0	0	0	0	0	0	0	0	0	0	0	0	0	0	0	0	0	3600
WA	-	7070	0	0	0	2357	0	0	1513	0	0	0	422	0	0	0	0	0	0
TRI	-	0	0	0	0	0	0	0	0	0	0	0	0	0	0	1819	0	0	0
MAL	-	0	0	0	0	0	0	0	0	0	0	0	0	0	1781	0	0	0	0
FA	-	0	0	0	0	0	0	0	0	0	703	1819	0	0	0	0	0	0	0
ME	-	0	0	0	0	0	1500	2690	0	0	0	0	0	0	0	0	0	0	0
O <sub>2</sub>	-	0	6285	0	0	0	0	0	0	1345	0	0	0	0	0	0	0	0	0
H <sub>2</sub>	-	0	0	0	786	0	0	0	0	0	0	0	0	0	0	0	0	0	0
CO <sub>2</sub>	5761	0	0	5761	0	0	0	0	0	0	0	0	0	0	0	0	0	0	0
CO	-	0	0	0	0	0	0	0	0	0	0	0	0	0	0	0	0	0	0
N <sub>2</sub>	-	0	0	0	0	0	0	0	0	0	0	0	0	0	0	0	0	0	0

**Table 24:** Material balance for Route B based on reference processes, stream numbers referring to Figure 2 in main manuscript.

	1	2	3	4	5	6	7	8	9	10	11	12	13	14	15	16	17	18	
	Mass flowrates $\dot{m}_i$ / kg per hour																		
OME <sub>3-5</sub>	-	0	0	0	0	0	0	0	0	0	0	0	0	0	0	0	0	0	3600
WA	-	8117	0	0	0	3008	0	0	1160	871	420	536	840	517	2	18	0	20	0
TRI	-	0	0	0	0	0	0	0	0	0	0	0	0	5	0	1819	0	0	0
MAL	-	0	0	0	0	0	0	0	0	0	0	0	0	0	1781	0	0	0	0
FA	-	0	0	0	0	0	0	0	0	0	706	1825	3	0	0	0	0	0	0
ME	-	0	0	0	0	0	1499	3018	0	0	0	0	0	0	0	0	0	0	0
O <sub>2</sub>	-	0	7215	882	0	450	0	0	0	1256	0	0	0	0	0	0	0	0	0
H <sub>2</sub>	-	0	0	0	902	0	0	0	70	0	0	0	0	0	0	0	0	0	0
CO <sub>2</sub>	6600	0	0	6600	0	409	0	0	412	0	0	0	0	0	0	0	0	0	0
CO	-	0	0	0	0	0	0	0	16	0	0	0	0	0	0	0	0	0	0
N <sub>2</sub>	-	0	0	2791	0	2791	0	0	4134	4134	0	0	0	0	0	0	0	0	0

### B.3 Pinch analyses for Route A

Pinch analysis is used to evaluate the heat integration potential of the investigated processes. Figure 25 to 30 show the respective composite curves. A splitting of the composite curves was not considered.

#### B.3.1 Scenario 1: All processes separately.

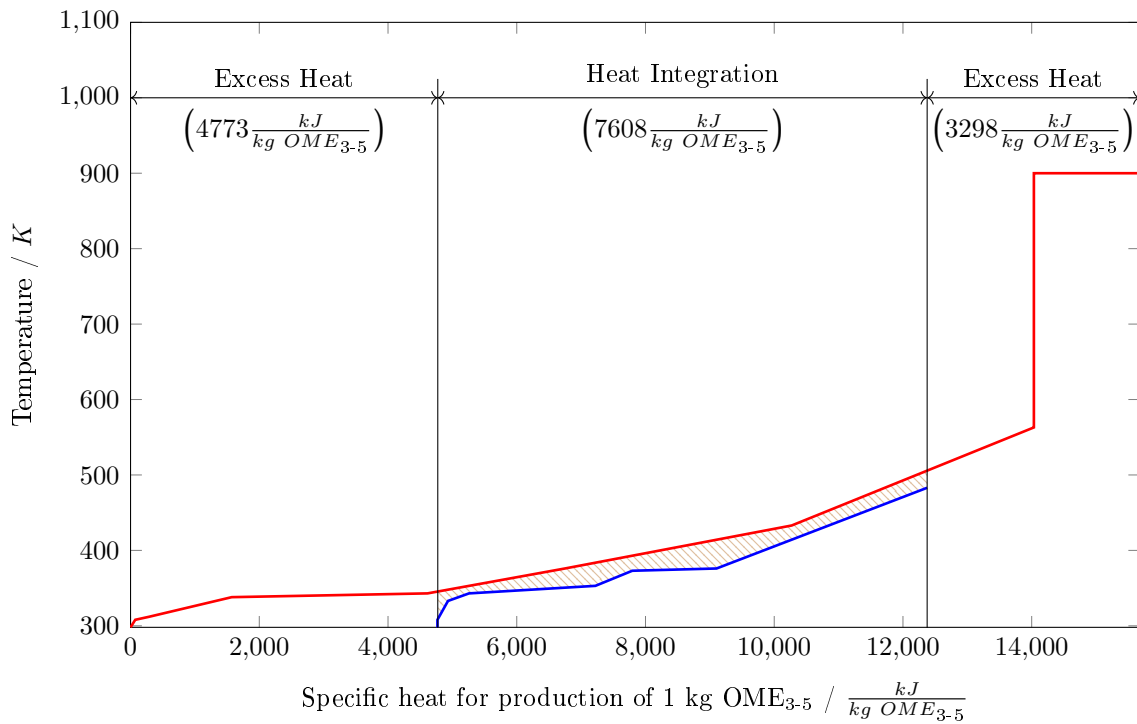


**Figure 25:** Hot and cold composite curve of the ME synthesis plant (Route A): Hot Composite Curve (red) and Cold Composite Curve (blue).

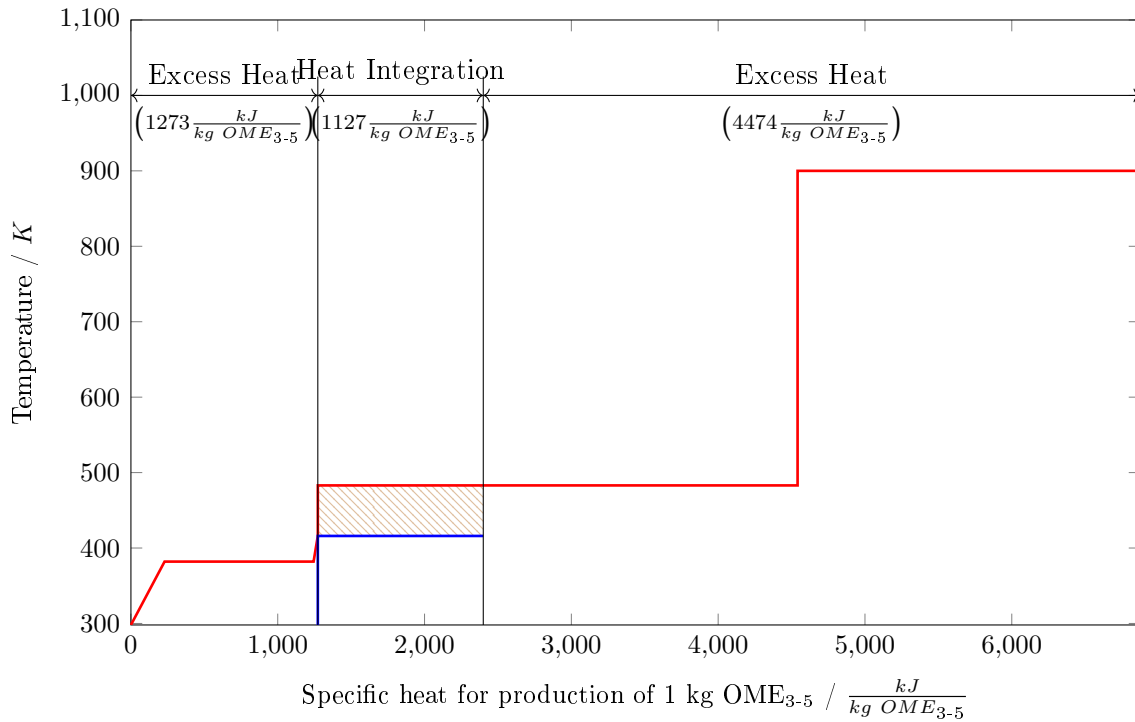


**Figure 26:** Hot and cold composite curve of the FA synthesis plant (Route A): Hot Composite Curve (red) and Cold Composite Curve (blue).

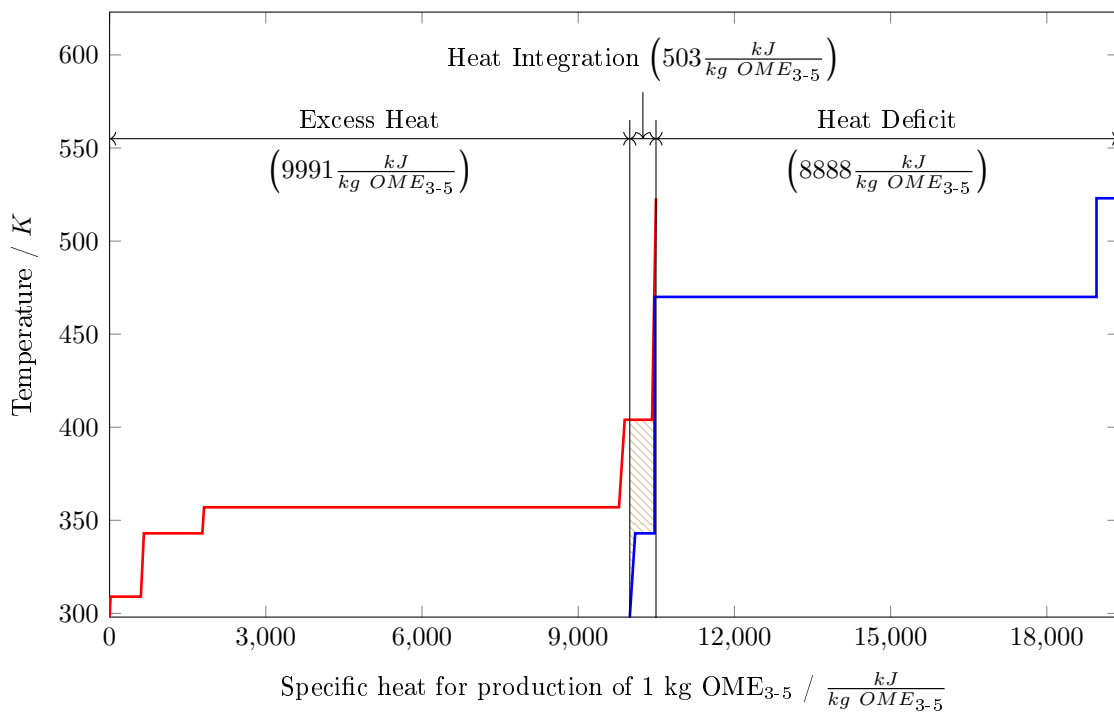


**Figure 27:** Hot and cold composite curve of the OME<sub>3-5</sub> synthesis plant (Route A): Hot Composite Curve (red) and Cold Composite Curve (blue).

## B.3.2 Scenario 2: Two blocks.

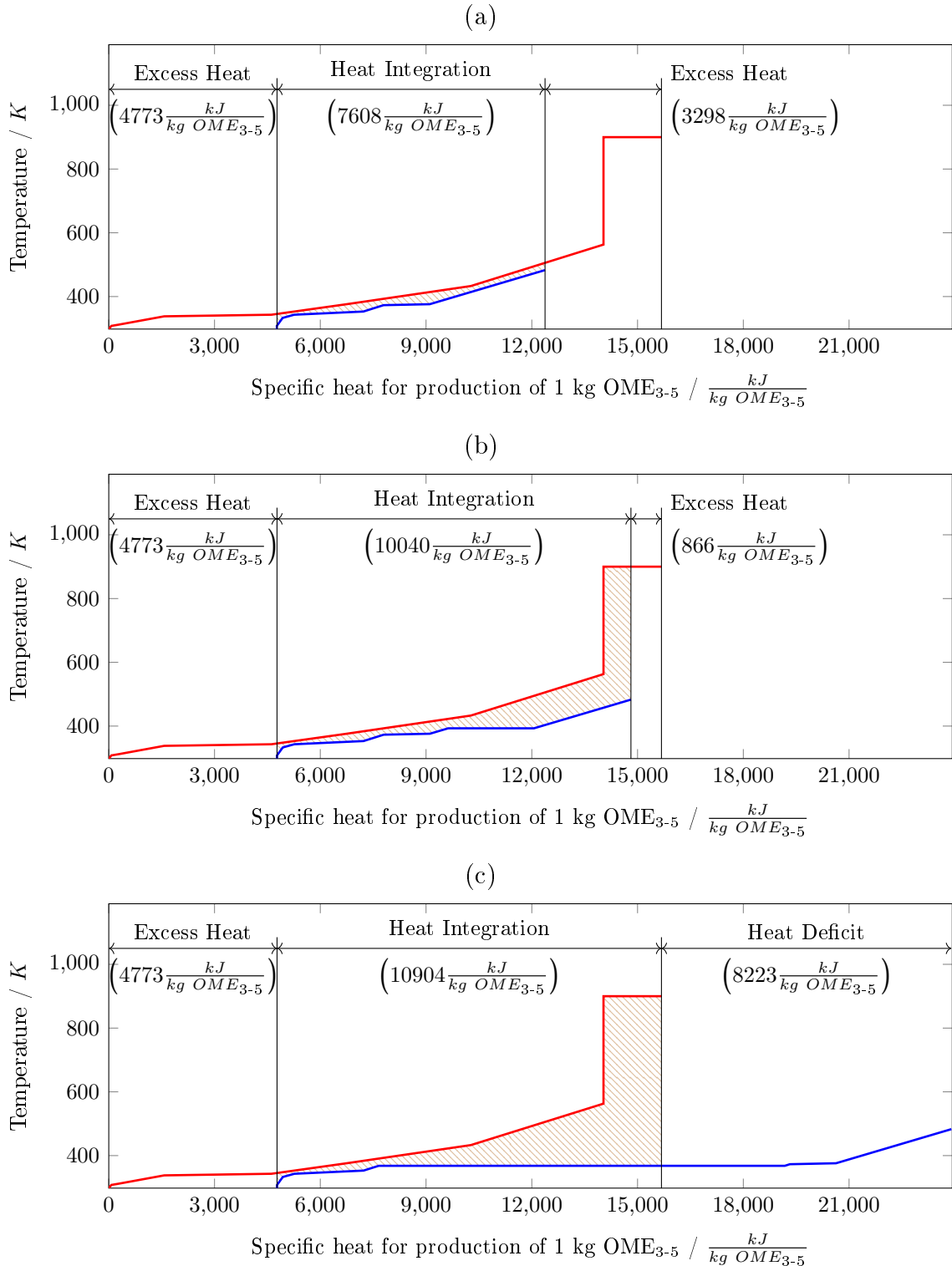


**Figure 28:** Hot Composite Curve (red) and Cold Composite Curve (blue) of the first block from CC to ME (Route A). Panels (a) to (c) give the composite curves for CO<sub>2</sub> supply via CPS (a), PCC (b), DAC (c).

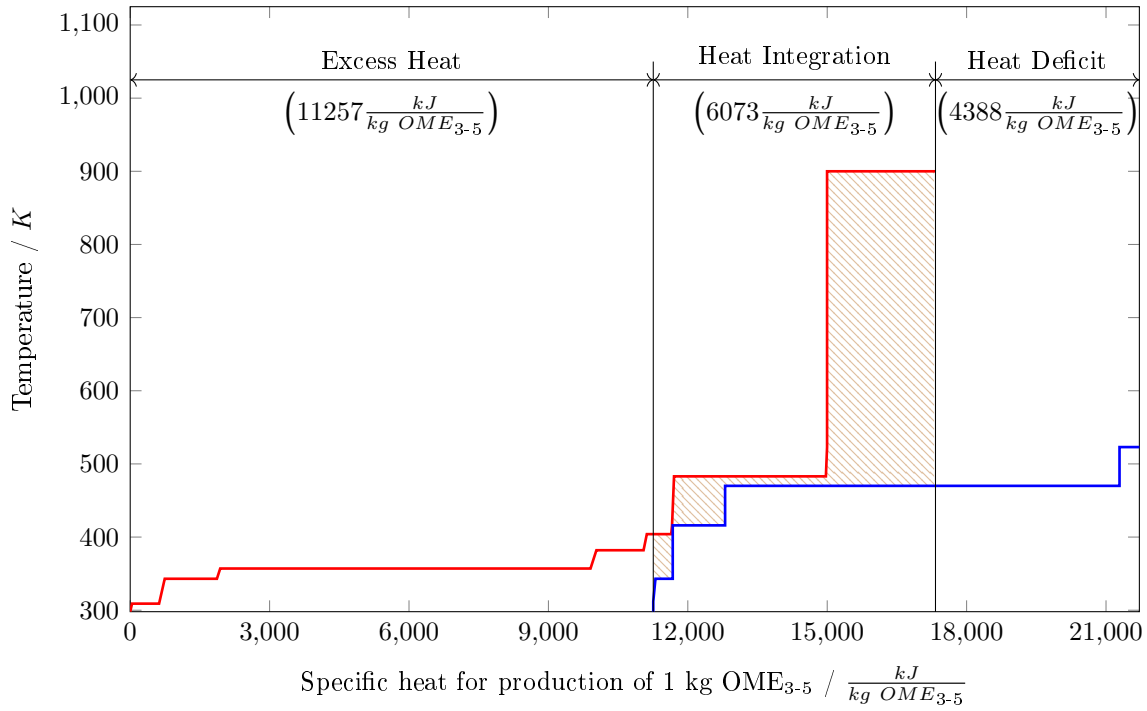


**Figure 29:** Hot and cold composite curve of the second block from FA to OME<sub>3-5</sub> (Route A): Hot Composite Curve (red) and Cold Composite Curve (blue).

## B.3.3 Scenario 3: One block.

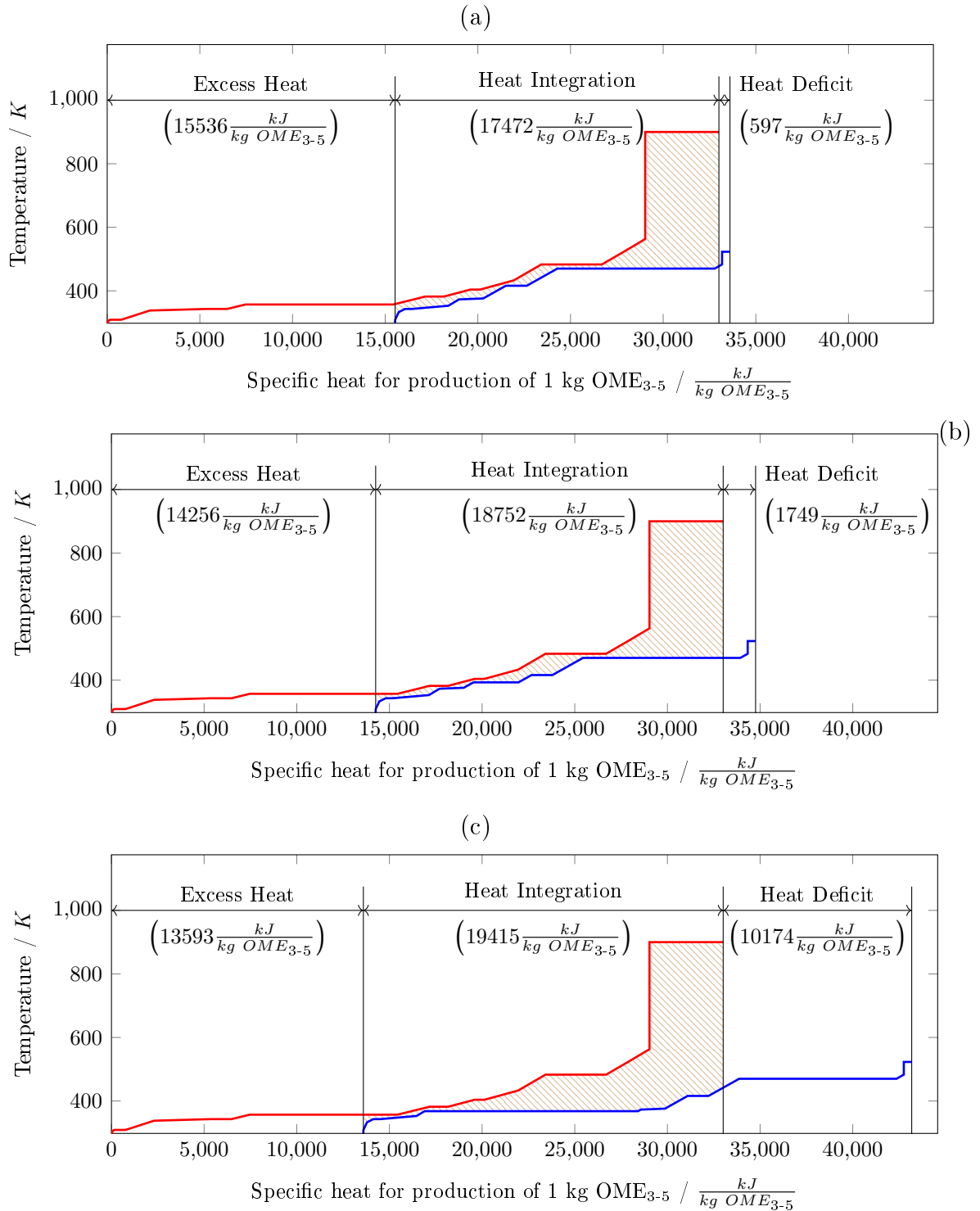


**Figure 30:** Hot Composite Curve (red) and Cold Composite Curve (blue) for overall heat integration (Route A). Panels (a) to (c) give the composite curves for CO<sub>2</sub> supply via CPS (a), PCC (b), DAC (c).

## B.4 Pinch analyses for Route B

Pinch analysis is used to evaluate the heat integration potential of the investigated processes, Figure 31 to 38 show the respective composite curves. A splitting of the composite curves was not considered.

### B.4.1 Scenario 1: All processes separately.

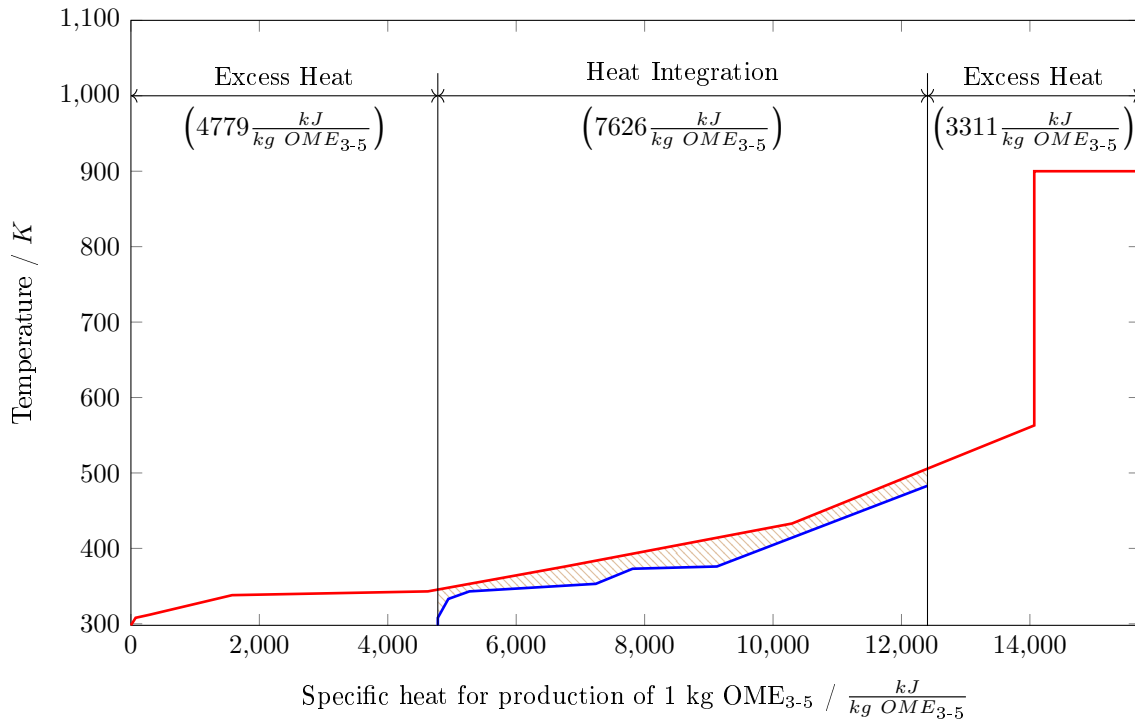


**Figure 31:** Hot and cold composite curve of the ME synthesis plant (Route B): Hot Composite Curve (red) and Cold Composite Curve (blue).



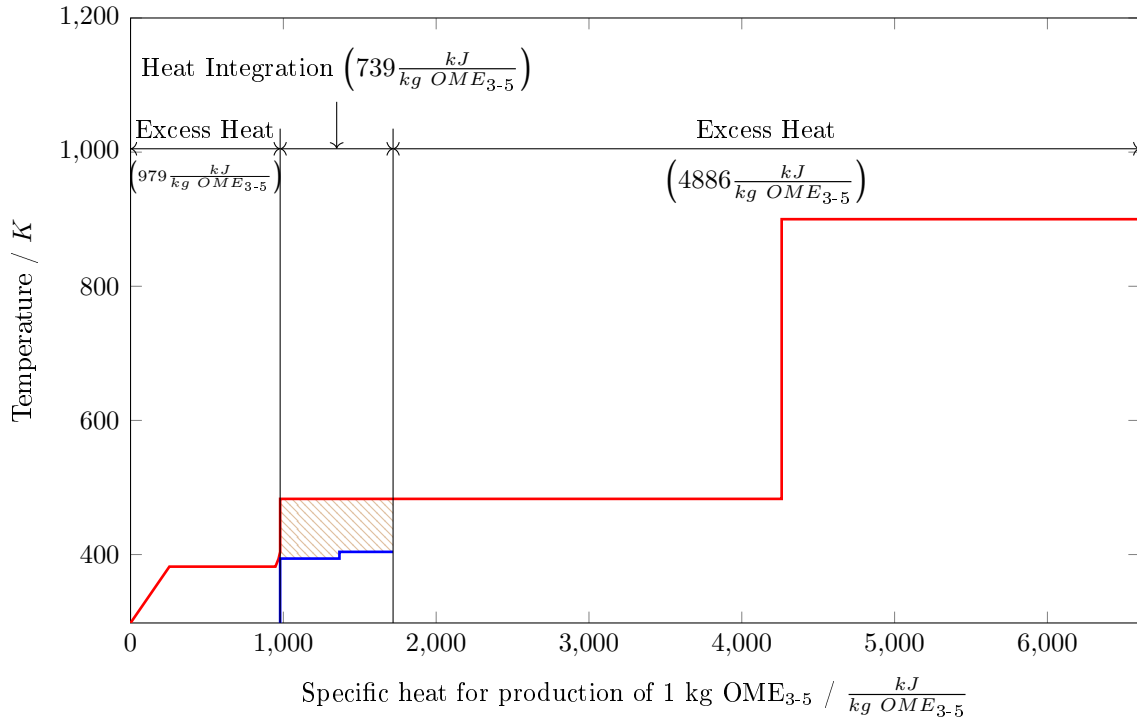


**Figure 32:** Hot and cold composite curve of the FA synthesis plant (Route B): Hot Composite Curve (red) and Cold Composite Curve (blue).

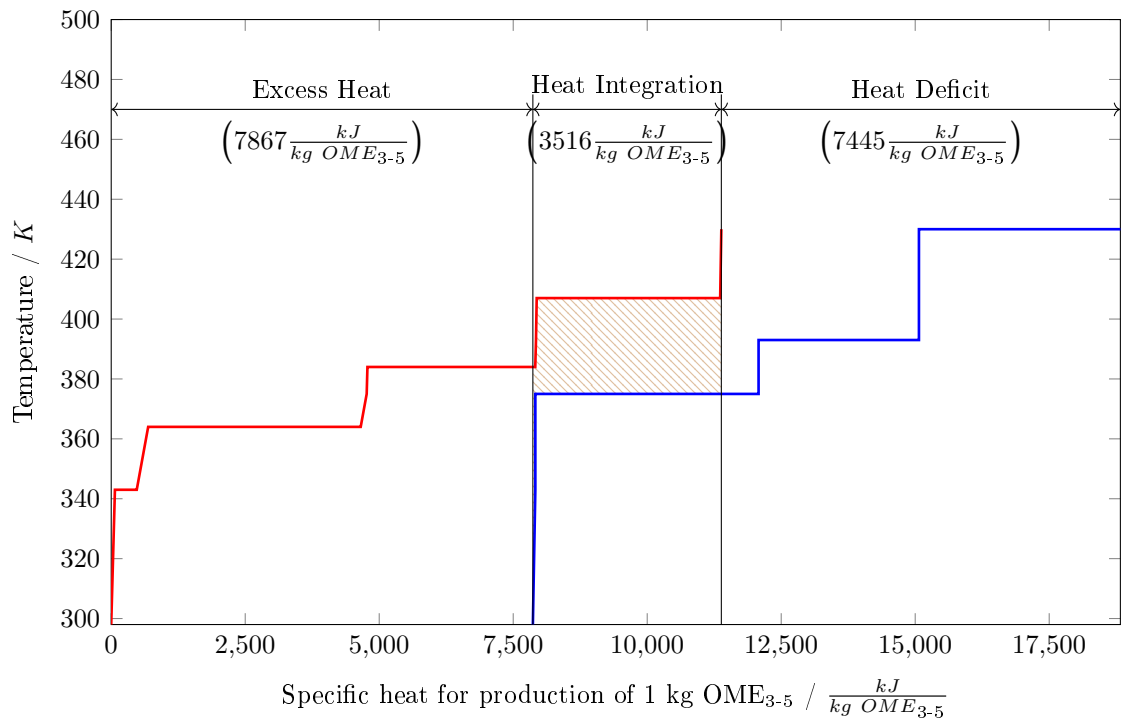


**Figure 33:** Hot and cold composite curve of the TRI synthesis plant (Route B): Hot Composite Curve (red) and Cold Composite Curve (blue).

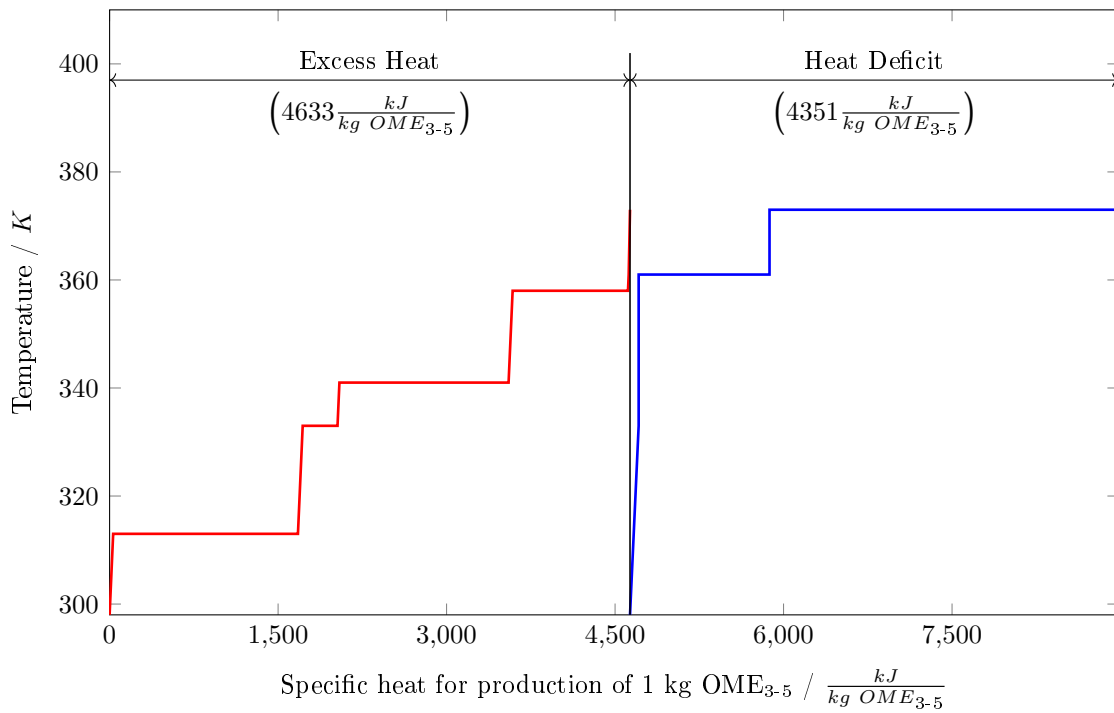


**Figure 34:** Hot and cold composite curve of the MAL synthesis plant (Route B): Hot Composite Curve (red) and Cold Composite Curve (blue).

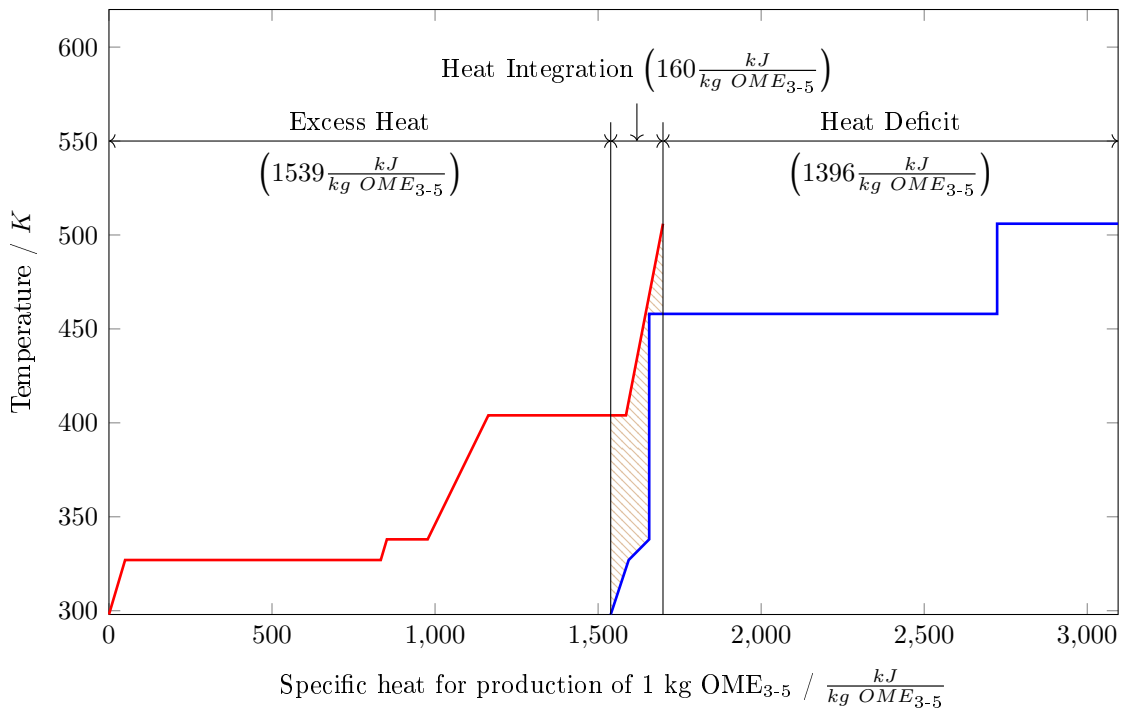


**Figure 35:** Hot and cold composite curve of the OME<sub>3-5</sub> synthesis plant (route B): Hot Composite Curve (red) and Cold Composite Curve (blue).

B.4.2 Scenario 2: Two blocks.

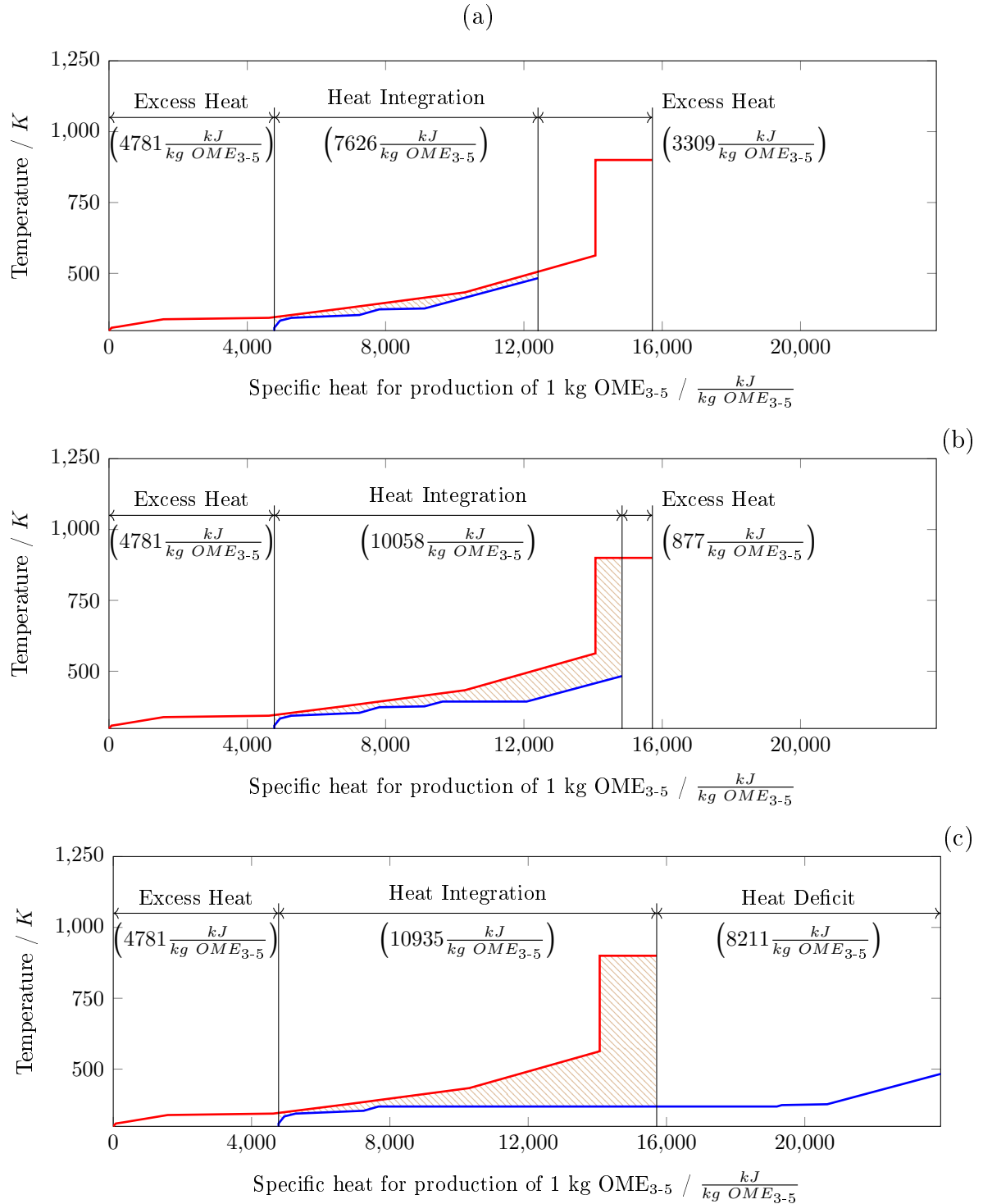


**Figure 36:** Hot Composite Curve (red) and Cold Composite Curve (blue) of the first block from CC to ME (Route B). Panels (a) to (c) give the composite curves for CO<sub>2</sub> supply via CPS (a), PCC (b), DAC (c).

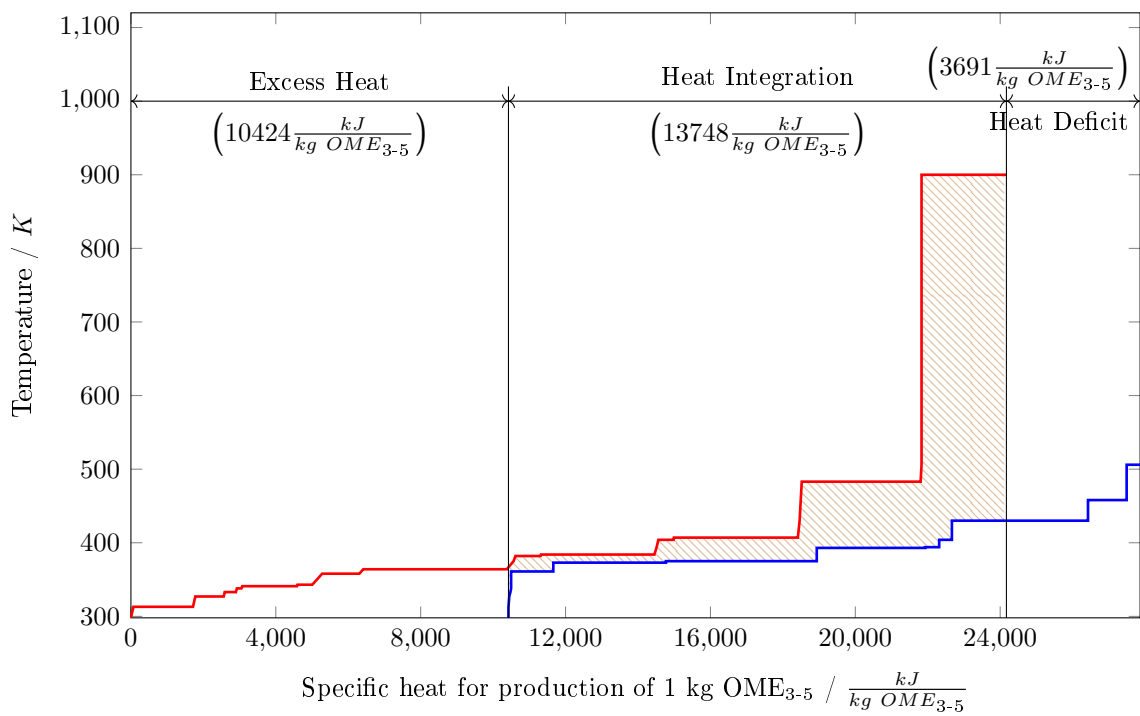


**Figure 37:** Hot and cold composite curve of the second block from FA to OME<sub>3-5</sub> (Route B): Hot Composite Curve (red) and Cold Composite Curve (blue).

B.4.3 Scenario 3: One block.

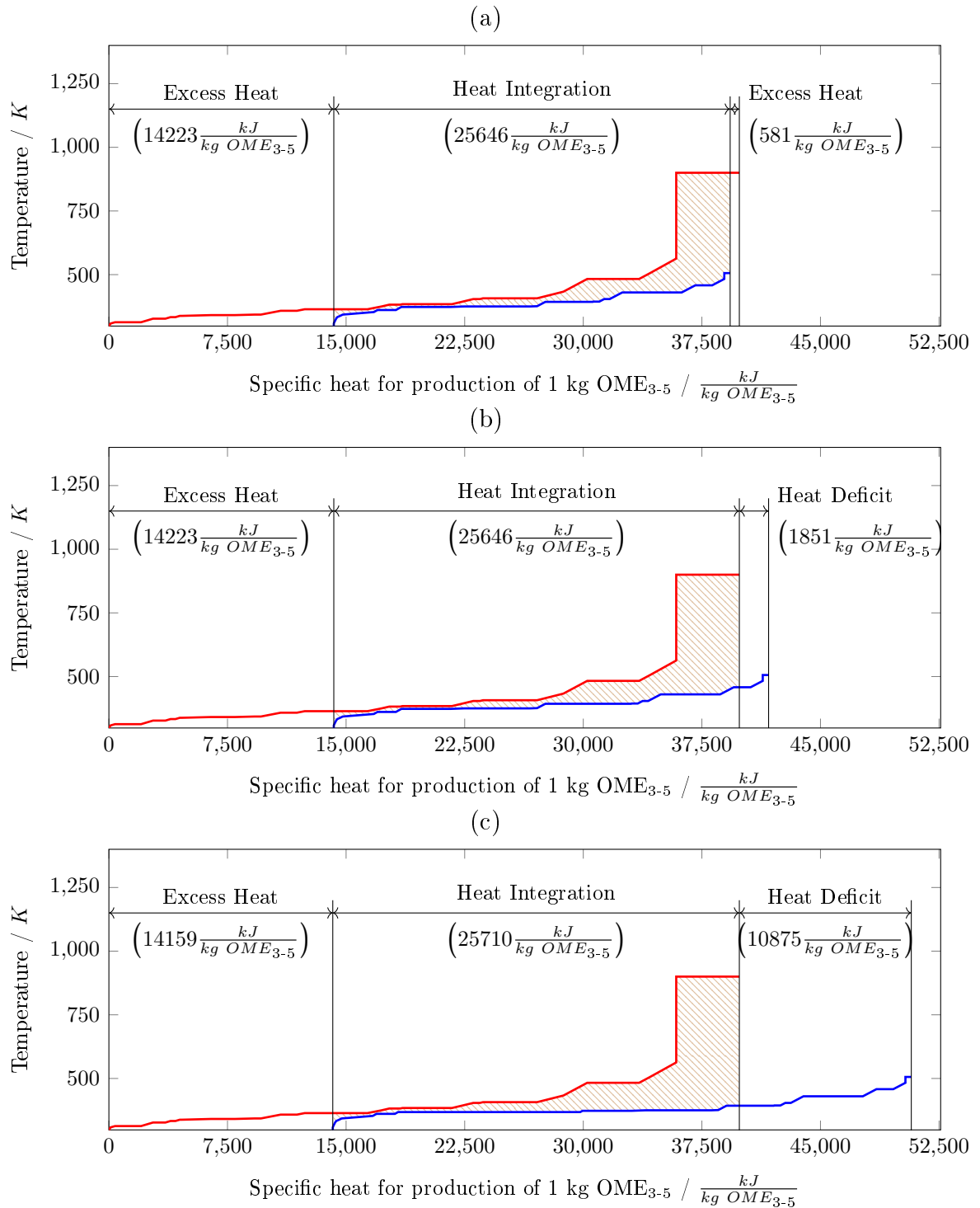


**Figure 38:** Hot Composite Curve (red) and Cold Composite Curve (blue) for overall heat integration (Route B). Panels (a) to (c) give the composite curves for CO<sub>2</sub> supply via CPS (a), PCC (b), DAC (c).

## B.5 Overall energy balance

Tables 25 and 26 give the overall energy balance for Routes A and B for three heat integration scenarios and three CC methods.

**Table 25:** Energy balance of different scenarios for Route A

Scenario/ Processes	Energy / kJ per kg OME <sub>3-5</sub>		
	<i>Q<sub>deficit</sub></i>	<i>Q<sub>excess</sub></i>	<i>w<sub>t</sub></i>
S1			
EL	0	14987	50031
CC(CPS)	0	0	0
CC(PCC)	2400	0	0
CC(DAC)	11500	0	1646
ME	0	8071	1400
FA	0	5747	43
OME	8888	9991	0
S2			
EL	0	14987	50031
ME +CC(CPS)	0	8071	1400
ME +CC(PCC)	0	5639	1400
ME +CC(DAC)	8223	4773	3046
FA+OME	4388	11257	43
S3			
EL	0	14987	50031
all+CC(CPS)	597	15536	1443
all+CC(PCC)	1749	14256	1443
all+CC(DAC)	10174	13593	3089

**Table 26:** Energy balance of different scenarios for Route B

Scenario/ Processes	Energy / kJ per kg OME <sub>3-5</sub>		
	$q_{deficit}$	$q_{excess}$	$w_t$
S1			
EL	0	15024	50158
CC(CPS)	0	0	0
CC(PCC)	2432	0	0
CC(DAC)	11520	0	1650
ME	0	8090	1404
FA	0	5865	43
TRI	7445	7867	0
MAL	4351	4633	0
OME	1396	1539	0
S2			
EL	0	15024	50158
ME +CC(CPS)	0	8090	1404
ME +CC(PCC)	0	5658	1404
ME +CC(DAC)	8211	4781	3054
FA + TRI+ MAL+ OME <sub>3-5</sub>	3691	10424	43
S3			
EL	0	15024	50158
all+CC(CPS)	0	14804	1447
all+CC(PCC)	1851	14223	1447
all+CC(DAC)	10875	14159	3097

## B.6 LHV efficiencies of Route A and B

Tables 27 and 28 give the overall energy efficiency for all investigated cases.

**Table 27:** LHV efficiency of Route A for different scenarios of heat integration and different carbon sources

	S1	S2	S3
Efficiency H <sub>2</sub> -to-OME			
CPS	0.469	0.528	0.591
PCC	0.443	0.528	0.570
DAC	0.354	0.414	0.437
Efficiency power-to-OME			
CPS	0.313	0.339	0.363
PCC	0.301	0.339	0.355
DAC	0.257	0.288	0.299

**Table 28:** LHV efficiency of Route B for different scenarios of heat integration and different carbon sources

	S1	S2	S3
Efficiency H <sub>2</sub> -to-OME			
CPS	0.423	0.537	0.600
PCC	0.401	0.537	0.567
DAC	0.327	0.420	0.430
Efficiency power-to-OME			
CPS	0.292	0.342	0.367
PCC	0.281	0.342	0.354
DAC	0.243	0.290	0.295

## B.7 Stream tables (ME to OME<sub>3-5</sub>)

### B.7.1 Stream tables for single processes in Route A.

Tables 29 to 31 show the stream tables of all processes in Route A.

**Table 29:** Stream table of the ME synthesis plant (Route A) based on Pérez-Fortes et al. [40], for stream numbers of Figure 24 (asterisk indicating a different temperature in the case of heat integration of the process into preceding or subsequent process)

	1	2	3	4	5	6	7
$p$ / bar	1.0	30.0	1.0	1.0	1.0	1.0	1.0
$T$ / K	298	298	293	525	298	298/312*	298
$\dot{m}_{\text{total}}$ / $\frac{\text{kg}}{\text{h}}$	6583	900	3664	4081	3005	1501	2592
Mass flowrates $\dot{m}_i$ / kg per hour							
CO <sub>2</sub>	6583	0	0	408	0	0	0
H <sub>2</sub>	0	900	0	0	0	0	0
O <sub>2</sub>	0	0	879	449	0	0	0
N <sub>2</sub>	0	0	2784	2816	0	0	0
WA	0	0	0	408	0	0	2592
ME	0	0	0	0	3005	1501	0



**Table 30:** Stream table of the FA synthesis plant (Route A) based on Reuss et al. [28], stream numbers referring to Figure 4 in main manuscript (asterisk indicating a different temperature in the case of heat integration of the process into preceding or subsequent process)

	1 / 2	3	4	5	6	7	8
$p$ / bar	1.0 / 1.4	1.4	1.4	1.4	1.4	1.4	1.4
$T$ / K		298	298	298	346	483	298
$\dot{m}_{\text{total}}$ / $\frac{\text{kg}}{\text{h}}$		5367	3005	3005	8372	8372	868
Mass flowrates $\dot{m}_i$ / kg per hour							
CO	0	0	0	0	0	16	0
CO <sub>2</sub>	0	0	0	0	0	411	0
O <sub>2</sub>	1251	0	0	1251	1251	0	0
N <sub>2</sub>	4116	0	0	4116	4116	4116	0
H <sub>2</sub>	0	0	0	0	0	70	0
ME	0	3005	3005	3005	3005	0	0
FA	0	0	0	0	0	2520	0
WA	0	0	0	0	0	1239	868

	9	10	11	12	13	14	15
$p$ / bar	1.4	1.4	1.4	1.4	1.4	1.4	1.4
$T$ / K	348	381	382	382	298	416	298 / 343*
$\dot{m}_{\text{total}}$ / $\frac{\text{kg}}{\text{h}}$	4658	4581	1615	1615	1615	2967	2967
Mass flowrates $\dot{m}_i$ / kg per hour							
CO	16	0	0	0	0	0	0
CO <sub>2</sub>	411	0	0	0	0	0	0
O <sub>2</sub>	0	0	0	0	0	0	0
N <sub>2</sub>	4116	0	0	0	0	0	0
H <sub>2</sub>	70	0	0	0	0	0	0
ME	0	0	0	0	0	0	0
FA	0	2520	0	0	0	2520	2520
WA	45	2062	1615	1615	1615	447	447

**Table 31:** Stream table of the OME<sub>3-5</sub> synthesis plant (Route A) based on Schmitz et al. [43], stream numbers referring to Figure 7 in main manuscript (asterisk indicating a different temperature in the case of heat integration of the process into preceding or subsequent process)

	1	2	3	4	5	6	7	8
$p$ / bar	1.5	1.5	1.5	1.5	1.5	1.5	1.5	0.3
$T$ / K	298/ 343*	343	298/ 312*	343	343	343	343	357
$\dot{m}_{\text{total}}$ / $\frac{\text{kg}}{\text{h}}$	2967	2967	1501	1501	4468	23562	23562	18713
Mass flowrates $\dot{m}_i$ / kg per hour								
FA	2520	2520	0	0	2520	10475	7957	7956
ME	0	0	1501	1501	1501	4661	3154	3154
WA	447	447	0	0	447	659	1083	1083
MAL	0	0	0	0	0	3766	3766	3766
OME <sub>2</sub>	0	0	0	0	0	2754	2754	2754
OME <sub>3</sub>	0	0	0	0	0	0	1796	0
OME <sub>4</sub>	0	0	0	0	0	0	1105	0
OME <sub>5</sub>	0	0	0	0	0	0	698	0
OME <sub>6</sub>	0	0	0	0	0	471	471	0
OME <sub>7</sub>	0	0	0	0	0	330	330	0
OME <sub>8</sub>	0	0	0	0	0	212	212	0
OME <sub>9</sub>	0	0	0	0	0	141	141	0
OME <sub>n<math>\geq</math>10</sub>	0	0	0	0	0	94	94	0

	9	10	11	12	13	14	15	16	17
$p$ / bar	1.5	1.5	1.5	0.3	1.5	0.03	0.03	0.3	0.3
$T$ / K	309	343	470	523	343	309	298	404	298
$\dot{m}_{\text{total}}$ / $\frac{\text{kg}}{\text{h}}$	17845	17845	4847	1248	1248	868	868	3600	3600
Mass flowrates $\dot{m}_i$ / kg per hour									
FA	7956	7956	0	0	0	0	0	0	0
ME	3154	3154	0	0	0	0	0	0	0
WA	215	215	0	0	0	868	868	0	0
MAL	3766	3766	0	0	0	0	0	0	0
OME <sub>2</sub>	2754	2754	0	0	0	0	0	0	0
OME <sub>3</sub>	0	0	1796	0	0	0	0	1796	1796
OME <sub>4</sub>	0	0	1105	0	0	0	0	1105	1105
OME <sub>5</sub>	0	0	698	0	0	0	0	698	698
OME <sub>6</sub>	0	0	471	471	471	0	0	0	0
OME <sub>7</sub>	0	0	330	330	330	0	0	0	0
OME <sub>8</sub>	0	0	212	212	212	0	0	0	0
OME <sub>9</sub>	0	0	141	141	141	0	0	0	0
OME <sub>n<math>\geq</math>10</sub>	0	0	94	94	94	0	0	0	0

### B.7.2 Stream tables for single processes in Route B

Tables 32 to 36 show the stream tables of all processes in Route B.

**Table 32:** Stream table of the ME synthesis plant (Route B) based on Pérez-Fortes et al. [40], for stream numbers of Figure 24 (asterisk indicating a different temperature in the case of heat integration of the process into preceding or subsequent process)

	1	2	3	4	5	6	7
$p$ / bar	1.0	30.0	1.0	1.0	1.0	1.0	1.0
$T$ / K	298	298	293	525	298	298/ 312*	298
$\dot{m}_{\text{total}}$ / $\frac{\text{kg}}{\text{h}}$	6600	902	3673	4091	3018	1499	2599
	Mass flowrates $\dot{m}_i$ / kg per hour						
CO <sub>2</sub>	6600	0	0	409	0	0	0
H <sub>2</sub>	0	902	0	0	0	0	0
O <sub>2</sub>	0	0	882	450	0	0	0
N <sub>2</sub>	0	0	2791	2823	0	0	0
WA	0	0	0	409	0	0	2599
ME	0	0	0	0	3018	1499	0

**Table 33:** Stream table of the FA synthesis plant (Route B) based on Reuss et al. [28], stream numbers referring to Figure 4 in main manuscript (asterisk indicating a different temperature in the case of heat integration of the process into preceding or subsequent process)

	1/ 2	3, 4	5	6	7	8	9
$p$ / bar	1.0/ 1.4	1.4	1.4	1.4	1.4	1.4	1.4
$T$ / K	298	298	298	346	483	298	348
$\dot{m}_{\text{total}}$ / $\frac{\text{kg}}{\text{h}}$	5390	3018	8407	8407	8407	871	4678
Mass flowrates $\dot{m}_i$ / kg per hour							
CO	0	0	0	0	16	0	16
CO <sub>2</sub>	0	0	0	0	412	0	412
O <sub>2</sub>	1256	0	1256	1256	0	0	0
N <sub>2</sub>	4134	0	4134	4134	4134	0	4134
H <sub>2</sub>	0	0	0	0	70	0	70
ME	0	3018	3018	3018	0	0	0
FA	0	0	0	0	2530	0	0
WA	0	0	0	0	1244	871	45

	10	11,13	14	15,16	17	18,20	21,22
$p$ / bar	1.4	1.4	1.4	1.4	1.4	1.4	1.4
$T$ / K		407/		394/ 333*		381/	404/ 343*
$\dot{m}_{\text{total}}$ / $\frac{\text{kg}}{\text{h}}$	381	298	394	298*	394	298	298*
$\dot{m}_{\text{total}}$ / $\frac{\text{kg}}{\text{h}}$	4601	567	4033	1126	2907	547	2360
Mass flowrates $\dot{m}_i$ / kg per hour							
CO	0	0	0	0	0	0	0
CO <sub>2</sub>	0	0	0	0	0	0	0
O <sub>2</sub>	0	0	0	0	0	0	0
N <sub>2</sub>	0	0	0	0	0	0	0
H <sub>2</sub>	0	0	0	0	0	0	0
ME	0	0	0	0	0	0	0
FA	2530	0	2530	706	1824,4	0	1824,4
WA	2070	567	1503	420	1083	547	536

**Table 34:** Stream table of the TRI synthesis plant (Route B) based on Grützner et al. [41], stream numbers referring to Figure 5 in main manuscript (asterisk indicating a different temperature in the case of heat integration of the process into preceding or subsequent process)

	1	2	3	4	5	6
$p$ / bar	1.0	1.0	1.0	1.0	1.0	1.0
$T$ / K	298/ 343*	343	343	343	375	343
$\dot{m}_{\text{total}}$ / $\frac{\text{kg}}{\text{h}}$	2360	2360	20842	20842	18482	18482
Mass flowrates $\dot{m}_i$ / kg per hour						
TRI	0	0	0	1825	0	0
FA	1825	1825	15871	14046	14046	14046
WA	536	536	4971	4971	4436	4436

	7	8	9	10	11	12	13
$p$ / bar	1.0	4.0	4.0	4.0	2.0	2.0	2.0
$T$ / K	365	430	298/ 338*	407	384	393	298
$\dot{m}_{\text{total}}$ / $\frac{\text{kg}}{\text{h}}$	10173	1838	1838	8336	7813	522	522
Mass flowrates $\dot{m}_i$ / kg per hour							
TRI	7059	1819	1819	5240	5235	5	5
FA	781	0	0	781	781	0	0
WA	2333	18	18	2314	1797	517	517

**Table 35:** Stream table of the MAL synthesis plant (Route B) based on Weidert et al. [62] and [42], stream numbers referring to Figure 6 in main manuscript (asterisk indicating a different temperature in the case of heat integration of the process into preceding or subsequent process)

	1	2	3	4	5	6	7
$p$ / bar	2.0	2.0	2.0	2.0	2.0	2.0	2.0
$T$ / K	298/ 333*	333	298/ 312*	333	333	333	333
$\dot{m}_{\text{total}}$ / $\frac{\text{kg}}{\text{h}}$	1126	1126	1499	1499	2625	7282	7282
	Mass flowrates $\dot{m}_i$ / kg per hour						
FA	706	706	0	0	706	708	58
ME	0	0	1499	1499	1499	5880	4485
WA	420	420	0	0	420	694	1085
MAL	0	0	0	0	0	0	1653

	8, 9	10	11	12	13	14	15
$p$ / bar	2.0	1.0	1.0	1.0	4.0	4.0	4.0
$T$ / K	341	373	298	313	358	361	298/ 338*
$\dot{m}_{\text{total}}$ / $\frac{\text{kg}}{\text{h}}$	4657	843	843	4573	2793	1782	1782
	Mass flowrates $\dot{m}_i$ / kg per hour						
FA	2	3	3	0	0	0	0
ME	4381	0	0	310	310	0	0
WA	274	840	840	1	0	1	1
MAL	0	0	0	4262	2482	1781	1781

**Table 36:** Stream table of the OME<sub>3-5</sub> synthesis plant (Route B), according to Burger et al. [44], stream numbers referring to Figure 7 in main manuscript (asterisk indicating a different temperature in the case of heat integration of the process into preceding or subsequent process)

	1	2	3	4	5	6	7	8
$p$ / bar	1.0	1.0	1.0	1.0	1.0	1.0	1.0	1.0
$T$ / K	343	327	298/ 338*	338	298/ 338*	338	338	338
$\dot{m}_{\text{total}}$ / $\frac{\text{kg}}{\text{h}}$	12252	6460	1781	1781	1819	1819	3600	12252
Mass flowrates $\dot{m}_i$ / kg per hour								
FA	32	32	0	0	0	0	0	32
TRI	491	490	0	0	1819	1819	1819	2310
MAL	3155	3155	1781	1781	0	0	1781	4936
OME <sub>2</sub>	2559	2558	0	0	0	0	0	2558
OME <sub>3</sub>	1905	209	0	0	0	0	0	209
OME <sub>4</sub>	1357	14	0	0	0	0	0	14
OME <sub>5</sub>	937	1	0	0	0	0	0	379
OME <sub>6</sub>	635	0	0	0	0	0	0	635
OME <sub>7</sub>	421	0	0	0	0	0	0	421
OME <sub>8</sub>	275	0	0	0	0	0	0	275
OME <sub>9</sub>	178	0	0	0	0	0	0	178
OME <sub>10</sub>	114	0	0	0	0	0	0	114
OME <sub>n&gt;10</sub>	192	0	0	0	0	0	0	192

	9	10	11	12	13	14	15	16	17
$p$ / bar	-	1.0	1.0	0.3	1.0	-	-	0.3	1.0
$T$ / K	-	338	458	506	338	-	-	404	298
$\dot{m}_{\text{total}}$ / $\frac{\text{kg}}{\text{h}}$	-	6460	5792	2192	2192	-	-	3600	3600
Mass flowrates $\dot{m}_i$ / kg per hour									
FA	-	32	0	0	0	-	-	0	0
TRI	-	490	1	0	0	-	-	1	1
MAL	-	3155	0	0	0	-	-	0	0
OME <sub>2</sub>	-	2558	1	0	0	-	-	1	1
OME <sub>3</sub>	-	209	1696	0	0	-	-	1696	1696
OME <sub>4</sub>	-	14	1343	0	0	-	-	1343	1343
OME <sub>5</sub>	-	1	937	378	378	-	-	558	558
OME <sub>6</sub>	-	0	635	635	635	-	-	0	0
OME <sub>7</sub>	-	0	421	421	421	-	-	0	0
OME <sub>8</sub>	-	0	275	275	275	-	-	0	0
OME <sub>9</sub>	-	0	178	178	178	-	-	0	0
OME <sub>10</sub>	-	0	114	114	114	-	-	0	0
OME <sub>n&gt;10</sub>	-	0	192	192	192	-	-	0	0

## B.8 Energy demand tables (ME to OME<sub>3-5</sub>)

In the following subsection, the energy demands of all individual processes are given. Depending on the level of heat integration, process inputs/ outputs are either heated up/ cooled down from/ to 298 K (indicated by a) or directly integrated from/ into the preceding/ subsequent process (indicated by b). For the ME production, the data of the given pinch analysis in Pérez-Fortes et al. [40] is extracted graphically (Hot/ Cold Composite Curve (HCC/ CCC) sections) and augmented with additional heat sources that can be used for heat integration. The combustion temperature during burning the waste stream will exceed the normal process temperatures. Hence, the heat can be used for heat integration in any case. As the specific temperature is of no further interest, it is arbitrarily set to 900 K. The descriptions of the energy streams are referring to the units in Figure 4 to Figure 7 of the main manuscript.

### B.8.1 Energy demand tables for single processes in Route A.

**Table 37:** Energy demand for the synthesis of ME (Route A) based on Pérez-Fortes et al. [40].  $T_{in/out}$ : inlet/ outlet temperature,  $q/w_t$ : specific heat/ electricity demand

Energy stream	$T_{in} / K$	$T_{out} / K$	$\frac{q \text{ or } w_t}{kg \text{ OME}_{3-5}}$
HCC section 1	563	433	-3763
HCC section 2	433	343	-5563
HCC section 3	343	338	-3027
HCC section 4	338	308	-1391
CCC section 1	308	333	164
CCC section 2	333	343	327
CCC section 3	343	353	1963
CCC section 4	353	373	573
CCC section 5	373	376	1309
CCC section 6	376	483	3272
B (Combustion of waste product)	900	900	-1644
HX1a (ME as input for FA process)	312	298	-41
HX1b (ME as input for FA process)	312	298	-41
HX2a (ME as input for OME <sub>3-5</sub> process)	312	298	-19
HX2b (ME as input for OME <sub>3-5</sub> process)	312	312	0
HX3	374	298	-230
Compression of educts	298	298	1400



**Table 38:** Energy demand for the FA synthesis plant (Route A) based on Reuss et al. [28].  $T_{in/out}$ : inlet/ outlet temperature,  $q/w_t$ : specific heat/ electricity demand

Energy stream	$T_{in} / \text{K}$	$T_{out} / \text{K}$	$q$ or $w_t / \frac{\text{kJ}}{\text{kg OME}_{3-5}}$
Column and evaporator HX2 fully heat-integrated	-	-	0
Reactor R	483	483	-3268
Combustion of waste product	900	900	-2333
TFE1 (thin film evaporator)	416	416	1127
CON1	382	382	-1015
HX1	298	298	0
HX3	382	298	-158
HX4a (FA input for OME <sub>3-5</sub> process)	416	298	-100
HX4b (FA input for OME <sub>3-5</sub> process)	416	343	-62
Compression of educts	298	298	43

**Table 39:** Energy demand for the OME<sub>3-5</sub> synthesis plant (Route A) based on Schmitz et al. [43].  $T_{in/out}$ : inlet/ outlet temperature,  $q/w_t$ : specific heat/ electricity demand

Energy stream	$T_{in} / \text{K}$	$T_{out} / \text{K}$	$q$ or $w_t / \frac{\text{kJ}}{\text{kg OME}_{3-5}}$
Reactor R	343	343	-1123
Reboiler at C1	470	470	8488
Condenser at C1	357	357	-7969
Reboiler at C2	523	523	427
Condenser at C2	404	404	-525
CON1	298	298	-587
HX1a	298	343	38
HX1b	343	343	0
HX2a	298	343	66
HX2b	312	343	47
HX3	343	343	372
HX4	523	343	-115
HX5	404	298	-180

### B.8.2 Energy demand tables for single processes in Route B.

**Table 40:** Energy demand for the synthesis of ME (Route B) based on Pérez-Fortes et al. [40].  $T_{in/out}$ : inlet/ outlet temperature,  $q/w_t$ : specific heat/ electricity demand

Energy stream	$T_{in} / K$	$T_{out} / K$	$q$ or $w_t$ $/ \frac{kJ}{kg OME_{3-5}}$
HCC section 1	563	433	-3772
HCC section 2	433	343	-5577
HCC section 3	343	338	-3034
HCC section 4	338	308	-1394
CCC section 1	308	333	164
CCC section 2	333	343	328
CCC section 3	343	353	1968
CCC section 4	353	373	574
CCC section 5	373	376	1312
CCC section 6	376	483	3280
B (Combustion of waste product)	900	900	-1648
HX1a (ME as input for FA process)	312	298	-41
HX1b (ME as input for FA process)	312	298	-41
HX2a (ME as input for MAL process)	312	298	-19
HX2b (ME as input for MAL process)	312	312	0
HX3	374	298	-231
Compression of educts	298	298	1404

**Table 41:** Energy demand for the FA synthesis plant (Route B) based on Reuss et al. [28].  $T_{in/out}$ : inlet/ outlet temperature,  $q/w_t$ : specific heat/ electricity demand

Energy stream	$T_{in} / K$	$T_{out} / K$	$q$ or $w_t$ / $\frac{kJ}{kg OME_{3-5}}$
Column and evaporator HX2 fully heat-integrated	-	-	0
Reactor R	483	483	-3282
Combustion of waste product	900	900	-2343
TFE (thin film evaporator)	393	393	702
CON1	373	373	-702
HX1	298	298	0
HX3	381	298	-55
HX4	381	298	-54
HX5a (FA input for MAL process)	394	298	-70
HX5b (FA input for MAL process)	394	333	-45
HX6a (FA input for TRI process)	404	298	-106
HX6b (FA input for TRI process)	404	343	-61
Compression of educts	298	298	43

**Table 42:** Energy demand for the TRI synthesis plant (Route B) based on Grützner et al. [41].  $T_{\text{in/out}}$ : inlet/ outlet temperature,  $q/w_t$ : specific heat/ electricity demand

Energy stream	$T_{\text{in}} / \text{K}$	$T_{\text{out}} / \text{K}$	$q$ or $w_t / \frac{\text{kJ}}{\text{kg OME}_{3-5}}$
Reactor R	343	343	-407
Reboiler at C1	375	375	4165
Condenser at C1	364	364	-3965
Reboiler at C2	430	430	3758
Condenser at C2	407	407	-3423
Reboiler at C3	393	393	2992
Condenser at C3	384	384	-3131
HX1a	298	343	46
HX1b	343	343	0
HX2	375	343	-276
HX3a	430	298	-124
HX3b	430	338	-91
HX4	393	298	-57

**Table 43:** Energy demand for the MAL synthesis plant (Route B) based on Weidert et al. [62] and Drunsel et al. [42].  $T_{\text{in/out}}$ : inlet/ outlet temperature,  $q/w_t$ : specific heat/ electricity demand

Energy stream	$T_{\text{in}} / \text{K}$	$T_{\text{out}} / \text{K}$	$q$ or $w_t / \frac{\text{kJ}}{\text{kg OME}_{3-5}}$
Reactor R	333	333	-310
Reboiler at C1	373	373	3109
Condenser at C1	313	313	-1645
Reboiler at C2	361	361	1165
Condenser at C2	358	358	-1027
CON1	341	341	-1506
HX1a	298	333	26
HX1b	333	333	0
HX2a	298	333	51
HX2b	312	333	31
HX3	373	298	-73
HX4a	361	298	-72
HX4b	361	338	-28

**Table 44:** Energy demand for the OME<sub>3-5</sub> synthesis plant (Route B), according to Burger et al. [44].  $T_{\text{in/out}}$ : inlet/ outlet temperature,  $q/w_t$ : specific heat/ electricity demand

Energy stream	$T_{\text{in}} / \text{K}$	$T_{\text{out}} / \text{K}$	$q$ or $w_t / \frac{\text{kJ}}{\text{kg OME}_{3-5}}$
Reactor R	338	338	-125
Reboiler at C1	458	458	1067
Condenser at C1	327	327	-784
Reboiler at C2	506	506	371
Condenser at C2	404	404	-422
HX1a	298	338	44
HX1b	338	338	0
HX2a	298	338	32
HX2b	338	338	0
HX3	327	338	42
HX4	506	338	-187
HX5	404	298	-181

# C Appendix: Novel process for the provision of methanolic formaldehyde solutions

## C.1 Model TFE: Influence of discretization

The number of stages  $N$  of the thin-film evaporator (TFE) was varied for fixed feed composition and temperature, while pressure, total heat duty  $Q_{\text{TFE}}$  and total residence time  $\tau_{\text{TFE}}$  are also kept constant. Table 45 gives the specifications of the study, Figures 39 and 40 the results. The first feed composition was adapted from a FA reactor product from the literature [131], the second is equal in composition to the feed of the TFE in the process (Case I, streams 3+6). The total heat duty was chosen so that the total vapor fraction is the same as in the desired operating point; however, the choice of the heat duty has no influence on the required discretization. The total residence time is calculated from the apparatus size in the experiment of Schilling et al. [135].

**Table 45:** Input parameters for the investigation of the discretization of the TFE model.

$x_{FA}^{Feed}$ /g/g	$x_{WA}^{Feed}$ /g/g	$x_{ME}^{Feed}$ /g/g	$T^{Feed}/circ$ C	$\dot{m}^{Feed}$ /kg/h	$p$ /bar	$\dot{Q}_{tot}$ /kW	$\tau_{tot}$ / s
0.451	0.241	0.308	75.16	1000	1	200	11.3
0.546	0.367	0.087	75.16	1000	1	200	11.3

The results show that increasing the stage number from one to two changes little in the composition of the top and bottom products. When using more than two stages, there is no change to the simulation results. Only comparably short residence times were investigated, as these are the only sensible operating point for the concentration of FA in TFEs. Medium to long residence times, which are not of interest here, could require more than one or two stages.

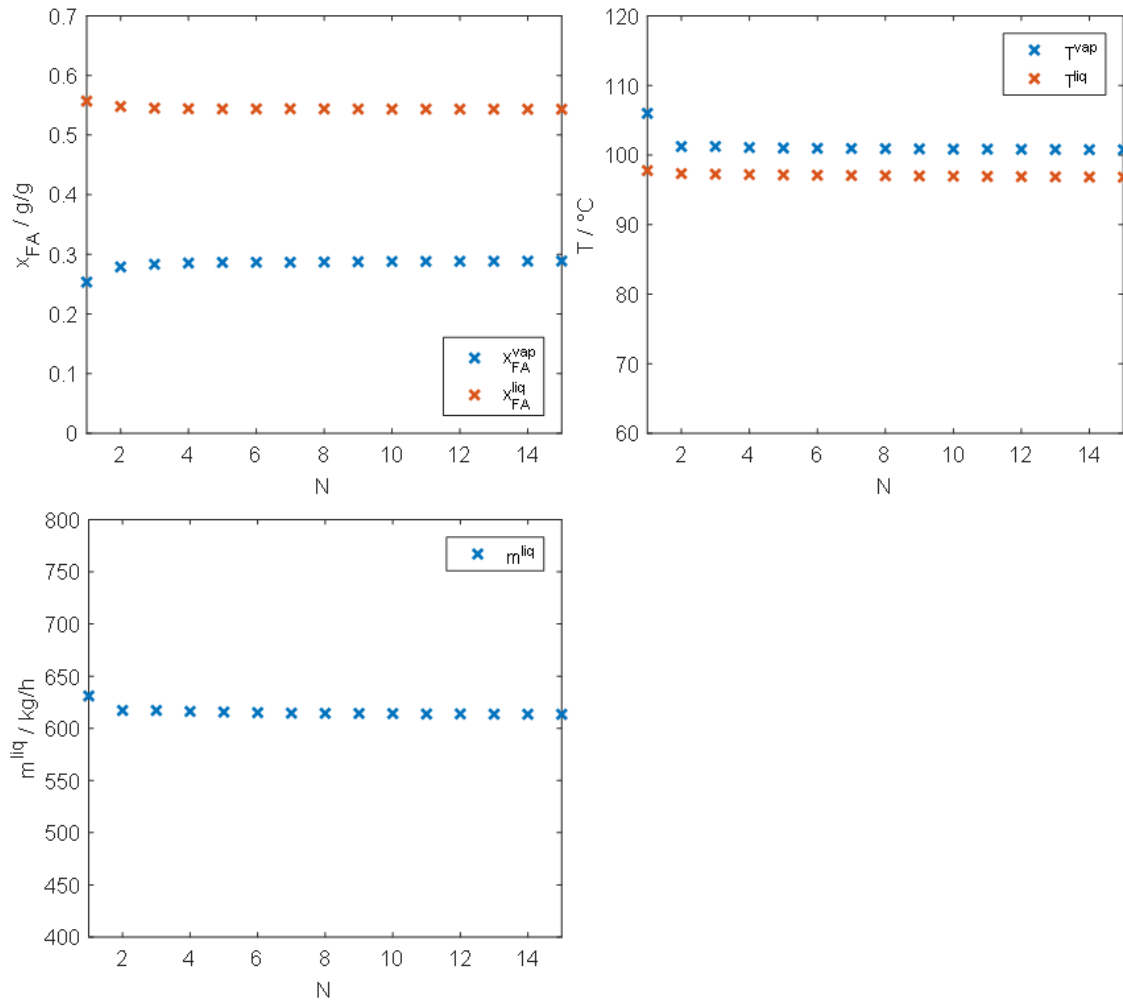


**Figure 39:** Influence of the number of stages on the composition, temperature, and mass flow rate of the products of the TFE for the feed given in row 1 of Table 45.

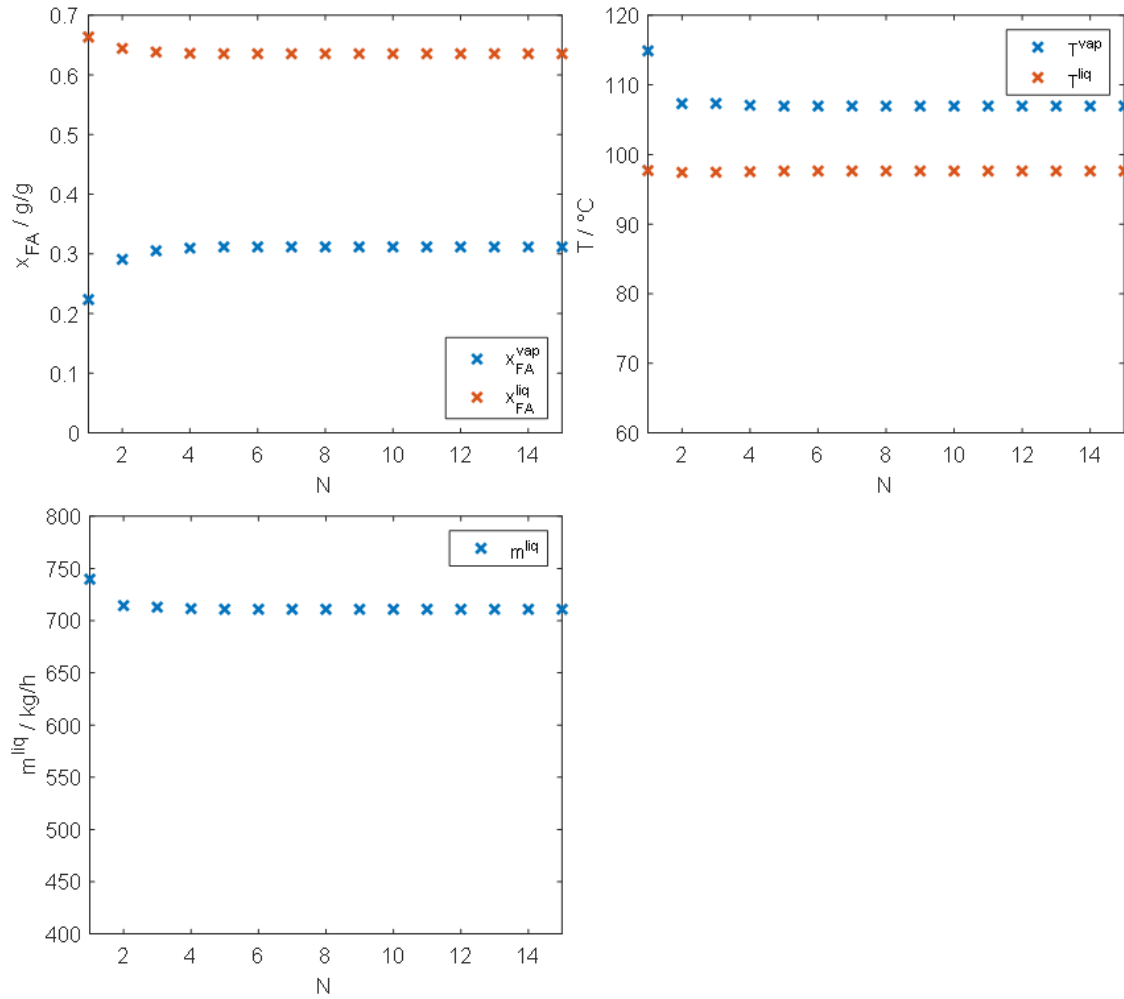


**Figure 40:** Influence of the number of stages on the composition, temperature, and mass flow rate of the products of the TFE for the feed given in row 2 of Table 45.

## C.2 Reactive vapor-liquid equilibrium topology of formaldehyde solutions

Figure 41 shows reactive distillation boundaries at various pressures in the system FA+WA+ME in a ternary map. Only overall mass fractions are displayed; the boundaries have already been shown by Ott et al. [33] and are reproduced based on the described property model of the present work.

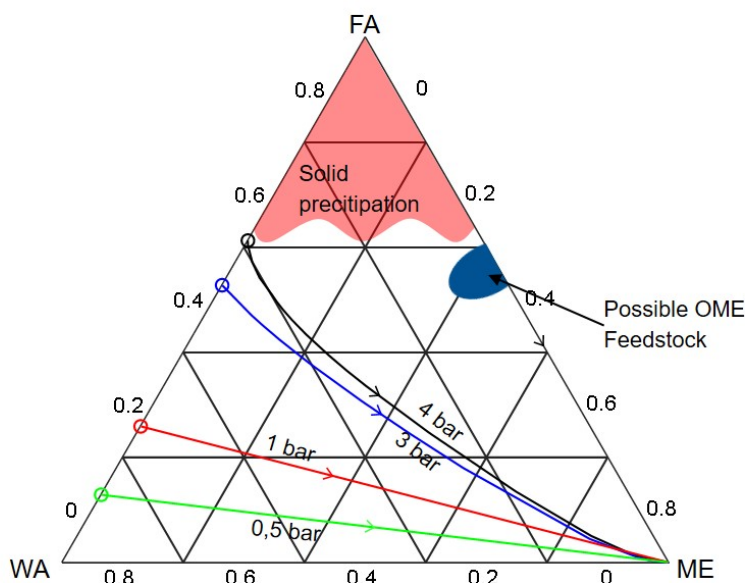


**Figure 41:** Distillation boundaries at various pressures in the system FA+WA+ME in a ternary map. The region of solid precipitation is highlighted qualitatively. FA mass fraction of the binary azeotropes FA/WA in g/g: 0.129 (0.5 bar); 0.259 (1 bar); 0.528 (3 bar); 0.613 (4 bar)

The desired product of the studied process is shown as the blue region in Figure 41. Removal of pure water via distillation is only possible if the column's feed is located on the WA-side of the boundary. Then, however, the column's other product still contains a lot of water. On the other side of the boundary, the OME feedstock is neither a feasible top nor a feasible bottom product of a distillation column, as long as water is still present. Therefore, it is impossible to produce OME feedstock by removing water from water-containing FA solutions via simple distillation. However, it is possible to produce highly concentrated FA solutions using thin-film evaporators. In TFEs the evaporation happens so fast that the chemical equilibrium in the liquid phase is not reached. This enables the production of concentrated FA solutions, which would otherwise show solid



precipitation. This also allows crossing the distillation boundary in Fig 41, as the evaporation in TFEs is governed by kinetic effects and not by the chemical equilibrium.

### C.3 Additional process data cases I and II

Table 46 gives the stream table of the process for the selected operating point for Case I, Table 47 for Case II.

**Table 46:** Stream table Case I, Pareto point 21

Stream	1	2	3	4	5	6	7	8
$\dot{m}$ / kg/h	1000.0	167.3	832.7	546.3	627.7	341.3	205.0	897.2
$p$ / bar	1.0	0.5	0.5	0.2	0.2	4.0	4.0	1.0
$T$ /°C	75.1	47.8	83.2	116.8	116.8	134.7	143.5	104.7
$x_i$ / g/g								
FA	0.503	0.000	0.604	0.254	0.800	0.405	0.003	0.560
WA	0.294	0.010	0.351	0.628	0.140	0.407	0.997	0.100
ME	0.203	0.990	0.045	0.118	0.059	0.188	0.000	0.340

**Table 47:** Stream table Case II, Pareto point 14

Stream	1	4	5	6	7	8
$\dot{m}$ / kg/h	1497.4	959.4	921.9	383.8	575.6	1380.6
$p$ / bar	1.0	0.2	0.2	4.0	4.0	1.0
$T$ /°C	75.1	122.1	122.1	136.2	143.5	101.4
$x_i$ / g/g						
FA	0.506	0.225	0.820	0.557	0.003	0.547
WA	0.494	0.775	0.180	0.443	0.997	0.120
ME						0.332

Table 48 and 49 give the optimization parameters of the Pareto front displayed in Figure 15 of the main document.

Figure 42 gives the results of the final  $N, Q$ -curves including feed stage optimization for columns C1 and C2 for case I, Figure 43 for C2 for Case II.

**Table 48:** Optimization parameters of the Pareto-optimal solutions in Case I

Case I	Opt. param.		
Pareto point	$RR_{C1}$	$Q_{TFE}$ / kW	$RR_{C2}$
1	6.064	137.187	1.585
2	6.064	143.705	1.636
3	6.050	151.414	1.642
4	6.070	159.151	1.624
5	6.077	166.693	1.637
6	6.059	171.409	1.812
7	6.082	180.889	1.693
8	6.096	187.602	1.751
9	6.136	195.492	1.735
10	6.216	201.452	1.746
11	6.131	212.398	1.786
12	6.266	218.186	1.831
13	6.194	229.295	1.756
14	6.237	234.122	1.776
15	6.218	240.473	1.804
16	6.317	253.183	1.827
17	6.248	260.307	1.860
18	6.248	259.942	1.872
19	6.282	274.298	1.951
20	6.163	300.912	1.795
21	6.093	307.482	1.814
22	6.126	334.025	1.805
23	6.073	342.979	1.921
24	5.982	350.340	1.780
25	5.999	361.858	1.950
26	5.983	389.225	1.798
27	5.945	404.795	1.454
28	5.944	422.911	1.929
29	5.948	391.797	2.631
30	5.891	384.844	2.800
31	5.859	431.969	3.397

**Table 49:** Optimization parameters of the Pareto-optimal solutions in Case II

Case II	Opt. param.	
Pareto point	$Q_{\text{TFE}}$ / kW	$RR_{\text{C2}}$
1	463.822	1.361
2	473.928	1.378
3	482.511	1.422
4	493.177	1.425
5	503.981	1.433
6	514.880	1.448
7	526.050	1.469
8	538.004	1.492
9	551.349	1.512
10	566.374	1.513
11	585.999	1.501
12	603.553	1.662
13	640.249	1.631
14	637.022	1.829
15	706.771	1.296
16	662.888	1.969
17	665.867	2.398
18	696.955	3.597
19	711.539	2.643

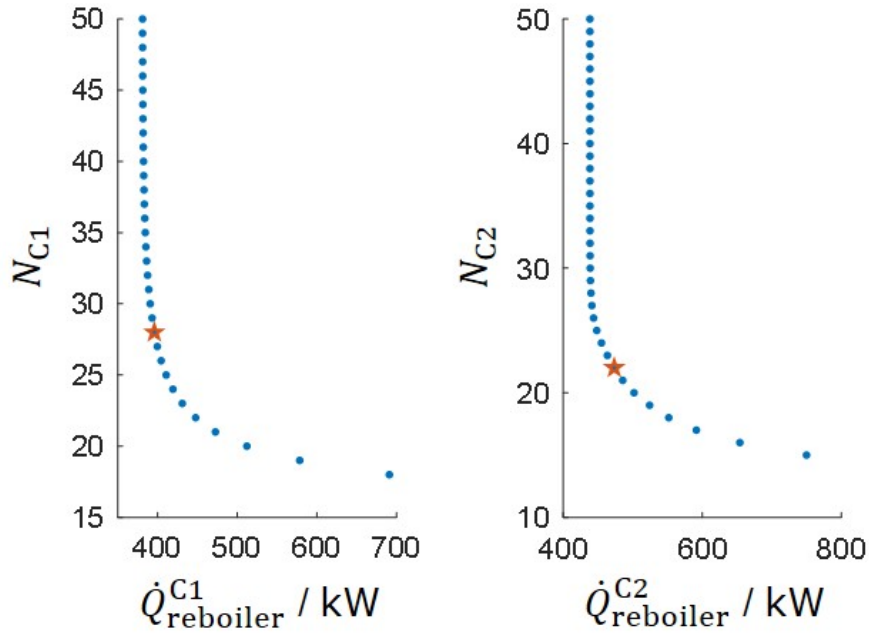


**Figure 42:**  $N, Q$ -curves for C1 and C2 for Case I in the final iteration of the optimization heuristic. The chosen operating point is highlighted as a star.

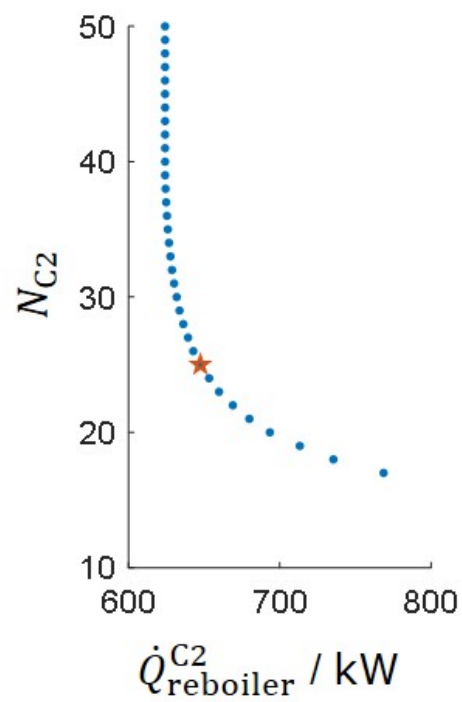


**Figure 43:**  $N, Q$ -curve for C2 for Case II in the final iteration of the optimization heuristic. The chosen operating point is highlighted as a star.

## C.4 Influence of the residence time in the TFE on $OP_I$

While a full investigation of the residence time in the TFE is beyond the scope here, its influence on the operating point  $OP_I$  was briefly studied. Fig 44 shows the shift in  $OP_I$  for increased residence time.

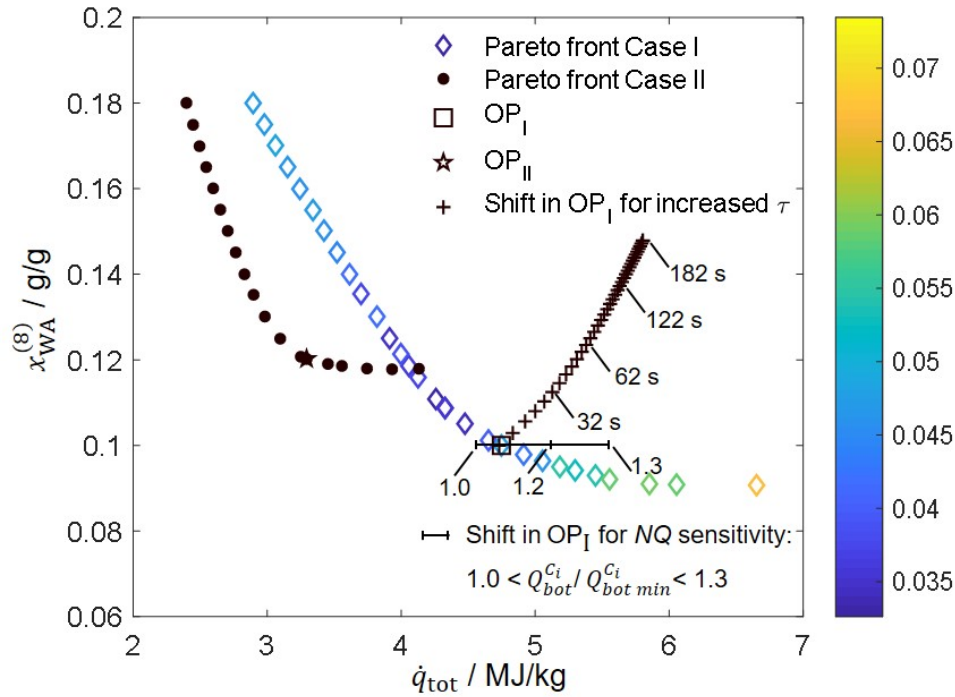


**Figure 44:** Results of the Pareto optimization in Case I (diamonds) and II (circles). For Case I, the mass fraction  $x_{ME}^{(3)}$  of ME in the bottom of C1 is highlighted as color code. The operating points selected in Step 3 of the optimization heuristic are highlighted as star/rectangle. The pluses show the influence of the residence time  $\tau$  in the TFE on  $OP_I$ . The bar shows the change in  $OP_I$  when the factor  $\frac{\dot{Q}_{bot}^{C_i}}{\dot{Q}_{bot\ min}^{C_i}}$  is chosen differently in step 4 of the optimization.

Figure 44 shows that increased residence times lead to higher energy demand and higher product water contents. It is, therefore, desirable to keep the residence time as low as possible. However, this has to be weight up against the increased investment for the TFE. The results further show that the designed process is still feasible even if residence times of only up to 60 s or even 120 s can be realized in a large-scale process.

Further, a sensitivity regarding the weighing of column height vs. heat duty when finding a compromise of both was performed. In step 4 of the optimization, the column stage number of C1 and C2 is chosen so that the factor  $\frac{\dot{Q}_{bot}^{C_i}}{\dot{Q}_{bot\ min}^{C_i}}$  equals 1.06. A low value was chosen to prioritize low-energy processes. The bar in Figure 44 shows the change in

OP<sub>I</sub> when this factor is chosen differently.

# D Appendix: Techno-economic analysis of OME production

## D.1 Additional information on the processes

This section gives process flow diagrams, stream tables, energy balances, and descriptions of the investigated processes. For processes for which the full stream and energy tables were not available in the original literature but calculated in the present work, the specifications used as input for the simulation are highlighted in **bold**.

### D.1.1 Process I: Production of FA with complete conversion of ME

Process I produces an aqueous solution of 0.5 g/g FA. We chose the BASF silver process, which uses a reactor with a silver catalyst and complete conversion of ME in one pass [28]. The left panel in Figure 45 shows the respective process flow diagram (PFD). The reactor conversion and selectivity as well as the composition of the Feed, the absorber off-gas, and the absorber bottom product are adopted from Ullmann's Encyclopedia of Industrial Chemistry [28].

Methanol (1) is evaporated in the evaporator E1 and mixed with steam, air (2), and recycled off-gas (9) from the absorber A1, mainly composed of N<sub>2</sub> and H<sub>2</sub>. The recycle mass flow rate is adjusted so that the resulting mixture is outside of the explosive limits. The explosive limits are calculated considering the limiting oxygen concentration of the mixture [161, 162]. The gaseous mixture (3) is superheated in heat exchanger HX1 and passed over a shallow bed of silver crystals. The water in the mixture enhances conversion and selectivity; the optimal molar ratio of ME to Water is **60/40** [163]. The product leaves the reactor at **680 °C**, conversion of ME is **99%**, the yield **90%** [28]. The reactor product (4) is immediately cooled in HX2 to prevent the disintegration of gaseous FA; the excess heat is utilized to produce steam.

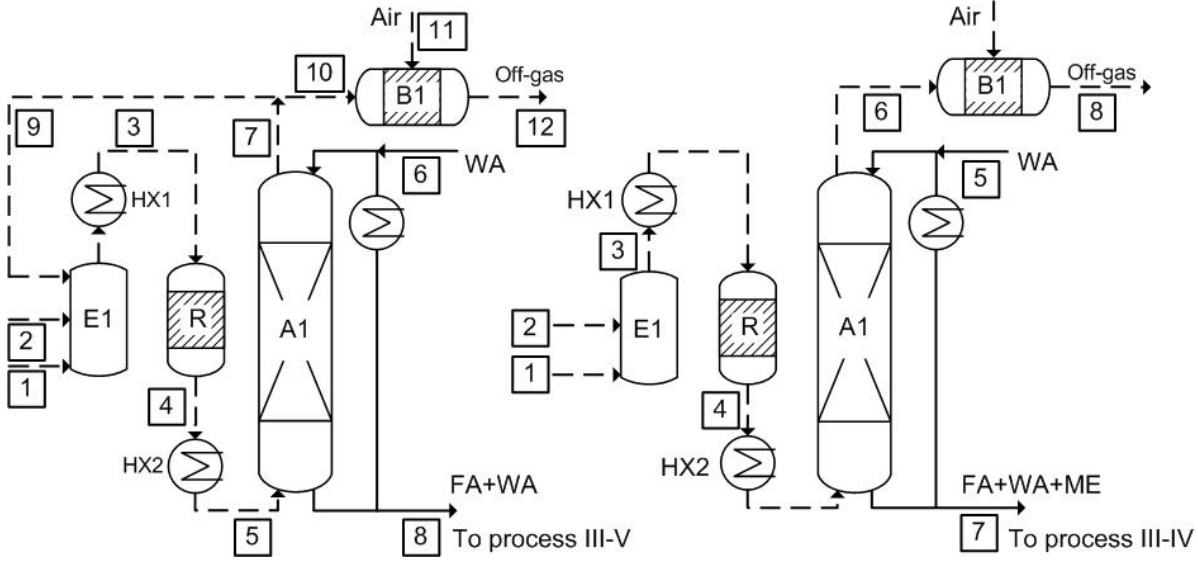


**Figure 45:** Process flow diagram of Process I (left panel) and Process II (right panel).

The cooled gases (5) are fed to the bottom of the absorption column A1, modeled with 4 vapor-liquid equilibrium (VLE) stages. At the bottom of A1, a liquid solution is drawn, cooled, and recycled to its top. Water is added to the top of A1 to enhance FA absorption. The off-gases (7) from the absorber contain small traces of FA and ME. Part of them are recycled as stream (9), the remainder is burned in the burner B1 with excess air (11) to generate steam. The solution (8) drawn from the bottom of A1 contains 0.5 g/g FA and WA with small traces of ME. Tables 50 and 51 give the stream table and unit data of the process.

**Table 50:** Stream Table Process I

Stream	1	2	3	4	5	6	7	8	9	10	11	12
$\dot{m}$ / kg/h	942.57	1354.52	4091.58	4091.59	4091.59	136.90	2991.55	1236.93	1794.50	1197.05	565.98	1763.03
$p$ / bar	1.00	1.00	<b>1.00</b>	1.00	1.00	1.00	<b>1.00</b>	1.00	1.00	1.00	1.00	1.00
$T$ / °C	25.00	25.00	241.97	<b>679.18</b>	160.00	25.00	<b>35.51</b>	65.61	35.51	35.51	25.00	160.00
$x_i$ / g/g												
FA	-	-	-	<b>0.153</b>	0.153	-	<b>0.001</b>	<b>0.504</b>	0.001	0.001	-	-
WA	0.216	-	<b>0.068</b>	<b>0.146</b>	0.146	1.000	0.042	0.492	0.042	0.042	-	0.105
ME	0.784	-	<b>0.181</b>	<b>0.002</b>	0.002	-	0.001	0.003	0.001	0.001	-	-
CO <sub>2</sub>	-	-	0.031	0.053	0.053	-	0.072	-	0.072	0.072	-	0.054
N <sub>2</sub>	-	0.767	0.634	0.634	0.634	-	0.868	-	0.868	0.868	0.767	0.835
O <sub>2</sub>	-	0.233	0.078	0.001	0.001	-	0.002	-	0.002	0.002	0.233	0.007
H <sub>2</sub>	-	-	0.005	0.009	0.009	-	0.012	-	0.012	0.012	-	-
CO	-	-	0.001	0.002	0.002	-	0.003	-	0.003	0.003	-	-



**Table 51:** Unit operations data Process I

Unit:	$T/^\circ\text{C}$	$p / \text{bar}$	$\dot{Q} / \text{kW}$
E <sub>1</sub>	49.04	1.00	405.03
HX <sub>1_1</sub>	140.00	1.00	129.11
HX <sub>1_2</sub>	210.00	1.00	103.18
HX <sub>1_3</sub>	241.97	1.00	46.68
R	680.00	1.00	-
HX <sub>2_1</sub>	300.00	1.00	-643.71
HX <sub>2_2</sub>	230.00	1.00	-110.37
HX <sub>2_3</sub>	160.00	1.00	-107.84
A <sub>1</sub>	35.51	1.00	-394.29
B <sub>1_1</sub>	300.00	1.00	-365.15
B <sub>1_2</sub>	230.00	1.00	-39.65
B <sub>1_3</sub>	160.00	1.00	-39.10

### D.1.1.1 Process II: Production of FA with incomplete conversion of ME

The production of FA with incomplete conversion of methanol is similar to Process I. The right panel in Figure 45 shows the respective PFD. Besides FA and WA, the reactor product (4) also contains unreacted ME. It is absorbed in water, resulting in liquid (7). The absorber off-gas (6) is burned with air to generate steam; a recycle is not required. An advantage is the reactor's lower conversions, which could lead to higher selectivities. We adopted the operating point of the reactor and the resulting absorber product from the literature; it consists of 0.509 g/g FA, 0.205 g/g ME, and Water [130]. Tables 52 and 53 give the stream table and unit data of the process.

**Table 52:** Stream Table Route A4 Process II

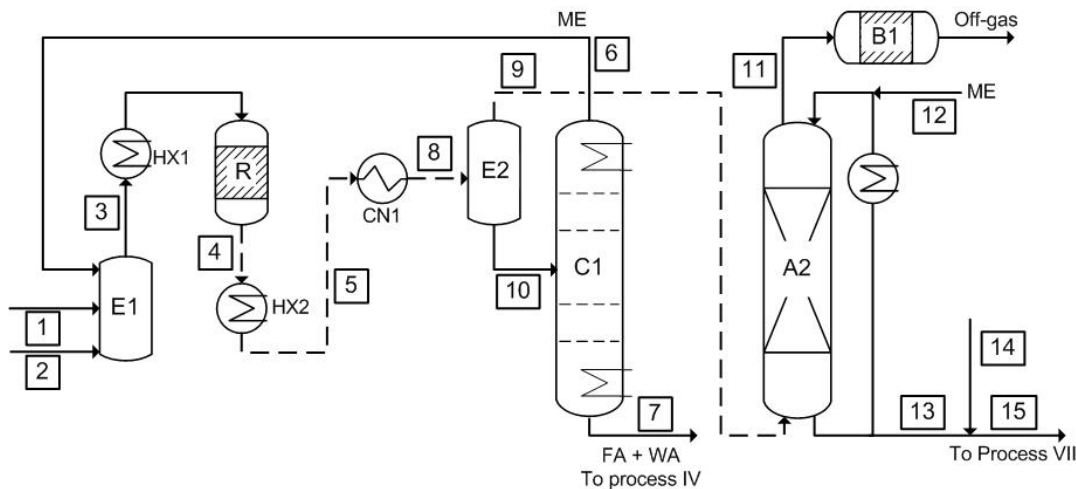
Stream	1	2	3	4	5	6	7	8
$\dot{m} / \text{kg/h}$	1125.20	1270.35	2395.55	2395.55	174.47	1345.57	1224.48	3002.25
$p / \text{bar}$	1.00	1.00	1.00	<b>1.00</b>	2.75	1.00	<b>1.00</b>	1.00
$T/^\circ\text{C}$	25.00	25.00	44.90	705.74	25.00	25.03	<b>69.50</b>	160.00
$x_i / \text{g/g}$								
FA	-	-	-	<b>0.264</b>	-	0.008	<b>0.509</b>	-
WA	-	-	-	<b>0.092</b>	0.876	0.016	<b>0.286</b>	0.144
ME	1.000	-	0.470	<b>0.106</b>	0.124	0.018	0.205	0.000
CO <sub>2</sub>	-	-	-	<b>0.112</b>	-	0.199	-	0.105
N <sub>2</sub>	-	0.770	0.408	<b>0.408</b>	-	0.727	-	0.751
O <sub>2</sub>	-	0.230	0.122	-	-	-	-	-
H <sub>2</sub>	-	-	-	0.018	-	0.032	-	-
CO	-	-	-	-	-	-	-	-

**Table 53:** Unit operations data Route A4 Process II

Unit:	$T/^\circ\text{C}$	$p / \text{bar}$	$\dot{Q} / \text{kW}$
E <sub>1</sub>	44.90	1.00	381.19
HX <sub>1_1</sub>	140.00	1.00	79.56
HX <sub>1_2</sub>	210.00	1.00	63.37
R	705.74	1.00	-
HX <sub>2_1</sub>	300.00	1.00	-480.84
HX <sub>2_2</sub>	230.00	1.00	-74.41
HX <sub>2_3</sub>	160.00	1.00	-71.65
B <sub>1_1</sub>	300.00	1.00	-1321.30
B <sub>1_2</sub>	230.00	1.00	-69.86
B <sub>1_3</sub>	160.00	1.00	-68.70
A <sub>1</sub>	25.00	1.00	-644.68

### D.1.1.2 Process II': Production of FA and fast condensation

A process proposed by Kloepper et al. [131] suggests the fast condensation of the reactor product of an FA plant with incomplete conversion. Fig 46 gives a PFD of the process. All stream compositions are adopted from the original work.


**Figure 46:** PFD of the process proposed by Kloepper et al..

The reactor product (4) (neglecting noncondensable components) consists of **0.445 g/g** FA and **0.314 g/g** ME and Water. It is subsequently cooled in HX1 to prevent the disintegration of FA. The obtained stream (5) is fed to condenser CN1. CN1 rapidly cools stream (5) to **53°C**, and the phase separator E2 splits it into the water-rich liquid (10) and the FA-rich gaseous stream (9). Stream (9) is absorbed in ME in the absorber A2 that has recirculation. The product (13) consists of 0.628 g/g FA, 0.311 g/g ME, and WA.

Stream (10) is fed to distillation column C1, where pure ME is recovered at the top (6)

and recycled, and aqueous FA solution is removed as the bottom product (7). Depending on demand, product (7) can be sold as aqueous FA solution. Here stream (7) is also converted to OME feedstock using a pervaporation unit (Process VI), allowing a better comparison to the other routes. Tables 54 to 56 give the stream table and unit data of process II', tables 69 and 70 of the added pervaporation process (cf. Section D.1.1.5). The mixed end product fed to process VII are 1030.61 kg of a solution of 0.603 g/g FA, 0.367 g/g ME and 0.03 g/g WA.

**Table 54:** Stream Table Process II'

Stream	1	2	3	4	5	6	7	8	9	10	11	12	13	14	15
$\dot{m}$ / kg/h	1438.22	1174.79	2613.00	2613.00	2613.00	335.30	670.94	2613.00	1605.87	1007.13	1220.60	33.30	418.56	29.70	448.27
$p$ / bar	1.00	1.00	1.00	1.00	1.00	1.00	1.00	1.03	1.03	1.03	1.03	1.03	1.03	1.03	1.03
$T$ /°C	25.00	25.00	43.89	810.12	160.00	64.57	99.20	<b>53.00</b>	<b>53.00</b>	<b>53.00</b>	11.18	16.00	23.99	25.00	26.22
$x_i$ / g/g															
FA	-	-	-	<b>0.242</b>	0.242	-	0.542	0.242	<b>0.167</b>	<b>0.361</b>	<b>0.004</b>	-	0.629	-	0.587
WA	-	-	-	<b>0.131</b>	0.131	0.014	0.451	0.131	<b>0.022</b>	<b>0.305</b>	0.007	-	0.059	-	0.055
ME	-	1.000	<b>0.450</b>	<b>0.171</b>	0.171	<b>0.985</b>	<b>0.007</b>	0.171	0.069	0.333	<b>0.011</b>	<b>1.000</b>	0.311	1.000	0.357
CO <sub>2</sub>	-	-	-	0.028	0.028	-	-	0.028	0.046	-	0.060	-	-	-	-
N <sub>2</sub>	0.770	-	0.424	0.424	0.424	-	-	0.424	0.689	-	0.907	-	-	-	-
O <sub>2</sub>	0.230	-	<b>0.127</b>	-	-	-	-	-	-	-	-	-	-	-	-
H <sub>2</sub>	-	-	-	0.004	0.004	-	-	0.004	0.007	-	0.009	-	-	-	-
CO	-	-	-	-	-	-	-	-	-	-	-	-	-	-	-

**Table 55:** Unit operations data Process II'

Unit:	$T$ /°C	$p$ / bar	$\dot{Q}$ / kW
E <sub>1</sub>	43.89	1.00	397.13
HX <sub>1_1</sub>	140.00	1.00	86.82
CN <sub>1</sub>	53.00	1.03	-629.44
R	810.12	1.00	-
HX <sub>2_1</sub>	300.00	1.00	-643.70
HX <sub>2_2</sub>	230.00	1.00	-76.11
HX <sub>2_3</sub>	160.00	1.00	-72.77
B <sub>1_1</sub>	300.00	1.00	-313.15
B <sub>1_2</sub>	230.00	1.00	-39.13
B <sub>1_3</sub>	160.00	1.00	-38.61

**Table 56:** Columns Process II'

Distillation columns	C <sub>1</sub>
$\dot{Q}_{top}$ / kW	-549.87
$T_{top}$ /°C	64.57
$\dot{Q}_{bot}$ / kW	605.37
$T_{bot}$ /°C	99.20
$p$ / bar	1.00
N	24.00
N <sup>Feed</sup>	10.00
RR	4.28

### D.1.1.3 Process III: Thin-film evaporation

The technology to produce stable, highly concentrated FA solutions using thin-film evaporators (TFE) is well established [57, 97, 135]. We adopted the process presented in Chapter 5 to produce OME feedstock and integrated it as Process III into Routes A1 and A4, Figure 47 shows a PFD.

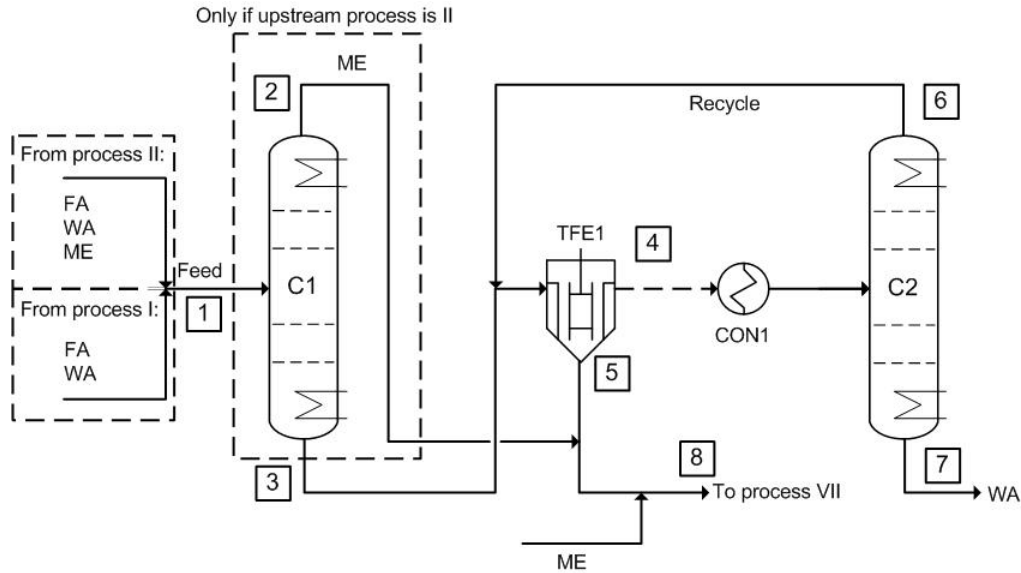


**Figure 47:** PFD of Process III. C1 is only required if the Feed contains methanol (Route A4)

Depending on the upstream FA production Process, the OME feedstock (8) is produced either from aqueous FA (Route A1, upstream Process I) or water-methanol formaldehyde solutions (Route A4, upstream Process II). For a detailed description of the process see Section 5.2.4.

Based on the fed FA solution, the OME feedstock contains 0.1 (Route A1) or 0.12 (Route A4) g/g water. Tables 57 to 59 give the stream table and unit data of the process for Route A1, tables 60 to 62 for Route A4.

**Table 57:** Stream Table Process III, Route A1

Stream	1	4	5	6	7	8
$\dot{m}$ / kg/h	1236.93	806.10	762.40	331.56	474.54	1135.98
$p$ / bar	25.00	0.20	0.20	4.00	4.00	1.00
$T$ /°C	65.61	120.47	120.47	136.19	143.47	100.73
$x_i$ / g/g						
FA	0.504	0.222	0.816	0.536	0.003	0.548
WA	0.492	0.772	0.178	0.449	0.997	0.120
ME	0.003	0.006	0.005	0.015	-	0.332

**Table 58:** Unit operations data Process III, Route 1

Unit:	$T/^\circ\text{C}$	$p$ / bar	$\dot{W}$ / kW	$\dot{Q}$ / kW
TFE	120.47	0.20	-	528.16
CON <sub>1</sub>	45.00	0.20	-	-535.84

**Table 59:** Columns Process III, Route A1

Distillation columns	C <sub>2</sub>
$\dot{Q}_{top}$ / kW	-439.44
$T_{top}/^\circ\text{C}$	136.19
$\dot{Q}_{bot}$ / kW	544.88
$T_{bot}/^\circ\text{C}$	143.47
$p$ / bar	4.00
N	24.00
N <sup>Feed</sup>	14.00
RR	1.73

**Table 60:** Stream Table Process III, Route A4

Stream	1	2	3	4	5	6	7	8
$\dot{m}$ / kg/h	1224.48	212.85	1011.63	619.15	771.79	379.31	239.84	1111.10
$p$ / bar	1.00	0.50	0.50	0.20	0.20	4.00	4.00	40.00
$T/^\circ\text{C}$	69.50	47.84	83.43	118.12	118.12	135.22	143.67	105.42
$x_i$ / g/g								
FA	0.509	-	0.616	0.264	0.806	0.428	0.003	0.560
WA	0.286	0.010	0.344	0.637	0.141	0.409	0.997	0.100
ME	0.205	0.990	0.040	0.100	0.053	0.163	-	0.340

**Table 61:** Unit operations data Process III, Route A4

Unit:	$T/^\circ\text{C}$	$p$ / bar	$\dot{Q}$ / kW
TFE	118.12	0.20	359.30
CON <sub>1</sub>	57.94	0.20	-373.22

**Table 62:** Columns Process III, Route A4

Distillation columns	C <sub>1</sub>	C <sub>2</sub>
$\dot{Q}_{top}$ / kW	-830.89	-580.75
$T_{top}/^\circ\text{C}$	47.84	135.22
$\dot{Q}_{bot}$ / kW	506.07	663.77
$T_{bot}/^\circ\text{C}$	83.43	143.67
$p$ / bar	0.50	4.00
N	28.00	22.00
N <sup>Feed</sup>	16.00	14.00
RR	6.13	2.60

**D.1.1.4 Process III\*, Thin-film evaporation**

Mantei et al. [10] previously suggested a simpler FA concentration based on thin-film evaporation. In their work, two thin-film evaporators are employed to produce OME feedstock, cf. Figure 48. The process is adopted without modification; the complete stream table and PFD were provided by Mantei et al. [10]

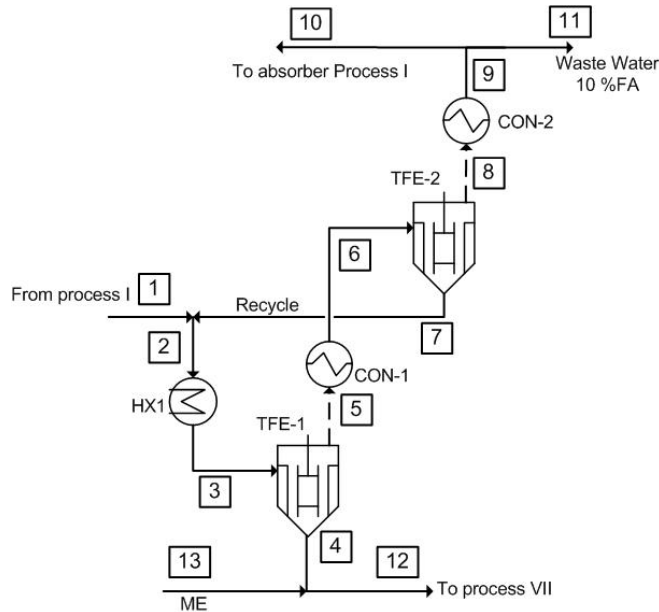


**Figure 48:** PFD of Process III\* adopted from Mantei et al. [10].

The aqueous FA solution from Process I (1) is preheated, fed to TFE1, concentrated to 0.86 g/g FA (4), and mixed with ME to produce OME feedstock (8). The top product of TFE1 (5) is condensed and fed to TFE2. The bottom product of TFE2 (7) is recycled and mixed with the feed. The top product (8) is condensed, and part of it is recycled to Process I to be used as an absorbent in the absorber; part of it is removed as wastewater. The material and energy balance was adopted from Mantei et al. [10]. 8 wt% of all fed FA is lost in the wastewater stream (11). Tables 63 to 64 give the stream table and unit data of the process.

**Table 63:** Stream Table Process III\*

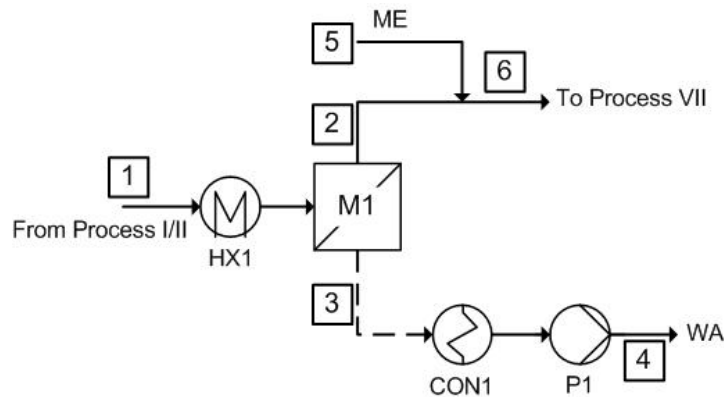
Stream	1	2	3	4	5	6	7	8	9	10	11	12	13
$\dot{m}$ / kg/h	1364.86	1598.12	1598.12	723.76	874.36	874.36	233.26	641.10	641.10	88.22	552.88	1099.42	375.66
$p$ / bar	0.07	0.07	0.07	0.07	0.07	0.20	0.20	0.20	0.20	1.00	1.00	1.00	1.00
$T$ / °C	44.83	45.30	50.00	50.00	50.00	40.00	40.00	40.00	30.00	30.12	30.12	25.00	25.00
$x_i$ / g/g													
FA	0.503	0.537	0.537	0.860	0.269	0.269	0.731	0.101	0.101	0.101	0.101	0.566	-
WA	0.490	0.458	0.458	0.137	0.723	0.723	0.269	0.888	0.888	0.888	0.888	0.090	-
ME	0.007	0.006	0.006	0.003	0.008	0.008	-	0.011	0.011	0.011	0.011	0.344	1.000

**Table 64:** Unit operations data Process III\*

Unit:	$T/^\circ\text{C}$	$p / \text{bar}$	$\dot{Q} / \text{kW}$
HX <sub>1</sub>	50.00	0.07	136.83
TFE <sub>1</sub>	50.00	0.20	415.45
CON <sub>1</sub>	40.00	0.20	-382.52
TFE <sub>2</sub>	40.00	0.20	282.35
CON <sub>2</sub>	40.00	0.20	-434.56

### D.1.1.5 Process IV, Pervaporation

Pervaporation has been successfully applied for the removal of water from various organic solvents, for example, ethanol [99, 100] and has been suggested for the removal of water from aqueous and methanolic FA solutions in patent literature [60, 128]. Furthermore, it has been proven in lab-scale experiments that pervaporation can be used to remove water from a stream composed of FA, WA, ME, and OME in the OME production process. In the referred study [59] suitable membrane materials have been identified regarding flux, permeate purity, and stability. Figure 47 shows a PFD for a pervaporation unit based on these works considered here for the removal of water from FA solutions.

**Figure 49:** PFD of the pervaporation unit including utility.

FA solution (1) is preheated in HX1 and fed to the membrane module M1 equipped with a hydrophilic polymeric membrane, PERVAP 4101 [59]. The pressure at the permeate side has to be sufficiently low to provide enough driving force; a pressure of 0.032 bar is chosen here. The water passes through the membrane to the permeate side; the module is adiabatic. The vapor (3) is condensed in CON1. The pump P1 conveys the condensed water, and a small auxiliary compressor attached to CON1 removes traces of inert gas. We assume the permeate has the same composition as in the original work [59] (**0.984 g/g water**). The retentate is mixed with methanol to produce OME feedstock. The permeate mass flow rate determines the remaining mass fraction of water in the retentate leaving the pervaporation unit (i.e., the produced OME feedstock). It influences both

the heat demand and the required membrane surface in process IV and the subsequent OME process VII. In a sensitivity study, the water content in the OME feedstock was varied in both processes. The overall heat demand is calculated in process simulation; the required membrane surface area is calculated from the correlation given by Schmitz et al. [59]. All other process parameters besides the water content in the retentate are kept constant. Figure 50 gives the resulting trade-off between membrane area and heat demand.

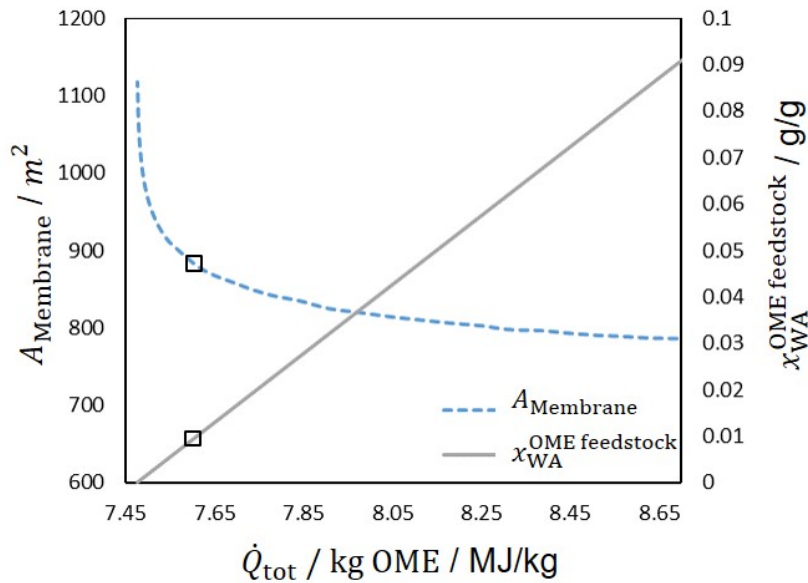


**Figure 50:** Membrane surface area and heat demand per kg OME in Process IV and in the OME process. The solid line shows the water fraction in the OME feedstock, and the dashed line the membrane surface area. The rectangles show the chosen operating point for the pervaporation unit.

The heat demand in the OME process increases significantly with higher water contents. This is because water inhibits OME formation in the reactor, leading to bigger recycle streams. The operating point (OP) for the pervaporation unit is chosen at  $x_{\text{WA}}^{\text{OME feedstock}} = 0.01 \text{ g/g}$  where both area and heat demand are close to their minima. Lower water contents are not advisable as they would lead to drastically higher membrane surfaces areas while saving little heat.

Depending on the setup of the plant, multiple pervaporation units can be employed in sequence to achieve the required membrane surface. In this case, HX1 serves as an intermediate heater to keep the retentate/feed at a constant operating temperature. Currently, the required membranes are not manufactured on a large scale, and estimating the future costs based on the limited information is difficult. In the present work, the membrane housing cost is estimated to  $50 \text{ \$/m}^2$  and the membrane cost to  $200 \text{ \$/m}^2$



[100, 164, 165]. Tables 65 to 66 give the stream table and unit data of the process for Route A2, tables 67 to 68 for Route A5 and tables 69 and 70 for Route A6.

**Table 65:** Stream Table Process IV, Route A2

Stream	1	2	3	4	5	6
$\dot{m}$ / kg/h	1252.31	636.45	615.85	615.85	373.65	1010.10
$p$ / bar	1.00	1.00	<b>0.03</b>	0.03	1.00	1.00
$T$ /°C	65.61	65.61	65.61	<b>25.00</b>	25.00	25.00
$x_i$ / g/g						
FA	0.505	0.978	<b>0.016</b>	0.016	-	0.616
WA	0.492	0.016	<b>0.984</b>	0.984	-	<b>0.010</b>
ME	0.003	0.007	-	-	1.000	0.374

**Table 66:** Unit operations data Process IV, Route A2

Unit:	$T$ /°C	$p$ / bar	$\dot{Q}$ / kW
HX1	65.61	0.03	403.54
CON1	25.00	0.03	-428.48

**Table 67:** Stream Table Process IV, Route A5

Stream	1	2	3	4	5	6
$\dot{m}$ / kg/h	1233.93	885.56	348.37	348.37	124.54	1010.10
$p$ / bar	1.00	1.00	<b>0.03</b>	0.03	1.00	1.00
$T$ /°C	69.50	69.50	69.50	<b>25.00</b>	25.00	25.00
$x_i$ / g/g						
FA	0.509	0.703	<b>0.016</b>	0.016	-	0.616
WA	0.286	0.011	<b>0.984</b>	0.984	-	<b>0.010</b>
ME	0.205	0.286	-	-	1.000	0.374

**Table 68:** Unit operations data Process IV, Route A5

Unit:	$T$ /°C	$p$ / bar	$\dot{Q}$ / kW
HX <sub>1</sub>	25.14	0.03	195.51
CON <sub>1</sub>	25.00	0.03	-213.74

**Table 69:** Stream Table Process IV, Route A6

Stream	1	2	3	4	5	6
$\dot{m}$ / kg/h	670.94	369.23	301.72	301.72	213.40	582.62
$p$ / bar	1.00	1.00	<b>0.03</b>	0.03	1.00	1.00
$T$ / °C	99.20	99.20	99.20	<b>25.00</b>	25.00	25.00
$x_i$ / g/g						
FA	0.542	0.972	<b>0.016</b>	0.016	-	0.616
WA	0.451	0.016	<b>0.984</b>	0.984	-	<b>0.010</b>
ME	0.007	0.012	-	-	1.000	0.374

**Table 70:** Unit operations data Process IV, Route A6

Unit:	$T$ / °C	$p$ / bar	$\dot{Q}$ / kW
HX <sub>1</sub>	69.50	0.03	190.30
CON <sub>1</sub>	25.00	0.03	-218.06

### D.1.1.6 Process V: Extractive distillation

A patent by Morishita et al. [61] suggests the production of gaseous FA of high purity from an aqueous FA solution via extractive distillation. Figure 51 shows the PFD of the process. Columns C2 and C3 and the compositions of their feed and product streams are adopted from the original work without changes; the recycle (6), column C1, evaporator E1, and absorber A1 were added in the present work. The compositions of the feed, top, and bottom products of the extractive distillation column as well as its size are adopted from the original literature.

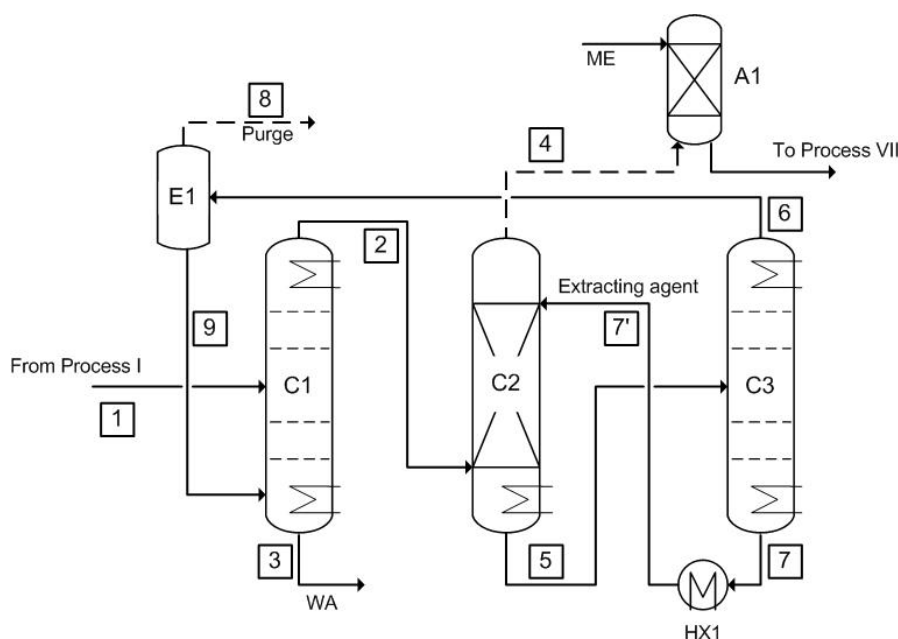


**Figure 51:** PFD of the extractive distillation process based on Morishita et al. [61].

Aqueous FA solution (1) is pre-concentrated in distillation column C1, and pure water (0.997 g/g) is removed at the bottom of C1. The top product (2) contains 0.65 g/g FA [61] and is fed to the lower part of the extractive distillation column C2. In the upper part of the column, a large stream of polyethylene glycol dimethyl ether (PEG) is added as an extracting agent at a temperature of 120 °C. Column C2 is equipped with a reboiler operated at 170 °C; there is no condenser at the top. Pure gaseous FA is recovered from the top as stream (4). In order to produce OME feedstock, we added a loss-free absorption of this gaseous FA in ME in absorber A1. Column C2's bottom product (5), comprised of PEG, water, and FA, is separated in column C3. We assume that PEG can be sharply separated from WA in distillation as bottom product (7) due to its low vapor pressure. Dilute aqueous FA solution (6) is removed at the top and recycled to convert all FA to OME feedstock. E1 evaporates and removes a small purge stream (8) to prevent an accumulation of small amounts of ME.

There is no property model readily available for the extracting agent. However, since there is no PEG present in C1, E1, and A1, the energy demand of these units is calculated via process simulation using the described model for FA, ME, WA. The energy demand of column C2 is trivially calculated since it has no condenser and the material balance and the heat capacity of PEG are available. For column C3 the condenser duty  $\dot{Q}_C$  is estimated from the enthalpy of vaporization  $\Delta h_{v,i}(T)$  of the components of the top product, their mass flow rate  $\dot{m}_i$ , and the reflux ratio  $RR$ , cf. Equation 27. The reflux ratio of C3 is estimated as 1.44 based on Underwood's equation using a relative volatility of WA/PEG of 230 [166]. The reboiler duty  $\dot{Q}_B$  is calculated via the energy balance of the whole column, cf. Equation 28. Tables 71 to 73 give the stream table and unit data of the process.

**Table 71:** Stream Table Process V

Stream	1	2	3	7'	4	5	6	7	8	9	10
$\dot{m}$ / kg/h	1251.19	1150.47	602.77	23009.42	623.15	23534.24	526.54	23009.42	24.50	502.05	1000.00
$p$ / bar	6.00	<b>6.00</b>	<b>6.00</b>	2.00	<b>2.00</b>	<b>2.00</b>	2.00	<b>2.00</b>	2.00	2.00	2.00
$T$ /°C	65.94	137.60	158.63	120.00	<b>120.00</b>	<b>170.00</b>	113.38	<b>170.00</b>	114.92	114.92	110.00
$x_i$ / g/g											
FA	0.504	<b>0.650</b>	0.003	-	<b>1.000</b>	<b>0.005</b>	0.237	-	0.328	0.236	0.623
WA	0.492	0.318	<b>0.997</b>	-	-	<b>0.017</b>	0.694	-	0.511	0.700	-
ME	0.003	0.032	-	-	-	-	0.069	-	0.161	0.064	0.377
PEG	-	-	-	1.000	-	<b>0.978</b>	-	<b>1.000</b>	-	-	-

**Table 72:** Unit operations data Process V

Unit:	$T$ /°C	$p$ / bar	$\dot{Q}$ / kW
E <sub>1</sub>	114.92	2.00	12.37
HX <sub>1</sub>	120.00	2.00	-694.92
A <sub>1</sub>	110.00	6.00	-251.98
HX <sub>2</sub>	40.00	1.00	-391.52

**Table 73:** Columns Process V

Distillation colmns	C <sub>1</sub>	C <sub>2</sub>	C <sub>3</sub>
$\dot{Q}_{top}$ / kW	-1285.78	-	-417.13
$T_{top}$ /°C	137.60	-	113.38
$\dot{Q}_{bot}$ / kW	1468.70	992.10	348.69
$T_{bot}$ /°C	158.63	<b>170.00</b>	<b>170.00</b>
N	24.00	<b>49.00</b>	<b>43.00</b>
N <sup>Feed</sup>	11.00	-	-
N <sup>Feed(9)</sup>	20.00	-	-
$p$ / bar	<b>6.00</b>	<b>2.00</b>	<b>2.00</b>
RR	1.42	-	1.44

### D.1.1.7 Process VI: Chemical separation of water and extractive distillation

A process proposed by Masamoto et al. [126] is based on the production of the intermediate MAL in order to remove pure WA. Figure 52 gives the PFD of the process.

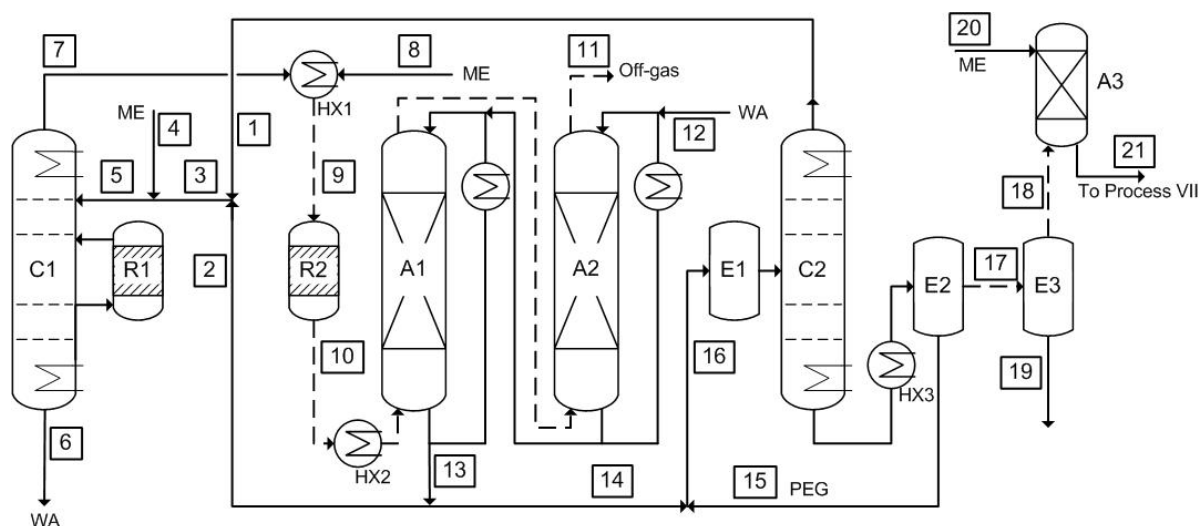


**Figure 52:** PFD of process proposed by Masamoto et al.

An aqueous solution of 0.39 g/g FA (3) produced in this process is mixed with ME (4) and fed to distillation column C1 as stream (5). Sidestreams of C1 are fed to three reactors (only one reactor shown, R1), where MAL is formed and recycled to the column and subsequently removed at the top as stream (7) (0.90 g/g MAL 0.1 g/g ME). Pure water is removed as bottom product (6). Stream (7) is combined with air (8) and fed to reactor R2 to produce FA. The reactor product (10) is absorbed in absorption columns A1 and A2 to produce a concentrated aqueous solution of 0.65 g/g FA (13). Part of stream (13) is recycled as stream (2).

The other part (14) is mixed with an extracting agent (PEG) (15) in the stirred vessel E1 and subsequently fed to column C2. In C2, a dilute aqueous FA solution of 27% FA is removed as the top product (1) and recycled. The bottom product of C2 is fed to the flash vessel E2, where pure PEG is recovered as a liquid product (15). The gaseous product (17) is fed to cooling trap E3, where pure FA gas is removed as stream (18), and small amounts of water and ME are removed as stream (19). The gaseous FA is absorbed in ME in Absorber A3 to produce OME feedstock. The recycled streams (2) and (1) form the aqueous FA solution (3) that is part of the feed. The absorbers A1 and A2 are modeled with 3 and 4 vapor-liquid equilibrium (VLE) stages, respectively. A liquid solution is drawn at the bottom of each absorber, cooled, and recycled to its top. The distillation column C1 is simulated rigorously using the described property model. The adiabatic reactors ascribed to it are modeled considering the chemical equilibrium

Reactions (7) to (12) in the main manuscript and the formation of MAL from FA and ME, Reaction (13) [64]. They draw and recycle solutions at stages 15, 18, and 21. Due to missing property data for PEG, column C2 is not simulated, but its heat demand is estimated based on the enthalpy of vaporization of the top product, the top and bottom product mass flow rates  $\dot{m}_i$ , and the reflux ratio, cf. column C3 in section D.1.1.6. A reflux ratio of 1.4 was assumed. All stream compositions are adopted from the original work [126], tables 74 to 75 give the stream table and unit data of the process.

Table 74: Stream Table Process VI

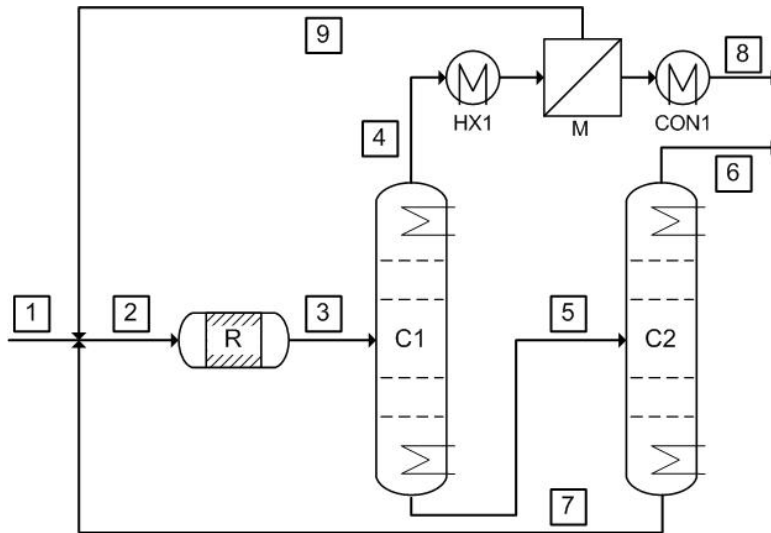
Stream	1	2	3	4	5	6	7	8	9	10	11	12	13	14	15	16	17	18	19	20	21	
$\dot{m}$ / kg/h	539.51	242.41	781.92	735.60	1510.61	655.24	858.02	7614.94	8472.96	8472.96	7560.47	497.90	1410.40	1167.99	1594.82	3720.44	628.48	611.92	16.36	388.08	1000.00	1000.00
$p$ / bar	1.00	1.00	1.00	1.00	1.00	1.00	1.00	1.00	1.00	1.00	1.00	2.00	1.00	1.00	1.00	1.00	1.00	1.00	1.00	1.00	1.00	1.00
$T$ / °C	56.33	67.30	59.99	25.00	59.86	99.62	41.38	25.00	40.00	340.00	39.98	25.00	67.30	67.30	140.00	96.47	140.00	-	-	25.00	25.00	25.00
$x_i$ / g/g																						
EA	<b>0.273</b>	0.650	0.390	-	0.202	0.001	-	-	-	<b>0.111</b>	<b>0.003</b>	-	<b>0.650</b>	0.650	-	0.372	<b>0.973</b>	<b>0.999</b>	-	-	-	0.612
WA	0.718	0.346	0.602	-	0.311	<b>0.999</b>	-	<b>0.013</b>	0.011	<b>0.039</b>	0.045	<b>1.000</b>	<b>0.346</b>	0.346	-	0.196	0.026	-	0.998	-	-	-
ME	0.009	0.004	0.008	1.000	0.487	-	<b>0.101</b>	-	0.010	<b>0.003</b>	0.002	-	0.004	0.004	-	0.003	-	-	-	1.000	0.388	-
CO <sub>2</sub>	-	-	-	-	-	-	-	-	-	-	-	-	-	-	-	-	-	-	-	-	-	-
N <sub>2</sub>	-	-	-	-	-	-	-	<b>0.897</b>	0.807	0.807	0.904	-	-	-	-	-	0.001	0.001	-	-	-	-
O <sub>2</sub>	-	-	-	-	-	-	-	<b>0.090</b>	0.081	0.037	0.042	-	-	-	-	-	-	-	-	-	-	-
H <sub>2</sub>	-	-	-	-	-	-	-	-	-	-	-	-	-	-	-	-	-	-	-	-	-	-
CO	-	-	-	-	-	-	-	-	-	0.003	0.003	-	-	-	-	-	-	-	-	-	-	-
MAL	-	-	-	-	-	-	<b>0.899</b>	-	0.091	<b>0.001</b>	0.001	-	-	-	-	-	-	-	-	0.002	-	-
PEG	-	-	-	-	-	-	-	-	-	-	-	-	-	-	1.000	0.768	-	-	-	-	-	-

Table 75: Unit operations data Process VI

Unit:	$T$ / °C	$p$ / bar	$\dot{Q}$ / kW	Distillation columns	
				C <sub>1</sub>	C <sub>2</sub>
HX <sub>1_1</sub>	140.00	1.00	71.44	-321.59	-340.30
HX <sub>3_1</sub>	40.00	1.00	137.78	41.58	56.33
R <sub>2</sub>	340.00	1.00	41.85	306.88	325.71
E <sub>1</sub>	79.98	1.00	-57.82	99.62	79.98
E <sub>2</sub>	79.98	1.00	353.97	1.00	1.00
E <sub>3</sub>	0.00	1.00	-42.06	32.00	<b>10</b>
A <sub>1</sub>	67.30	1.00	510.71	15.00	<b>1</b>
A <sub>2</sub>	39.98	1.00	-750.91	2.05	1.40
A <sub>3</sub>	25.00	1.00	-418.61		

### D.1.1.8 Process VII: OME production

The OME production process is adopted from Schmitz et al. [43]. All compositions and mass flow rates are adopted without modifications, Figure 53 gives a PFD.



**Figure 53:** PFD of the OME process proposed by Schmitz et al. [43].

The OME feedstock is mixed with the recycle streams 7 and 9 and fed to the isothermic reactor R. R is operated at 68 °C and 2 bar and is filled with Amberlyst 46 as a catalyst. 0.277 kg of catalyst is required per kg of produced OME<sub>3-5</sub> per hour. The reactor product (3) is fed to distillation column C1, where OME<sub>3</sub> and all longer chained OME are yielded in the bottom product.

The bottom product (5) is fed to column C2, where all OME<sub>n>5</sub> is separated as the bottom product (7) and recycled, the top product (6) is the product OME<sub>3-5</sub>. The top product of C1 (4) is fed to a pervaporation unit M1 to remove pure water (8) as permeate. The retentate (9) is recycled to the reactor. Tables 65 to 66 give the stream table and unit data of the process. Note that the process data is given exemplary for route A4, where 0.10 g/g of water is present in the OME Feedstock. However, the OME process has been simulated with the corresponding amount of water in the feed for every route.



**Table 76:** Stream Table Process VII

Stream	1	2	3	4	5	6	7	8	9
$\dot{m}$ / kg/h	1111.10	8101.00	8100.99	7145.08	955.92	893.78	62.13	217.31	6927.77
$p$ / bar	1.00	<b>2.00</b>	<b>2.00</b>	<b>1.40</b>	<b>1.40</b>	<b>0.10</b>	<b>0.10</b>	1.40	1.40
$T$ /°C	70.00	68.51	68.00	68.27	184.97	96.41	202.71	68.27	68.27
$x_i$ / g/g									
FA	0.560	0.207	0.130	0.148	-	-	-	-	0.152
WA	0.100	0.018	0.031	0.036	-	-	-	1.000	<b>0.005</b>
ME	0.340	0.153	0.106	0.120	-	-	-	-	0.124
MAL	-	<b>0.393</b>	<b>0.393</b>	0.445	-	-	-	-	0.459
OME <sub>2</sub>	-	0.195	0.195	0.221	-	-	-	-	0.228
OME <sub>3</sub>	-	0.027	0.086	<b>0.030</b>	<b>0.502</b>	0.536	-	-	0.031
OME <sub>4</sub>	-	-	0.036	-	0.302	0.323	-	-	-
OME <sub>5</sub>	-	-	0.014	-	0.121	0.129	-	-	-
OME <sub>6</sub>	-	0.004	0.006	-	0.047	<b>0.011</b>	<b>0.567</b>	-	-
OME <sub>7</sub>	-	0.002	0.002	-	0.018	-	0.276	-	-
OME <sub>8</sub>	-	0.001	0.001	-	0.007	-	0.104	-	-
OME <sub>9</sub>	-	-	-	-	0.003	-	0.039	-	-
OME <sub>10</sub>	-	-	-	-	0.001	-	0.014	-	-

**Table 77:** Unit operations data Process VII

Unit:	$T$ /°C	$p$ / bar	$\dot{Q}$ / kW
R	68.00	2.00	-39.06
HX <sub>1</sub>	68.27	1.40	114.64
CON <sub>1</sub>	5.46	0.03	-157.08

**Table 78:** Columns Process VII

Distillation columns	C <sub>1</sub>	C <sub>2</sub>
$\dot{Q}_{top}$ / kW	-1597.75	-162.49
$T_{top}$ /°C	68.27	96.41
$\dot{Q}_{bot}$ / kW	1656.66	119.21
$T_{bot}$ /°C	184.97	202.71
$p$ / bar	<b>1.40</b>	<b>0.10</b>
N	13.00	13.00
N <sup>Feed</sup>	7.00	6.00

## D.2 Assumptions Techno-Economic Assessment

Tables 79 to 82 give the assumption and sources for the Techno-Economic Assessment of Routes A1-A7.

**Table 79:** Factors for CAPEX and OPEX estimation based on Peters et al. [145].

<b>Factors for CAPEX estimation</b>	Factor	Basis
<i>Direct Investment Costs</i>		
Equipment costs	1	EQ costs
Installation	0.47	EQ costs
Instrumentation and controls	0.36	EQ costs
Piping	0.68	EQ costs
Electrical systems	0.11	EQ costs
Buildings	0.18	EQ costs
Yard improvements	0.1	EQ costs
Service facilities	0.7	EQ costs
<i>Indirect Investment Costs</i>		
Engineering and supervision	0.33	EQ costs
Construction expenses	0.41	EQ costs
Legal expenses	0.04	EQ costs
Contractor's fee	0.22	EQ costs
Contingency	0.44	EQ costs
Fixed Capital Investment (FCI)	5.04	EQ costs
Working Capital (% of TCI)	15%	TCI
Total Capital Investment (TCI)	5.93	EQ costs
<b>Factors for OPEX estimation</b>		
<i>Direct Operating Costs</i>		
Insurance and taxes	0.02	FCI
Maintenance labor (ML)	0.01	FCI
Maintenance material (MM)	0.01	FCI
Operating supplies (OS)	0.15	ML+MM
Operating supervision (OV)	0.15	OL
Laboratory charges	0.2	OL
Plant overhead costs (PO)	0.5	OL+OV+OS
Administrative costs	0.25	PO
Distribution and selling costs	0	NPC
Research and development costs	0	NPC

**Table 80:** Further boundary conditions for economic estimation and further estimation factors.

	Value	Base	Reference
<b>Economic Parameters</b>			
Reference year	2018		
Operating hours per year	8000		
Depreciation period in years	20		
WACC	0.05		
Annuity	0.08	FCI	
<b>Material Factors</b>			
Carbon steel	1		[145]
Aluminium and bronze	1.07	Carbon steel Equipment	[145]
Cast steel	1.1	Carbon steel Equipment	[145]
304 stainless steel	1.3	Carbon steel Equipment	[145]
316 stainless steel	1.3	Carbon steel Equipment	[145]
321 stainless steel	1.5	Carbon steel Equipment	[145]
Hastelloy C	1.55	Carbon steel Equipment	[145]
Monel	1.65	Carbon steel Equipment	[145]
Nickel and Inconel	1.7	Carbon steel Equipment	[145]
<b>Location Factors</b>			
United States Gulf Coast	1		[145]
Germany	1.11	Equipment cost US Gulf Coast	[145]
<b>Chemical Engineering Plant Cost Index</b>			
	Jan 10	532.9	[167]
	2018	603.1	[167]
	2019	607.5	[167]
<b>Exchange Rate</b>			
EUR/USD (2018)	0.8464		[168]

**Table 81:** Direct Costs for OPEX estimation.

	Value	Unit	Reference
<b>Raw Materials</b>			
Methanol	401.75	EUR/t	[169]
Water	1	EUR/t	Own assumption
Air	0		Own assumption
<b>Utility Costs</b>			
Power	50	EUR/MWh	Own assumption
Natural gas	28.2	EUR/MWh	[170]
Cooling water	0.005	EUR/kWh	Own assumption
Steam 4 bar, 150 °C	22.8	EUR/t	Based on Turton [171]
Steam 20 bar, 220 °C	23.1	EUR/t	Based on Turton [171]
Steam 70 bar, 290 °C	23.5	EUR/t	Based on Turton [171]
Cooled water	0.0075	EUR/kWh	Own assumption
Cooling Agent (Salt Solution)	0.015	EUR/kWh	Own assumption
<b>Consumables</b>			
Catalyst	700	EUR/kg	Own assumption
Extraction agent	2996.19	EUR/t	[126]
<b>Labor costs</b>			
Hourly wages	41.91	EUR/h	Own assumption

**Table 82:** Heat Transfer coefficients [140].

Type	Value	Unit
<b>Shell-and-tube heat exchangers</b>		
- without phase change -		
Gas (1 bar) inside - Gas ( 1 bar) outside	20	W/m <sup>2</sup> K
Gas (200 bar ) inside - Gas ( 200 bar) outside	325	W/m <sup>2</sup> K
Liquid - Gas (1 bar)	42.5	W/m <sup>2</sup> K
Gas, high pressure (200 bar) inside - Liquid outside	300	W/m <sup>2</sup> K
Liquid inside - Liquid outside	625	W/m <sup>2</sup> K
Superheated steam outside - Liquid inside	750	W/m <sup>2</sup> K
- Evaporator -		
Natural circulation - low viscosity	600	W/m <sup>2</sup> K
Natural circulation - high viscosity	1250	W/m <sup>2</sup> K
Forced circulation	2000	W/m <sup>2</sup> K
- Condenser -		
Cooling water inside - Steam outside	750	W/m <sup>2</sup> K
<b>Waste heat boiler</b>		
Gas inside - Boiling water outside	32.5	W/m <sup>2</sup> K
<b>Double pipe</b>		
Gas (1 bar) inside - Gas ( 1 bar) outside	22.5	W/m <sup>2</sup> K
Gas (200 bar) inside - Gas ( 1 bar) outside	40	W/m <sup>2</sup> K
Gas (200 bar ) inside - Gas ( 200 bar) outside	325	W/m <sup>2</sup> K
Gas, high pressure (200 bar) inside - Liquid outside	400	W/m <sup>2</sup> K
Liquid inside - Liquid outside	850	W/m <sup>2</sup> K
<b>Plate heat exchanger</b>		
Flat channels   Gas - Water	40	W/m <sup>2</sup> K
Flat channels   Liquid - Water	575	W/m <sup>2</sup> K
Profile plates   Liquid - Liquid	2500	W/m <sup>2</sup> K
<b>Cooling</b>		
Min temperature Difference	10	K
<b>Heating</b>		
Steam Network available		
Boiling Water at pressure level of steam network available		

# Student theses

The following student theses were prepared under the supervision of the author of the present doctoral thesis in the frame of his research:

- Caio Yuiti Tamaki Furukawa: Simulation and optimization of a process for the synthesis of formaldehyde, 2020.